Modelling the Thermal Potential and Operation of Salinity Gradient Solar Ponds

Sirajadien Alzin

A Thesis Submitted in Fulfilment of the Requirements for the Degree of Doctor of Philosophy in Chemical and Process Engineering

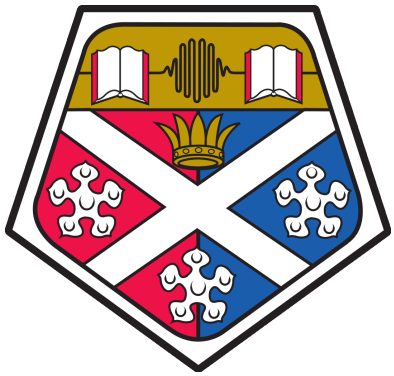

Chemical and Process Engineering Department

University of Strathclyde

2020

Declaration

'This thesis is the result of the author's original research. It has been composed by the author and has not been previously submitted for examination which has led to the award of a degree.' 'The copyright of this thesis belongs to the author under the terms of the United Kingdom Copyright Acts as qualified by University of Strathclyde Regulation 3.50. Due acknowledgement must always be made of the use of any material contained in, or derived from, this thesis.'

Acknowledgement

I would like to express my sincere gratitude to my supervisor Dr Leo Lue for the continuous support of my PhD study, for his patience, motivation, guidance, and immense knowledge. I could not have imagined having a better supervisor and mentor for my PhD study.

Special thanks go to my parents who have sacrificed their lives for myself and provided everlasting support, love and care. They have always encouraged me to explore my potential and pursue my dreams. I love them so much, and I would not have made it this far without them.

I especially thank my wonderful wife and daughter for their love, care and moral support during my academic progression.

Contents

List of Figures

List of Tables

Nomenclature

A Aspect ratio

Bi Biot number

C Salt concentration [kg m^{-3}]

C_p Specific heat [J Kg^{-1} K^{-1}]

CV Control volume

D Mass diffusinn coefficient [m^2 s^{-1}]

D_{st} Soret coefficient [$^{\circ}C^{-1}$]

DDC Double-diffusive-convection

De Declination angle of the sun

FEM Finite element method

Fr Froude number

FVM Finite volume method

H Height [m]

h_c Convection heat transfer coefficient [W m^{-2} K^{-1}]

h_e Evaporation heat transfer coefficient [W m^{-2} K^{-1}]

I Solar intensity [W m^{-2}]

J Diffusion flux [$cm^{-2}s-1$]

K Thermal conductivity [W m^{-1} K^{-1}]

LCZ Lower convective zone

$LDPE$ Low-density polyethylene

Le Lewis number

MD Membrane distillation

$MDPE$ Medium density polyethylene

MED Multi-effect distillation

$MED-TVC$ Multi-effect-desalination thermal vapour compression

$MEMS$ Multi-effect multi-stage

MSF Multi-stage-flashing

N Buoyancy ratio

N Buoyancy ratio

n_w Water reflection index

n_{air} Air reflection index

NCZ Non-convective zone

P Dimensionless pressure

p Pressure [N m^{-2}]

PDF Partial differential equations

pH potential of hydrogen

ppm Part per milion

Q_c Heat loss via convection [W m^{-2}]

Q_e Heat loss via evaporation [W m^{-2}]

Q_r Heat loss via radiation [W m^{-2}]

Q_w Heat from make up water [W m^{-2}]

Q_{cn} Heat conducted [W m^{-2}]

Q_g Heat loss to ground [W m^{-2}]

Q_{loss} All heat loss [W m^{-2}]

Q_{sra} Heat absorbed [W m^{-2}]

Ra_ρ Stability criteria

Ra_C Solutal rayleigh

Ra_I Internal rayleigh

Ra_T Thermal rayleigh

RO Reverse osmosis

Sc Schmidt number

$SGSP$ Salinity gradient solar pond

T Temperature [°C] or [K]

t Time [s]

$T.D.S$ Total dissolved solids

T_w Temperature from make up water [°C]

T_s Sky temperature [°C]

UCZ Upper convective zone

V Dimensionless velocity

v Velocity [m s^{-1}]

W Width [m]

X Dimensionless horizontal coordinate

Z Dimensionless vertical coordinate

z Depth [m]

SGSP Salinity gradient solar pond

Greek symbols

α Thermal diffusivity [m^2 s^{-1}]

β_C Solutal expansion coefficient [m^3kg^{-1}]

β_T Thermal expansion coefficient [K^{-1}]

g Gravitional acceleration [m s^{-2}]

ΔC	Salt concentration difference [kg m^{-3}]
ΔC_s	Salinity difference $\%$
ΔT	Temperature difference [°C]
$\dot{m}_e$	Rate of water addition [kg/s]
ϵ	Hemisperical emissivity of water
λ	Wavelengtg [μm]
λ_h	Relative humidity
$\nabla \cdot \mathbf{X}$	Divergence of $\mathbf{X}$
∇	Gradient
∇^2	Laplace Operator
ν	Kinematic viscosity [cm^2 s^{-1}]
ϕ_V	Test function [Velocity]
ϕ_θ	Test function [Temperature]
ϕ_φ	Test function [Salt concentration]
$\Re$	Refractance in Fresnel's equation
ρ	Density [kg m^{-3}]
σ_o	Stefan Boltzmann constant [Wm^{-2}K^{-4}]
$\tau(z)$	Solar radiation transmission
τ_s	Fraction of radiation penetrates the surface
θ	Dimensionless temperature
θ_i	Incident angle
θ_R	Refraction angle
θ_r	Reflection angle
φ	Dimensionless salt concentration
ϑ	Crank Nicolson time step

Subscripts/Superscripts

$_r$	Reference
$_S$	Solutal
$_T$	Thermal
z_0	LCZ-ground interface
z_1	NCZ-LCZ interface
z_2	UCZ-NCZ interface

Abstract

Access to freshwater is crucial for socio-economic development. In Libya, the demand for freshwater is soaring, but the supply is limited. Freshwater is intrinsically linked to energy where the paramount consideration for its sustainability is the amount of energy required to guarantee sufficient supplies of freshwater through seawater-desalination. This emphasises two paramount needs that should be promptly sought as a national priority, first stringent water conservation, and second the employment of sustainable energy sources to power desalination.

Salinity Gradient Solar Pond (SGSP) can be one of a mix of technologies leading to a future based on sustainable energy. This study models the potential and operation of SGSPs as a source of thermal energy in Libya. The study makes an original contribution to knowledge by explaining the essence (when, how, and where) of the SGSP operational instability. It also investigates the optimum zone thicknesses ratio of the three different salinity zones constituting the SGSP; Upper Convective Zone (UCZ), middle Non-Convective Zone (NCZ), and Lower Convective Zone (LCZ) while implementing the double-diffusive convection (DDC) phenomenon.

One-dimensional and two-dimensional numerical studies are conducted. The results indicate that SGSP has the potential to provide hot saline-water at a temperature exceeding 70 °C for multi-effect desalination thermal vapour compression units which require a minimum top brine temperature of 60 - 65 °C. At a SGSP thermal output of 55 W m^{-2}, 46.8 m^2 of land is required for the production of 1 m^3 per day of distillate. The two-dimensional study explains the nature of the operational instability where the occurrence and expansion of convective cells at the interfaces of the NCZ due to DDC leads to instability. This study also gathered evidence on the effect of buoyancy ratio. Salt concentration differences separating the UCZ and the LCZ should be sustained at 300 kg m^{-3} to maintain stability. The optimum zone thicknesses for an average SGSP of 2 m height are 0.4, 1.2, and 0.4 meters for the UCZ, the NCZ, and the LCZ, respectively.

Chapter 1

Introduction

Energy and freshwater are inseparable resources that are essential for human life and civilisation. The importance of freshwater can hardly be overstressed as the establishment of habitats principally rely on its availability. Energy is necessary for development; it puts all human activities in operation. Boiling freshwater is needed to generate energy. Energy is required to deliver and produce freshwater. In Libya in 2019, the freshwater and energy supply scenarios are complicated. The demand for energy and freshwater is increasing, while the supplies are limited.

Libya has a population of about 7 million with an average freshwater demand for drinking and other domestic uses of approximately 250 litres per capita per day [1]. Thus, the average water demand in the country is 1.75×10^6 m^3/day (0.638×10^9 m^3 / year). Practically, the watery supply scenario; surface water accounts for (ca. 2.3 %), recycled sewage effluent provides (ca. 0.9 %), while water from desalination covers only (ca. 0.7 %) of the annual national demand. Thus, (ca. 96 %) of Libya's freshwater supply is a groundwater [2]. About 75 % of this groundwater comes from the man-made river reservoirs.

From the Sahara desert, 1.46×10^9 m^3 of fresh groundwater is withdrawn annually via the Man-Made River pipelines shown in Fig. 1.1, for municipal, agricultural and industrial purposes in the coastal areas as most Libyans live in these areas where the groundwater is salty (8×10^3 ppm) and unacceptable for drinking and other domestic use. The world health organisation states that the maximum salinity of drinking water is 1000 ppm [3, 4]. The two major reservoirs in the Libyan desert have fresh groundwater with total dissolved solids T.D.S.

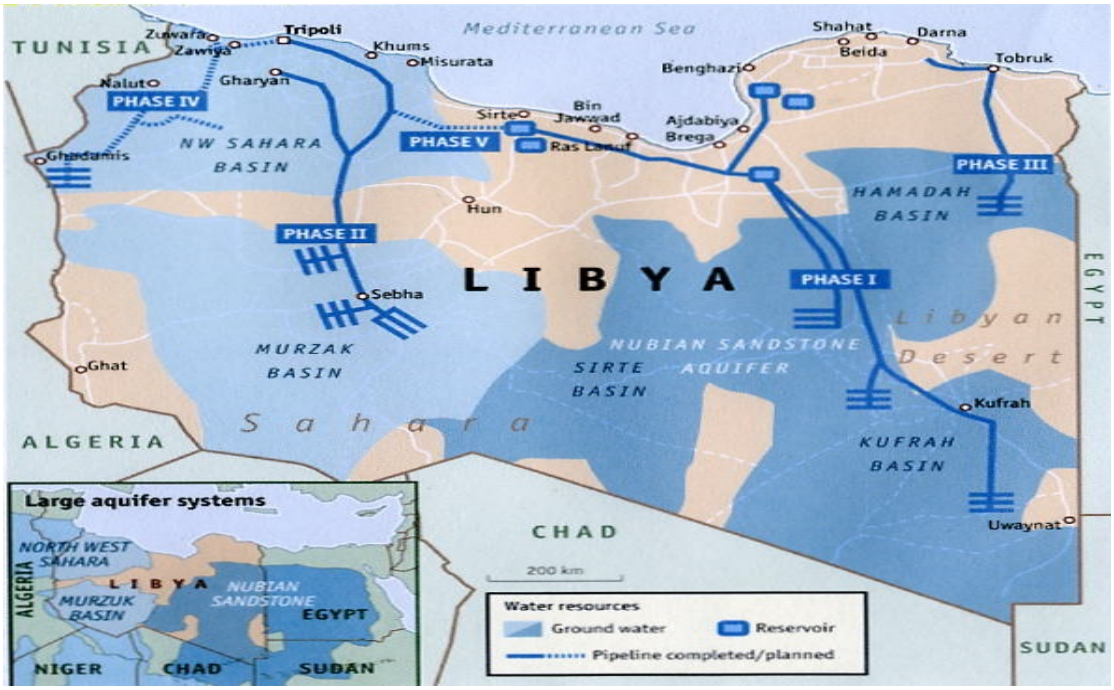

FIGURE 1.1. Libya water resources map [6].

$< 5 \times 10^2$ ppm. They contain fossil water that maybe ten thousand years old, which had accumulated during the last ice age. The first reservoir is located in Kufra/Sarrir plain (South East); its estimated storage capacity is 3.4×10^{12} m^3 of freshwater, its depth is 2 km below the ground surface, and it covers an area of 700×10^6 m^2. The second reservoir is located in Murzak basin; its estimated storage capacity is 4.8×10^{12} m^3 of freshwater, its depth is 1 km below the ground surface, and it covers an area of 350×10^6 m^2. Other relatively smaller reservoirs are located in Sirte, Tazerbo and Fezzan [2, 1, 5].

The reservoirs, though gigantic, are finite. As demand is soaring, the Man-Made River pipelines are getting longer, and the groundwater levels are falling. The freshwater supply situation has become even more complicated with a rapid increase in population. The population growth rate is approximately 3.3 % per year (one of the highest and least sustainable in the world) [2]. Thus, an urgent recognition of this problematic water consumption and supply scenario is crucial if to improve the country's standard of living and to guarantee economic security for future generations. Consequently, developing non-conventional sources of freshwater supply is drastically needed. Seawater desalination is one of the available options [2].

Unfortunately, desalination systems are energy-intensive processes. The typical

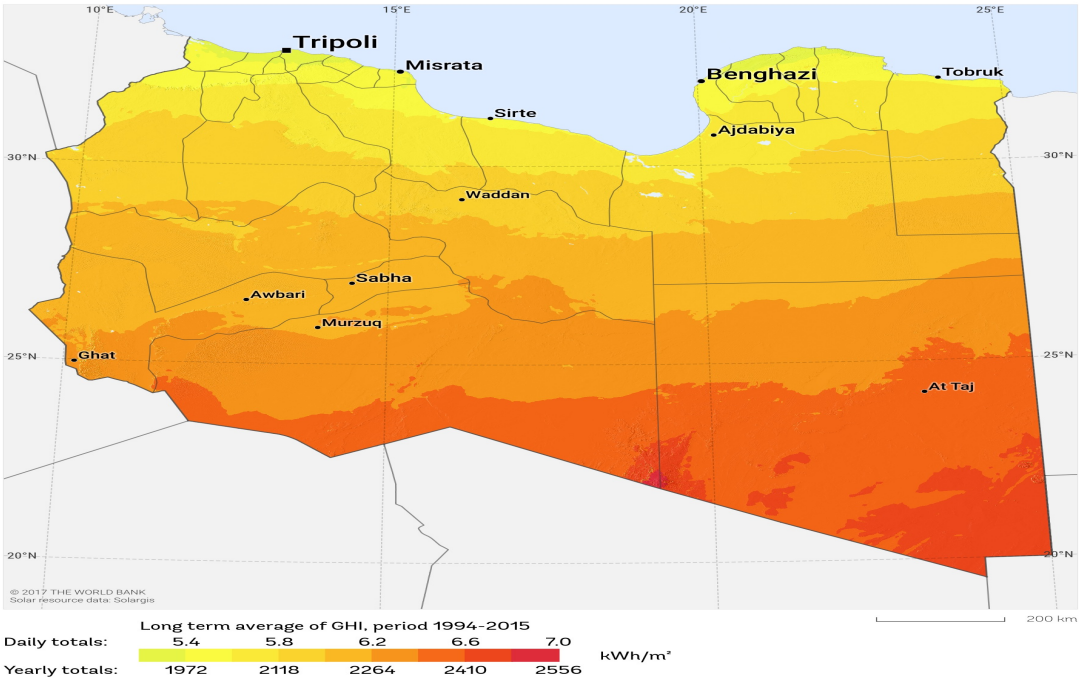

FIGURE 1.2. Libya solar resources map [8].

multi-effect-distillation energy consumption is approximately 1.8 kW h m^{-3} of distillate, while for the multi-stage-flashing unit is 4 kW h m^{-3} of distillate [7]. Desalination costs are between US. \$0.60 to US. \$1.0 per cubic meter (excluding distribution expenses). About 50 % of desalination costs come from energy costs [2]. Even if desalination cost is dropping internationally due to the current advancement in the desalination units; the rise of energy cost cancels out the advantage of more advanced technology. The energy supply situation in Libya became even more problematic, due to the civil war in the country, and the decline of fuel resources which urged researchers to find alternative sustainable energy options. The paramount consideration for freshwater sustainability for future generations is the amount of energy required to sustain a sufficient supply of freshwater through desalination.

Fortunately, there is a correlation between regions of freshwater scarcity (consequently desalination requirement) and the abundance of solar energy. Consequently, there is an excellent potential for exploiting solar-powered desalination as an attractive option in Libya. Giving the recent advancements in thermal desalination units, solar-powered desalination is a promising option. Libya has an average daily global solar radiation rate of around 7 kWh m^{-2}day^{-1} on a horizontal surface, as shown in Fig. 1.2 [8]. One of the intrinsic properties of solar energy is that it is diffuse and requires a massive investment of capital

and material resources to collect it and harness it. At present, conventional collection and storage systems are expensive and often uneconomic. It is crucial to reduce the cost of collection and storage to make them economically feasible. The material cost of a conventional collection and storage system, such as solar panels, is close to 75% of the total cost and, as such, the prospect of reducing the price of a conventional system does not seem to be very likely [9].

Among all solar technologies (i.e. solar panels, photovoltaics), salinity gradient solar ponds (SGSPs) offer an inexpensive, simple and promising method for converting solar energy to thermal energy that subsequently can be used to drive desalination units. The SGSP concept has captured the imagination of an increasing number of researchers, as there are no devices that are less costly than a pond holding water, and the picture of areas of otherwise unused tract producing substantial amounts of heat is powerful image [10]. Typically, a SGSP is a large body of water that ranges between 1 and 3 meters in depth with a salinity gradient in the middle. Solar radiation that reaches the bottom of the SGSP is trapped and stored; due to high densities in the bottom (high salt concentration) which, makes the solution heavy and hinders the heat loss via convective movement, subsequently, the heat collected at the bottom can be utilised to supply thermal energy for desalination unit [9, 11, 12]. If the energy collection by SGSPs can be sustained at an adequate level without too much expense, then SGSPs has the potential to be one of a mix of technologies helping to lead the Earth's population to a tomorrow based on sustainable energy.

The concept of SGSP appears to be simple; however, in reality, SGSP is an extremely complex non-equilibrium fluid system, and it is subject to instability due to the number of physical phenomena involved in its operation. Previous studies provide an insight into SGSP operation; however, neither the operational stability has been fully explained, nor the essence (when, how and where) of the hydrodynamic instability has been simulated in sufficient detail. In addition to the stability issues, SGSP also has some design issues. Previous models sizing SGSPs zones, excluding the double-diffusive convection DDC effect have limited accuracy. Thus, more complicated models considering the DDC effect are needed to understand how to design better SGSPs that can perform efficiently and for the longest period.

The present study aims to model the potential and operation of SGSP as a

source of thermal energy according to Libya geographical and climate conditions. Also, investigates the optimum zone thicknesses where the SGSP has the best thermal performance and longest-term operational stability. In order to meet this aim, several objectives are addressed:

The concept, design, construction and the physics of salinity gradient solar ponds are described. Existing SGSPs are reviewed in order to shed light upon current design and operation challenges. The thermal potential of SGSP to derive thermal desalination units is assessed according to Libya climate. The long term operational stability of the SGSP is investigated. The formation and changes occur to the zones of the SGSP during operation are studied, and an optimal zone thicknesses ratio is recommended. Furthermore, a procedure for long term operation that will help maintain the optimum thickness of the zones where the SGSP can sustain performing at its best is proposed. The thesis is structured as follows:

Chapter 2 explains the SGSP concept, design, and construction. It reviews the significant previous pertinent research on SGSP physics, thermal behaviour and stability and finds the literature gap. **Chapter 3** shows the development of theoretical and mathematical models of the SGSP where mass and energy balances are applied to yield a set of governing nonlinear partial differential equations that govern the system. **Chapter 4** presents a 1-D numerical study that assesses the thermal potential of SGSP to derive desalination units where the governing equations are solved numerically applying the finite volume method for a proposed SGSP located in Libya within the latitude and longitude of (32.54° N, 13.11° E). **Chapter 5** presents a 2-D numerical study that explains the thermo-hydrodynamic behaviour and the hydrodynamic instability of SGSPs. The starting point of the analysis in this chapter is the incompressible Navier-Stokes equations; the Boussinesq approximation is applied where advanced dimensionless analysis has been performed and utilised to perform the study. **Chapter 6** the 2-D model used in chapter 5 is utilised to investigate the effect of zone thicknesses, buoyancy ratio and heat recovery on the operation stability; this helps to recommend an optimal zone thickness ratio and provide a procedure that helps the SGSP to perform at its best. Finally, **Chapter 7** presents the conclusion, the recommendations and the future work.

Chapter 2

Salinity gradient solar ponds

2.1 Overview

Today in 2019, Libya has to adopt two strategies for energy and freshwater sustainability; the first is adopting powerful water conservation techniques and the second is reducing the expense of freshwater production through renewable-energy based desalination units. Solar power has a promising future as it stands-out amongst the most promising sustainable energy sources in Libya; however, unfortunately, most solar technologies require a substantial investment of capital and material resources, thus, to have a transition to a country energy supply based on solar energy and if this goal is to be achieved in the future, it is necessary to deploy extremely low-cost solar collectors. In the spirit of low-cost solar collectors, salinity gradient solar ponds combine low collection cost with long term storage and can provide heat for a variety of low-grade temperature thermal applications. The present chapter aims to establish the basis for understanding the concept, the design, and the construction of salinity gradient solar ponds. In addition to that, in this chapter, a detailed review of the major previous pertinent research on SGSP thermal performance and operation is given.

In the present chapter, the fundamentals and the concept of SGSPs are explained. The basics of the SGSP scientific theory is introduced, and this mandates providing theoretical definitions of some important termonologies. These theoretical definitions help to explain the SGSP principle of operation where the SGSP and its associated natural phenomenons are related to each other to form

complete theory. Reviews for different solar ponds that were designed and constructed worldwide are presented to shed light upon the past and the current design and operation challenges. The design and construction of SGSPs are explained in detail where critical design and operation factors such as site selection, salt type, forming the salinity gradient, lining and heat extraction methods are discussed. The prospects in the works done on SGSPs to improve its performance and pertinent literature concerned with SGSP operational stability are reviewed. In this chapter, the operational instability sources are divided into three main categories. That includes design and construction factors of instability, mechanical factors of instability and thermal hydrodynamic sources of instability. Finally, the limitations of previous work and literature gaps are identified, and a summary of the chapter is presented.

2.2 Concept

Before proceeding with the concept of salinity gradient solar ponds, it is useful first to shed light upon some fundamentals and define some terms that are relevant to the physics and working principle of the technology. In particular, methods of heat transfer and also some hydrodynamic and fluid flow terminologies [13, 14]

⇒ **Conduction**: Heat transfer by successive atomic collisions and motion.

⇒ **Convection**: Heat transfer as a result of the movement of fluid.

⇒ **Radiation**: Heat transfer in the form of electromagnetic wave light.

It is also useful to define some of the physical phenomena involved in salinity gradient solar pond operation:

⇒ **Diffusion**: is the movement of a substance from a region of higher chemical potential to a region of lower chemical potential.

⇒ **Buoyancy**: It is an upward force applied by a fluid that resists the weight of an immersed object and it is the engine that turns heat into motion.

⇒ **Convection currents**: Heated fluid grows and ascends because of the buoyant force where a cooler, denser fluid falls and takes its place. This cycle builds up a circular current (convection currents) that stops just when the heat is uniformly disseminated all through the fluid. This phenomenon alongside diffusion is two important yet problematic natural phenomena in SGSP operation; however, the aim is not to generate and enhance them but to halt and suppress.

Now, having defined these terms. Reviewing what occurs in a standard, normal or typical pond (e.g. a garden pond) is a good point to start from.

2.2.1 Typical pond

As a part of the sunlight incident on a pond (e.g. a garden pond), the sunlight gets transmitted and absorbed, which leads to the heating of the pond and formation of convection currents everywhere inside the pond as shown in Fig. 2.1.

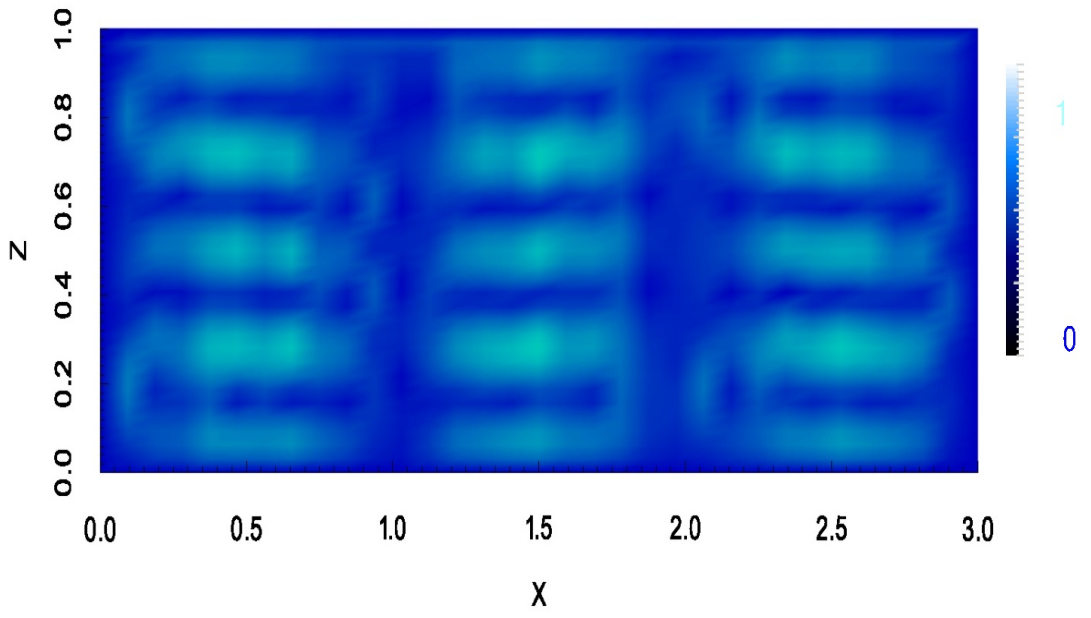

FIGURE 2.1. A 2-D illustration of the hydrodynamic behaviour of a typical pond with no salt gradient established. The dark blue indicates low fluid velocity, light blue indicates relatively higher velocity due to convective movement.

The heated fluid becomes less dense and ascends to the surface where it loses a portion of its heat due to the differences between the warm surface temperature and the colder surrounding air. The heat loss from the surface is through evaporation, convection, and radiation. As the fluid at the surface area cools, it becomes denser and descends to the bottom of the pond. Due to densities difference between the hot and cold fluid and the buoyancy effect, continuous mixing occurs inside the pond.

Therefore, due to the continuous chaotic mixing, as it has been depicted in Fig. 2.1, it is almost impossible to accumulate and store a significant amount of heat in such a pond. Salinity gradient solar pond SGSP is simply intended to suppress the generated thermal convective currents at the bottom, thus, maintain the heat at the bottom of the pond by the artificial formation of a salinity gradient between the bottom (high salt content injected) and top of the pond (almost freshwater) acting as a transparent insulating layer. Further explanation of the SGSP operation is in the next section.

2.2.2 Salinity gradient solar pond

Salinity gradient solar pond, as the name suggests, is a mass of water in which a salinity gradient is built in the middle to separate the bottom where the high salt content is placed from the top where freshwater is added. It works as a solar receiver, collector and heat storage medium. As depicted in Fig. 2.2, SGSP consists of three zones (layers).

Upper convective zone

The upper convective zone (UCZ) which is a small layer of almost freshwater. It protects the salinity gradient solar pond from the external sources of instability such as the rain and wind.

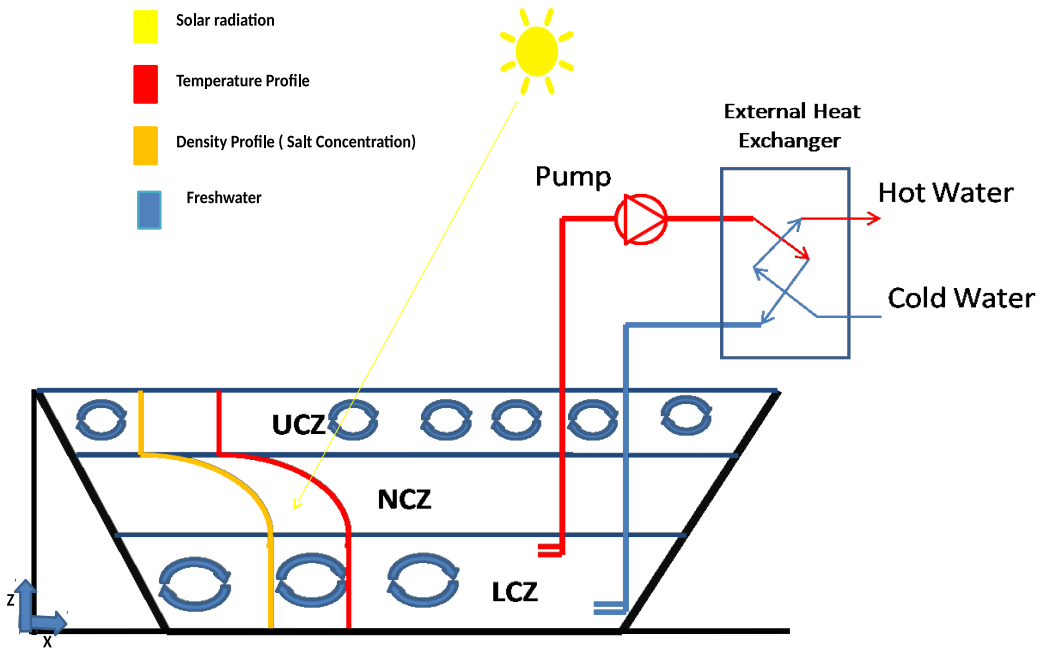

FIGURE 2.2. Schematic diagram of salinity gradient solar pond showing the positions of the three zones (i.e. UCZ, NCZ and LCZ).

Non-convective zone

The non-convective zone (NCZ) is a zone in which salt gradient is created, and it is positive downward. It works as transparent insulation between the top and the bottom of the pond.

Lower-convective zone

The third and final zone is the lower convective zone (LCZ) or the storage zone where the concentration of salt is very high, dense and uniform. It works as a heat storage medium.

The operational concept is simple. As depicted in Fig. 2.2, a portion of the solar radiation incident on the SGSP, is absorbed in the bottom zone of the pond (LCZ) which subsequently leads to the heating of the water available in this region. Water in this zone will not be able to rise due to the less salt content available in the water above (less dense). Likewise, water in the top (UCZ) cannot drop to the lower zone as the water below it is denser due to the higher

salt content. Consequently, the formed convective currents in the lower convective zone due to the heating effect are suppressed, and heat transfer from the heated lower convective zone to the relatively colder upper convective zone solely occur via conduction. Given the weak thermal conductivity of water, the non-convective zone (NCZ) functions as translucent insulation, allowing solar radiation to be transmitted, absorbed and stored in the form of useful heat in the bottom zone and halts it from loss to the top [14, 13].

Therefore, SGSPs are principally designed to suppress convection currents via the NCZ and to retain the heat in the LCZ, where heat can be removed to provide the required energy to power a process (e.g. desalination) [14].

Despite the simplicity of the general design concept and operating mechanism, the vast amount of natural phenomenons associated with its functioning and operation makes any comprehensive explanation of the system a complex problem from both physical and the mathematical viewpoints. Even though the physics of every phenomenon is significantly well-known, the coupling between the phenomena (how they work collectively towards destabilizing the pond) requires more investigations in order to help to improve the technological potential and subsequently, the technological feasibility of SGSPs for future implementations.

Throughout this chapter. Detailed knowledge of salinity gradient solar pond physics, design, construction and operational related issue are presented. Furthermore, the underpinning logic of developing the theoretical models to study and understand the thermal behaviour and operational stability adequately is established.

2.3 Chronology

Salinity gradient solar pond was first introduced in 1902 by Kaleciusky who witnessed that Madre lake in Transylvania (42° 44′N, 28° 45′E) was recording high temperatures at a depth of 1.3 m through the summer season. Rudolph Bloch [15] explained this as solar radiation absorbed in the body of the lake causes a temperature rise in the lower regions. Due to a natural salt concentration gradient in the lake, lower regions remain denser even when warmer.

Thus, convection that would typically occur is prevented via this gradient (insulating) layer. The steady lake absorbs and stores solar radiation as thermal energy. And the majority of the absorbed energy is maintained in the lower regions, almost at 1.3 meters depth. The only mechanism of heat loss from the lower regions to the top of the lakes is via conduction. Given the poor conductivity of water, the heat loss is minimal. The salt concentration gradient is preserved through salt precipitates and deposit at the bottom region of the lakes, which guarantee near saturation concentrations in the lower regions. The freshwater currents which run transversely on the top of the lake form a small upper zone that would protect the erosion of the gradient layer and minimize the heat loss to the environment which suggest the importance of flushing and adding fresh water to the UCZ. Towards the end of the summer, temperatures as high as 70 °C have been marked at a depth of 1.3 meters. Rudolph Bloch [15] stated that adopting controlled conditions; an increase in temperature could be anticipated.

In 1948, the concept of constructing man-made SGSPs was first introduced by the same man, Bloch [15]. Later, Tabor [16] and Hull [14] published a series of experimental and theoretical studies of SGSP. These works introduced the technology to the world [17]. Since then, the theory of SGSP has been explained in the literature which includes, amongst other subjects, physics [14, 18, 19], hydrodynamics [20]; and engineering [16, 21, 22, 23].

Research on SGSPs became active again just in the few past decades, due to the increasing environmental problems, declining fuel resources and advancement in low-grade heat applications. Thermal energy generated by SGSPs became one of the most attractive options for providing heat for low-grade heat applications such as thermal desalination units when the geographical and climate conditions are suitable.

2.4 Worldwide examples of SGSPs

Many SGSPs have been constructed worldwide, and some have been operating for years [24, 11, 25, 26, 27]; however, various operational, performance and stability issues have also been encountered. Next, are examples from sites across the world.

2.4.1 El-Paso solar pond (U.S, 1983)

The El Paso salinity gradient solar pond that is shown in Fig. 2.3 started as an illustration project managed by Texas university in El Paso region and was financed by the US office of reclamation and the state of Texas. The project was launched in 1983. The El Paso SGSP has been in operation since that time, and over the years of operation, experimentation and research was taking place. The El Paso SGSP has contributed positively and provided invaluable, detailed knowledge and illustration to the multiple utilisation and integrations of SGSP with other applications. To the best of the author's knowledge, it is considered as the first SGSP to produce process thermal energy to an industrial corporation, and that was in 1985. El Paso was also the first US experimental SGSP powered desalination facility in 1987 [25, 28, 26].

FIGURE 2.3. The El-Paso salinity gradient solar pond [26].

The El Paso salinity gradient solar pond covers an area of approximately 3000 m^2. The height of the SGSP is around 3.25 m. The UCZ is $\approx$ 0.7 m, NCZ is $\approx$ 1.2 m, whereas LCZ is $\approx$ 1.35 m. The salt utilised is predominately sodium chloride NaCl. The 3000 m^2 SGSP depicted in Fig. 2.3 recorded an LCZ temperatures ranges between 70-93 °C [25, 28, 26].

In order to make SGSP more reliable, stable, productive, and efficient technology, a range of systems have been developed and examined at the El Paso SGSP project [25, 28, 26]. These systems include; instrumentations for SGSP monitoring; advanced scanning and injection procedure for advanced salinity gradient formation and maintenance; innovative liner set; and enhanced heat recovery arrangement [28, 26].

Throughout its years of operation, El Paso SGSP used to provide heat for various processes, such as electricity generation unit and thermal desalination units. Electricity generation was not a successful application for SGSP as it was not economically feasible because of the relatively low temperatures achieved in these ponds during autumn and winter which makes solar-to-electricity conversion fairly inefficient; however, SGSP assisted desalination is considered one of the most promising SGSP assisted applications as some desalination systems requires low-grade heat that ponds can provide consistently. Research has also shown that for locations where conditions are suitable, SGSPs are as efficient and less expensive than any other solar collector [29, 30, 31, 32].

SGSP has demonstrated special technological practicability when used to provide thermal energy to a multi-effect desalination unit. The desalination unit worked effectively, delivering a high-quality distillate. The price of freshwater produced fluctuates at US $\$1.06/m^3$ for a 3,800 m^3 per day plant capacity [25] in comparison to conventional energy powered medium to small scale units-total fresh water cost hovering around US $\$ 0.6$ - $1.0/m^3$. About 50 $\%$ of desalination costs come from energy costs [2].

2.4.2 Bhuj solar pond (India, 1987)

The Bhuj SGSP in India is another medium size pond of about 6000 m^2 which was created and run at the Kutch dairy, Bhuj, India, see Fig. 2.4.

The SGSP provides hot water to the dairy. The maximum temperature recorded was 84 °C [33]. The high thermal performance of Bhuj SGSP has made a base where a commencement could take place for industrial exploitation of SGSP. More than 20 million litres of hot water was supplied to the dairy between

FIGURE 2.4. Bhuj solar pond, India [33].

September 1993 and March 1997. Kumar cited that the payback time was expected to be shorter than five years (neglecting any subsidy or incentives), which could be satisfactory for an upcoming alternative energy technology [24]. While the Bhuj SGSP project added a significant contribution towards the advancement and improvement of SGSPs, further advanced research still needs to be conducted [24].

The critical point was the brine containment, as there was a leakage as a result of the failure of the liner when the temperature of the SGSP reached nearly 84 °C without heat recovery measures [24]. This emphasizes the importance of heat recovery and installing a high-quality liner to avoid such problematic scenario. Heat recovery and liner technologies will be discussed in the design and construction section.

2.4.3 Pyramid Hill solar pond (Australia, 2000)

Another example of a SGSP is the Pyramid Hill SGSP in Australia [26]. The SGSP project that is shown in Fig. 2.5 was constructed at Pyramid Hill.

FIGURE 2.5. Pyramid Hill solar pond, Australia. The floating rings shown are wind suppressors to minimize the wind effect [26].

The project is a collaborative work including two industrial partners and RMIT University. It is centred around the use of SGSP for industrial process heating. The SGSP was created with a height of 2.3 m. The LCZ was 0.8 m thick, the NCZ 1.2 m thick whereas the UCZ was approximately 0.3 m thick. The maximum temperature achieved was 90 °C. This 3000 m^2 SGSP supplies about 60 kW of thermal energy for industrial salt production company [34]. Such a facility is a reliable model of a SGSP composed for a particular application. Hydrodynamic instability issues were encountered during the operational years [26].

Sherman and Imberger [35] investigated another 1600 m^2 SGSP at Alice Springs in Australia where a storage zone (LCZ) temperature in a range between 85 °C and 90 °C was consistently maintained. According to these studies, SGSP is suited to Australia geographical and climate conditions. Interestingly, the pyramid Hill SGSP has a different thermal performance from Alice Springs, which raises the question of wither there is an optimum design and operational specification for SGSP to work at its best.

2.4.4 Granada solar pond (Spain, 2014)

Solvay Minerals in Granada (south Spain) is a leading industrial SGSP that was set up recently in Europe, in the year of 2014, see Fig. 2.6.

FIGURE 2.6. Granada industrial solar pond, Spain. The barrels role is to protect the pond from the wind [27].

The goal of this SGSP is to preheat water to 60 °C and exchange this heat with the reagents in the mineral flotation plant. Fuel oil was utilised for this objective in the past. The establishment of the SGSP contributed significantly towards decreasing fuel oil burning and reducing its environmental harm, that is principally correlated with carbon dioxide emissions [27]. The emission factor of the fuel oil consumed is estimated to be around 2.868 kg CO_2/L; consequently, 31.7 and 22.5 tons of CO_2 emissions were avoided during the first and second periods of operation due to the use of the salinity gradient solar pond [27]. The surface area of the SGSP is approximately 500 m^2, and it has a height of 2.2 m. The LCZ is 0.6 m thick, the NCZ is 1.4 m thick, and the UCZ is approximately 0.2 m thick. The maximum temperature achieved was 90 °C in August 2014 [27]. The SGSP was able to provide the heat required for the application; however, lining and salinity gradient degradation issues were encountered [27]. The next section provides more insight into SGSP design, construction and challenges.

2.5 Design and construction

This section provides an insight into the SGSP design and construction principles. Understanding the design and construction of the SGSP is essential to understand its operation. Fortunately, today, in 2019, salinity gradient solar ponds can employ well-established techniques for the most part of their construction and operation, including, salt type, controlling biological organisms, maintaining pond transparency, building earth embankments and installing SGSP liners, pumping fluids and delivering thermal energy to a load; however, some areas require more investigation and improvement. The present section covers, selection of site, salt type and dissolving methods, excavation, embankment and lining, forming the salinity gradient and monitoring systems.

2.5.1 Site selection

A salinity gradient solar pond is a horizontal solar radiation collector and cannot be tilted like solar panels. As a consequence, sites selected for SGSP application must not be far from the equator. They should be within a latitude, where a high level of solar radiation is available year-round. The site decided for setting up a salinity gradient solar pond must also have other specific characteristics. A source of inexpensive salt or brine has to be accessible nearby to stock a substantial inventory of salt required to establish the SGSP and to evade all extra transportation costs. The place has to be reasonably levelled to minimize the ground shifting job to a minimum. Except if the flawless lining of the SGSP is ensured, it is not advised to create a SGSP when underground freshwater is available near the surface to avoid the leaks of salt and heat to groundwater. Whether the SGSP is (insulated) or not the case, it has not to be overlaying near to an underground water aquifer. Such aquifers, whether of freshwater or brackish water, can cause structural and thermal obstacles. In case the underground water movement is fast, heat is going to be wasted from the base of SGSP as the soil below is not ideally insulated. A low-cost source of water is required to be ready to compensate for convection and evaporation losses from the SGSP [16, 14].

Accordingly, SGSP is fitted to arid and semi-arid regions, such as the potential

FIGURE 2.7. Libya map illustrates locations of Sebha (south of the country) and Tripoli (north of the country) cities [36].

sites will be considered in this study, which is located in Libya. And that is due to the intensity of solar radiation and existence of the extensive sabkhas (salty areas), vast arid lands and natural salt lakes at zero cost which indicates a high potential for the utilization of salinity gradient solar ponds. The site has been selected located in the city of Tripoli at 32.54°N, 13.11°E, the city location is illustrated in Fig. 2.7, is exhibited to solar radiation throughout the year with prolonged hours during day time. It has an average diurnal solar radiation rate of approximately 7 kWh $m^{-2}day^{-1}$ on a horizontal surface on the coast (Tripoli) [37]. The geographical and climate conditions for the potential site are applicable to the technology and considered in this study. Later, in this work, analytical and numerical studies will be performed in order to predict the thermal potential of SGSP according to these sites climatology data, the results and discussion will be presented in chapters 4, 5 and 6.

2.5.2 Excavation, embankment and lining

In most places, the pond excavation is carried out with heavy earth moving equipment, as shown in Fig. 2.8. In smaller ponds, manual labour alone could be employed. The amount of earth that must be moved to make a pond of specified depth is not the volume of the pond, but the volume of earth moved

FIGURE 2.8. Installation of the flexible polypropylene geomembrane liner [25].

is only what is needed to build up an embankment around the perimeter of the pond. For Libya, SGSP, the earth can be excavated to a certain depth, and the excavated soil could be used for the formation of embankment around the perimeter of the SGSP to a height of the SGSP required from the ground level. Solid walls are also essential for the protection of a pond, and a firm base should be provided for lining installation [26].

Embankments should be sufficiently compacted to avoid slumping and the falling or sinking of material down the sidewall. The compaction of the embankment can be performed manually using hand-pulled stone rollers. The dry density of the soil could be estimated from the samples collected from various locations of the sloped wall of the pond [25].

Pond bottom and side walls insulation are essential, as two types of leakages could occur: leakage of water out of the base of the pond and leakage of thermal energy into the soil. The leakage of hot brine cannot be tolerated as it loses both heat and salt. Besides, if SGSP is close to underground water, this water will be contaminated. So lining is crucial. Liners (blackened plastic film) at the bottom of the SGSP as shown in Fig 2.9 are used to prevent these leakages and to enhance the absorption of solar radiation that arrives at the ground of the SGSP [12].

2.5.3 Salt type and quality

The salt used for a salinity gradient solar pond should grant the following inherent characteristics to sustain the pond's performance and long term stability [38]; (I) The solubility of the salt should be high in order to fit the level of solution density needed. (II) The solubility of the salt must not vary significantly with temperature. (III) After dissolving the salt in water, the solution should be transparent enough in order to allow solar radiation to transmit to the lower region of the solar pond. (IV) The salt should not has any harmful environmental impacts, and it must not contaminate the groundwater. (V) The salt should be affordable and plentiful and located close enough to the pond's location to avoid any additional transportation costs. (VI) The molecular diffusivity of the salt must not be high [39].

The salt diffusivity rate is a critical factor when it comes to enhancing SGSP long term stability. Fundamentally, the molecular diffusivity of all salt types is always a function of temperature and salinity. For instance, the solubility of sodium chloride (Na Cl) at 90 °C can be five times greater than its solubility at 10 °C [40]. In addition to that, different salts also have different properties [9].

The molecular diffusivities of different types of salt at room temperature are given by Ref. [9]; however, Hull et al[9] also reported that the diffusivities at

FIGURE 2.9. SGSP with liner system installed at El Paso [25].

various temperatures had not been examined. Nevertheless, it is agreed that the diffusion coefficient increases typically at high temperatures, which leads to boosting the upward salt flux in ponds [9].

Sodium chloride is regarded as the common salt by far for loading and running salinity gradient ponds worldwide. Sodium chloride is the main and most recommended type of salt by many researchers to be used in SGSPs [9]. Some of its inherent advantages are; it has the lowest molecular diffusivity, its solubility value is high enough to meet the highest solution density required, and its solubility does not change significantly with temperature. It is also crucial to mention here that the salt used in SGSPs should also be non-toxic, and ecologically acceptable to avoid any environmental and economic risks, subsequently, lining (insulating) the bottom of the SGSP which has been discussed in the previous section is crucial not only to reduce heat wastes to the soil but also to protect the environment.

2.5.4 Forming the salinity gradient

The critical requirement of SGSPs is that a salinity gradient must be established and maintained [9]. The first primary task to implement a SGSP is to create a gradient salt concentration profile efficiently, in order to function as an insulating non-convective layer that suppresses convection in the bottom of the pond and, consequently, disallowing pond overturn and heat loss.

Many ideas and methods to build the gradient zone have been introduced and experimented in operational SGSPs [9, 41]; (I) Rab and Nielsen method, (II) Fixed level injection method, and (III) Scanning and injecting method. The selection of what technique is the most effective depends on whether salt and salty water are accessible, the size of the pond, the significance of wind disruption anticipated, and the equipment available [20]. This section not only reviews the three procedures used of creating a salinity gradient but also explains the physics behind setting up a salinity gradient and forming the three zones of the SGSP explicitly.

The first well-documented method goes back to 1974. In June 1974 Rabl and Nielsen [22] built the US first experimental pilot plant salinity gradient solar

pond in Columbus at Ohio State University. Since then, Nielsen has tried to resolve several practical difficulties connected with creating a salinity gradient. The first technique he used to fill the pond was to mix the brine of a proper concentration in tanks available close from the pond location. This brine solution created was permitted to run through a pipe over a board that placed on a pond surface. As the pond filled, the salt concentration was made smaller to obtain the correct density gradient. This method is not practical due to the long period of time required to fill in the SGSP and to create the gradient using this method. In this particular solar pond, Nielsen would sometimes discharge water at different heights through a relatively large hose to drain out leaves and other unwanted objects that fall in the pond. After the filtering process, the solution would be pumped back in at the height it had been withdrawn [22]. This filtering process is unpractical. It produces the onset of internal convection currents in the gradient non-convective zone of the pond. These particular internal convection currents cannot be easily observed. The simplest straightforward technique for tackling such an issue when noticed was to withdraw the fluid at that particular height, inject enough salt to make the fluid heavier and prevent convection. This technique can only be effective for small salinity gradient solar ponds [22]. For large scale solar ponds, other techniques should be considered.

The second method is the fixed level injection method for creating the salinity gradient which has been proposed at the University of New Mexico, which is at that time considered as the easiest and most expedient method to build and adjust the gradient layer [41]. This does not need supplementary tanks, and it can be suitable for solar ponds of any size. In this method, the primary parameters that should be planned for each injection step are the upper and the lower limits or elevations, and also the amount of freshwater needed to be added. The lower limit of the first injection step will be the elevation of the interface between the non-convective zone and the lower convective zone. The lower limit is maximized by almost 5 cm for each following step. The amount of water injected at each step is decided to depend on the required salt concentration profile; the salt concentration profile results from the previous injection step. Complete injection process until the fluid level in the pond approaches the upper interface of the designated gradient layer. And lastly, add freshwater onto the surface via a floating diffuser in order to not cause any mixing, until the SGSP is full [26].

The critical parameter for the fixed level injection method is the Froude number Fr. It is a dimensionless number that represents the ratio of the kinetic energy to the gravitational potential energy of the injected fluid. In order to accomplish full mixing at the injection diffuser level, the Froude number should always be kept at a fixed value of almost 18 [42]. At smaller Fr values the injected fluid rises, via buoyancy force, and consequently, mixes just above the diffuser level. On the other hand, when Fr value is greater than 18, the injected fluid tends to entrain large volumes of fluid from underneath the diffuser level. Either of those scenarios drives to correct gradient profile.

In order to meet the Fr condition throughout the whole injection process applying the fixed level method, the diffuser geometry and the flow rate must be customised to suit the density changes of the ambient fluid at all injection steps. Usually, the radius of the diffuser is fixed, and the flow rate is maintained close enough to the highest value possible to decrease the time of construction. Accordingly, the gap of the injection diffuser requires to be modified and adapted repeatedly throughout the fixed level injection process [24].

Generally, the diffuser gap is 2–3 mm [9], and the gap is customarily limited at 10–20 mm [24]. The restriction of using the ultimate diffuser gap and the necessity for using and maintaining the critical Fr number, restrict the injection of the highest flow rate possible; consequently, more time is required for the gradient establishment. When the required non-convective zone gradient profile is established, the natural physical phenomenon of diffusion transports salt from the lower zone to the upper zone at low rates. If entrainment at the interfaces or internal gradient instabilities happens, salt transportation to the top layer is increased above the molecular transport. All this salt must be discharged from the upper layer by flushing the upper layer with freshwater [20]. The fixed level injection process has been adopted at the El Paso salinity gradient pond before the year of 1995, the gradient layer formation or creating was time-consuming, tiresome, and also labour intensive.

The third method, which is the scanning injection method. In the year 1995, it was proposed. It is a similar, but more innovative scanning injection technique was introduced as a new method creating the salinity-gradient profile in SGSPs. This new approach was first practised to modify and adjust the gradient profile [43] and later used successfully to construct the salinity gradient. It slightly

differs from the fixed injection method where; instead of remaining at a fixed level, the diffuser is actuated up and down in a precise manner within a preset area throughout the injection process.

FIGURE 2.10. Fresh water flushing system for the upper convective zone [26].

Zangrando described this technique as a simple method to create a salinity gradient. Zangrando technique can be performed in three steps [20]. Firstly, a solution at a high level of concentration is poured to fill the depth of the LCZ, including also almost half the depth of the NCZ. Afterwards, freshwater to be added to the solution in precise amounts to create the wanted gradient zone. This particular action will weaken the concentration of the solution and will form a gradient zone. The third and final step is to add a final layer of almost freshwater to fill the UCZ. This technique is the accepted technique of filling SGSP and is widely used. The major issue is to maintain the density gradient for long times. In order to do so, salt should be injected into the lower zone, while the surface is regularly flushed with freshwater [9]. The procedure is mature and has been successfully practised to build the 1.3 m thick gradient in Miamisburg, Ohio, pond, which is one of the largest operational SGSPs in the US, with a surface area of 2000 m^2 [41]. Furthermore, the Zangrando technique has also been used to adjust the gradient of the Ohio State pond [44, 41].

Even though the theory of this method appears to be easy; it is a complicated task from the physical and practical point of views. For a greater understanding of the technique, a detailed procedure is given here: Assume that a pond with

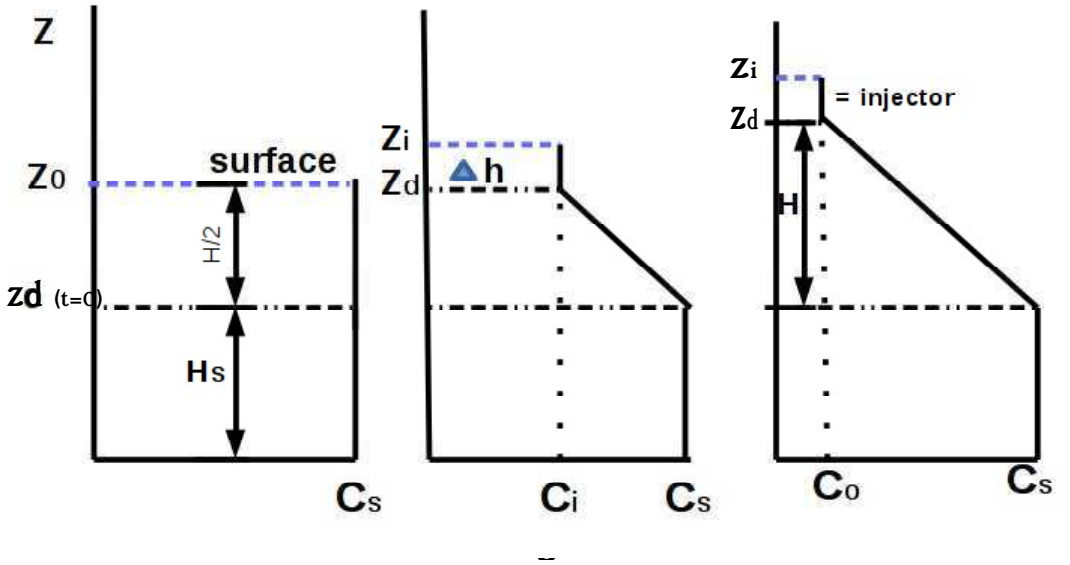

FIGURE 2.11. Schematic diagram of relative positions of injector and surface during establishment of the gradient.

vertical walls (constant area A) needs to have a salinity gradient created. The pond should have a lower convective zone (Storage Zone) of Height H_s, a gradient of height H, and an upper layer of height Z_o. Assume that H must have a linear gradient profile of salt concentration, from the highest salinity or concentration C_s to the lowest concentration C_o. Neglecting the little differences in volume during the time of the fluids being mixed, the average salt concentration of the gradient insulating layer is $\frac{1}{2}(C_s + C_o)$. When the pond is filled with a heavy solution of salty water to a height, $H_s + \frac{1}{2}$ H. The pond holds all the salt required yet needs a volume A($\frac{1}{2}$ H + Z_0) of almost freshwater. Due to the fact that the lower convective zone is present and can not be displaced, place the Z axis at H_s, move Z positive upward, and examine the development of the gradient zone. A schematic diagram of relative positions of injector and surface during the establishment of the gradient is depicted in Figure 2.11 [45, 41].

The freshwater is added via a diffuser; this freshwater would experience a buoyancy force, and it rises to the surface entraining fluid along its path. The entrainment process is very efficient at mixing the entire volume above the position Z_d of the diffuser (Fig. 2.12 illustrated the diffuser used to set up the gradient), Z_i indicates the surface level, so the concentration above Z_d is nearly

homogeneous, but it varies as a function of time [20].

$$\frac{\partial C}{\partial t} = \frac{\partial}{\partial t}\left(\frac{M_a}{V_a}\right) = -\frac{C(t)\frac{\partial Z_i}{\partial t}}{Z_i - Z_d} \tag{2.1}$$

where M_a and V_a are the mass and volume of the brine above the diffuser. In case the diffuser position has not changed, the brine above it is going to be diluted at a rate $C = C_s\ (Z_o / Z_i)$ as the surface rises. In case, the diffuser is moved at twice the rate of rise of the surface then $\frac{\partial Z_d}{d_t} = 2\ \frac{\partial Z_i}{d_t}$, the diffuser reaches to the surface at height H and the salt concentration profile left behind becomes [20]:

$$C_z = C_s\left(\frac{H - Z}{H}\right) \tag{2.2}$$

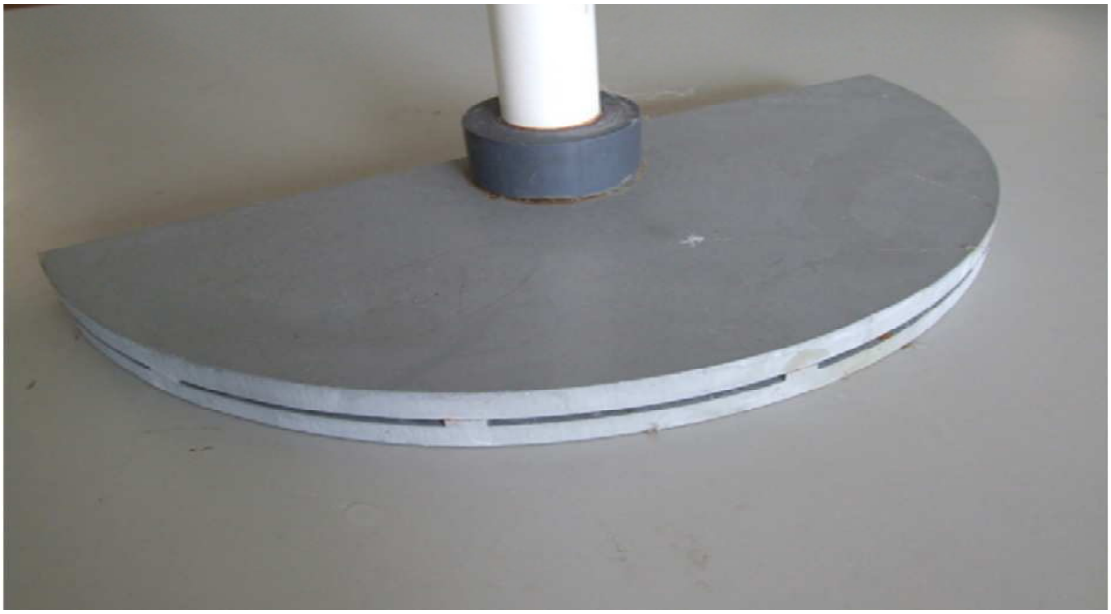

FIGURE 2.12. Diffuser used to setup gradient [26].

After building the gradient zone, almost freshwater should be injected to the upper zone using a flushing procedure, as shown in Fig. 2.10. If this layer of almost freshwater is not created, ambient turbulence will mix the fluid at the top, and that will be at the expense of the gradient zone. Any salt gradient profile can be creating adopting this technique [20].

Compared to a fixed level injection, the scanning injection method has many

advantages. Firstly, the accomplished gradient profile is much accurate and neat, also resulted in a perfect match with the required profile. Secondly, the scanning method is straightforward and simpler to be used; it is far less labour intensive and can be accomplished in short time[26]. For instance, in the El Paso salinity gradient solar pond, the scanning method lessened the time required for establishing the gradient profile by 50 % as compared with the fixed level injection technique [25, 26]. Moreover, the scanning injection method is not as sensitive to the Froude number. The single condition for the scanning injection method is that the injection velocity at the exit of the diffuser needs to be adequate for obtaining a minimum Fr of almost 18 to guarantee an adequate level of mixing [25, 26].

2.5.5 Salt dissolving and recharging

It is crucial to have a brine tank at the site, as shown in Fig. 2.13, to compensate the salt loss from the bottom of the pond via diffusion during the pond operation. A salt charger is used to charge salt into the pond. The salt charger typically has openings, as shown in Fig. 2.13. The heights of the openings define the location of the lower boundary of the non-convective zone. This tank could also be used as a salt mixing tank during the initial filling of the pond. Such a tank has been provided at the pond site. Also, in case of an emergency, it is also possible to drain the salt solution to the sea without polluting the environment [25].

Different investigators have used various other methods for dissolving the salt in water. Some of the methods, ponds located very close to sea and salt works directly use concentrated end brine/bitterns for SGSP establishment. For example, Tabor and his team have used the end brines directly pumped from the Dead Sea for all their ponds, including the largest ones. The only cost involved in this is the pumping cost. Macdonald et al.,[46] have used bitterns from seawater desalination for their ponds. The bitterns were stored in a separate pond and pumped into the main solar pond. Hull [9] while establishing this pond, pneumatically pumped solid salt into the pond. Water was added, and the salt was left to dissolve over the winter. The excess salt left salt piles that persisted for many years without detrimental to the pond operation.

Collins [47] has reported a fast salt dissolving technique that uses a "lixator", a down-draft salt dissolver. The dissolver consists of a pit about 1 m in depth, filled with salt crystals with a sprayer on top. As the freshwater moves through the salt, it eventually becomes saturated. Due to the filtration action of the salt stored in the lixator, the solution coming out of the lixator is reportedly a clean, very clear saturated brine. Direct dumping of salt into the main solar pond and allowing it to dissolve on its own will take a long time. Further, this causes localized excess loading of the pond floor due to the salt dumping at a few locations. Additionally, the bottom of the salt pile will collect either decreased or nil insolation at its bottom because of the opaqueness and reflectivity of the salt pile.

Moreover, if the salt crystals are directly dumped on any membrane liner, it may get damaged because of the sharp edges of the NaCl crystals loaded on it [47]. Otherwise, they have to be powdered, which involves excess labour and energy to crush the salt into powder. In the lixator type of salt distribution process, salt has to be periodically and gradually added into the salt pit, which may require constant feeding of salt into it, which may require a scooper machine to do it or workforce attention is continuously necessary to load the lixator with a constant periodicity. Moreover, there is a possibility of clogging of the silt inside the lixator, which may reduce the brine discharge rate delivered into the pond [47].

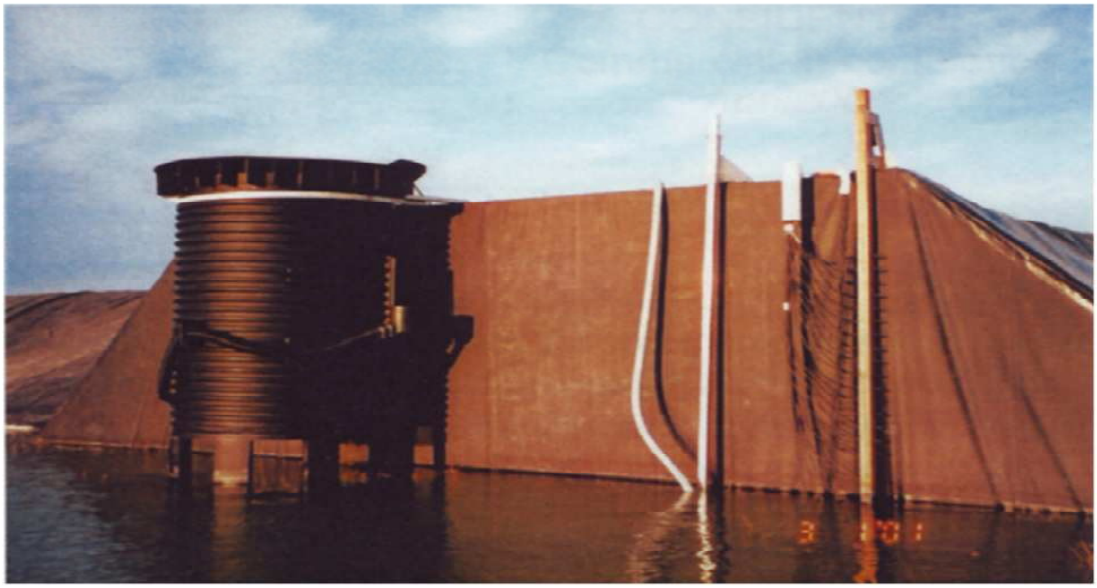

FIGURE 2.13. Salt charger fixed to interface wall [26].

According to literature, for salt storing and dissolving techniques, the forced circulation method could be used for the dissolution of the salt as this is simple and less time-consuming. Further, the scum and other materials which float on top during mixing could be removed, and the silt which gets settled at the bottom could also be removed after pumping the brine into the main tank. The same pump which is used for salt dissolution in the small mixing tank could be used for establishing the salinity gradient when adopting Zangrando's method.

2.5.6 Monitoring and control

Reliable instrumentation and careful monitoring schemes are crucial for successful SGSP operation. Critical data, such as temperature and salt concentration distribution in the SGSP, hydrodynamic stability, and clarity condition, should all be observed and examined regularly. At the El Paso SGSP, for an instant, the parameters which are monitored and controlled on a regular basis and routinely include density, temperature, turbidity, and the PH; furthermore continuous salt management analysis, thermal behaviour and stability analysis are conducted [25, 26].

FIGURE 2.14. Instrumentation tower shown in yellow in the middle of the pond [26].

After the examination of many measurement techniques and instrumentation

and monitoring systems from 1986 to 1992 at El Paso SGSP, an automated, integrated instrumentation system had been introduced there. This instrumentation system utilises a scanner technology integrated with the computer-controlled data logger. The newly introduced automated instrumentation system at that time has a drum-cable scanner, sensor head, sample pump, "U" tube density meter, pH probe, cooling heat exchanger, turbidimeter, and computer. The sensor head was mounted on the scanner. The scanner and sample pump were mounted on the deck of an instrumentation tower, as shown in Fig. 2.14. The density meter, pH probe, turbidimeter and heat exchanger were all mounted in the same enclosure on the SGSP bank close from the instrumentation tower [25, 26].

The computer that is used for control purpose and data logging is placed in an instrumentation and control compartment near the pond. With the integrated monitoring and control instruments, all the measurement required can be performed in around 3 hours. This supports a near "real-time" representation of the SGSP status, thereby allowing more accurate gradient maintenance and consequently higher thermal efficiency [25, 26].

Salt concentration, pH, and turbidity are examined almost every week, as these variances happen at a slow rate. On the other hand, the temperature is measured daily, or during extreme operation conditions times a day. The spatial interval of measurement is critical. As the minimum thickness for the internal convective zones (gradient breakdown) is of the order of 5 cm [9]; however, in some critical situations, such as gradient adjustment, the measurement interval is decreased to 2.5 cm or even 1 cm. For the purpose of reducing the impact of the turbulence on the accuracy of the measurements, the scanner is moved downward carefully. A similar monitoring system was also adapted by Pyramid hill solar pond and could be adapted in future solar ponds like the proposed Libya SGSP. For more detailed information regarding the monitoring system, see Refs. [25, 26].

2.6 Heat recovery and integration with desalination

Heat recovery is the main aim of establishing a SGSP. This section discusses heat recovery techniques and the possible SGSP -thermal desalination integrations. The heat recovery process can be performed by submerging a heat exchanger in the bottom of the SGSP, where a heat transfer fluid circulates in a closed cycle via the internal heat exchanger and transfers its thermal energy to an external heat exchange, another way of heat recovery is accomplished by pumping out hot brine from the bottom of the SGSP at one side of the SGSP and after exchanging that heat in an external heat exchanger, the (cooled) fluid returned at a lower level at another side [9], as shown in Fig. 2.15.

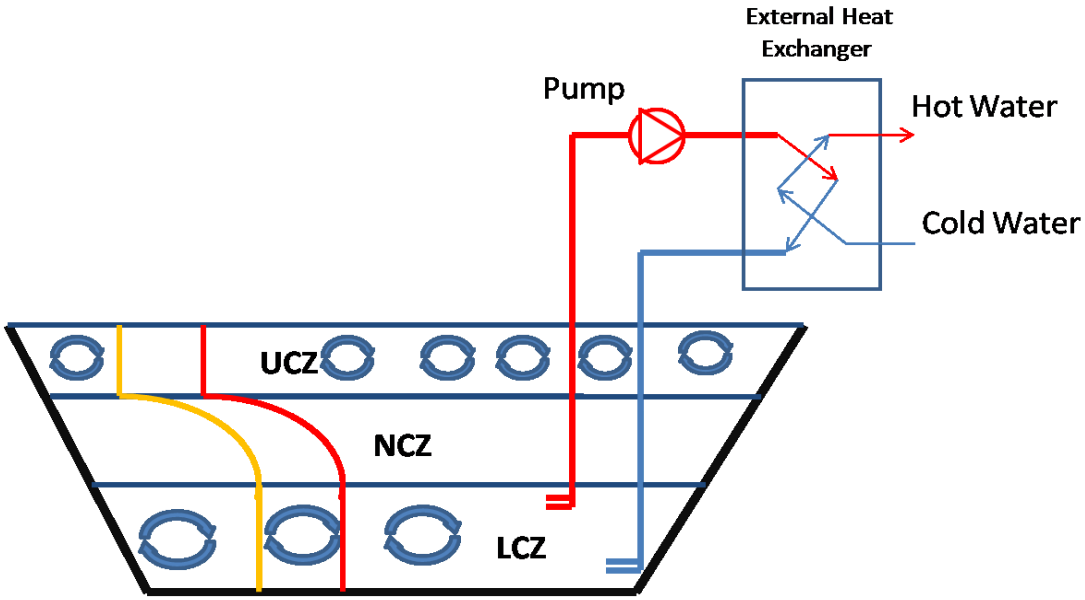

FIGURE 2.15. Conventional method of heat extraction using an external heat exchanger.

At the El Paso SGSP, heat recovery has been achieved by adopting the fluid-withdrawal technique that is shown in Fig. 2.15. Where the hot fluid in the bottom of the SGSP is withdrawn from the lower convective zone by using an extraction diffuser depicted in Fig. 2.16 that has been placed in the lower convective zone, the fluid exchange heat in an external heat exchanger before it is returned to the LCZ via another return diffuser [25, 28, 26].

At Pyramid Hill and Granada salinity gradient solar ponds [26], the heat recovery process is accomplished by circulating fresh water through an internal heat

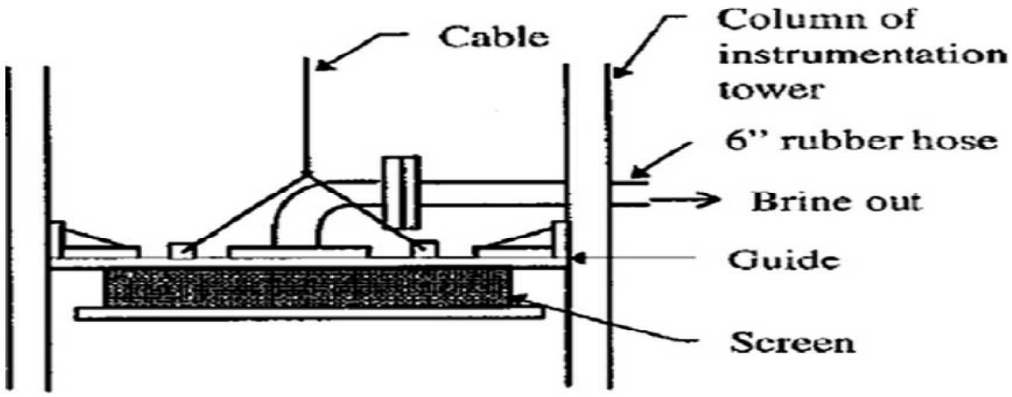

FIGURE 2.16. Schematic of suction diffuser of heat extraction system [25].

exchanger placed in the lower convective zone of the pond, and later transporting the heated water to an external heat exchanger that is located 200 m far and then to the thermal application as depicted in Figs. 2.17 and 2.18.

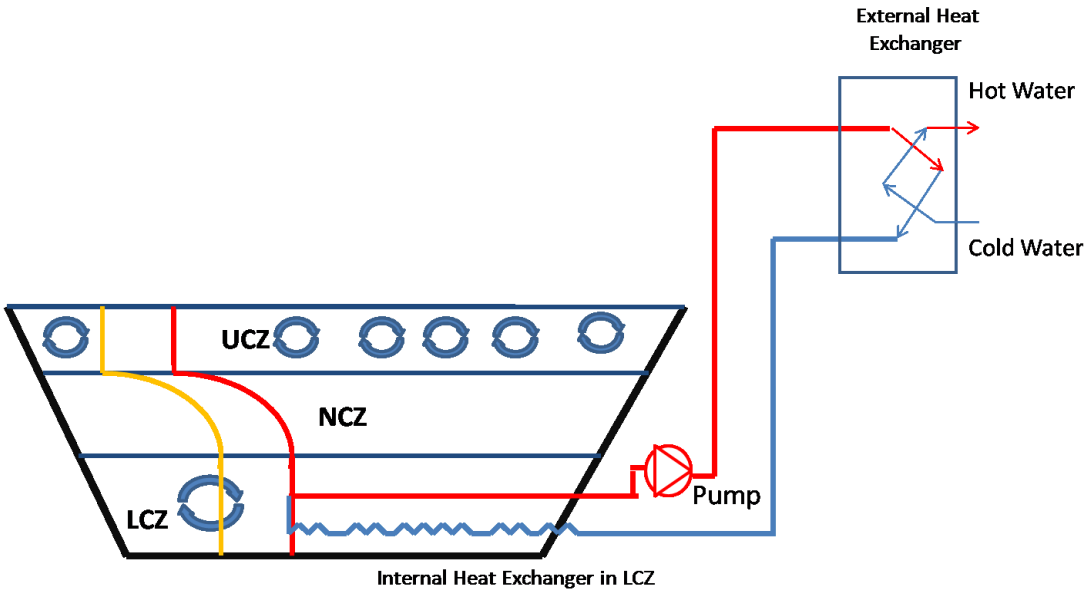

FIGURE 2.17. Conventional method of heat extraction using an internal heat exchanger.

At Pyramid Hill salinity gradient solar pond [26], the tubes of the internal heat exchanger positioned inside the lower convective zone, precisely below the NCZ-LCZ interface, the tubes are made from Iplex Polyplex Blueline Medium Density Polyethylene (MDPE 80 B) plastic pipes (26 mm inside diameter, 31 mm outside diameter) in order to resist corrosion. The heat transfer surface area is increased in order to compensate for the low thermal conductivity of the (MDPE 80 B) plastic tubes (0.37 W/m °C). In total, 48 heat extraction (MDPE

FIGURE 2.18. Heat exchanger (1200 m in length) in the Granada, Spain, distributed in six independent spirals of 200 m each. Fixation of the heat exchanger pipes was done by the use of concrete bricks [27].

80 B) tubes were placed, the length of each one of these tubes is about 60 m, as shown in Fig. 2.19.

FIGURE 2.19. Heat extraction tubes and inlet manifold at Pyramid Hill [26].

The heat extraction (MDPE 80 B) tubes are attached to 2 polyethene manifold pipes (72.9 mm ID, 90 mm OD) manufactured from the exact same material and covered with 40 mm expanded polystyrene. Considering the saturated brine

density which is about 1200 $\mathrm{kg\,m^{-3}}$ compared to only 1000 $\mathrm{kg\,m^{-3}}$ for pure-water and approximately 943 $\mathrm{kg\,m^{-3}}$ for the (MDPE 80 B) tubes, the pipes have undergone an up thrust and consequently had to be upheld in place by using an extra anchoring equipment. The pipes were connected to barbells coated with plastic to secure them in a specific place. Those design measures were taken before creating the gradient profile. Furthermore, the pipes were insulated from the top interface of the non-convective zone to the manifold by 9 mm thick Armaflex insulation (32 mm ID). Moreover, larger plastic pipes (56.8 mm ID, 63 mm OD) was additionally inserted over the insulation in order to inhibit heat loss from the pipes when the going fluid moves via the progressively colder layers over the lower convective zone and out to the atmosphere [26], as shown in Fig. 2.20.

FIGURE 2.20. Heat extraction tubes with insulation and outer tubes [26].

A 1.5 kW centrifugal pump was utilised to circulate the fluid in the heat exchangers. The designed inlet and outlet fluid temperatures were roughly 62 and 57 °C, respectively [26].

Accordingly, both heat recovery techniques are efficient for extracting heat without a significant destabilizing effect on the gradient profile; however, in the withdrawal technique, the velocity and temperature of the fluid being pumped have to be monitored accurately in order to inhibit erosion of the gradient zone.

Process integration

Desalination units powered by SGSP is a promising solar thermal desalination technique when the geographical conditions and more importantly, the climate conditions are favourable, and the resources are plentiful [25]. Even though SGSPs provide comparatively low-grade heat, that can be less than 100 °C; they are still regarded as a well-suited technology for providing thermal energy for thermal distillation units. Notably, in the past decade, and that is due to a massive improvement in thermal desalination units as some thermal desalination units can operate at top brine temperature of almost 60 °C [48, 49, 50].

There are a number of desalination techniques that have been utilised globally. A few of the techniques are completely matured and have even been employed on medium to large scales to desalinate brine water (considered in this study), while some techniques are yet undergoing to improvements and have just been accepted for demonstration purposes or at best at small scales. Desalination systems can be classified according to the energy source such as; thermal, mechanical, electrical and chemical energy sources. Another classification depends on the desalination process: evaporation-condensation, filtration, and crystallisation technique. Some of the desalination technologies are still under development such as; solar chimney, greenhouse, natural vacuum, adsorption desalination, membrane distillation (MD), membrane bioreactor (MBR), forward osmosis (FO), an ion-exchange resin (IXR). The reverse osmosis (RO) followed by multi-stage flashing (MSF) and multi-effects distillation (MED) systems are the most worldwide implemented desalination technologies [48, 49, 50].

In order to utilize SGSP heat for medium to large scale desalination purposes, different mature SGSP - thermal desalination configurations have been assessed [51, 52, 10, 53]. The assessed configurations below are the most matured and used medium to large scale desalination systems worldwide.

2.6.1 Multi effect desalination (MED)

The multi-effect desalination system functions by passing vapours from one effect via a pipe to the following effect. This procedure or process makes the

vapours condense in the following effect, while the produced heat throughout the condensation process is utilised to heat the water in the following effect. In order to accomplish such a process effectively, each effect is sustained at a specific pressure point, which consequently, drives to a different boiling point temperature for the water at each effect; however, there is an essential condition here, which is to maintain the temperature of the seawater at a lower degree than that of the condensing steam. This condition is crucial for the effective and efficient functioning of the multi-effect process; otherwise, the following effect will not get enough thermal energy to perform the task [54].

Generally, MED is deemed to be among the highest performing thermal desalination techniques. The evaporation process and condensation process occur concurrently in the heat exchanger and the different effects [30]. The features of the MED method are listed [30]; (I) MED operates with low-heat supplies such as solar radiation collectors. (II) The MED units can efficiently run at a top brine temperature (inlet of the first stage) of 60 - 65 °C as in MED-TVC [48, 49, 50]). Additionally, it can handle a high concentration ratio of the reject brine even at saturation conditions. (III) MED systems tolerate operational conditions. Operating at a low temperature makes the system able to avoid scaling and corrosion. (IV) MED process tolerate the fluctuations in seawater quality (such as salinity or turbidity); consequently, it provides stable behaviour and performance. (V) Multi-effect desalination system with thermal vapour compression (MED-TVC) particularly has low energy consumption [7].

2.6.2 Multi effect desalination - thermal vapor compression

In multi-effect desalination thermal vapour compression units MED-TVC, a mechanical compressor is utilised to compress the water vapour. The water vapour that has been compressed then transport inside a number of tubes, which drives to condensation. Figure 2.21 shows a schematic diagram of a mechanical vapour compression distillation system coupled with MED powered by a salinity gradient solar pond. Thermal vapour compression is usually coupled with multiple-effect distillation, which utilises water vapour produced in each effect [55, 49, 50].

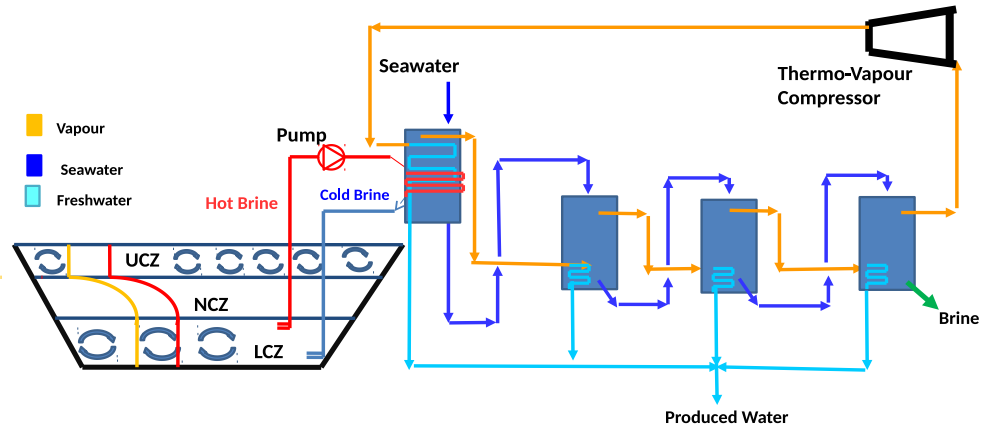

FIGURE 2.21. Schematic diagram of SGSP coupled with MED-TVC plant.

MED-TVC is characterized by low energy consumption, high-performance ratio, easier operation and low maintenance requirements [7]. The MED-TVC units can efficiently run at a top brine temperature of 60-65 °C [48, 49, 50].

Having reviewed some thermal desalination units. Turning now to studies on solar thermal desalination processes have been carried out. Since 1987 at El Paso SGSP [56] research on SGSP-thermal desalination has been conducted. Research conducted on desalination might be split into two phases. The first phase from (1987–1994) which centred around testing the technical practicability of SGSP coupled desalination systems. Throughout this phase, two single-effect, 24-stage falling-film desalination units MSF, and a multi-effect,multi-stage(MEMS) flash evaporator were experimented [57]. The second phase commenced in 1997, which concentrated on enhancing the efficiency and thermo-economics of SGSP coupled desalination system.

The first phase had three significant functions: (I) to advance the thermodynamic effectiveness of the SGSP-MSF unit; (II) to examine and experiment other low-temperature thermal desalination integrations; and (III) to improve the overall systems strategy which combines SGSP coupled with multi-process desalination units and brine concentration methods.

An old MED unit was renovated and fitted at the El Paso SGSP in September

from the same year [28]. The later system was examined under various operational circumstances, including changeable heat input, temperature level, and various sources of brackish water. The influential elements affecting distillate output and energy consumption rate were recognised. It was observed that the water at the SGSP surface could signify an efficient cooling source for thermal desalination, and power consumption could be lessened, thereby omitting the need for cooling tower [28].

Membrane distillation (MD) have likewise been investigated. In order to decide the technical feasibility and operational efficiency of MD coupled with a SGSP, a small MD system (about 350 L/day) experimented at El Paso in 1999. The laboratory outcomes proved that SGSPs serve a possible source of electric power to drive a relatively small MD desalination unit [28]. It was evident from the experimental research that desalination units that are thermally driven, such as MSF and MED are more promising than electrically driven such as MD.

Seawater desalination seems to be a promising utilisation of SGSP thermal energy. Besides producing clean, green energy to derive desalination units, SGSPs can also help to utilize the waste concentrate. Brine concentrate management and disposal are recognised as one of the main impediments for desalination applications. Domestic desalination of salty water must regard not only the facilities and energy needed to run the units but also environmentally suitable and economically feasible brine concentrate management and disposal processes.

Coupling SGSP with desalination could lead to better brine management as the situation in El Paso, where the rejected brine from the desalination system is re-injected to the SGSP thereby compensating the need for disposal, and subsequently transformed to a contamination-free energy source for desalination units [28]. In order to scrutinise the technical and economic feasibility of the approach mentioned above, and to gather data and information for a so-called 'zero discharge plant, a brine Concentrator and Recovery System (BCRS) was constructed in 1999 and experimented in 2000 at El Paso. Extensive details of this concept are discussed in Ref. [28].

Saleh et al. .[11] reported a 3000 m^2 SGSP integrated with desalination in a location close to the Dead Sea was able to provide an annual average production

rate of 4.3 L/min of freshwater, compared with 3.3 L/min that would be delivered by El Paso SGSP and at lower price [25], though, it has approximately similar surface area [11]; however, at the near Dead Sea SGSP, the appearance of gassing was witnessed. When the ground below the SGSP touched a temperature of over 60 °C, gas bubbles developed at the base of the SGSP which created mixing and turbidity. At the point, it was supposed that this gassing was as a result of anaerobic decomposition of organic material below the SGSP, however, after that, it was noted to be due to the proximity of underground water which released dissolved air into the SGSP [11].

Geographical and climate conditions play a significant role in SGSP thermal performance. Thus, each potential site should be assessed separately. In addition to that, thermal desalination units have advanced significantly during the past two decades. Recently, some desalination units such as the MED-TVC are reported to be working at an extremely low-grade heat. Consequently, a new assessment of SGSP-Thermal Desalination is required. The next section will review the literature (experimental and numerical) studies concerns with SGSP thermal potential, behaviour and stability.

2.7 SGSP: thermal performance

Different thermal performances (maximum recorded LCZ temperature) have been reported, El Paso [25] recorded LCZ temperatures range between 70-93 °C, Bhuj [33] 84 °C, Pyramid Hill [26] 90 °C, and Granada [27] also recorded 90 °C. This section reviews pertinent experimental, theoretical and numerical studies concerned with understanding the determining factors of the salinity gradient solar pond thermal behaviour and performance.

2.7.1 Experimental approaches

Rudolph Bloch In 1948, [15] proposed the first artificial solar pond to investigate SGSP thermal performance. Later, Tabor [16] and Rabl and Nielsen [22] reported a series of experimental studies of salinity gradient solar pond. Several experimental pieces of research have been conducted after that and up to this date in order to study the SGSP thermal behaviour [58, 59, 60, 61, 62].

Experimental work has principally focused on thermal measurements to investigate the thermal behaviour of SGSP under different conditions. The thermal performance differs from one experiment to another, as different experimental set-ups were used (e.g. different sizes for the zones, different salt types, etc.).

It can be concluded that experimental approaches to study the thermal behaviour and performance of salinity gradient solar pond can be time-consuming and sometimes expensive. Any change in pond parameters necessitates a change in the experimental set-up. For instance, any damage to the non-convective zone requires a new salt gradient formation. Due to the long-time requirements for the pond to heat, long time to detect season variations, and the need for a completely new set-up in the case of any instability occurs to the zones. The computer simulations can provide an alternative approach to study the effect of parameters on pond performance in a shorter time, with different parameters for any location.

2.7.2 Theoretical modelling and simulation approaches

Computer simulations can provide an excellent alternative approach to investigate the effect of various parameters on SGSP thermal behaviour.

SGSP was theoretically investigated by Weinberger in 1964 [63], who made the first documented attempt to described the physics of salinity gradient solar ponds. Weinberger, in his study, also predicted the thermal behaviour of SGSPs by resolving the heat and mass diffusion equations analytically. The partial differential equations PDFs analytical solution was accomplished considering an exponential solar radiation transmission function of the radiation absorption throughout the SGSP. In his model, Weinberger also made other assumptions, where he assumed that ignoring sides losses is fair as the SGSP considered to be well insulated, the upper convective zone temperature of the SGSP is supposed to be equal to the ambient, the UCZ-NCZ and LCZ-NCZ interfaces are fixed. He stated that analytical solutions are useful for simple indications [17]; however, it can be argued that if more complicated conditions (complicated boundary conditions) are considered, then numerical methods have to be used to reach more precise predictions of thermal behaviour and performance.

Followed, in 1975, Rabl and Nielsen [22] used the Weinberger's model; however, this time, they have divided the SGSP into a two-zones with LCZ and NCZ. The top of the non-convective zone temperature (practically the UCZ) assumed to be equivalent to dry bulb temperature of the ambient air, and all solar radiation transmitted to the lower convective zone is absorbed in that layer. Basically, Rabl and Nielsen extended Weinberger's theoretical model, but this time considering, heat is permitted to be a loss to the ground, considering the thermal conductivity and heat capacity of the earth.

At that time, Rabl and Nielsen's model was a more realistic approach to be taken in order to study SGSP thermal performance, considering that work has been done before the advancement of insulation liners. In comparison to Weinberger theoretical model where he neglected the heat loss to the ground problem altogether.

Bryant and Colhcck [64] have used the Rabl Nelsen model to estimate the temperature of SGSP suited to the climate conditions of London. They have estimated that a SGSP with an area almost equal to the area of a residential house is required for its space heating, with a cost comparable to the cost of using gas for heating. During their effort, they managed to develop a relationship for the fraction transmitted of solar radiation reaching any depth of SGSP, from 1 cm to 10 m, that closely matches the equation developed by Rabl and Nielson and used in their model [22].

Kishore and Veena Joshi have developed a steady-state model for non-convective SGSP [65], taking into consideration the heat losses from the top surface and the bottom of the SGSP. In their model, the UCZ boundary condition of the governing heat diffusion equation is not fixed to the ambient temperature at the SGSP location. Alternatively, it adopts the climate temperature for each month and calculates the heat loss from the surface. Their study has shown that, depending on climate conditions, the thermal performance of the SGSP can deviate substantially from that when UCZ temperature is fixed, and issues like heat losses from the surface were not considered.

Subhakar and Srinivasamurthy [66] have developed a simulation procedure in which a set of nonlinear PDEs of mass and energy balances of the three zones UCZ, NCZ and LCZ have been solved numerically using the weighted average finite difference method to predict the transient thermal behaviour of a saturated SGSP. Thermo-behaviour is considered to be dependent on the hourly variation of solar radiation, relative humidity, air velocity, ambient temperature. They concluded that the pond thermal performance indicates that the upper convective zone heat losses contribute significantly to the total heat losses from SGSP. As well as that, the impact of a ground heat loss appears too little in comparison to the top heat losses. It was also concluded that saturated SGSP had not proved any significant improvement in terms of thermal performances over a similar unsaturated SGSP, apart from its stability.

According to the reviewed literature, in terms of method of solving the governing equation of SGSP, analytical methods are beneficial for simple cases and indications; however, when more complicated boundary conditions are considered, numerical methods have to be employed.

The reviewed literature above are not the only efforts that have been made to study the SGSP thermal behaviour and performance, but they were the first efforts to set the basis for future research. Following that, there were several numerical methods and numerical solutions of the partial differential energy equation governing the salinity gradient solar pond in the literature. Similar assumptions and simplifying hypothesis to those made by previous researchers have been made. Hull [67], Rubin et al. [68], and Kurt et al. [61], Safwan [69] have used a finite difference method, while Jayadev et al.[70] and Panahi et al. [71] have applied a finite element technique.

All these efforts helped to understand the thermal performance of SGSP; however, interestingly, SGSP had different thermal performance even when similar assumptions and simplifying hypothesis were made, which drives the author of this research to this conclusion; SGSPs are not off the shelf technology.

SGSPs by their nature exhibit a surprising degree of climatology-specific behaviour and subsequently, different thermal performances. The interaction between the pond and the environment seems to be always of fundamental importance. This fact implies that one best not presuppose that a SGSP can be built and operated at any site, in the short or the long term, by blindly following a simple construction manual. Instead, for future applications, one must accurately assess and evaluate each potential SGSP via experimental (inflexible to parameters change, time-consuming and expensive, option), or via computer simulations, and then assess the application of pond, on its merits.

In order to assess the thermal potential of SGSP as a source of thermal energy according to the geographical conditions of Tripoli, a study considering Tripoli climatology should be conducted. Unlike all numerical used in the literature (finite element and finite Difference), finite volume method will be adopted this time. Both finite element and finite volume are easy to define up to second-order accuracy on unstructured grids; however, the finite volume is a new approach to be used this time for 1-D SGSP thermal potential study. The 1-D study should provide an indication of the SGSP thermal performance as a stable system.

2.8 SGSP: operational stability

This section aims to review factors that negatively affect SGSP thermal performance and long term operational stability. According to experiences from the reviewed salinity gradient solar ponds [25, 33, 26, 27]. Table. 2.1 summarizes the most common factors that tend to deteriorated SGSP thermal performance, behaviour and bring instability [24, 11, 26, 27]. Luckily, there have been considerable theoretical [24, 67, 68, 12, 72] and experimental [73, 61, 34] studies addressing some of the issues, which include analytical and numerical models [74, 75, 76], laboratory testing, construction and performance analyses [24, 77]. Factors that affect the SGSP thermal performance and bring instability could be divided into three main categories (I) Design and construction issues, (II) Mechanical sources of instability, and (III) Thermal and hydrodynamic sources of instability.

TABLE 2.1. Factors affect SGSP thermal performance and stability [78, 14, 79, 11, 26, 27].

Design and construction	Mechanical factors	Thermal and hydrodynamic factors
The site selection	Heat extraction system	Double diffusive convection
Underground-water table depth	Surface flushing	Interfaces motion
Liner quality	Wind turbidity	
Salt type and quality		
Thickness of zones		

A review of the previously conducted research studying and investigating these factors is conducted in the next sections in order to highlight issues that either have not been studied or has not been investigated in sufficient detail.

2.8.1 Design and construction sources of instability

Fortunately, today, in 2019, salinity gradient solar ponds can employ well-established techniques for the most part of their construction and design. The present section covers the effect of, selection of site, salt type and dissolving methods, lining, water clarity and Zones thickness.

Improper site selection

According to the reviewed ponds [25, 33, 26, 27], it can be stated that SGSPs are not off the shelf technology. SGSPs by their nature exhibit a surprising degree of site-specific behaviour and subsequently, different thermal performances as it has been shown in the previous section. El Paso [25] recorded LCZ temperatures range between 70-93 °C, Bhuj [33] 84 °C, Pyramid Hill [26] 90 °C, and Granada [27] 90 °C.

Underground-water table depth

In the near dead-sea SGSP, the phenomenon of gassing was observed. When the ground under the pond reached a temperature of just over 60 °C, gas bubbles appeared at the bottom of the SGSP which caused mixing and turbidity. At the time, it was believed that this gassing was due to anaerobic decomposition of organic material under the pond but was then believed to be due to the proximity of underground water which released dissolved air into the pond according to Saleh's study [11]. This shows the importance of the right site selection and using a liner to insulate the bottom of the SGSP.

Low-quality liners

Various lining practices have been applied in SGSPs, such as flexible membrane liners and compacted plastic/clay concealed liners. Kumar [24] for example, stated that Bhuj SGSP provided thermal energy for around two years, which is enough evidence of the competence of the lining system used. Nonetheless,

it may not be considered as a high-grade option fundamentally due to linear Low-Density Polyethylene LDPE and LDPE-variants are not intended for high-temperature settings. Studies conducted on the LDPE film (Liner Section) indicate that the LDPE film undergoes degradation due to oxidation process and reduction in mechanical characteristics such as tensile strength and puncture resistance as a result of which it fails to contain the pond brine leading to leakage when the temperature of brine is in excess of 80 °C. In the third year of operation, the site experienced leakage because of the failure of the LDPE liner, when the temperature of the SGSP was allowed to be close to 85 °C without any heat removal [24].

Throughout the earlier years, the El Paso SGSP had encountered liner collapses [80], where three distinct types of liners have been applied: a geosynthetic clay liner (GCL), an XR-5 8130 liner and a polypropylene liner.

The XR-5 liner, a PVC covered polyester fabric, have been applied in the 1970s in many SGSPs. This liner, possessing a 1.0 $\mathrm{kg\,m^{-2}}$ weight, was introduced at the El Paso SGSP in 1984 as part of a double lining arrangement with a present Hypalon liner under making a secondary containment. The forecasted endurance of the XR-5 liner was about 20 years. Nonetheless, it collapsed in 1992 after 7 years of SGSP operation. Over 100 holes were spotted on the XR-5 liner on the deeper bottom of the side walls. Failure analysis showed that the XR-5 liner, close to the LCZ in the SGSP, at points the liner exhibited to high temperature, tended to be very fragile and the durability of the material worsened to as low as 10 % of its primary strength [81].

The GCL was another option to a geomembrane liner which is a compacted plastic/clay lining system GCL applied for SGSPs in Mexico. A GCL provides many improvements, including, inexpensive option and extraordinary puncture endurance. Yet, the features and expenses of GCL are quite location-oriented and might diversify based on the expertise who construct it[82]. It might be too challenging to attain a proper regional or domestic clay for GCL. At El Paso, five local clays had been examined in order to decide the best compaction, mineralogical composition and hydraulic conductivity. Unfortunately, none of the clays demonstrated satisfactory level for use in a SGSP.

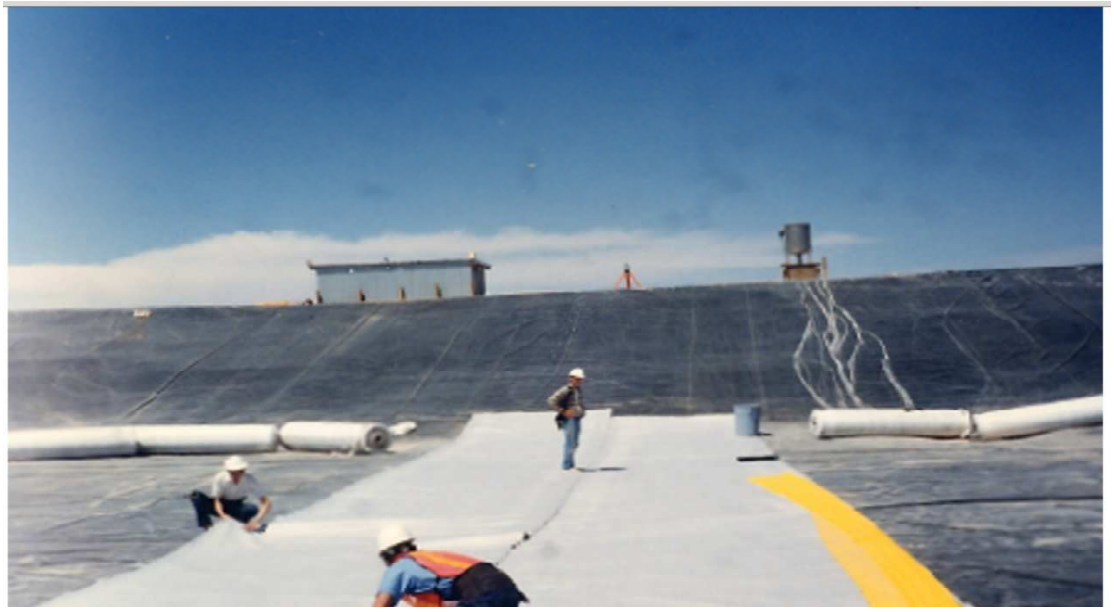

FIGURE 2.22. Installation of Geo-textile between the polypropylene liner and GCL [25].

Following an examination of different kinds of insulation schemes, two separate insulation schemes, a flexible polypropylene geomembrane and a geosynthetic clay liner (GCL) for the SGSP base were decided and composed especially for the El-Paso SGSP. The GCL applied at the El Paso SGSP composed of a layer of sodium bentonite clay adhered to 30 mm polypropylene. The GCL is overlain and thus needs no cementing, causing the installation to be simpler and economical. The bentonite possesses a 92 % montmorillonite content and is formed to combat the impacts of pollution and contaminants from saltwater. Both liner arrangements were introduced and applied in May 1994. The process of installation of the liner system is shown in Figs. 2.22 and 2.9.

The liner used for sidewalls was approximately a 40 mm polypropylene seamed liner placed above a 30 mm polypropylene auxiliary containment liner. The particular GCL was placed on the base of the SGSP with the clay side below to reduce contact between the brine from one side and the bentonite from the other side. Inbetween the GCL and the adjustable polypropylene liner, a film of geo-textile was fitted to preserve the GCL from damage. The layers of the GCL were overlaid 30–50 cm and a 146 kg m^{-2} overburden of soil were placed as prescribed by the producer. A waste scheme introduced below the GCL was created to support the monitoring of the leakage percentage. The following was hydration with freshwater, which is needed for the creation of the SGSP, dense concentrate brine with dry salt was injected into the SGSP from other

evaporation ponds at the site. Thus, a salinity gradient was created in March 1995. According to some recorded leak measures, the hydraulic conductivity of the GCL was determined to be on the order of 2×10^{-6} cm/s [81, 83].

Lastly, a polypropylene liner was used. In summer 1996, around 2 years after the establishment of the geosynthetic liner, the 40 mm polypropylene liner on the SGSP sides collapsed. Due to an inappropriate UV stabilizer was combined with the resin material while manufacturing, the liner deteriorated because of the exposure to ultra-violet UV. Cracks and splits occurred above the SGSP waterline, particularly in the north, east, and west sides of the SGSP. Subsequently, the SGSP was emptied, and the whole SGSP was lined with an upgraded 60 mm polypropylene liner. It had run competently since that point and was still in excellent shape by the end of the year of 2003 [25].

A thick Nylex Millennium polypropylene liner was used for Pyramid Hill SGSP. To observe and follow the state of the liner, the bottom of the SGSP a sump was created. A pipe was fixed below the liner to permit scrutinising the level of water in the sump. The water volume in the sump should show whether the liner is effective or not. This time, the liner was sturdy and gave excellent results [26].

According to reviewed work, thick Nylex Millennium polypropylene liner is highly advised. It was chosen for its strength to endure brine at high temperatures that could go up to 100 °C and also its unique resistance ability to the ultraviolet type of radiation [26]. The lining represents a considerable, and critical, the cost in SGSP economics.

Low-quality salt type

According to experiment [25], the topmost three types of salts in terms of resistance to temperature changes are sodium chloride (NaCl), magnesium chloride ($Mg\ Cl_2$) and sodium sulphate ($Na_2\ SO_4$), respectively, [25].

Sodium Chloride; this particular salt makes the most part (77%) of the ocean and seawater salts. Moreover, it is considered to be one of the most exceptionally stable salts with temperature change. Furthermore, the transparency of Na

Cl brine is relevantly high, and it is cheap in comparison to other types of salts mentioned earlier. Sodium Chloride has the capacity to be dissolved in water up to 27-30 % prior to approaching full saturation, which is deemed to be comparatively low. Most of the USA SGSPs use Na CL [9].

Magnesium chloride (Mg Cl_2) is another commonly used type of salt in salinity gradient solar ponds. It is deemed the second-highest salt constituent of the seawater. Moreover, it makes the most significant portion of salt in the Dead Sea. This mainly salt is stable during the pond operation, and it manifests high solubility in creating a brine that is so dense. Mg Cl_2 is capable of dissolving within a range of 35 to 40 % depending on the water temperature. In comparison with Na Cl, magnesium chloride is capable of providing a slightly higher salinity. Also, it is more stable during the pond's operation. The only disadvantage it holds in comparison to Na Cl, it is much more costly and not as abundant [9].

Other types of salts; Murthy and Pandey [84] studied fertilizer salts for operating solar ponds. Kurt [61] performed both experimental and numerical investigations of the performance of sodium carbonate salt gradient ponds under simulated solar radiation. While [85] assessed the performance of magnesium chloride saturated solar ponds. Hassairi et al. [86] used natural brine. The highest temperature achieved in the natural brine salinity gradient ponds is slightly less than the Na Cl and Mg Cl_2 salinity gradient solar ponds [86].

In summary, according to previous experiences, it is not surprising that sodium chloride is regarded as the common salt by far for loading and running salinity gradient ponds worldwide. Sodium chloride is the main and most recommended type of salt by many researchers to be used in SGSPs [9]. Some of its inherent advantages are; it has the lowest molecular diffusivity, its solubility value is high enough to meet the highest solution density required, and its solubility does not change significantly with temperature.

It is crucial to mention here, that the salt used in SGSPs should also be non-toxic, and ecologically acceptable to avoid any environmental and economic risks, subsequently, lining (insulating) the bottom of the SGSP which has been discussed in the previous section is crucial not only to reduce heat wastes to the soil but also to protect the environment.

Hight turbidity

After the salinity gradient pond is established, controlling the brine transparency plays an important part in the thermal efficiency of the SGSP. The clarity of the pond by lessening and preventing any presence of algae or dust contributes to the thermal performance of the pond directly and indirectly. Certain measures should be taken to remove debris and leaves that are less dense than water and tend to float on the top of the SGSP by skimming them off. Dust sank to the bottom of the SGSP does not affect the absorption of solar radiation. However, any of the dust that is floating in the non-convective zone should be ended by adding powdered alum. The growth of algae can be managed by injecting copper sulphate. However, it should be noted here that if the SGSP water is alkaline, copper sulphate might not dissolve. Hull [9] has recommended various methods of algae control.

Improper pond size and zone thicknesses

Improper sizing of the SGSP zones could lead to counterproductive results. Kooi [87] has developed a steady-state three zones salt gradient solar pond model also with the assumption that the UCZ temperature is equal to the wet-bulb temperature of the ambient air. In his model, SGSP was considered as a flat plate solar energy collector, and hence the Hottel-Whiller-Bliss form of equations was applied for the pond in Kooi study. The resultant efficiency of the SGSP has been compared with that of a flat plate collector. He demonstrated that, for given surface temperature, heat collection temperature and insolation, there is an optimum thickness of the non-convective zone NCZ of 1.2 m for which the heat collection efficiency is maximum.

In 2008, Garman [88] conducted a sizing and thermal study of salinity gradient solar ponds and reported that 1.1 m is optimum NCZ thickness which is in a good agreement and very close to the figure suggested by Kooi [87]. However, none of the previous works provided a procedure to maintain a SGSP at the recommended pond-zone thickness.

Stability of the zones is crucial in order to maintain the overall pond thermal performance and stability. Tabor [89] noticed that even when no washing of

the surface was performed the density gradient at the top of the pond was lost at the rate of 1 cm/week and mixing caused the appearance of a convecting zone at the top, thus indicating that a UCZ is automatically formed at the cost of NCZ. Tabor and Matz [16] have reported that a surface wave amplitude of 2 cm, developed a mixing zone of 20 cm. To keep wave amplitudes down to these levels would require windbreaks and wave breaks at 50 - 100 m intervals. In their SGSP with no wind or wave breaks, the top mixed zone always reached an asymptotic depth of 20 cm. In order to keep the UCZ at 0.40 m, Tobar and Doron [89] in their 150 k/W pond used spaced plastic nets to float on the surface to reduce the fetch and to dissipate the wind. Though Al-Marafie et al. [90] have selected a UCZ thickness of 0.4 m, they found it very difficult to maintain it because of the heavy seasonal winds of that region (Kuwait) and reported severe wind-induced mixing between UCZ and NCZ which resulted in the UCZ thickness increasing from 0.4m to 0.9 m.

Tabor and Doron [89] have selected 0.4 m as UCZ thickness and have maintained it by floating plastic nets which attenuates the mixing of the upper waters. Motiani et al. [24] have used 0.5 m as UCZ thickness, considering the windy location of Bhuj and have used a wave suppression system to reduce NCZ erosion due to wind mixing. Similarly, Mac Donald et al. [46] have used 0.5 m as UCZ thickness and maintained it by floating ring wave suppressors on the surface. Srinivasan [33] has maintained the UCZ thickness of his pond between 0.3 m and 0.6 m. Higher values such as 0.6 m have been maintained during heavy rainfall to take care of rain penetration dilution at the UCZ-NCZ boundary. Patel and Gupta [91] have suggested a UCZ thickness of 0.3 m - 0.5 m for the SGSPs in tropics.

Kooi [87], Wang and Akbarzadeh [79, 26] Bansal and Kaushik [92] and Motiani et al. .[24] have made theoretical modelling studies on a solar pond and have suggested a UCZ thickness as thin as possible, ranging from 0.1 to 0.5 m, in order to have maximum solar collection efficiency.

From the theoretical investigations of the present study, it has been concluded that a UCZ thickness ranging from 0.1 to 0.5 m could be used for the solar pond. This conclusion is consistent with the findings arrived at by several investigators given above using altogether different models/from their experience on practical ponds. Cha et al. [93, 94] have theoretically analysed the

effects of wind velocity on the wavelength of surface waves generated by the wind, by keeping the fetch as the parameter. They have given a graphical relation between wind velocity over the pond surface and wavelength of the surface waves, for different constant values of fetch length of the pond. They have shown that the UCZ thickness could be 1.6 times the wavelength of surface waves to take care of the wind effects. The findings of the studies of the various investigators show that a thin UCZ layer gives maximum solar collection efficiency. But difficulties are encountered in keeping the UCZ thickness as small as possible, because of the, (I) Wind shear causing the top convective layer to rotate horizontally leading to mixing al the interface, (II) Surface water evaporation requiring daily addition of freshwater for make-up on the top zone and, (III) Rain penetration causing the UCZ thickness to get increased at the cost of the NCZ thickness.

For maximum solar energy collection, the UCZ thickness could be between 0.1 and 0.5 m, as the wind velocity is high in Libya during some seasons (dusty wind from desert). And the country does not get rains so often. So, a relatively thick UCZ is reasonable. The procedure given by Cha et al. has been considered in this study to fix the UCZ thickness. Therefore following Cha et al. [93, 94], a UCZ thickness of 0.4 m will be selected. This UCZ thickness of 0.4 m is within the upper limits given by Kooi (30), Wang and Akbarzadeh [79, 26] Bansal and Kaushik [92] and Motiani et al.[24] for maximum solar energy collection. The UCZ thickness selected for the proposed Libya SGSP takes care of the rain penetration effect also the wind effect. The UCZ thickness must be fixed based on the climatic condition of the pond site and the LCZ temperature required.

The theoretical investigations of Kooi [87] and Bansal [92] have shown that as when the NCZ thickness decreases from the set-up thickness, the pond efficiency falls rapidly. Rabl and Nielsen [22] have shown in their theoretical investigations that smaller NCZ would give only a low temperature for the pond. And Ref. [24] while working with their pond in India have observed, that there is low efficiency and massive conduction loss from LCZ to UCZ and they have attributed these to a thin NCZ used by them. They have also found that if the NCZ thickness is less than the optimum value, the temperature gradient at the NCZ - LCZ boundary is positive and not fixed. The respected researchers have not proposed an optimum value for NCZ, and they instead meant the initial set-up value.

Al-Marafie el al. [90] while working on a SGSP in Kuwait had noted that when the NCZ thickness was 0.45 m (i.e. 55% < the initial set-up value) the pond could not sustain the temperature difference between the LCZ and UCZ and the SGSP experienced heat losses. They stated that for the NCZ thickness (less than the initial) the efficiency and pond temperatures are low and losses are high. The theoretical investigations discussed had shown that as the NCZ thickness increases from the initial value, the efficiency falls very slowly initially and then falls rapidly but not as rapidly as the case when the NCZ thickness was less than the initial. So it is imperative that the optimum NCZ thickness is used for the pond so that it can have maximum collection efficiency without disturbing the NCZ - LCZ boundary. The researchers have not proposed an optimum value for NCZ, and they instead meant initial set-up value.

Tabor [21] has pointed out that the optimum thickness of NCZ depends on pond clarity, the temperature of operation and the local insolation. And did not provide any ratios or values for NCZ to other zones thickness. Kooi's [87] theoretical analysis reveals that a salt gradient solar pond will have maximum collection efficiency only for a particular optimum value of NCZ thickness, which has been found to be in the range of 1.2 to 1.4m. Wang and Akbarzadch [95] have made theoretical studies on the pond parameters, including ground heat loss and reported an NCZ thickness of 1.5 m as the optimum thickness, for maximum solar energy collection. Pacetti and Principi [96] have used an NCZ thickness of 1.5 m based on the heating requirement estimated using computer code. Srinivasan [33] has constructed a 240 m^2 bottom area solar pond al Bangalore, using 1.0 m as NCZ depth of a total thickness of 2.4 m. This optimum NCZ depth of 1.0 m has been obtained from his theoretical investigation. Motiani et al.[24] have used 1.5 m as NCZ thickness based on the observation that it reduces the upward diffusion of salt from the storage zone.

Bansal and Kaushik [92] have predicted in their parametric studies on SGSPs that for maximum collection efficiency, the NCZ thickness has to be 1.5 m. It could be noted that the NCZ thickness used by a large number of respected investigators in different locations ranged between 1.0 to 1.5 m. However, there is no fixed ratio and a specific procedure for choosing the optimum thickness of this zone. In this thesis, optimum zone thicknesses ratios will be investigated by means of 1-D and 2-D models; a procedure will be suggested to choosing the NCZ:LCZ optimum thickness ratio.

The observations of Tabor and Doron [89] have indicated, that the diurnal variation of temperature has to be very small to consider a small LCZ thickness and if it is very much excess of 2 °C/day LCZ thickness should be large enough. A small thickness can lead to more rapid seasonal warm-up of the lower zone, which may result in a large average value of boundary temperature gradient and resultant gradient zone erosion. For example, Patel and Gupta [97] have selected an LCZ thickness of 0.5 m, and have found that the diurnal variation of temperature was around 3 °C in the LCZ. They have noticed massive gradient zone erosion, and in such cases, steady-state conditions cannot be applied. The LCZ thickness should be such that when the heat is extracted by the brine withdrawal method and re-injected into the pond, the bottom layers of the gradient zone are not disturbed. Tabor and Doron [89] have selected an LCZ thickness as large as 2.5 m, in their solar pond, so that withdrawal of heat from the storage zone at very high flow rates does not lead to erosion of bottom layers of the gradient zone and the diurnal variation is less than 1 °C; however, lower LCZ temperature is obtained in the latter. And more salt requirement will be needed. Such large thickness should be economically justified when discussing large SGSPs.

In order to operate a low-grade heating pond, Newell et al. [98] at the University of Illinois, have selected an LCZ depth of 1.8 m, with the intention of operating it without daily and/or weekly involvement of personnel. Similarly, Motiani et al. [24] have used 1.4 m as LCZ depth, so that hot brine withdrawal does not erode the bottom portion of the NCZ Layers. Swift et al. (57) in their 3355 m^2 SGSP initially used 0.6 m as LCZ thickness and extracted heat and later used 1.0 m as LCZ thickness so that there could be no adverse effect on the gradient zone and they could get a diurnal variation of nearly 1 °C. Hawlader and Brinkworth [99] in their study have suggested an LCZ depth of 1.0 m for maximum energy collection to be obtained in a shorter pond heating period. Kooi [87] has found the optimum LCZ depth for maximum heat collection for a fixed UCZ depth. In Bansal and Kaushik [92] parametric study on a three-zone solar pond model and found that a thickness of 1.2 m for LCZ as appropriate.

Agha [100] used a 1-D model to investigate the thermal characteristics and economic of SGSP coupled with MSF plant, where the size of the SGSP and the number of stages for the MSF unit were examined counting the changes in the quantity of thermal energy provided by the SGSP between the seasons in Libya.

One result was that over-sizing the SGSP, lead to a decline in the seasonal yield ratio; however, because of the current advancement in desalination units, an up to date assessment to the thermal potential of the technology is needed. Additionally, Agha model did not consider and misses the DDC effect; thus, it would, therefore, has limited accuracy in sizing pond zones as it neglects the changes occur to the zones during operation. MSF plants require a TBT of 90 °C. Considering desalination units, that has a lower TBT could lead to better results. Garman also [88] used a 1-D model to size the SGSP zones, he stated that there is a linear relationship between the needed thermal energy for the desalination system and the surface area of the SGSP and also concluded that optimum thickness for the UCZ is 0.3 m, for NCZ is 1.1 and as large as 4 m for the LCZ. It can be argued that the lower convective zone thickness influences the maximum temperature obtained by the pond. A small depth may lead to higher LCZ temperature, which may disturb the gradient stability of the pond by increasing the rate of salt diffusion to the UCZ. Furthermore, the high temperature may also lead to failure of the liner material. As a matter of fact, several SGSPs discussed in the liner section earlier in this thesis had a leakage problem due to the failure of the liner material on account of high temperatures. On the other hand, the large thickness may lead to a lower temperature and high salt requirements, which can not be economically justified.

Thus, three factors to consider when choosing the LCZ thickness, (I) performance, (II) Stability and (III) Economics. Previous studies used 1-D models to study the zone thickness effect and neglected the stability factor altogether. 2-D models are needed to investigate the sizing and hydrodynamic stability collectively. The gradient zone or non-convective zone is the region which does not allow the heat from the storage zone of the pond to be lost to the ambient air by convection, and it is important to maintain this layer at its optimum thickness during the operation. In previous work, all the attempts were focusing on investigating the optimum NCZ thickness, without focusing on the thermal and hydrodynamic sources of instability and the changes occur to the NCZ thickness during the operation of the pond due to this instability sources.

Thus, a 2-D model coupling the heat, mass and hydrodynamic (velocity) approach could lead to more accurate results and predictions. A 2-D study to investigate the optimal NCZ: LCZ zone thickness ratio will be conducted in the present research.

2.8.2 Mechanical sources of instability

The mechanical sources of instability can significantly affect the salt concentration profile, especially at the boundaries of the non-convective zone. Nonetheless, if mechanical instability sources such as the energy extraction system, the surface flushing process, and the wind suppression and protection systems are adequately designed, then the prime causes of mechanical instabilities and shearing flows will be halted. Mechanical instability sources are, shearing-flows induced by fluid injection, withdrawal, the top surface or the gradient profile adjustment and energy extraction which affect the interior interfaces and, wind-driven surface flows which in return affects the upper interface.

Fortunately, mechanical instability sources have been taking care of and extensively investigated by several researchers. And potential solutions to the problems have also been provided. The heat extraction and UCZ flushing issue have been investigated by Refs. [96, 89, 101, 25], and the wind-driven surface flow has been studied by Refs. [102, 103, 104].

Heat extraction systems

Heat recovery is the main aim of establishing a SGSP; however, improper heat extraction technique could damage the gradient layer (Mechanical source of instability). The heat extraction process has been investigated by Refs. [96, 89, 101, 25]. Thus, well-established techniques that have been experimented are available.

The experience at the El Paso pond shows that the fluid-withdrawal technique is efficient and favoured. The extraction diffuser can be mounted at a depth of maximum temperature in the lower convective zone while the return diffuser is located just underneath it. Applying this technique admits the placing both diffusers at a close point. Additionally, this technique guarantees that the colder fluid is injected to the bottom, minimizing any heat loss to the ground [26].

Following many years of operation, the diffusers had rusted at some points. Along with the corrosion issue, the free ions of iron were suspected to be a

cause of the clarity problem in the SGSP. After this occurrence, the heat recovery system was replaced in 1994, where steel diffusers were substituted with polypropylene plate, connected by 15 cm rubber hose to the external piping system [26].

As the potential for a SGSP to become unstable as a result of the fluid withdrawal from the bottom of the pond is become suspected. Extreme withdrawal procedure and/or reinjection procedures produces a turbulent flow that signifies potential erosion of the gradient layer. This particular problem was first noticed in the 2000 m^2 Ohio SGSP, where the uneven returning flow was the main cause given for non-convective zone erosion, while the main reason was the high brine withdrawal rates [26].

Nevertheless, various SGSP that adopted this technique has shown that fluid withdrawal was not an issue when the procedure and the system are appropriately employed [102]. For instance, the suction point must be some centimetres below the interface of the lower zone and the non-convective zone, while the colder fluid should be returned at a lower level [9]. Additionally, it is advised that the re-injected brine temperature must be below the lower convective zone temperature to avoid the erosion of the NCZ [9]; even though there is no underpinning scientific logic, it could be translated to meeting the natural convection condition, since the colder, denser brine would tend to flow.

At Pyramid Hill and Granada salinity gradient solar ponds, the heat recovery process is accomplished by circulating fresh water through an internal heat exchanger placed in the lower convective zone of the pond, and later transporting the heated water to an external heat exchanger that is located 200 m far and then to the thermal application as depicted in Figs. 2.17 and 2.18. The technique was effective and efficient throughout the years of operation [26].

Accordingly, both heat recovery techniques are reliable and efficient for extracting heat without a significant destabilizing effect on the gradient profile. However, in the withdrawal technique, the velocity and temperature of the fluid being pumped have to be monitored accurately in order to inhibit erosion of the gradient zone.

Surface flushing and wind effect

Another mechanical source of instability is the surface flushing process which might affect mainly the NCZ, which in turn affects the stability of the gradient pond. If the flushing process has not been performed correctly. The NCZ can easily get eroded. Surface flushing method has been discussed in the design and construction section.

Macdonald et al. [46], Hull et al. [9], and Al-Marafie et al. [90] have all reported that high wind speed does not just cause the dust accumulation in the pond, but it also increases evaporation losses appreciably and destabilize the salt gradient layers. Several investigators, like Tabor and Doron [89] used artificial windbreakers and wave breakers to offset the effects of high wind speeds, an example of windbreaks is shown in Fig. 2.5.

Tabor and Matz [16] have reported that a surface wave amplitude (crest to trough) of 2 cm, developed a mixing zone of 20 cm. To keep wave amplitudes down to these levels would require windbreaks and wave breaks at 50 - 100-metre intervals. In their solar pond with no wind or wave breaks, the top mixed zone always reached an asymptotic depth of 20 cm. In order to keep the UCZ at 0.4 m depth, Tobar and Doron [89] in their 150 KW pond used spaced plastic nets to float on the surface to reduce the fetch and to dissipate the wind energy.

The wind factor is worth mentioning because of the significant effects that it could cause. Using a thicker upper convective zone of at least 0.4 m is preferable in Libya to minimize the negative effect that might be caused by the wind, and wave breakers can also provide more protection to offset the effects of high wind speeds.

2.8.3 Thermal and hydrodynamic sources of instability

Here are some examples of sources of hydrodynamic instabilities; the heat loss from the top surface of the pond UCZ by radiation, convection, and evaporation. The latter represents the most significant source of SGSP heat losses. It has been argued by some researchers that the convection circulation (overturn) in

the UCZ may be one of the causes which may encourage turbulence and may grow with time [104].

On the other hand, the thermal energy stored at the lower zone in the form of hot brine that has high temperatures may reach its boiling point; subsequently, one of the worst instability scenarios could occur, called pond overheating which leads to the rapid formation of convection currents inside the gradient layer and destroy it. This kind of catastrophic collapse has been witnessed in a few SGSPs, and it appears to be that the appearance of air bubbles was the catalyst that initiated the mixing [9].

The salt contribution to SGSP stability is another factor; this was addressed by Ref. [38] as it has also been discussed earlier in this chapter. It has pointed out that a regular salt for salinity gradient solar pond should possess some inherent characteristics to improve the SGSP thermal performance and long term stability. The majority of salinity gradient solar pond thermal and hydrodynamic behaviour studies [9, 63], stated that the stability of the SGSP significantly depends on the mass transport rate. Where the mass transfer rate per unit area in a uniform temperature binary solution depends on the concentration gradient and the molecular diffusivity, thus, the migration or diffusion of salt from the high concentration lower convective zone to the upper convective zone would significantly contribute to the damaging of the gradient profile of the non-convective area and subsequently the SGSP destabilization. This process could be expressed mathematically as follows.

Based upon Fick's law of diffusion, (J) which represents the diffusion flux is related to the density gradient by Ref. [101]:

$$J = -D\frac{\partial C}{\partial z} \tag{2.3}$$

The mass transport can be represented as following [9]:

$$\frac{\partial C}{\partial t} = D\frac{\partial^2 C}{\partial z^2} \tag{2.4}$$

where C is salt concentration, D is the diffusion coefficient, t is time, and z

is the depth. This relationship is used by SGSP researchers, and its scientific underpinnings stem from the assumption that the mass salt transfer is only driven by the concentration gradient [9]. Mass diffusion issue is investigated and explained in more detail in chapters 3,4,5, and 6.

According to Ref. [105], the mass diffusion equation Eq. 2.4 can be utilized only when the diffusion calculations consider the molecular diffusion of salt solely in the SGSP; however, when a significant temperature gradient is there, the Soret effect should be considered.

$$\frac{\partial C}{\partial t} = -\overrightarrow{\nabla} \cdot \left[- D\overrightarrow{\nabla} C - D_{st} C \left(1 - \frac{C}{\rho} \right) \overrightarrow{\nabla} T \right] \tag{2.5}$$

where D_{st} is Soret coefficient, T is temperature, t is time and ρ is density. Only a small amount of research used the Soret coefficient; to the best of the author's knowledge, its value is not documented, particularly at high salt concentration like that in SGSPs and at high temperatures; however, it is assumed to be in the order of 1×10^{-3} to 3×10^{-3} by some researchers, and it is a positive number for sodium chloride in water. According to Nielson's study at the Ohio State University SGSP, the difference between the salt diffusion calculations with and without considering Soret term is less than 10%. Thus, the Soret term can be neglected. Hull, in his research, supported these findings, stating that the Soret diffusion effect can be overlooked due to its negligible effect [9, 105, 106].

Thermal sources of instabilities that can contribute to overturning the SGSP, all of them must work against gravity. The potential overheating in the SGSP can lead to double-diffusive convection over stable oscillations which affects the gradient interior. And natural Convection in the LCZ could lead to entrainment by eddy sweeping of the interface which affects the Lower interface of the SGSP.

Double diffusive natural convection phenomenon

Double-diffusive convection is a fluid hydrodynamics phenomenon that represents a form of convection driven by two different density gradients, that have different rates of diffusion [107].

Convection in fluids is inspired mainly by variations in densities under the influence of gravity. These density differences might be created by gradients in the structure of the fluid, or by variations in temperature or concentration via thermal expansion β_T and β_C, which is the salinity expansion coefficient. Thermal and compositional gradients usually diffuse with time, decreasing their capability to induce convection, and demanding that gradients in other areas of the flow exist, so the occurrence of convection continues. A typical place where DDC occur is SGSPs, as heat and salt concentrations exist with different gradients and diffuse at differing rates [107].

Considering a fluid in which salt concentration and temperature both increase downward as in SGSP, beside the gradients being such that where and fluid density is uniform and their respective contributions to the density gradient are balanced, in this case, the fluid in the system is statically stable; as there is no buoyancy force to generate scale of motion; however, if we provide conditions that would allow a fluid component of density ρ at a particular Z be shifted down to another location of (Z + ΔZ), in which the ambient density is yet ρ however the temperature now is (T + ΔT) and the salt concentration is (C + ΔC). As the thermal diffusivity is considerably greater than salt diffusivity, the fluid component reaches the ambient temperature more quickly than it reaches ambient salinity; consequently, it becomes less dense and undergoes to an upward force [107].

If solely double-diffusive consequences are critical, then just the relative balance between temperature and concentration plays a role in the density field, which is interpreted by the stability number Ra_ρ, sets the stability constraints. Alternatively, if the predominant mixing stems from an asymmetry between inertia and buoyancy, expressed as Ra_ρ or the mathematically equivalent buoyancy ratio N, then solely the overall density distribution concerns, regardless of the temperature and concentration. The heat helps to reduce the local density, but it does not engage directly in generating the overturning [107, 20].

In SGSPs, it is just the contribution of the salinity distribution that produces enough gravitational opposition to the mixing, due to the fact that temperature just weakens the density distribution. So, to counterbalance this natural source of instability, the salt concentration contribution $\beta_C \Delta C$ to the local net density must be greater than the temperature contribution $\beta_T \Delta T$. The stability criteria

Ra_ρ given by [107, 20]:

$$R_\rho = \frac{Ra_C}{Ra_T} \geq 1 \quad which \quad is \simeq N = \frac{\beta_C \Delta C_s}{\beta_T \Delta T} \geq 1, \tag{2.6}$$

where ΔC_s is the salinity differenc and ΔT is the temperature difference, Ra_T is the thermal Rayleigh, Ra_C is the solutal Rayleigh, N is the buoyancy ratio, β_C and β_T are the thermal and solutal expansion coefficient given by [20]:

$$\beta_C = \frac{1}{\rho}\frac{\partial \rho}{\partial C}|_C \tag{2.7}$$

$$\beta_T = -\frac{1}{\rho}\frac{\partial \rho}{\partial T}|_T \tag{2.8}$$

$$Ra_C = \frac{g\beta_S \Delta C H^3}{(\alpha\nu)} \tag{2.9}$$

$$Ra_T = \frac{g\beta_T \Delta T H^3}{(\alpha\nu)} \tag{2.10}$$

The buoyancy ratio condition implies that the density differences must be more significant in order to meet the stability criteria. Both Ra_ρ and N are equal quantities from the mathematical point of view.

Experimental approaches to study DDC effect

Several experimental approaches to study the SGSP stability had been conducted. Nielsen [22] has studied the stability of salinity gradient solar pond at Ohio. The pond has a 200 m^2 surface area and was lined with a black plastic liner. The temperature that has been recorded in the lower convective zone of this SGSP was 62 °C in June 1976 and 69 °C in August 1977. Nielsen stated that the equilibrium thickness of the gradient non-convective zone is controlled by the upward salt diffusion and the erosion at the interfaces due to the fluid motion in the adjacent convecting layer.

Leshuk [108] studied the long term stability of the pond experimentally. He made a similar conclusion to that of Nielsen where he noted a steady growth of convection currents in the LCZ and UCZ during heat collection and storage.

The external source of instability did not seem to trigger any form of instabilities. The middle parts of the gradient were extraordinarily stable and have the ability to recover artificially as the rate of instability growth could be controlled by increasing initial salinity gradients and utilizing natural diffusion. Additionally, he concluded in his research that more conclusive evidence is needed and that requires further experimentation.

Modelling and simulation approaches to study DDC effect

Studies considering velocity factor of the fluid and investigating the double-diffusive convection phenomena in SGSPs and how they affect the SGSP stability, and the overall thermal performance has been conducted, where, several respected efforts for applying numerical solutions for the partial differential energy equation governing solar pond are in the literature [109, 110].

A one-dimensional model cannot describe fluid flow or the hydrodynamic stability of the system. Two-dimensional models are required. The hydrodynamic sources of instability (DDC) have been investigated by a few researchers [111, 72] where efforts for applying numerical solutions for the partial differential energy equation governing salinity gradient solar pond are conducted [111, 72].

The first realistic 2-D numerical approach seems attributed to [111, 72] who have used commercial codes to simulate two-dimensional double-diffusive convection problem in a pond with height (1 m height).

Suarez [111] developed a transient double-diffusive convective model for salinity gradient solar pond where an energy and mass balance over the zones of the SGSP were applied. The governing Navier Stokes equations, equations of continuity, momentum, heat and mass transfer, were coupled with the density of the fluid approximation and considered to be linear with temperature and salinity. The code that was used is the Fluent commercial computational fluid dynamics code. The numerical method was adopted to solve the governing equation is the finite volume discretization. Suarez stated that the formation of convective currents in the upper convective zone and the lower convective zone clearly indicates that erosion of the non-convective zone happens as a result at some

point. Model results also showed that in a period of two weeks, the temperature in the lower convective zone of the salinity gradient solar pond rose from 20 °C to around 52 °C. Although the non-convective region was eroded due to the double-diffusive convection (convective mixing above and below), the salinity gradient solar pond sustained its stability; however, the reduction in thickness of the non-convective zone decreases the thermal performance of the salinity gradient solar pond.

Suarez [111] concluded that convective mixing has a severe impact on the stability of salinity gradient solar pond, and his results prove the need to control the mixing process in order to maintain the stability of the non-convective zone. Suarez also concluded that results from models that underestimate or completely ignore double-diffusive convection are not accurate and they overestimate the salinity gradient solar pond performance. This is a reasonable argument; however, the salinity gradient solar pond thermal performance depends on other factors such as solar intensity and zone thicknesses.

Followed, Boudhiaf [72, 110] conducted a 2-D study to study the hydrodynamic behaviour of SGSPs. The body of the simulated SGSP is the typical pond enclosure of height H and length L with an artificially created non-convective zone to suppress convective currents motivated by solar energy absorption and to stabilize the salinity gradient solar pond. The bottom and the sidewalls of the SGSP is insulated and impermeable, while the free-surface is subjected to heat losses by convection, evaporation and radiation. The system is governed by equations of continuity, momentum, thermal energy and mass transfer. The numerical method utilized to discretize the governing equations is the finite volume method in transient regime. In Boudhiaf study [72], the pressure-based segregated solver was chosen, and spatial discretization on cell centre and second-order upwind weighting were used. The gradients and derivatives were assessed utilising the Green-Gauss cell-based technique; the semi-implicit method for the pressure linked equations algorithm was used for the pressure-velocity coupling, and because the fluid is buoyancy-driven, the staggering pressure scheme was chosen to interpolate the pressure. To guarantee the independence of the numerical results with respect to spatial discretization, several grids were examined. Cells of 0.02 m were determined to be suitable. In the results, the velocity profile shows the appearance of small convective currents in the UCZ and relatively larger convective currents in the LCZ.

However, in both studies by Boudhaif and Suarez, there is no real indication of how and where precisely these convective currents start to form. Furthermore, the results do not show the expansion or the reduction of the non-convective zone. Boudhiaf studied the effect of buoyancy ratio. He concluded that the buoyancy ratio plays a vital role in the reduction of temperature in the upper convective zone and the maintenance of high temperature in the lower convective zone. The higher the buoyancy ratio, the better is the SGSP thermal performance. It also points to the importance of maintaining the thickness of the gradient layer in order to halt heat losses upwards; however, no optimum zone thickness ratio was suggested.

The recently reviewed studies pointed out that the degree of success in the design, operation and obtaining the best thermal performance of SGSP is regulated by the absence of convection in the insulating non-convective zone and by keeping the NCZ at its optimum thickness; however, none of the studies reviewed explained the essence of shrinking or expansion of the NCZ during pond operation (how and where it starts to erode); and, no definitive procedure was proposed to maintain the NCZ at its designated thickness for the most prolonged period. In addition to that, no optimum NCZ: LCZ zone thickness ratio for the longest term of stability and best thermal performance was advised considering the DDC effect. Subsequently, A 2-D study to address these issue, provide more details to SGSP operational stability and answer the question of optimum zone thickness ratio is to be conducted.

2.9 Summary

Salinity gradient solar pond has several advantages as a solar energy device. It combines both heat collection and heat storage in one device. It is able to store heat at no additional storage cost. It utilizes low technology components, is simple in design, and is fairly easy to maintain. The most sophisticated part of a solar pond is probably the plastic pond liner. Hopefully, an appropriate clay or other material substitutes will be found to replace plastic for use as a liner.

The limitation of SGSPs is that they do require significant surface area and large quantities of salt. Other types of solar collectors can be incorporated onto roofs or into other building structural elements. It does not appear feasible to do this

with solar ponds, which might limit their use to rural areas. Environmental contamination from the salt required by solar ponds could also be a problem. Solar ponds must be built so that salt does not leak from them, and salt runoff from the surface must be contained.

A large number of physical phenomena involved in SGSP operation makes the full prediction of the system behaviour a challenging problem from both the physical and the mathematical points of view. In fact, although the physics of each phenomenon is quite well known, the coupling between the phenomena need further investigations and understanding to help improving technical viability and subsequently, the feasibility of SGSPs for future implementations.

SGSP cannot operate without a stable non-convective gradient zone. In the reviewed literature and to the best of the researcher knowledge, neither the questions of how and where the erosion of the non-convective gradient zone has been answered nor have the transient behaviour of the zone due to the double-diffusive convection effect been simulated in adequate detail (Shrinking and Expansion of the Zone); however, in major recent studies by the respected researchers, it has been pointed out that the degree of success in the design, operation and best thermal performance of SGSP is measured by the absence of convection in the insulating gradient layer and keeping the zones at their optimum thickness.

However, and also according to the survived literature and to the best of the author's knowledge, none of the studies in the literature; covers the optimum zones design thickness ratio considering the DDC effect and the hydrodynamic behaviour of the zones (No LCZ to NCZ zone thickness ratio was advised) and no procedure was proposed to maintain the SGSP zones at an optimum thickness. Previous models sizing SGSPs zones, excluding the double-diffusive convection DDC effect have limited accuracy. Thus, more complicated models considering the DDC effect are needed to understand how to design better SGSPs that can perform efficiently and for the longest period.

Thus, in this thesis, 1-D and also 2-D models will be developed where the mass conservation for water and species, momentum, and energy equations will be coupled with the equation of fluid density to predict the transient thermal behaviour accurately and operational stability of salinity gradient solar pond

zones and the changes occurs to these zones during energy collection and storage according to Libya Climatology. Subsequently, the present study will supply by computations detailed knowledge of the hydrodynamic, thermal and solutal structures of the transient fluid flow developed in a salinity gradient solar pond during the collection and the storage of energy. Which will help to understand the formation and changes occur to the zones and subsequently, to find the optimum zone thickness ratio and to develop a procedure that can help to maintain the optimum thickness of these zones where SGSP can perform at its best.

The next chapter is devoted to explaining the physical concept and to develop the mathematical formulation necessary to adequately study the thermal behaviour and hydrodynamic stability of salinity gradient solar ponds.

Chapter 3

Theoretical modelling

3.1 Overview

In the previous chapter, the concept and design principles of salinity gradient solar pond are explained. SGSP thermal performance and stability pertinent literature are reviewed. It was concluded that SGSP is not off the shelf technology and by nature, it exhibits a surprising degree of site-specific behaviour. Subsequently, any potential application should be assessed accordingly. Furthermore, as the concept of the SGSP appears to be simple. In reality, SGSP is an extremely complex fluid system in non-equilibrium. The vast amount of natural phenomena associated with its work makes the complete explanation of the system a challenging task from the physical and the analytical perspective. In point of fact, albeit the science of each phenomenon is totally and thoroughly comprehended, connecting the phenomena and the way these phenomena tend to destabilize the system needs further investigation. This chapter aims to describe the physical concept and develop the equations required to, adequately simulate, predict and assess the thermal potential of SGSP. Furthermore, to develop the governing mathematical formulation necessary to investigate the SGSP long term operational stability issue.

In this theory chapter, the SGSP general model configuration is presented, this illustrates the features of the mathematical models that will be developed in order to simulate and predict the thermal potential of SGSP according to Libya climatology and to investigate SGSP operational stability. Firstly, the solar radiation transmission in SGSP is modelled where a system of equations is derived from which will be computed the portion of the solar radiation transmitted and

absorbed in the salinity gradient solar pond. Secondly, 1-D steady-state and 1-D transient heat and mass transfer models are developed by applying mass and energy balances over the zones of the SGSP which yielded a set of partial differential equations that governs the system. Finally, in this chapter also, in order to study the hydrodynamic behaviour of SGSP, a 2-D model is developed, the 2-D model includes equations that govern velocity, concentration, and temperature, which are linked simultaneously with an integral relationship connecting temperature and density.

3.2 Mathematical configuration

Before proceeding with theoretical modelling of SGSPs, its beneficial to explain how the system works in the first place. Once solar radiation I hits the surface of the SGSP, part of the incident, solar radiation is absorbed in the lower zone of the SGSP. The term $\tau(z)$ is the fraction of the incident solar radiation transmitted to depth z, as shown in Fig. 3.1. Thus, $I\tau(z)$ represents the solar radiation absorbed. The next section explains the development of the solar radiation model in detail.

The solar radiation absorption drives to the heating of the fluid in the LCZ. The fluid in this particular zone does not arise as the fluid overhead is less dense due to the lower salt content. Likewise, the fluid in UCZ does not sink as the fluid underneath is denser due to the higher amount of salt content. Accordingly, convection currents are suppressed, and the heat transfer from the heated lower convective zone to the cold upper convective zone solely occur via conduction, as shown in Fig. 3.1. Due to the weak thermal conductivity of water and the presence of the NCZ, which functions as natural insulation, thermal energy is confined in the lower zone fulfilling SGSPs main design concept which is to suppress convection currents via an NCZ and retain the heat at the LCZ from where the heat extraction to provide the thermal energy to applications occur. This is the ideal operational situation for a SGSP; however, heat loss could occur via convection Q_c, radiation Q_r and evaporation Q_e from the uppermost surface of the SGSP as shown in Fig. 3.1 which in return affects SGSP thermal performance [9].

It is essential to set up the configuration and features of the system, and the

mathematical model will be developed. The SGSP mathematical configuration is depicted in Fig. 3.1.

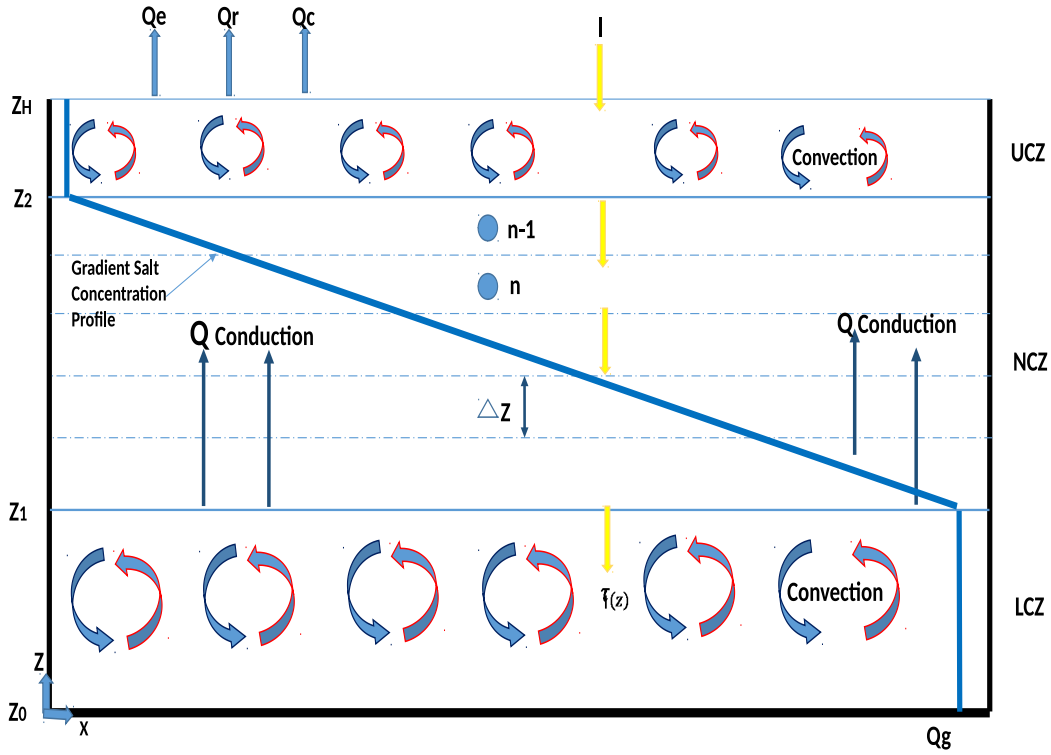

FIGURE 3.1. Salinity gradient solar pond model configuration.

The SGSP consists of three main zones, as presented in Fig. 3.1. Each zone of the three zones has different heights and salt concentration profile. Z_2 is the location of the (UCZ - NCZ interface), Z_1 is the location of (NCZ - LCZ interface), Z_0 is the bottom of the pond, and Z_H is the top surface of the SGSP. The sides of the SGSP are assumed to be well insulated.

3.3 Solar radiation model

The Sun is the most abundant source of renewable energy, and it is one of the greatest options to replace non-renewable energy sources. It is the seat of thermonuclear processes that provides an immense quantity of energy. Notwithstanding the substantial gap between the Sun and the Earth as depicted in Fig. 3.2, the significant amount of radiation emitted by the Sun and striking the Earth is still huge. This radiation is called solar energy [112].

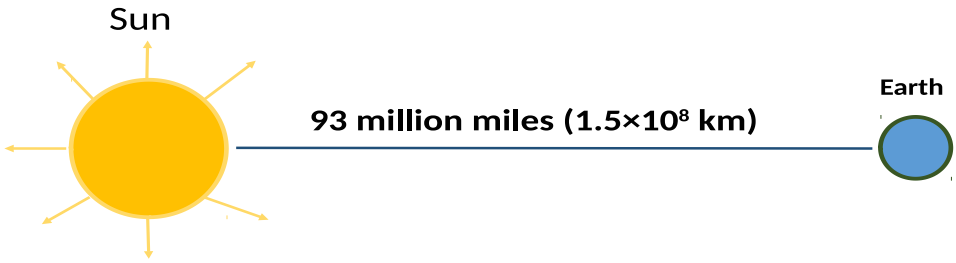

FIGURE 3.2. Sun-Earth relationship.

Therefore, solar energy can be defined as the electromagnetic wave come from the Sun. The emitted solar energy as a function of the wavelength is called the solar spectrum, which is composed of a constant emission with relatively superimposed line structures. The wavelengths range from as little as fractions of angstroms to as much as hundreds of metres as depicted in Fig. 3.3. It should be noted that solar radiation is solely the electromagnetic radiation varying in wavelength from approximately 0.2 to slightly over 3.2 μm, counting and inclusive of the near-ultraviolet UV, visible light, and near-infrared IR radiation [112].

The Sun's entire radiation yield is roughly similar to that of a blackbody at almost 5776 K. The energy radiated by the Sun travels through space until it strikes the Earth; but, approximately only 50 % of the extraterrestrial solar radiation is attenuated throughout its course to the Earth's surface. For instance, the bulk of the ultraviolet solar radiation, with wavelengths between 0.1 and 0.2 μm, is absorbed by the ozone gas available in the Ozone layer. While the ultraviolet band which is smaller than 100 A, Gamma rays and X-rays are mostly absorbed by the nitrogen and oxygen atoms available in the atmosphere. On the other hand, the infrared waves longer than 0.7μ m in wavelength, are partly absorbed by carbon dioxide gas, ozone, and water vapour available in the atmosphere [112].

Part of the solar radiation can be scattered or reflected to the sky; while the excess is received by the Earth, as shown in Fig. 3.4. The portion of the incident solar radiation that is reflected and backscattered to space is called the albedo.

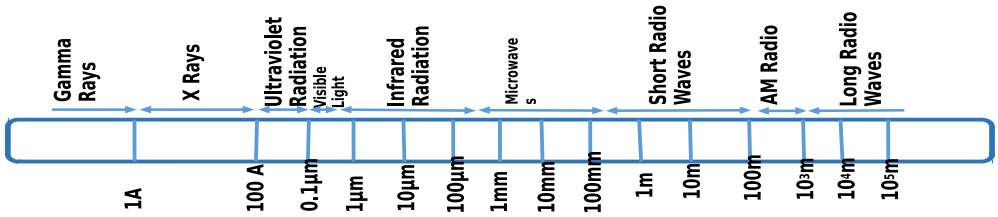

FIGURE 3.3. Electromagnetic spectrum.

The solar radiation emanating and approaching the Earth straight from the Sun and received at the surface of the Earth is termed as direct beam solar radiation. While diffuse beam solar radiation is the scattered radiation arriving from all other different directions. The total of both elements, when received on a horizontal surface, is termed as global solar radiation [112, 113].

Before proceeding with describing the behaviour of solar radiation arrival on the Earth's surface, it is crucial to explain some other common terms in this field:

Solar Constant: The whole quantity or the rate at which solar energy reaches the surface of the Earth, approximated to be 1388 W/m^2 [112].

Solar altitude angle: This angle can be defined as the angle located between the Sun's ray centre and a horizontal plane, as depicted in Fig. 3.5.

Solar zenith angle: This can be described as the angle located between the Sun's ray centre and the zenith, as presented in Fig. 3.5.

Solar energy incident on the surface of the SGSP is constituted of direct beam solar radiation element and diffuse solar radiation elements. The radiation intensity, polarization, and also the spectral composition of each component depending on the zenith angle, the azimuthal of the Sun (angle underneath zenith

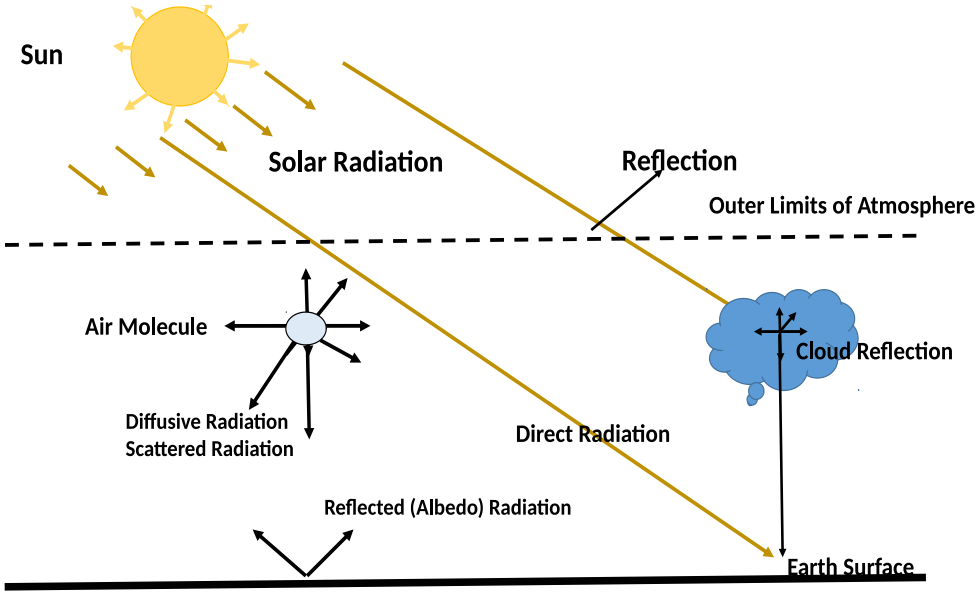

FIGURE 3.4. Solar radiation journey to the Earth.

angle as shown in Fig. 3.5), characteristics of the sky as well as the sun position [12].

3.3.1 Diffuse solar radiation

The diffuse component can be readily incorporated into the analysis of the thermal behaviour of the salinity gradient solar pond; however, since the transmission of radiation through water is so strongly dependent on wavelength, the diffuse component gives particular difficulties in the thermal analysis of SGSPs. The reason for the difficulties is that the spectral distribution of diffuse component changes dramatically with sky conditions and cloud cover. Accurate measurements of the spectral composition as a function of sky condition and angle of incidence do not yet exist, and one must make many assumptions to model the diffuse component [9]; however, Hull [9] was the first to formulate a model of the transmission of diffuse sky radiation in SGSPs. The key feature in his model is the assignment of a "colour temperature" to the diffuse component according to sky conditions as suggested by photographic handbooks. The sky condition is then correlated with the clearness index K_T so that the energy associated with the diffuse component can be calculated according to a Liu-Jordan type correlation [14, 9].

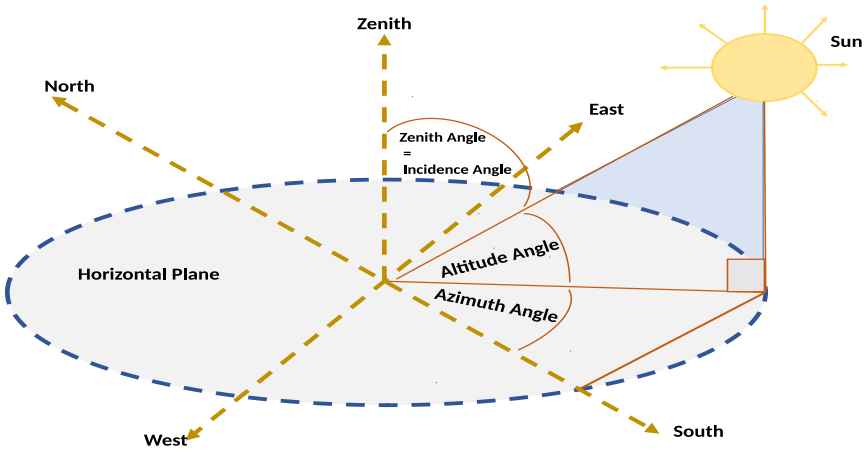

FIGURE 3.5. Earth's orbit around the sun.

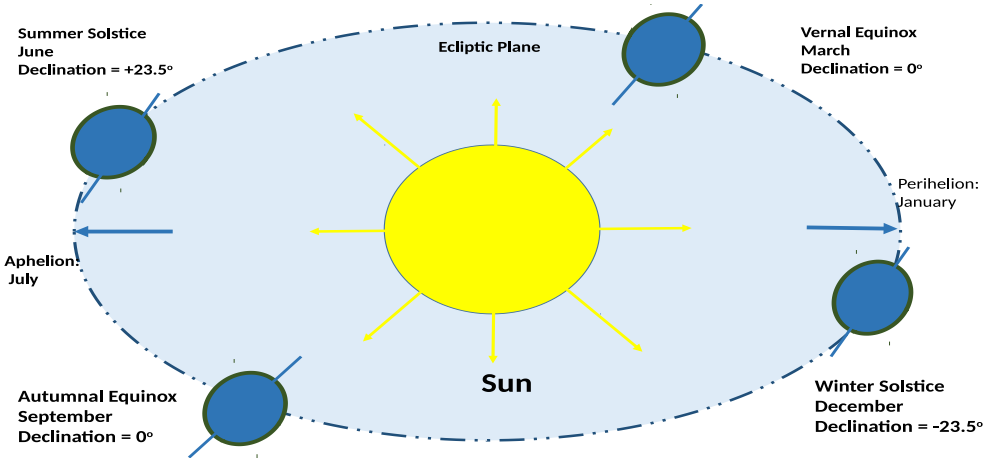

FIGURE 3.6. Sun position.

Understanding the effect of the diffuse component on the transmission function is useful for appreciating that the variations in SGSP efficiency may be anticipated to sky condition, and for recognizing the problems might be involved with calibrating underwater radiation sensors, especially those with limited spectral response range [67, 9]. However, many researchers [71, 69] have chosen to ignore the diffuse component problem altogether, arguing that the number of assumptions in any a priori estimate of the transmission function will be enormous. This is a reasonable argument, due to the uncertainty, the latter point of view is considered in this study.

3.3.2 Direct incident solar radiation

The portion of solar radiation that reaches the surface of the Earth unchanged or affected by any of the atmospheric entities is termed as a direct beam or direct solar radiation [112, 113]. This solar radiation incident on a horizontal surface (The SGSP surface) is dependent on latitude, the day, the time, and climatology. The zenith angle which is also recognized as the angle of incidence θ_i changes also with the time of the day and the year according to [9]:

$$\cos\theta_i = \cos\ La\ \cos De\ \cos(2\pi t_h/24) + \sin\ La\ sin\ De \tag{3.1}$$

in which t_h = time in hours (noon = 0), La = latitude, and De is the declination angle of the sun. De is given by the equation:

$$\sin\ De = \sin\ E\ \cos\ (2\pi/t_D\ 365) \tag{3.2}$$

with E = declination of the sun over summer season = 23° as shown in Fig. 3.6, and t_D = time in days. The time constant of the salinity gradient solar pond is big so that a value for insolation averaged over some time interval is enough to predict seasonal thermal behaviour precisely. This is fortunate because insolation measurements available are normally for hourly or daily totals of global horizontal insolation [9].

3.3.3 Arrival of solar radiation at SGSP

When a ray of solar radiation is incident at angle θ_i at the air/water interface of the SGSP, as depicted in Fig. 3.7, part of the ray is reflected back into the air at an angle θ_r, and part is transmitted into the SGSP at an angle θ_R, as depicted in the same Fig. 3.7. The angles θ_r and θ_i are equal. The reflection, transmission and absorption processes are explained in the next sections.

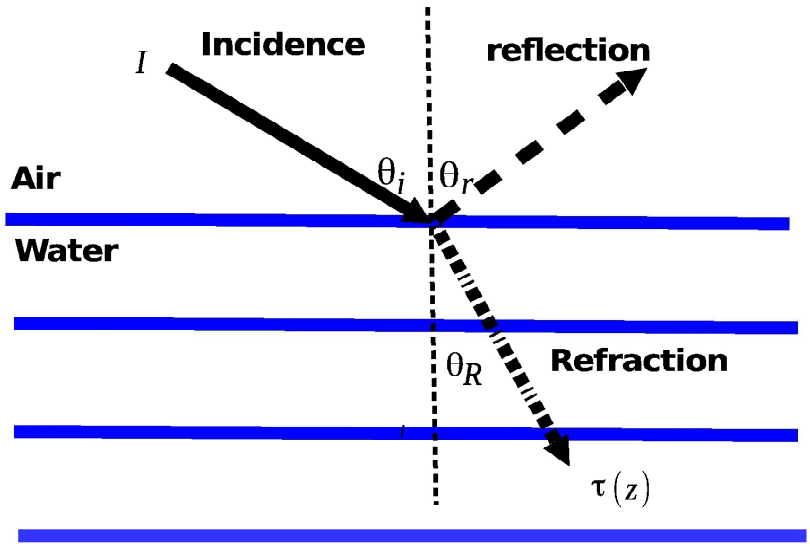

FIGURE 3.7. The distribution of the solar radiation. I represents solar intensity (Energy Flux) , where $\tau(z)$ is the fraction of the incident solar radiation transmitted to depth z. Thus, $I\tau(z)$ represents the solar radiation absorbed.

3.3.4 Solar radiation reflection

The portion of the solar radiation reflected towards the sky depends on the Sun's location and the water's surface conditions. When the water surface is stationary or just slightly turbulent, the reflection can be calculated using Fresnel's equation [112, 113]. Thus, the incident ray may be analyzed in terms of electric field vectors either perpendicular (s) or parallel (p) to the plane of incidence. The reflectance $\Re$ of the p or s component is given by Fresnel's equation as follows [114]:

$$\Re_s = \frac{\sin^2(\theta_i - \theta_R)}{\sin^2(\theta_i + \theta_R)} \tag{3.3}$$

$$\Re_p = \frac{\tan^2(\theta_i - \theta_R)}{\tan^2(\theta_i + \theta_R)} \tag{3.4}$$

The reflectance of either polarisation is minimal at small angles of incidence but approaches unity for incident rays that graze the surface. A harsh surface condition can absorb more solar radiation while a surface that is glass-like can be more reflective, though, the harsher surface can also have a little effect as

long as wind speed does not exceed 15.4 m/s [115].

3.3.5 Solar radiation transmission and absorption

The incident solar radiation part that enters through the water surface and is refracted into the water medium can be predicted by Snell's Law: The refracted angle is given by Snell's law [114]:

$$n_w \sin \theta_R = n_{air} \sin \theta_i \tag{3.5}$$

where n_w is the water reflection index, n_{air} is the air refraction index. The index of reflection depends on the solar radiation wavelength. The solar radiation travels deeper in the water depending upon the wavelength and the transparency of the water. Water pollutants can scatter and/or absorb the incident solar radiation; on the other hand, pure and transparent water enables it to progress further; consequently, the SGSP water should be sustained as transparent as possible. For solar radiation striking the water normal to the interface, $\Re = 0.020$ for $n_w = 1.33$. Thus, for any incident ray, the fraction τ_s of the radiation that penetrates the surface is [9]:

$$\tau_s = 1 - \Re \tag{3.6}$$

The air/water interface is usually assumed to be flat for calculating τ_s. When surface waves are present, the average angle of incidence is increased for nearly vertical rays, but it is reduced for nearly horizontal rays. The result is a slight increase in the reflectance for almost vertical rays plus a substantial decrease in reflectance for almost horizontal rays. Including and considering all ray directions, waves insignificantly increase the amount of time-averaged diffuse solar radiation penetrating water, but the most utmost of this increment is at significant incidence angles plus refraction for which the solar radiation penetrating the body of water has a long absorption path length. The reflectance of direct-beam solar radiation is influenced likewise by surface-waves, and the average effect will include the integral over all solar angles of elevation [9].

The solar radiation absorption process is complicated, and there is such limited accessible data on solar radiation attenuation and transmission in water. Some researchers have tried to formulate equations that govern the process in order to describe it mathematically. Nevertheless, it has been observed that the absorption of solar radiation cannot be defined and characterized by a single exponential equation [22]. As before-mentioned absorption depends on the solar radiation wavelength. For instance, the near-infrared may be absorbed within the first millimetres of the surface. And the most utmost visible light wavelengths may be absorbed within 10 metres; however, short wavelengths could progress up to 150 meters; according to available data, none reaches further than this depth, even in extremely clear and pure water [22]. Solar radiation extinction is described mathematically at a definite wavelength by applying Beer's law [112]:

$$B(\lambda, z) = B(\lambda, 0) \cdot \exp[-E(\lambda) \cdot z] \tag{3.7}$$

where, B(λ,0) represents the energy in the solar spectrum at the wavelength λ at z equals zero, (just below the free liquid surface), when z represents the optical depth or more precisely the depth in the SGSP with zero angles of incidence (sun overhead). B(λ, z) represent the energy that has been transmitted at depth z, and E(λ) represents the extinction coefficient which includes both, absorption, and scattering at wavelength λ [112, 113].

There is more than one mathematical expression has been used to predict solar radiation transmission. One of the widely used is Rabel and Nelsen [22]. Rabl and Nielsen, and according to Defant's [9] research in 1961, distributed the wavelength spectrum within 0.2 and 1.2 μm into four bands after that defined the solar radiation fraction and average extinction coefficient for each of the four bands. They assumed that water is opaque to wavelengths more significant than the infrared spectrum (1 μm) [22]. Hull developed a similar absorption function to determine the absorption coefficient and radiation fraction values in each band. Though, Hull split the radiation spectrum into 40 wavelength bands which yielded a transmission function that was almost 0.10 higher than that of the Rabel and Nelsen model. In an effort to derive a more straightforward transmission function, a 4-part transmission function was fitted to the transmission function formed by the 40- part spectrum [9, 67]. Through this, it

can be stated that Hull's method is more accurate as it has been derived from greater accuracy of 40 terms.

Furthermore, the absorption data and transmission function developed by Hull match excellently with spectral transmission measurements performed in natural lakes that contain pure water [9]. Thus, solar radiation intensity enters into the body of water decays exponentially with depth, as water layers absorb this incoming solar energy. The decay rate depends on the wavelength of the incoming solar radiation. In other words, the transmissivity is a function of the solar radiation wavelength, and the whole spectrum of wavelengths can be described in the transmission function below and as it has been illustrated in Table. 3.1 [9, 67]:

$$\tau(z) = \tau_s \sum_{i=1}^{4} S_i \exp \delta_i \left(\frac{-z}{\cos \theta_R} \right) \tag{3.8}$$

TABLE 3.1. Parameters for a four-term Hull series fit of water transmision [9]

$Wavelength$	S_i	δ_i / m
0.90-1.20	0.190	20
0.75-0.90	0.230	1.75
0.6-0.75	0.301	0.0656
0.2-0.6	0.141	0.0102

where $\tau(z)$ in the equation above represents the fraction of the incident solar radiation transmitted, θ_R is the refraction angle, S_i and δ_i represent the parameters for a four-term Hull transmission function [9].

Once the solar radiation has penetrated the air/water interface, it travels through one or more meters of water and reaches the storage zone/LCZ to provide useful heat. The smoothness of the transmission process of solar radiation within SGSP is a critical factor in SGSP thermal efficiency. In practice, the high transmission never occurs because SGSP is susceptible to the environmental changes and conditions, especially, at the surface where dust and other entities may enter the SGSP. Heavier particles quickly sink, while finer elements might stay hung for long periods. These fine elements and any other living

micro-organisms in the SGSP, absorb and scatter solar radiation moreover will degrade the transmission in the SGSP [9].

Although scattering in pure water acts a negligible role in radiation transfer, for SGSP, scattering may influence the transmission in the pond [14]. Analysis of the effects of scattering on radiation transmission in water bodies has been presented in the scientific literature [41]. For most relatively clear waters, the scattering is highly forward. And the exponential beam attenuation model discussed earlier can provide results equivalent to those from models that involve scattering. If scattering is significant so that the exponential beam attenuation models may not appropriately account for the transmission in the SGSP, consequently, SGSP efficiency will likely be too low, and water clean-up will be needed [41]. Careful pond transparency management practices can help keep the degradation to a minimum and subsequently maximize transmission and absorption. SGSP water in this study assumed to be pure and clear. Water clarity and transparency measures have been explained in chapter 2.

3.4 One-dimensional steady state model

The aim of this section is to develop a steady-state heat and mass transfer model in addition to providing a great first prediction to the thermal performance of SGSPs. The steady-state model can provide an initial indication of SGSP thermal potential as well as a physical insight into the parameters to be used for a given design.

The salinity gradient solar pond is divided into three zones; the upper convective zone, the non-convective zone and the lower convective zone as depicted in Fig. 3.1. The horizontal temperature fluctuations are deemed to be small, and consequently, negligible. Accordingly, the temperature and salt concentration distributions in the SGSP are 1-D. Mass transfer is also one-dimensional. The temperatures and density in the UCZ and the LCZ are assumed to ideally mixed, and they are uniform. In this simple model, the heat losses via the bottom are not considered, assuming insulation provided by the liner. The sidewalls of the SGSP are assumed to be insulated perfectly. The heat loses from the top via radiation Q_r and evaporation Q_e are minimal values that can be neglected in this simple model. So, the only heat losses might be considered the

one via convection Q_c from the upper convective zone; however, as the transient term is neglected in this model, the UCZ temperature is just fixed to the ambient.

Heat transfer

The vertical distribution of temperature for the SGSP, could be calculated or predicted from the steady-state heat conduction equation derived from an energy balance over the gradient zone NCZ:

$$\overbrace{k\frac{\partial^2 T}{\partial z^2}}^{\text{Conduction}} = \overbrace{I\frac{\partial \tau(z)}{\partial z}}^{\text{Radiation Absorption}} \tag{3.9}$$

The initial SGSP temperature is measured in °C, and it is equal to the ambient when starting the SGSP's operation. The first boundary is located at Z_2 (UCZ - NCZ interface) while the second boundary is located at Z_1 (NCZ - LCZ interface). At both NCZ boundaries, the heat flux is described as follow:

$$T|_{z_2} = \overbrace{T_r}^{\text{Reference Temperature (Ambient)}} \tag{3.10}$$

$$-k\frac{\partial T}{\partial z}\bigg|_{z_1} = \overbrace{I\tau_{z_0} - I\tau_{z_1}}^{\text{Solar Radiation Absorped}} \tag{3.11}$$

where T_r is the reference temperature that is equivalent to an average ambient temperature, k is the thermal conductivity of water 0.59 $\mathrm{W\,m^{-1}\,K^{-1}}$ [52], I is the average insulation in Libya = 300 $\mathrm{W\,m^{-2}}$ [37], $\tau(z)$ is fraction of I transmitted to depth z which has been mathematically described in Eq. 3.8. The vertical temperature distribution in the LCZ is uniform, and UCZ is subject to the boundary conditions above Eqs. 3.10 and 3.11. These are the boundary conditions for the heat conduction equation Eq. 3.9 which has a z dependent variation only in the NCZ. Solving Eq 3.9 analytically yields the temperature distribution equation

written below Eq. 3.12:

$$T(z) = -\frac{I}{k}\tau_s \sum_{i=1}^{4} S_i \delta_i \cos\theta_R \exp\left(-\frac{H-z}{\delta_i \cos\theta_R}\right) + T_r \tag{3.12}$$

The temperature distribution in the NCZ is for a SGSP that has a UCZ thickness of 0.4 m, NCZ thickness of 0.8 m, and LCZ thickness of 0.8 m. The thermal performance is simulated according to Libya climate, in a location within the latitude and longitude of (32.54° N, 13.11° E) [37].

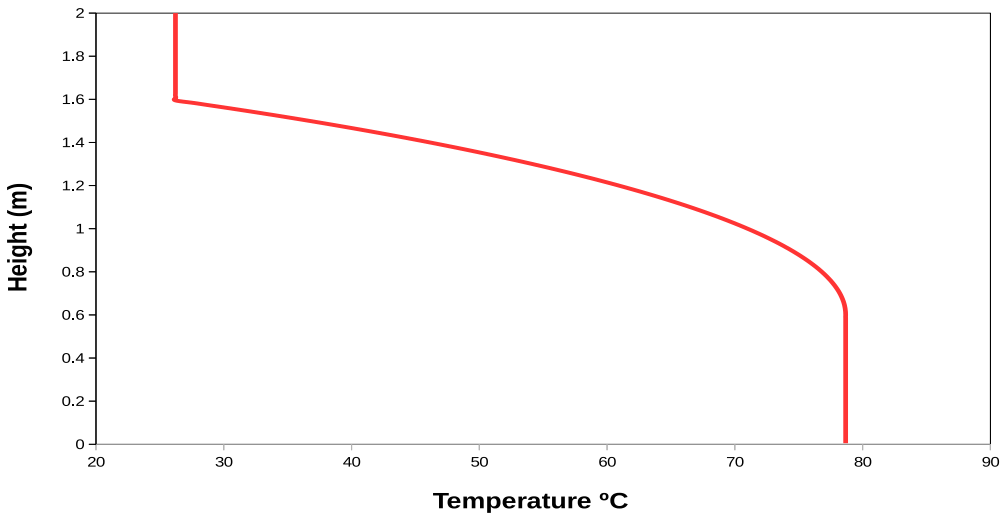

FIGURE 3.8. Temperature profile for Libya SGSP at an average solar intensity of 300 W m^{-2}, UCZ= 0.4 m, NCZ= 1.0 m and LCZ= 0.6 m.

For the given SGSP, the steady-state model has a large number of simplifying hypothesis; however, it still does its aim and provides an indication of the pond performance and behaviour. The steady-state model yielded the gradient zone temperature profile, as shown in Fig. 3.8. The temperature of the UCZ and LCZ are considered uniform. The UCZ temperature is equivalent to the ambient while the LCZ temperature is the maximum temperature obtained. The temperature distribution is given in Fig. 3.8 shows the overall thermal performance of the SGSP according to the data used.

The non-convective zone provides thermal insulation. It does not, however, act simply as an insulator with a uniform temperature gradient. Rather, the radiation it absorbs results in a temperature gradient that is non-uniform and

greater far from the surface, as shown in Fig. 3.8. The energy absorbed and conducted upward also contributes to the temperature gradient, increasing the temperature gradient at the boundary with the lower zone, and reducing heat conduction out of the lower zone, and thereby increasing and sustaining the LCZ temperature of the pond.

For the purpose of this 1-D steady-state mode, only one SGSP set-up has been considered and particular data utilized. Investigating different set-ups, different conditions, and finding the optimum design thickness ratio, which can be defined as the NCZ/LCZ thickness ratio that yields the maximum temperature will be conducted later in this thesis considering more complex models, where the transient thermal behaviour of the zone is considered. Therefore, further investigation of the SGSP thermal behaviour is to be conducted considering more complex models where transient terms are activated and a wider range of data utilized.

Mass transfer

The distribution of salt concentration C can be obtained from the equation of mass below derived from Fick's law:

$$J = \overbrace{-D\frac{\partial C}{\partial z}}^{\text{Mass Diffusion}}. \tag{3.13}$$

where J is the diffusive flux, and D = 3×10^{-9} m^{2}s^{-1} is the diffusion coefficient [33]. The boundary conditions for the mass equation are determined, considering that the LCZ is in an almost saturated state. And the salt concentration is high while the salt concentration is sustained at a low value at the UCZ. The salt concentration of UCZ C_0 = 0 kg m^{-3}, and LCZ C_1 = 300 kg m^{-3} are specified, and both layers assumed to be perfectly mixed. The UCZ and LCZ are regarded as owning infinite capacity permitting, the values of salt concentration at the boundaries of the NCZ to be fixed.

The solution of the mass equation requires the initial condition, which is the salt concentration at the UCZ and LCZ and two boundary conditions. Hence,

the first boundary condition is particularised at Z_2 and the second at Z_1.

$$C|_{z_1} = C_1 \tag{3.14}$$

$$C|_{z_2} = C_0 \tag{3.15}$$

Applying these assumptions the steady-state solution of the mas diffusion equation can be simply written as:

$$J = D\frac{C_1 - C_0}{z_1}(z_2 - z_1) \tag{3.16}$$

where z_1 and z_2 are the interfaces of the gradient layer. This equation should gives an indication of the rate at which salt is moving into the LCZ. The concentration profile is shown in Fig. 3.9 illustrates the distribution of salt in the SGSP. Steady-state models are useful as they provide an indication of the thermal behaviour of the system, but in order to further investigate the system, more complicated transient models are needed. As in this section, the time effect was neglected, which is a simplifying hypothesis. A transient model will be developed in the next section in order to study the evolution and behaviour of both temperature and concentration profiles.

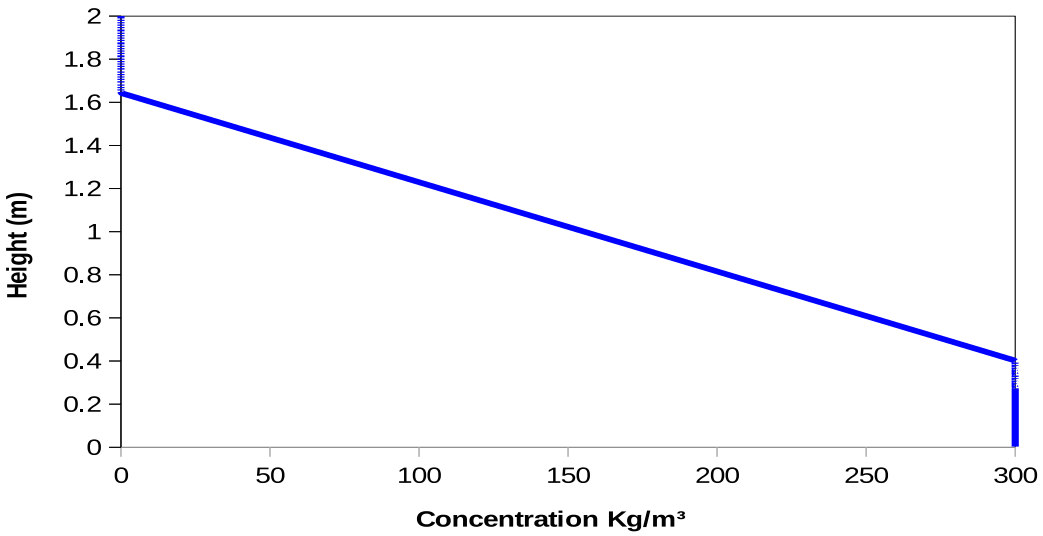

FIGURE 3.9. Vertical concentration distribution in SGSP, UCZ= 0.4 m, NCZ= 1.2 m and LCZ= 0.4 m.

3.5 Transient one-dimensional model

The use of a 1-D model to study the thermal performance and behaviour of salinity gradient solar ponds is widely adopted as SGSPs are normally built on massive scales with a wide surface area. In such salinity gradient solar ponds, the horizontal changes of temperature at a particular depth are insignificant, in comparison to the temperature changes with the depth and consequently. Thus, it is logical to consider 1-D models for predicting the temperature distribution while neglecting the end effects. In the steady-state study section, no attempt was made to describe the transient behaviour of the SGSP. This model should provide an insight to not only the thermal performance but also the thermal behaviour of the SGSP over a period of time. Which will allow simulating the thermal potential of SGSP as a source of thermal energy to drive thermal desalination units over the course of one year or even two years.

3.5.1 Heat transfer

In this section, a 1-D heat and mass transfer transient model is developed. The salinity gradient solar pond mathematical configuration is depicted in Fig. 3.1. An energy balance is carried out to all three zones of the pond.

NCZ energy balance.

The gradient layer NCZ operates like a solid transparent, insulating layer transporting the heat from the LCZ to the UCZ just via conduction. Conduction is the mechanism by which most of the heat is transferred within the SGSP. The direction of this transfer is in general, upwards from the lower convective layer to the surface through the insulating layer.

Applying energy balance over the NCZ, the general 1-D equation for temperature profile for a conducting non-convective zone that is transmitting and absorbing solar radiation is:

$$\overbrace{\rho C_p \frac{\partial T}{\partial t}}^{\text{Accumulation}} = \overbrace{k\frac{\partial^2 T}{\partial z^2}}^{\text{Conduction}} - \overbrace{I\frac{\partial \tau(z)}{\partial z}}^{\text{Radiation Absorption}} \tag{3.17}$$

where z is distance measured as positive upward, C_p is heat capacity, ρ is density, t is time, the derivative $\frac{\partial \tau}{\partial z}$ is negative so that the term $-I\frac{\partial \tau(z)}{\partial z}$ is energy flux into the medium from radiation absorbed. To solve the equation, at least two boundary conditions are needed. The two boundary conditions are derived from an energy balance over the UCZ and LCZ.

UCZ energy balance

The UCZ temperature can be derived from an energy balance of the entire upper zone. In practice, the upper zone may not have a homogeneous temperature during day time hours of high insolation; however, the temperature stratification is seldom more than a few degrees, and the approximation of a uniformly mixed upper convective zone is probably sufficient for most purposes. In a practical solar pond, the heat losses from UCZ happen via convection Q_c, radiation Q_r and evaporation Q_e. The accumulated heat in the UCZ is thermally supplied by solar irradiation absorption and also the conducted heat from the LCZ; however, a portion of this heat can be lost by the three processes mentioned.

The equation below represents the general energy balance for the UCZ where the UCZ heat losses are expressed in the right side of the equation:

$$\overbrace{Q_{sra} + Q_{cn} + Q_w}^{\text{UCZ Heat Accumulation}} = \overbrace{Q_r + Q_e + Q_c}^{\text{Heat Loss}} \tag{3.18}$$

where Q is heat flux, and the subscripts are defined as follows: sra, is the solar heat absorbed; cn, heat gained by conduction from the gradient zone; w, heat

gained from make up water; r, heat loss via radiation; e, heat loss via evaporation; c heat lost via convection. Solar heat absorbed is giving by:

$$Q_{sra} = I(\tau(H) - \tau(z_2)) \tag{3.19}$$

Note, because the energy balance is over the entire upper zone, it is only needed to know the quantities at UCZ. Heat conducted from NCZ is given by:

$$Q_{cn} = k\frac{\partial T}{\partial z}\bigg|_{z_2} \tag{3.20}$$

where k is the thermal conductivity of water. Heat obtained from make up water or rain is given by:

$$Q_w = \dot{m}_e C_p (T_w - T_{UCZ}) \tag{3.21}$$

where $\dot{m}_e$ is the rate of water addition, T_w is temperature of make-up water, T_{UCZ} is the UCZ temperature, and C_p is specific heat of water in 4.184 J Kg^{-1} K^{-1} . Q_w will be ignored as makeup water is always comes from an open water source, thus T_w = T_{UCZ} and consequently one may set Q_w = 0.

In order to predict and evaluate the temperature profile for SGSP corresponding to the accessible solar radiation and weather conditions, it is important not to underestimate the heat loss Q_{loss} to the atmosphere. Heat loss from the UCZ of SGSP is an issue, as they can deteriorate and severely affect the SGSP thermal performance. If the operator's objective is to determine the relation between UCZ and ambient temperature precisely for an operating SGSP (and the relation will vary with operating conditions, such as the amount of heat extracted and the solar input), the most straightforward procedure is to measure the temperature. Average obtained from perhaps several observations per day over the year would be entirely adequate. However, it is also possible to model the surface zone to investigate different operating conditions.

The convective heat transfer from the UCZ to the atmosphere depends mostly

on factors such as the speed of the wind in the site and the temperature difference between the atmosphere T_r and the UCZ temperature T_{UCZ}. More detailed explanation on correlations for the wind convection coefficient are reviewed by Palyvos in 2008 [116]. Eq. 3.22 is to be utilized because it can predict both free and forced (mixed) convection heat transfer and it has been also experimentally validated [117]. Moreover, Lior [117] in 1990 stated that Eq. 3.22 is the only mathematical method to predict the convection heat transfer until recently. Heat loss due to convection is given by [118]:

$$Q_c = h_c(T_{UCZ} - T_r) \tag{3.22}$$

$$h_c = 5.7 + 3.8v \tag{3.23}$$

where T_r is the reference temperature which equals the ambient temperature, h_c is convection heat transfer coefficient in W m^{-2} K^{-1}, and v is the wind speed in m s^{-1}.

Heat loss by radiation is the heat transfers between UCZ and the sky due to radiation, and it is a function of the sky temperature, the temperature of the surface and the UCZ, heat loss by radiation can be described as following:

$$Q_r = \sigma_o \epsilon[(T_{UCZ})^4 - (T_s)^4] \tag{3.24}$$

where σ_o = 5.6$\times 10^{-8}$ $Wm^{-2}K^{-4}$ is the Stefan Boltzmann constant, hemispherical emissivity of water ϵ = 0.97 [9], A is surface area, T_s is the temperature of the sky and it can be calculated using the formula sugested by Swinbank's [119]:

$$T_s = 0.0552 \quad T_r^{1.5} \tag{3.25}$$

The heat loss via evaporation Q_e [9]:

$$Q_e = h_e[C_1(T_{UCZ} - T_a) - C_2(1 - \lambda_h)] \tag{3.26}$$

where C_1 = 2.933, C_2 = 39.1150, λ_h is relative humidity that is available for any location, h_e is the evaporation heat transfer coefficient in W m^{-2} K^{-1}, and it can be calculated using the formula from [120]:

$$h_e = 8.88 - 7.82\upsilon \tag{3.27}$$

Thus, the energy balance of UCZ and also the boundary condition for the one-dimensional Eq. 3.17 for temperature T in a conducting non-convecting medium that is transmitting and absorbing radiation can be written as:

$$\overbrace{(H - z_2)\,\rho C_p \frac{\partial T}{\partial t}\bigg|_{z_2}}^{\text{Accumulation}} = \overbrace{k\frac{\partial T}{\partial z}\bigg|_{z_2}}^{\text{Heat Conducted}} + \overbrace{I(\tau(H) - \tau(z_2))}^{\text{Heat Absorbed in UCZ}} - \overbrace{Q_r + Q_e + Q_c}^{\text{Heat Loss}} \tag{3.28}$$

LCZ energy balance

For a one-dimensional heat conduction unsteady state model. The equation below represents the energy balance for the LCZ where the heat losses from the ground of SGSP are expressed in the right side of the equation:

$$\overbrace{Q_{sra} - Q_{cn}}^{\text{LCZ Heat Accumulation}} = \overbrace{Q_g}^{\text{Heat loss to ground}} \tag{3.29}$$

Solar heat absorbed is giving by:

$$Q_{sra} = I(\tau(z_0) - \tau(z_1)) \tag{3.30}$$

Note, because the energy balance is over the LCZ zone, it is only needed to know the quantities at LCZ. Heat conducted from LCZ is given by:

$$Q_{cn} = -k\frac{\partial T}{\partial z}\bigg|_{z_0} \tag{3.31}$$

The work could be generated is given by:

$$\Delta w = \dot{m}Cp\Big((T_h - T_c) - T_C \quad \ln(\frac{T_H}{T_C})\Big) \tag{3.32}$$

Most of the heat loss from the LCZ happens through the bottom and the sides when the SGSP is not insulated properly with a high-quality liner, depending on the SGSP surface area and the type of the soil, i.e., the heat loss from the bottom can be larger when the SGSP surface area is enormous while in a small surface area SGSPs, the sidewalls may form the main and most significant heat loss. The distance between the bottom of the SGSP and the underground water can also affect the amount of heat loss from the bottom; a small distance drives to more heat exchange between the underground water and the LCZ. This heat exchange is also influenced by soil type, as dry soil can insulate better than wet soil as illustrated in Table. 3.2. Wang and Akbarzadeh [95] investigated ground heat loss in wet soil, and they advised that the SGSP should always be well insulated, especially when the groundwater level is near to the bottom of the SGSP. Davis and his group [121] affirmed; except that if the bottom of the SGSP is well insulated, around 20% of the SGSP heat could be lost to the ground.

TABLE 3.2. Measured values of different soils [9]

Material	Thermal conductivity W m^{-1} K^{-1}	Thermal diffusivity m^2 s^{-1}	Density kg m^{-3}	Specific heat J Kg^{-1} K^{-1}
Dry soil	34-68	175-260	NA	NA
Wet mud	176	190	1.5	0.6
Sandstone	545	980	2.6	0.12

Heat loss to the ground is given by [122]:

$$Q_g = k_g \left|\frac{\partial T}{\partial z}\right|_{z_g} \tag{3.33}$$

where k_g is the thermal conductivity of the ground W m^{-1} K^{-1}, T is temperature distribution through the lower convective zone in °C at time t and height z

measured from the top of the pond and z_0 is the (LCZ and ground interface).

The information above considering heat loss to the ground is just for reference and to show the importance of perfect insulation via high-quality liners. Today 2019, due to the advancement in liners technology and the dry nature of Libyan soil and far distance of the water table depth, in the present study the SGSP is assumed to be always perfectly insulated from the bottom via a high-quality liner.

The heat loss from the surface and bottom of the SGSP have been discussed in detail, there are other forms of heat loss which are the sides heat losses, these kinds of losses have been neglected as they are minimal, and with proper insulation, this kind of heat loss can be avoided. So the only heat losses considered are the major ones which are the ones from the top of the SGSP.

The energy balance of LCZ and also the boundary condition for the one-dimensional Eq. 3.17 in a conducting non-convecting zone that is transmitting and absorbing radiation can be written as:

$$\overbrace{(z_1)\ \rho C_p \frac{\partial T}{\partial t}\bigg|_{z_1}}^{\text{Accumulation}} = \overbrace{-k\frac{\partial T}{\partial z}\bigg|_{z_1}}^{\text{Heat Conducted}} + \overbrace{I(\tau(z_1)-\tau(z_0))}^{\text{Heat Absorbed in LCZ}} \tag{3.34}$$

The solution of NCZ equation Eq. 3.17 need initial and also two boundary conditions. The initial condition, in this case, is the ambient temperature which is the initial SGSP temperature when starting the SGSP operation. The first boundary condition is defined at z_2 (UCZ - NCZ interface) which is governed by Eq. 3.28 while the second boundary condition is defined at z_1 (NCZ - LCZ interface) which is governed by Eq. 3.34.

3.5.2 Mass transfer

This section aims to develop the mathematical formulation necessary to simulate the SGSP solutal behaviour adequately. The mass transfer model will help to provide an insight into the solutal behaviour in SGSPs. In the mass transfer model, the total system mass in control volume is constant. The mass transfer

process occurs due to molecular diffusion. In this model, it has been assumed that the mass transfer process and thermal processes are independent. According to Fick's law of diffusion, (J) which is the diffusion flux is related to density gradient this time by [101].

$$J = -D\frac{\partial C}{\partial z} \tag{3.35}$$

Assuming a constant D, the mass diffusion equation that represents the concentration profile can be written as:

$$D\frac{\partial^2 C}{\partial z^2} = \frac{\partial C}{\partial t} \tag{3.36}$$

where C reperesents salt concentration in kg m^{-3}, the salt water (brine) diffusion coefficient, D = 3$\times$10^{-9} m^{2}s^{-1} [33].

The mass diffusion equation solution requires an initial condition which is the mass of salt at the UCZ and LCZ with linear density gradient at the NCZ and two boundary conditions; applying mass balance. The first boundary condition is defined at z_2 (UCZ - NCZ interface) while the second boundary condition is defined at z_1 (NCZ - LCZ interface).

Applying a simple mass balance over the upper convective zone yields the first boundary condition:

$$-D\frac{\partial C}{\partial z} = \left.\frac{\partial C}{\partial t}\right|_{z_2}(H - z_2), \quad (z = z_2, t > 0). \tag{3.37}$$

Applying mass balance over the lower convective zone yields the other boundary condition:

$$-D\frac{\partial C}{\partial z} = \left.\frac{\partial C}{\partial t}\right|_{z_1}(z_0 - z_1), \quad (z = z_1, t > 0). \tag{3.38}$$

The salt density gradient occurring due to salt concentration variance magnitude in a SGSP is described as a positive gradient because it leads to creating the required gradient profile for the NCZ, i.e. the salt gradient is concentrated

downward. In the proposed 1-D model, the system total mass in the particular control volume is constant; also, the mass transfer process is simply the consequence of molecular diffusion process, and the heat transfer and the mass transfer processes are considered to be completely independent. According to these assumptions, the 1-D transient mass diffusion numerical study will be carried out.

SGSP can not function without a stable concentration profile. However, salt in water tends to diffuse from high concentration regions to regions at lower concentrations. In the case of SGSP, it is from the bottom of the SGSP to the surface. If to consider the diffusion scenario, which is inevitable, although, this might happen slowly over time if continuously, such behaviour will de-homogenize the pond in the long run [9], this diffusion will result in mixing. Thus, the SGSP will also become hydro-dynamically unstable. One-Dimensional Models can not address SGSP hydrodynamic instability. They can not describe velocity fields and the movement of the fluid, as it requires at least two dimensions to occur. Subsequently, developing a two-dimensional and conducting a 2-D study is required.

3.6 Transient two-dimensional model

The One-Dimensional steady-state and transient models provide a great insight into SGSP thermal and solutal behaviour. However, they can not address SGSP hydrodynamic and operational stability. They can not describe velocity and convection, as it requires at least two dimensions to occur. Consequently, a fully coupled two-dimensional model is needed. In this section, the physical concept and hydrodynamics are explained; moreover, the mathematical formulation necessary to describe the behaviour of a fully coupled system is developed.

Before proceeding with the mathematical formulation of the 2-D model. It is beneficial to start with describing the nature of the fluid behaviour inside SGSPs. Assume that cold freshwater over hot salty water as shown in Fig. 3.10, the fluid relocated vertically downwards absorbed heat by diffusion, and so overshoots when rising to the surface. This drives to an oscillation of growing amplitude, or in other terms an oscillatory instability. Both sorts of diffusion

(Heat and Mass) can contribute to the motion, and the mixing happens inside SGSPs.

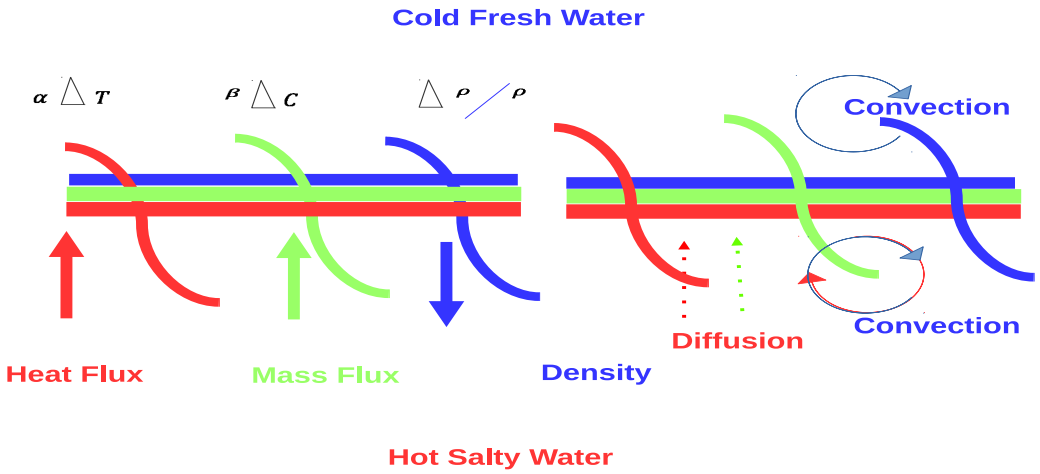

FIGURE 3.10. Double diffusive convection.

In the previous analysis (1-D steady-state and 1-D transient), the velocity fields were completely neglected where a uniform salinity and temperature profiles and fixed zone thickness were assumed. These were simplifying hypothesis as there should be a motion of the fluid resulted directly or indirectly from the effect of double-diffusive convection which is the fluid dynamics phenomenon which defines a particular pattern of convection induced and generated by two different density gradients, that also have varying rates of diffusion as shown in Fig. 3.10.

It is understood that diffusion is the motion of a particle or a molecule from a region of high concentration to another region with lower concentration. While convection is mainly generated due to density differences influenced by the impact of gravity. The difference in density can be created because of gradients in the fluid composition, or due to variations in concentration or temperature created by differences in β_C and β_T. Compositional gradients and thermal gradients usually diffuse with time, lessening their capability to stimulate convection, and consequently for convection to occur and continue, gradients in other areas of the flow have to exist [107].

A mathematical model to further investigate the thermal behaviour, hydrodynamic behaviour and operational stability of the SGSP is developed in the present section; the model includes the equations that govern the system, the governing equations are for velocity, concentration and temperature, as well as a constitutive association of temperature and density. The compressible Navier Stokes explains the velocity correctly many physical applications; however, these equations are challenging to study analytically or even to integrate numerically; thus, they could be avoided when there is no substantial deviation for density field from hydrostatic equilibrium as the situation in SGSPs. Pressure-driven flows that posses weaker density differences could surely be approximated as having almost constant densities, utilizing the incompressible Navier Stokes equations.

The Navier-Stokes is a vector equation derived by applying Newton's Law of Motion to a fluid element and is also termed as the momentum equation. It is supplemented by the continuity equation, a mass conservation equation, and the energy equation. It is assumed that the fluid inside the SGSP is Newtonian and incompressible. All properties of salt and water mixture inside the SGSP are considered constant, except in buoyancy-driven flows, as density changes cannot be completely neglected as they generate motion as it has been mentioned earlier. Thus, the ideal compromise is to apply the Boussinesq approximation, which has been considered in this numerical study. The Boussinesq approximation was first suggested by Joseph Boussinesq (1842-1929). Buoyancy-driven flow, the density changes could be ignored everywhere in the equation of momentum apart from the gravitation term. The Boussinesq approximation has been widely employed in order to simplify the Navier-Stokes equations. The model first-order derived from Boussinesq approximation for density variation with temperature amounts to, Eq. 3.40 [20]:

$$\rho = \rho_r \Big[1 - \beta_T (T - T_r) + \beta_C (C - C_r)\Big] \tag{3.39}$$

where ρ_r, T_r, C_r are reference density, temperature and salt concentration respectively, β_T is thermal expansion coefficient and β_C is salinity expansion coefficients.

The equation below represents the gravitational force per unit mass on the fluid [72]:

$$\mathbf{f} = \Big[1 - \beta_T(T - T_r) + \beta_C(C - C_r)\Big]\mathbf{g} \tag{3.40}$$

The velocity, temperature, and concentration variation are solely considered in x and z directions. Consequently, the velocity, temperature, and concentration distributions in the SGSPs are 2-D. And the assumption is that density changes are only considered in the buoyancy force. Thus, mass conservation for water and species (i.e., continuity and convective-diffusive equations), momentum (i.e., Navier-Stokes), and energy conservation equations are coupled with the density of the fluid, assumed to be linear with temperature and salinity. These equations can be written as:

3.6.1 Continuity equation

The continuity equation is developed simply by employing the law of conservation of mass for a volume element within flowing fluid. Most fluids and so water are incompressible; consequently, their densities are constant considering a wide range of flows. Since the density of the fluid is constant and incompressible flows must satisfy the constraint:

$$\nabla \cdot \mathbf{v} = 0 \tag{3.41}$$

3.6.2 Momentum equation

The equation of momentum is a description of Newton's second law; it correlates the entirety of the forces acting upon a fluid element to its acceleration or more precisely to its rate of change of momentum. Since the density of the fluid is constant, incompressible flows must satisfy the constraint:

$$\frac{\partial v_x}{\partial t} + \mathbf{v} \cdot \nabla v_x - \nu \nabla^2 v_x = -\frac{1}{\rho_r}\frac{\partial P}{\partial x} \tag{3.42}$$

$$\frac{\partial v_z}{\partial t} + \mathbf{v} \cdot \nabla v_z - \nu \nabla^2 v_z = -\frac{1}{\rho_r}\frac{\partial P}{\partial z} - \Big[1 - \beta_T(T - T_r) + \beta_C(C - C_r)\Big]g \tag{3.43}$$

where ν is kinematic viscosity $\mathbf{v}$ is velocity, (x,z) are Cartesian coordinates, and P is the pressure. At the bottom and the surface of the SGSP, a zero flux of mass is imposed. The boundary conditions for the continuity and momentum equations at the bottom of the SGSP are:

$$V_x = 0 \quad V_z = 0, \quad at \quad z = 0 \tag{3.44}$$

Therefore, the bottom of the pond is impermeable, which physically indicates using a high-quality liner. The boundary conditions the continuity and momentum equations at the top surface of the salinity gradient solar pond are:

$$V_z = 0, \quad V_x = 0, \quad at \quad z = H \tag{3.45}$$

where H is the height of the SGSP and is taken as a reference for the spatial coordinate z.

3.6.3 Energy equation

$$\frac{\partial T}{\partial t} + \mathbf{v} \cdot \nabla T - \alpha \nabla^2 T = \frac{I}{\rho C_P} \frac{\partial \tau(z)}{\partial z} \tag{3.46}$$

The boundary condition for the thermal energy equation at the bottom of the SGSP is:

$$\frac{\partial T}{\partial z} = 0 \quad at \quad z = 0 \tag{3.47}$$

Which indicates a complete insulation to the bottom of the SGSP. The boundary condition for the thermal energy equation at the top surface of the SGSP is:

$$-\hat{\mathbf{n}} \cdot (\alpha \nabla T) = h(T - T_r) \quad at \quad z = H \tag{3.48}$$

where α is thermal diffusivity and the term with $-\hat{\mathbf{n}}$ is a vector that is normal to top surface points outwards from the pond, all these assumptions which do not

modify the principles of the system will be considered in the numerical study part of the thesis for simplifying the analysis.

TABLE 3.3. Illustrates, parameters, units and values of all parameters in the dimensional equations [72, 123, 9].

Dimensional Equation Parameters	
Term (symbol)	Value
Solar intensity (I)	300 W m^{-2}
Thermal diffusivity (α)	1.2 $\times 10^{-6}$ m^2 s^{-1}
Thermal Expansion Coefficient (β_T)	5.24 $\times 10^{-4}$ K^{-1}
Diffusion Coefficient (D)	3.39 $\times 10^{-9}$ m^2 s^{-1}
Solutal Expansion Coefficient (β_C)	6.82 $\times 10^{-3}$ (Wt Pct)$^{-1}$
Gravitional acceleration (g)	9.8 m s^{-2}
Kinematic Viscosity (ν)	1.8 $\times 10^{-6}$ cm^2 s^{-1}

3.6.4 Mass equation

$$\frac{\partial C}{\partial t} + \mathbf{v} \cdot \nabla C = D \nabla^2 C \tag{3.49}$$

There is no loss of salt from the bottom of the pond, thus, the boundary condition for the mass equation at the bottom of SGSP is:

$$\frac{\partial C}{\partial z} = 0 \quad at \quad z = 0 \tag{3.50}$$

Boundary condition for the mass equation at the top surface of the SGSP is:

$$\frac{\partial C}{\partial z} = 0 \quad at \quad z = H \tag{3.51}$$

The boundary condition for the mass equatin can also be written as:

$$-\hat{\mathbf{n}} \cdot \nabla C = 0 \tag{3.52}$$

Thus, both the sidewalls and the bottom of the SGSP are considered to be well insulated with high-quality liners. Thus, no salt or heat leakage from the SGSP. And the solar radiation that enters the SGSP is completely absorbed.

3.6.5 Dimensionless analysis

The dimensional equations Eqs. 3.41 - 3.49 of continuity, momentum, heat and mass which were described in chapter 3 are written in a non-dimensional form. In the non-dimensional analysis performed, a non-dimensional value (or more accurately, a value with the dimensions of 1) is a value that has no real physical units and consequently a real number. Such a value is typically described as an output or ratio of values that do have physical units, in a way where all the units cancel out [124].

In order to analyse the system behaviour and find the characteristic quantities. The following dimensionless groups are defined:

$$A = \frac{W}{H}, \quad \theta = \frac{T - T_r}{\Delta T}, \quad \varphi = \frac{C - C_r}{\Delta C}, \quad P = \frac{pH^2}{\rho_r \alpha^2}, \quad \mathbf{V} = \frac{\mathbf{v}H}{\alpha},$$
$$t = \frac{\alpha t}{H^2}, \quad X = \frac{x}{H}, \quad Z = \frac{z}{H}$$

where $\mathbf{V}$ is dimensionless velocity components (note that no attempt was made to describe velocity in the 1-D study), θ is dimensionless temperature, φ is dimensionless concentration, P is dimensionless pressure and t is the dimensionless time of heating. A represents the aspect ratio, X is the dimensionless horizontal coordinate which also corresponds to the width W width of the SGSP, Z is the dimensionless vertical coordinate that represents the height H of the SGSP, ΔT and ΔC are dimensional temperature difference and salt concentration difference, respectively. The dimensional equations Eqs. 3.41 - 3.49 are written in a non-dimensional form as follow:

Continuity and momentum equations

$$\nabla \cdot \mathbf{V} = \mathbf{0} \tag{3.53}$$

$$\frac{\partial V_x}{\partial t} + \mathbf{V} \cdot \nabla V_x - Pr\nabla^2 V_x = -\frac{1}{\rho_r}\frac{\partial P}{\partial X} \tag{3.54}$$

$$\frac{\partial V_z}{\partial t} + \mathbf{V} \cdot \nabla V_z - Pr\nabla^2 V_z + \frac{\partial P}{\partial Z} = PrRa_T(\theta - N\varphi) \tag{3.55}$$

where Pr is the Prandtl number, and N is the buoyancy ratio, see Table. 3.4 for the mathematical definitions of these parameters. The boundary conditions on the vertical walls of the salinity gradient solar pond are $\mathbf{V}$ = 0. The boundary conditions for the continuity and momentum equations at the bottom of the SGSP are:

$$V_x = 0 \quad V_z = 0, \quad at \quad Z = 0 \tag{3.56}$$

Therefore, the bottom of the pond is perfectly insulated, which physically indicates using a high-quality liner. The boundary conditions for the continuity and momentum equations at the top of the salinity gradient solar pond are:

$$V_z = 0, \quad V_x = 0, \quad at \quad Z = 1 \tag{3.57}$$

where 1 is the dimensionless height of the SGSP which corresponds to 2 m dimensional height and is taken as a reference for the spatial coordinate Z.

Energy equation

$$\frac{\partial \theta}{\partial t} + \mathbf{V} \cdot \nabla \theta - \nabla^2 \theta = \frac{Ra_I}{Ra_T}\frac{\partial \sigma}{\partial Z} \tag{3.58}$$

$$\sigma = \tau_s \sum_{i=1}^{4} S_i \quad \phi \quad exp\Big[- \phi(1 - Z)\Big] \tag{3.59}$$

where σ represents the dimensionless transmission approximation $\tau(z)$ and ϕ equals $\frac{\delta_i}{\cos\theta_R(H)}$. The boundary conditions on the vertical sidewalls of the salinity gradient solar pond are θ = 0. The boundary conditions the energy equation at the bottom of the SGSP are:

$$\frac{\partial\theta}{\partial Z} = 0, \quad at \quad Z = 0 \tag{3.60}$$

Therefore, the bottom of the pond is perfectly insulated, which physically indicates using a high-quality liner. The only heat loss from the SGSP is the heat loss from the top surface to the atmosphere via convection. The boundary conditions for the energy equation at the top surface of the salinity gradient solar pond are:

$$\frac{\partial\theta}{\partial Z} = -Bi\theta, \quad \theta = 0 \quad at \quad Z = 1 \tag{3.61}$$

where Bi is Biot number, it is a non-dimensional heat transfer coefficient quantity used in heat transfer calculations. It provides a simplistic ratio index of the heat transfer resistances within and at the surface of a body of fluid.

Mass equation

$$\frac{\partial\varphi}{\partial t} + \mathbf{V}\cdot\nabla\varphi = \frac{1}{Le}\nabla^2\varphi \tag{3.62}$$

where Le is Lewis number. The boundary conditions for the mass equation at the bottom boundary of the SGSP is:

$$\frac{\partial\varphi}{\partial Z} = 0, \quad at \quad Z = 0 \tag{3.63}$$

The boundary conditions on the sidewalls of the salinity gradient solar pond are φ = 0. While the boundary conditions for the mass equation at the top of the salinity gradient solar pond are:

$$\frac{\partial\varphi}{\partial Z} = 0, \quad -\hat{\mathbf{n}}\cdot(\frac{1}{Le}\frac{\partial\varphi}{\partial Z}) = 0 \quad at \quad Z = 1 \tag{3.64}$$

where $-\hat{\mathbf{n}}$ is a vector that is normal to top surface points outwards from the pond and the term $-\hat{\mathbf{n}}.(\frac{1}{Le}\nabla\varphi)$ = 0 on the boundaries due to no flux directed at

that area.

TABLE 3.4. Illustrates, the mathematical definetions of the dimensionless equations parameters [124, 72, 125].

Term (symbol)	Definition
Schmidt Number (Sc)	$\frac{\nu}{D}$
Prandtl Number (Pr)	$\frac{\nu}{\alpha}$
Lewis Number (Le)	$\frac{Sc}{Pr}$
Biot Number (Bi)	$\frac{hH}{k_w}$
Buoyancy ratio (N)	$\frac{\beta_C \Delta C}{\beta_T \Delta T}$

The dimensionless parameters in the governing equations can be divided into two groups; (I) Dimensionless parameters that characterize material properties of the fluid, (II) Dimensionless parameters or characteristic quantities that characterize the fluid flow and consequently the salt gradient solar pond hydrodynamic behaviour. Table. 3.4 illustrates the mathematical definition of these parameters.

If the double-diffusive convection consequences are critical, then the relative balance between temperature and concentration can play a role in SGSP stability. The effect of DDC on SGSP operational stability and the measures that could be taken to minimize this effect will be investigated in chapters 5 and 6.

3.7 Summary

In this chapter, the mathematical configuration of the SGSP is presented where the SGSP divided into three zones with different heights and salt concentration profiles. Other features, such as areas of potential heat loss, are also shown. This mathematical configuration will be referred to throughout the thesis.

The solar radiation transmission model is developed where the physical concept and mathematical formulation necessary to adequately predict the solar radiation transmission in SGSP are introduced. The obtained solar radiation transmission function will be used in all the studies conducted in this thesis.

A 1-D steady-state and 1-D transient heat and mass transfer models are developed by applying mass and energy balances over the zones of the SGSP which yield a number of nonlinear partial differential equations. The developed 1-D Model in this chapter will be used to numerically investigate the thermal potential of salinity gradient solar pond as a source of thermal energy for thermal desalination applications according to the geographical and climate conditions of Libya. Previous studies might provide an insight into SGSP performance; however, the current development in thermal desalination units necessitates a new assessment of the potential of SGSP as a source of thermal energy for desalination applications. According to the reviewed experimental and theoretical work in Chapter 2, SGSPs, by their nature, appear to exhibit a surprising degree of site-specific behaviour and various thermal performances. Consequently, one must accurately assess and evaluate each potential SGSP, and the associated application of the SGSP heat according to its merits. The 1-D study, considering Libya climatology, will be presented in chapter 4.

A 2-D model is developed where the physical model and governing equations are presented after the problem of hydrodynamic, transient heat and mass transfer in the SGSP is formulated using a dimensional and dimensionless forms of Navier Stoke equations. To the best of the author's knowledge, studies that fully explain how SGSP becomes hydro-dynamically unstable have not been conducted. In particular, how, when, and where convection current start to form to damage the gradient (non-convective zone) have not been explained nor have the transient behaviour of the fluid been simulated in great detail. Thus, the 2-D model developed in this chapter will be utilized to investigate the hydrodynamic instability of SGSP by (I) Investigating the hydrodynamic behaviour of the transient fluid flow developed in the UCZ, NCZ, and LCZ during the collection and the storage of energy in the presence of the DDC effect, (II) Investigating the changes that occur to the zones during operation due to the DDC effect and answering the questions of how and where convection currents start to form in the non-convective zone, (III) Comparing the thermal performance of the 1-D SGSP where the SGSP is assumed to be stable and the

2-D model where the SGSP is subject to the DDC effect. The 2-D study will be presented in chapter 5.

Finally, to the best of the author's knowledge, a design key question like, what the optimum (Best thermal performance and longest term of stability) zones thickness ratio has never been answered in sufficient detail considering the DDC effect. Thus, a numerical study to investigate the optimum (best thermal performance and long term stability) NCZ: LCZ thickness ratio will be conducted utilizing the 2-D model developed in this chapter. The effect of zone thicknesses, buoyancy ratio and heat recovery 2-D studies will be presented in chapter 6.

Chapter 4

1-D transient heat and mass transfer study

4.1 Overview

In chapter 2, the concept, design and construction of SGSPs are explained. The previous pertinent experimental and theoretical work is reviewed, and the current operation challenges are identified. In chapter 3, the solar radiation transmission inside the SGSP is modelled, and the mathematical formulations necessary to adequately predict and investigate the thermal potential and operation of SGSP are developed. Hence, previous 1-D studies provide an insight into SGSP thermal performance, the fact that SGSP is not off the shelf technology, and with the current development in thermal desalination units necessitates a new assessment to the potential of SGSPs as a renewable source of thermal energy for desalination applications. Recently, it has been reported in the literature that Multi-effect thermo-vapour compression desalination units were operated at lower top brine temperature of 60-65 °C [49, 50]. This chapter aims to predict the thermal performance and potential of salinity gradient solar pond as a source of thermal energy under Libya geographical and climate conditions.

Consequently, in this chapter, the features of the proposed SGSP physical model are presented. The governing equations and the assumptions that are considered to investigate the thermal performance of the proposed SGSP are introduced. The numerical method adopted to solve the governing equations of the system is explained. The generation of the mesh, the discretisation of the governing equations, the logic of the programming code and the general logic flow of the computer model are all illustrated. Moreover, the numerical code precision in simulating the thermal performance is compared and validated with

an experimentally measured temperature data obtained from Granada and El Paso salinity gradient solar ponds which were already reviewed in chapter 2.

The numerical study results for the proposed SGSP are then presented, where (I) The thermal performance is examined under different zone thickness ratios where the SGSP is run for the same average solar intensity and the same period for all thickness ratios. Consequently, the generated temperature profiles are plotted against the height of the SGSP. Accordingly, a zone thickness ratio that has the best thermal performance (highest LCZ temperature) is identified. Furthermore, (II) The thermal and solutal behaviour of Libya SGSP is assessed and studied in more detail in order to understand how both the temperature and the concentration profiles evolve with time. (III) The heat recovery from SGSP is studied where the integration potential of different desalination plants is assessed, and the thermal potential of SGSP being a consistent thermal energy supply for low-grade heat thermal desalination units is evaluated. Finally, a summary of the chapter is presented.

4.2 Physical model and governing equations

This section provides an insight into the proposed SGSP model configuration. This section also highlights the governing equations of the system and introduces the assumptions that are made to perform this study.

4.2.1 Physical model

The proposed SGSP is located in Tripoli, Libya within a latitude and longitude of 32.54° N, 13.11° E. The SGSP is divided into three zones, UCZ, NCZ and LCZ as depicted in Fig. 3.1. The UCZ thickness is maintained as small as 0.4 m in order to minimise heat losses to the atmosphere and to reduce the effect of wind erosion at the surface. Chapter 2 explains in detail the underpinning logic of choosing this particular height for the UCZ. The upper convective zone of the proposed SGSP is assumed to be susceptible to heat losses via convection only, as convection represents the most significant heat loss from the UCZ. For the NCZ and the LZC thicknesses, different NCZ: LCZ zone thicknesses ratio are

to be examined as there is no definite optimum zone thicknesses ratio for those zones in the literature.

The shape of the SGSP is another debatable subject. Dehghan et al. [62] demonstrated in his experiment that, for a large surface area SGSP, circular-shaped SGSPs have better thermal performance than square-shaped SGSPs. This advantage is mainly associated with the smaller heat losses from sidewalls and linked to, the fewer edges and bends per unit area of the circular-shaped SGSPs [62]. In practice, small surface area SGSPs (of less than 500 m^2) are recommended to be circular-shaped, while larger SGSPs can be either rectangular-shaped or circular-shaped, as the heat losses via their sidewalls will be less significant and critical than those happening in small SGSPs.

Due to the advancement in liner technology and the high-quality liners available today (E.g. Nylex Millennium polypropylene liner, see, chapter 2). In this particular study, the sidewalls and the bottom surface of the SGSP are assumed to be perfectly insulated, hindering any heat loss. Consequently, the solar radiation reaching the lower convective zone is effectively absorbed.

4.3 Numerical method

This section deals with the numerical method. In this sections, the finite volume method is explained, the discretisation of the governing equations is performed, the logic flow of the computer model is introduced, and a validation study to assess the precision of the developed code is also performed.

4.3.1 Finite volume

The finite volume (FVM) is a discretisation method for partial differential equations, particularly those that originate from physical laws of conservation. The finite volume method applies a volume integral formulation of the problem with a finite partitioning set of volumes to perform the discretisation of the equations. The method is in wide use for discretising computational fluid dynamics equations [126].

The utilisation of the finite volume method, mesh generation and the general form of finite volume method discretisation are explained in detail in the next sections.

4.3.2 Mesh generation

In order to use the finite volume method, the domain of the solution should initially be divided into non-overlapping polyhedral cells or elements, as shown in Fig. 4.1a. A solution domain is divided or distributed in such a way the final pattern or form is commonly defined as a mesh. A mesh includes faces, vertices and cells, as shown in Fig. 4.1a.

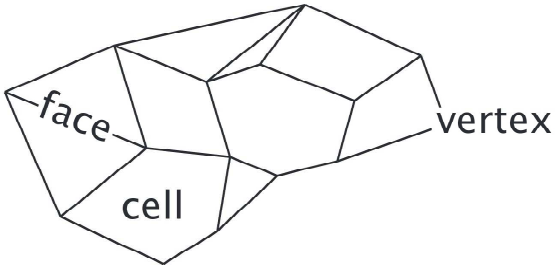

(A) A mesh consists of cells, faces and vertices.

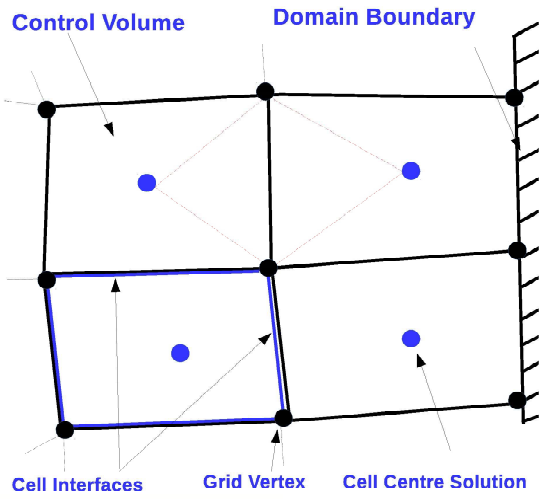

(B) Cell centred finite volume method.

FIGURE 4.1. A mesh consists of cells, faces and vertices. The divider between two cells is termed as a face at all of the dimensions]A mesh consists of cells, faces and vertices. The divider between two cells is termed as a face at all of the dimensions [127, 128].

In the finite volume method, variables are averaged over control volumes CVs. Furthermore, these control volumes are characterised and defined by the cells' centres. In the cell-centred CC-FVM shown in Fig. 4.1b, the control volumes are shaped by the cell of the mesh with the centre of the cell, saving the average variable value in the control volume.

The face fluxes are approximated using the variable values in the two adjacent cells surrounding the face. This low order approach has the benefit of being

effective and demanding low bandwidth matrices (the bandwidth is equal to the number of cell neighbours plus 1) and consequently, the low requirement for storage. Nevertheless, the mesh topology is bound because of conjunctionally and orthogonality requirements. The value at a face is considered to be the average value over the face. On an unstructured mesh, the face centre might not occupy the place on the line connecting the centres of the CV, which will, in return, drive to an error in the face interpolation. FiPy currently utilises the CC-FVM which is used in this study [127, 128].

Before preceding with the programming code and the logic flow of the computer model. For more clarification to the numerical method, the discretisation of the heat conduction equation that governs the heat transfer inside the SGSP is explained. The same concept and numerical method are used to discretise the mass equation.

4.3.3 Discretization of governing equations

The initial step to discretize the governing equatoin Eq. 3.17 using the CC-FVM is integrating over a control volume and after that making a suitable approximations for fluxes across the boundary of each control volume. In this particular section, each term in Eq. 3.17 is performed separately to understand the approach used to solve the equation of heat transfer. For the heat accumulation part (transient term) in the heat diffusion governing equation, the integral discretionary $\int_V$ over the volume of a CV is:

$$\overbrace{\int_V \rho C_p \frac{\partial(\ T)}{\partial t} dV}^{\text{Heat Accumulation}} \simeq \frac{(\rho_P C p_P T_P - \rho_P^{old} C p_P^{old} T_P^{old}) V_P}{\Delta t} \tag{4.1}$$

where T_P is the average value of T in a control volume that is centred on a point P, the previous time-step value is defined by the superscript "old" while V_P in the equation represents the volume of the control volume, and Δt is the time step size. The term is also described as the "Transient term". The discretization

of the diffusion term (heat conduction) is given by:

$$\overbrace{\int_V \frac{k\partial^2(T)...}{\partial z^2} dV}^{\text{Heat Conduction}} = \int_s k(\hat{\mathbf{n}} \cdot \nabla ...) dS \simeq \sum k_f (\nabla ...)_f A_f \simeq \sum k_f A_f \frac{T_A - T_P}{d_{AP}} \quad (4.2)$$

$$(\hat{\mathbf{n}} \cdot \nabla ...)_f \simeq \frac{(...)_A - (...)_P}{d_{AP}} \quad (4.3)$$

where ... indicates a recursive application of the specified operation on T, which works in a manner that enables calculating the variable T at every control volume, A_f is the area of each surface, ∇ is the diffusion term. The term is represented in the code as "Diffusion Term", the term $(\hat{\mathbf{n}} \cdot \nabla ...)_f$ represents the flux estimate and is figured via Eq. 4.3. The term d_{AP} represents the distance between the neighbouring cell centres.

The discretisation of the source term (Solar Energy Absorption). As the term cannot be formulated in any of the previous forms and is regarded as a source S. The discretisation of the source term is:

$$\overbrace{\int_V S dV}^{\text{Solar Energy Absorption}} \simeq S V_P. \quad (4.4)$$

A dependence can be included in a linear manner, thus Eq. 4.4 becomes

$$V_P(S_0 + S_1 T_P), \quad (4.5)$$

where S_0 represents the source that is independent of T, while S_1 represents the coeficient of the source that is also linearly dependent on T. The source term is defined and written in FiPy the same way it is represented in the mathematical form in the heat diffusion equation. Combining Eqs. 4.1, 4.2, and 4.5, the complete discretization of Eq. 3.17 can be written for each CV as:

$$\frac{\rho_P C p_P (T_P - T_P^{old}) V_P}{\Delta t} - \sum k_f A_f \frac{T_A - T_P}{d_{AP}} = V_P(S_0 + S_1 T_P) \quad (4.6)$$

The discretization for Eq. 3.36 for mass transfer can be written for each CV as:

$$\frac{(C_P - C_P^{old})V_P}{\Delta t} = \sum D_f A_f \frac{C_A - C_P}{d_{AP}} \tag{4.7}$$

4.3.4 FiPy: a finite volume PDE solver using python

FiPy [128] is an object-oriented, partial differential equation (PDE) solver, written in Python, based on a standard finite volume (FVM) approach. FiPy solves the equation at the centres of the cells of the mesh, shown in Fig. 4.1b. The way it works, the 1-D domain has 100 solution points, NZ is defined, the NCZ is divided into layers that have an equal size with a specified total height for the zone. The grid object represents a structured linear grid and grid spacing (set to unity). Thus, a CellVariable object introduced in order to store or save the values of the solution for the equation of heat diffusion T and mass diffusion C. Transient terms and Coefficients are also set.

The set of boundary conditions are supplied to the equation essentially as a Python tuple or list (the distinction is not usually necessary to FiPy). The outer faces on the upper interface or boundary of the domain are extracted by mesh.faceGrad[0] while mesh.faceGrad[1] for the lower boundary. Alternatively, to using the solve() system equation, the sweeping method is used; it is often called sweep() instead. Both systems or methods behave the same, but the later returns the residual which next can be used as part of the exit condition. The next section explains the general logic flow of the computer model to perform the simulation.

4.3.5 The general logic flow of the computer model

Python codes using FiPy are developed to solve the 1-D finite volume for the mass and heat transfer governing equations. The computer program works in the manner shown in Fig. 4.2, it starts with an initial pond temperature that equals to the ambient, given standard insolation data for the location proposed. The upper convective zone and the lower convective zone are considered as a

single grid point. The third step of the program calculates the radiation input to each of the layers. This is done with the solar radiation data and the angle of incidence of direct solar radiation, all solar radiation is assumed to be direct, and the effect of day and night shifts for solar radiation are not considered. The fourth step of the program is to perform the heat and mass transfer iterations. Thus, the output of the simulations is the temperature and concentration profiles for the proposed salinity gradient solar pond. Fig. 4.2 shows the general logic flow of the SGSP computer simulation. For clarification, only the heat equation is explained. However, the same concept is applied and used to solve and predict solute behaviour.

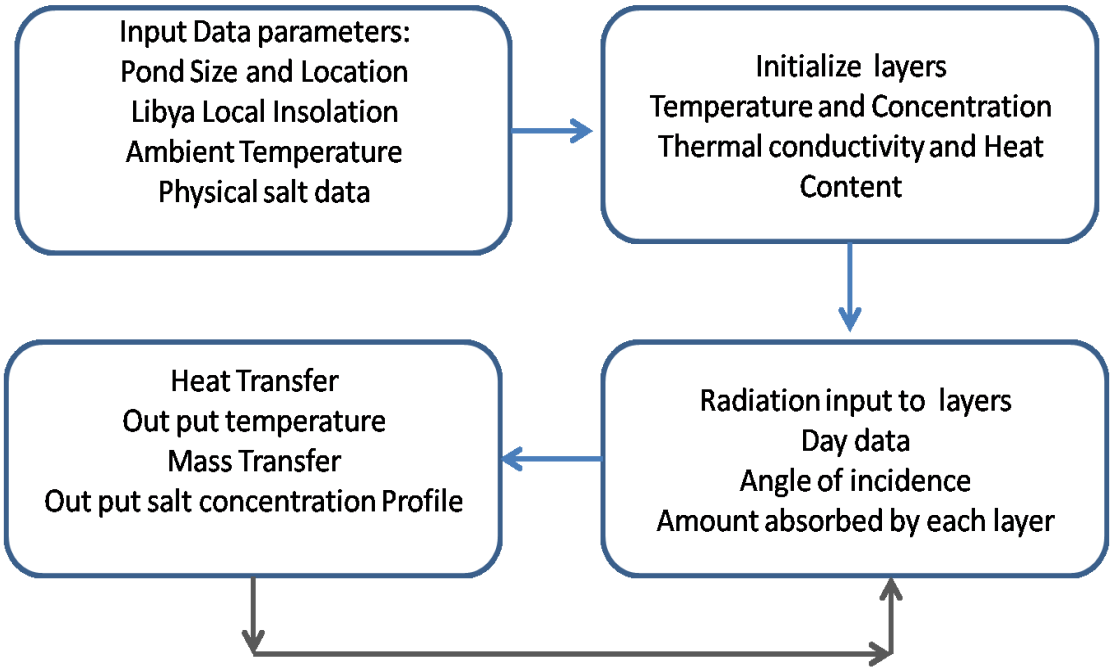

FIGURE 4.2. General logic flow of the computer model.

The numerical model addressed with attention to avoid any simplifying hypotheses that may lead to inaccurate estimates, which are not compatible with the process and the system characteristics. So far, the computer model developed in this study incorporated some of the assumptions as that in the Hull, Rabl and Nielsen mathematical model [9]; however, at this point, the program is set to try and model the UCZ temperature more accurately, taking in consideration heat loss from the top surface. Indeed, the analysis will provide useful insight into the potentiality of a solar thermal desalination process according to Libya geographical and climate conditions. Two code precision validation studies are conducted in the next section.

Time step sensitivity analysis

A time step sensitivity study of different time schemes is conducted, as shown in Fig. 4.3. The study shows that the same output can be achieved by applying lower-order or higher-order time schemes.

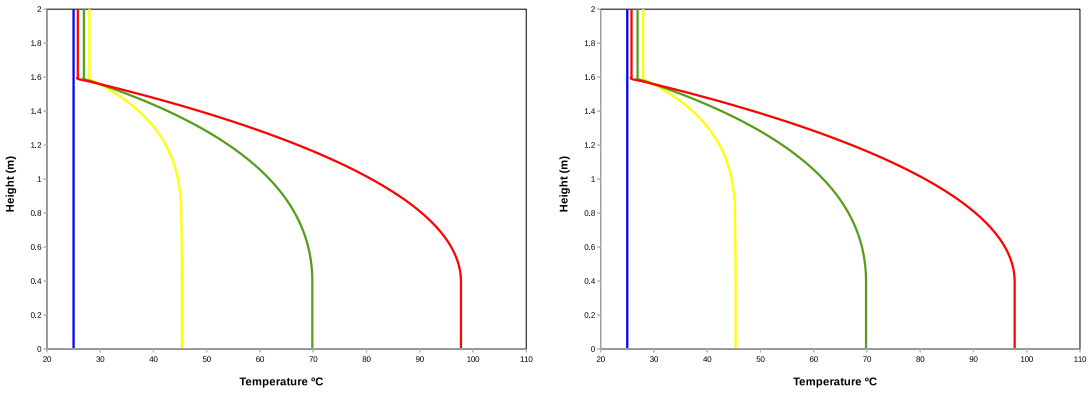

(A) Time step = 30 seconds. (B) Time step = 1 minute.

FIGURE 4.3. The evolution of salt temperature profile inside the SGSP till SGSP reached steady state, at NCZ (1.2 m) and I = 300 W m^{-2}, ■ Initial, ■ 20 Days, ■ 70 Days, ■ 90 Days (Steady State).

The results indicate that it is possible to reduce or increase the time steps required to predict the evolution of concentration, temperature or velocity profiles till steady state is reached. However, the smaller size of the time step results in the increased total number of iterations. The analysis for the 1-D numerical study shows that the numerical method provides a good balance between the size of time step and number of iterations. A time step of 1 minute is used in the simulation. With 1 minute the computational time for one month is about an hour and a half while with 30 seconds the computational time is approximately 3 hours. Consequently, a time step of 1 minute found to be appropriate and gives the shortest runs time.

4.3.6 Validation of the model

To validate the developed numerical code precision in simulating the thermal performance of the SGSP. Two validation studies are conducted and compared against experimental data for two different locations. The first SGSP is the

Granada solar pond in Spain which has been reviewed in chapter 2. The metrological data and the operational parameters for Granada SGSP are obtained from [129, 27]. The data is for the year of 2014-2015. The second SGSP is El Paso in the US, which was also reviewed in chapter 2. The metrological data and operational parameters for El Paso SGSP are obtained from [130, 25, 26]. The data is for the years between 1991-1993. Data concerning the location and design specification are illustrated in Table. 4.1.

TABLE 4.1. Location and design specification data [130, 129, 25, 27, 26].

i	Granada SGSP	El Paso SGSP
Location	Spain	US
Latitude	37.18° N	31.7° N
Longitude	3.6° W	106.4° W
Height	2.2 m	3.25 m
UCZ Thickness	0.2 m	0.7 m
NCZ Thickness	1.4 m	1.2 m
LCZ Thickness	0.7 m	1.35 m

Granada SGSP

The distribution of temperature for short-run (temperature profile) is validated with experimentally measured temperature data from Granada SGSP [129, 27].

The monthly averaged solar radiation incident and the average ambient temperature are obtained from [129, 27]. As illustrated in Table. 4.1 The dimensions of SGSP zones are 0.2 m, 1.4 m and 0.6 m for the UCZ, NCZ and LCZ respectively. The bottom of the SGSP is insulated. A more detailed review of this SGSP design and operation is performed in chapter 2.

It can be noticed that the temperature profile of the current study and the experimental data from Granada have a good agreement. There is a slightly different in behaviour at the interfaces. This could be due to the formation of convective currents at these regions. This could not be detected by the 1-D model where a uniform temperature is assumed in the UCZ and LCZ. The difference in the LCZ thermal behaviour can also be linked to the degradation of the bottom insulation (liner degradation). There could be a ground heat loss in the Granada

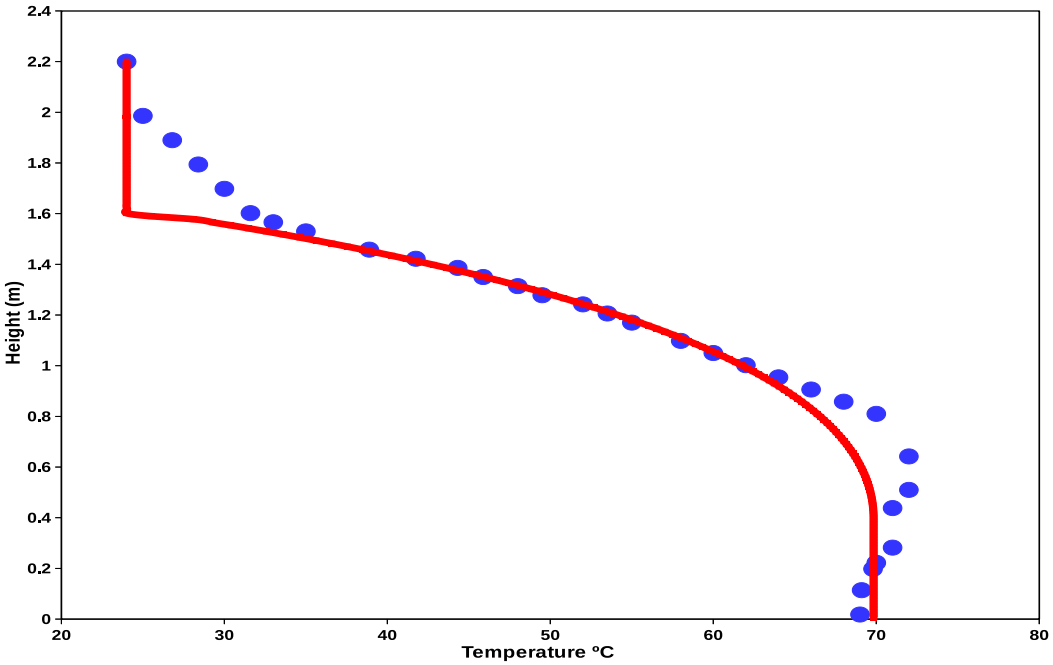

FIGURE 4.4. Validation of Temperature Distribution Results for the Present model with an experimental data 2014-2015 [129, 27], ■ Experimental (Granada Solar Pond), ■ Present Study.

SGSP which caused this sudden decrease in temperature in the bottom of the pond. In the present study model, the liner assumed to be efficient and perfectly insulates the bottom of the SGSP. The middle zone temperature gradient profile looks almost identical, and the same applies to the final temperature 70°.

El Paso SGSP

To check the validity of the current study model for the long-run behaviour, the simulated temperature of the El Paso SGSP is compared to an experimentally measured data obtained from the same pond [25]. El Paso SGSP is located at latitude 31.7° N. The location and design specification data are illustrated in Table. 4.1. More operational details regarding El Paso SGSP are in Chapter 2.

The El Paso SGSP temperature profile shown in Fig. 4.5 is taken for one year over an average of 2 years of operation 1991-1993. The same data is used to validate the present model. The result of the comparison is shown in Fig. 4.5. The red colour represents the present study model, while El Paso data is represented with black and grey colours.

There is an excellent agreement between the current study model and the data compared to. However, a slight difference in thermal behaviour is noticed. This slight difference could be due to thermal conductivity coefficients value variation between actual in the site and the modelled one (0.59 $\mathrm{W\,m^{-1}\,K^{-1}}$) [52].

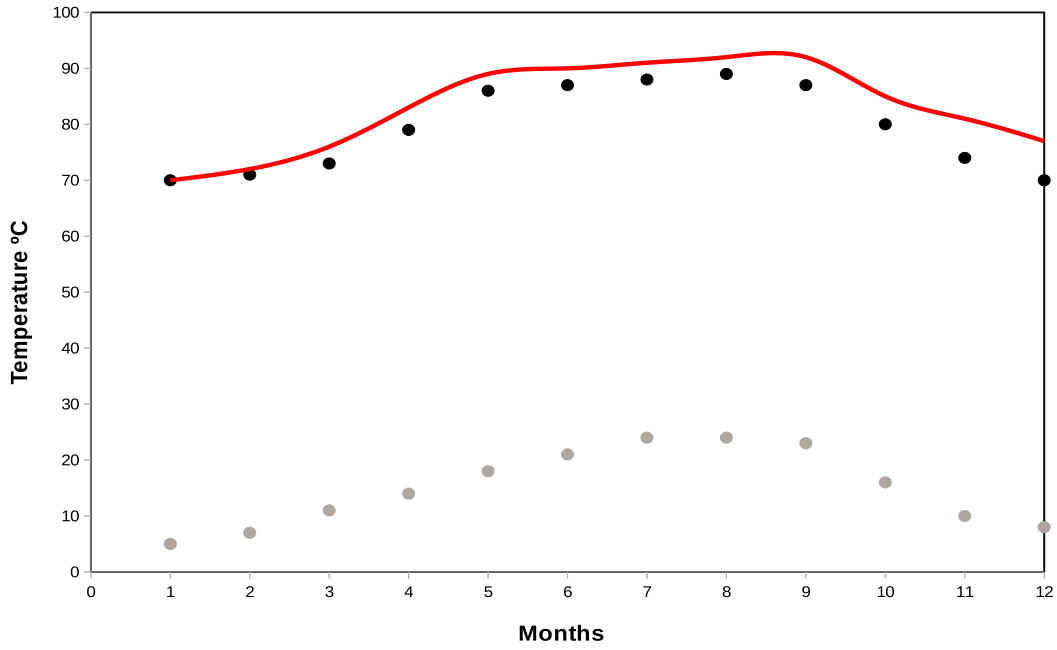

FIGURE 4.5. Comparison of the LCZ average temperature over two years of operation (1991-1993), ■ El-Paso pond ambient temperature [130], ■ Present study, ■ El-Paso SGSP LCZ temperature.

As illustrated in Fig. 4.5, for the present model, the thermal behaviour is almost similar to the El Paso SGSP. The temperature in the LCZ reaches its maximum value by the end of August for El Paso SGSP and the same for the present model. Furthermore, a progressive reduction in temperature is detected after September in both cases. The slight differences in thermal behaviour are more likely for the following reasons. It could be due heat transfer coefficients difference between actual in the site and assumed one. Additionally, factors like the clarity and transparency of the SGSP, as the El Paso was on for a long time before the measurements were taken so that means the water transparency might have deteriorated. Moreover, changes occur to zones during operation due to the DDC effect, might play a role in this slight change in behaviour.

To sum up, the codes successfully simulates two existing SGSPs for two different locations with different SGSP dimensions. The present model shows a good agreement with the experimental data.

4.4 Libya SGSP thermal potential: Numerical study

This particular study aims to predict the thermal potential of the salinity gradient solar pond as a source of thermal-energy for thermal desalination applications according to Libya climatology. The features of the physical model and governing equations are described in section 4.2. The numerical method and the logic flow of the computer model are explained in section. 4.3. This section introduces the data that is utilised to conduct the study. In this section also, five studies are conducted, the first study evaluates the thermal performance of SGSP at three-zone thickness settings (variations) in order to find the optimum zone thicknesses ratio, where SGSP has the highest thermal performance. The second and third studies are devoted to studying the thermal performance and solutal behaviour for the SGSP in short and the long run, respectively. The final two studies are devoted to study the potential of heat recovery from SGSP and to evaluate the thermal potential of integrating SGSP with desalination units.

4.4.1 Parameters

The thermal properties of the salt-water solution are illustrated in Table. 4.2, which provides values for the thermal diffusivity, the thermal conductivity, k, the specific heat, C_p, and the density ρ for salt-water solutions at conditions that match operational ponds. The differences in the thermal properties of pure water to a salt-water solution are introduced in the same table.

TABLE 4.2. Thermal properties of salt water [52, 125, 131]

Water type	Thermal conductivity	Thermal diffusivity	Density	Specific heat
	$W\,m^{-1}\,K^{-1}$	$m^2\,s^{-1}$	$kg\,m^{-3}$	$J\,kg^{-1}\,K^{-1}$
Pure water	0.6	1.43×10^{-7}	998	4184
Salt-water	0.59	1.34×10^{-7}	1100	3989

The dissolved salts concentration in seawater is almost uniform everywhere in this globe; it is around 35,000 ppm at all the World's oceans [52]. As the impact of some uncertainties such as the variation of the thermal properties

with temperature and concentration can be insignificant, in this study, constant values for the properties of the salt-water solution are considered [9].

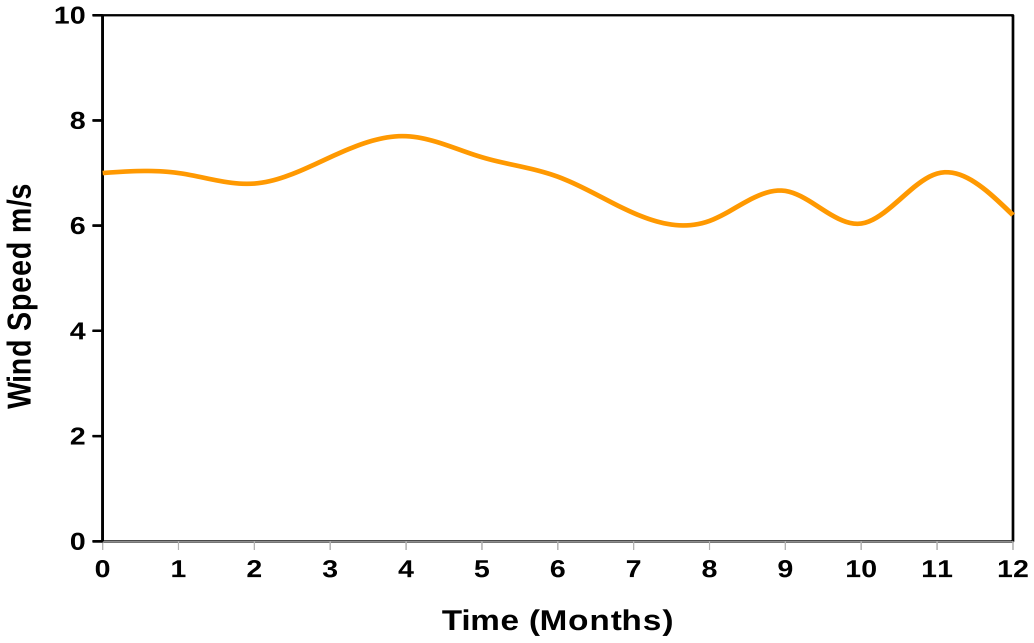

FIGURE 4.6. ■ Average wind speed during the year in Tripoli[37].

The SGSP is located in Tripoli within a latitude and longitude of 32.54° N, 13.11° E. The solar radiation data and wind speed data are obtained from NASA [37]. Table. 4.3 shows the average solar radiation for the city of Tripoli. Fig. 4.6 shows the monthly average wind-speed for Tripoli.

SGSP design parameters; Different zones thickness ratios will be studied as there is no fixed optimum zone thickness ratio anywhere in the literature to be considered. The type of salt considered is sodium chloride. The salt concentration of each layer is specified; the UCZ has 0 $\mathrm{kg\,m^{-3}}$, and 300 $\mathrm{kg\ m^{-3}}$ for the LCZ where salt content at both layers assumed to be perfectly mixed. The salt-water (Brine) diffusion coefficient D equals 3×10^{-9} $\mathrm{m^2\ s^{-1}}$ [33]. UCZ and LCZ thermal conductivities are 0.6 $\mathrm{W\ m^{-1}\,K^{-1}}$, 0.59 $\mathrm{W\ m^{-1}\,K^{-1}}$ and their specific heat are 4.184 $\mathrm{kJ\ kg^{-1}\,K^{-1}}$ and 3.989 $\mathrm{kJ\ kg^{-1}\,K^{-1}}$ respectively [52, 125, 72, 131]. The results are calculated according to the monthly averaged insolation incident on a horizontal surface for the city of Tripoli.

TABLE 4.3. Global radiation on horizontal surface for Tripoli from NASA [37].

Month	Insolation (I) W/m^2
(0-1) Jan	138
(1-2) Feb	151
(2-3) Mar	206
(3-4) Apr	258
(4-5) May	295
(5-6) Jun	312
(6-7) Jul	329
(7-8) Aug	290
(8-9) Sep	241
(9-10) Oct	183
(10-11) Nov	144
(11-12) Dec	122

Incident insolation during the year

It is essential to show the profile of the incident solar radiation in the area of the proposed SGSP in order to relate and notice how it will correspond to the temperature profile that will be developed later in this study.

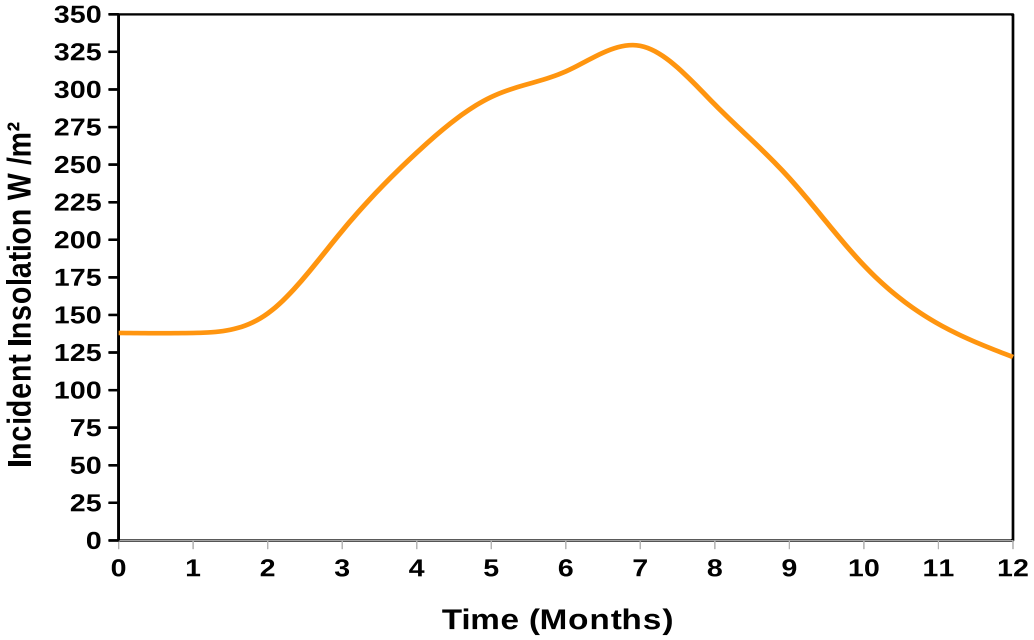

FIGURE 4.7. Solar radiation profile for Tripoli during one year, ■ Incident Insolation (I) W/m^2 [37].

The solar radiation profile can help to recognise the variations in the radiation intensity throughout the year. To be able to observe when it is high and intense or low and weak. The solar radiation profile is shown in Fig. 4.7 is for the city of Tripoli. It is apparent from Fig. 4.7 that the solar radiation intensity rises in a regular pattern from winter season to the summer season, and it records its maximum value in June, July and August.

The seasonal variation in the solar radiation intensity can have a significant impact on the behaviour of the SGSP.

4.4.2 Zones thicknesses

As there is no catalogue anywhere in the literature that suggest the optimum NCZ: LCZ zone thicknesses ratio. Subsequently, this study evaluates the thermal performance of three-zone thicknesses settings in order to find an optimum thickness ratio, where SGSP has the highest thermal performance (highest LCZ temperature). The different NCZ: LCZ zone thicknesses ratios will be investigated are illustrated in Table. 4.4. The UCZ thickness is fixed to 0.4 m as it is crucial to keep this layer at this fixed thickness to minimise heat losses via convection from the top surface. The NCZ thickness has been changed from 0.8 m to 1 m and then to 1.2 m with 0.2 m intervals. Simultaneously, the LCZ thickness has been changed from 0.8 m to 0.6 m and then to 0.4 m with 0.2 m intervals. While maintaining the thicknesses of the upper convective zone to 0.4 m during the simulation. The NCZ: LCZ zone thicknesses ratios are illustrated in Table. 4.4.

TABLE 4.4. Different NCZ: LCZ thicknesses ratios.

i	UCZ thickness m	NCZ thickness m	LCZ thickness m	NCZ : LCZ thickness ratio
1	0.4	0.8	0.8	1:1
2	0.4	1.0	0.6	2:1
3	0.4	1.2	0.4	3:1

The SGSP is run from June - August and for the same period (90 days) for all thickness ratios. The used parameters have been explained in previous sections in this chapter. Temperature profiles are plotted against the height of the SGSP, as shown in Fig. 4.8. Note that the model assumes all solar radiation that reaches the non-convective zone–lower convective zone interface is absorbed in the lower convective zone.

Figure. 4.8 shows that with a small non-convective zone thickness of 0.8 m, the LCZ temperature is the lowest, as the maximum obtained temperature is approximately 65 °C. In Fig. 4.8 it is also observed that increasing the NCZ thickness from 0.8 m to 1.2 m results in a positive impact on the overall thermal performance of the SGSP. The increase of the NCZ thickness improves the effectiveness of the thermal insulation provided by the gradient zone, and that is

by lessening the upward heat loss from the lower convective zone to the upper convective zone, and that can be noticed at the UCZ temperature. It can also be affirmed that this increase in temperature of the lower convective zone is due to the increase of the thickness of the non-convective zone, which works as a transparent guard or insulator sustaining all the absorbed heat in the LCZ. Therefore, modifying the non-convective zone thickness from 0.8 to 1 m leads to an increase in the LCZ temperature. The LCZ temperature increase is by almost 15 °C to reach almost 79 °C. An additional increase of the NCZ thickness to 1.2 m improves the maximum temperature to reach approximately 98-99 °C, by providing further insulation that helps to reduce the upward heat loss from the lower convective zone to the upper convective zone.

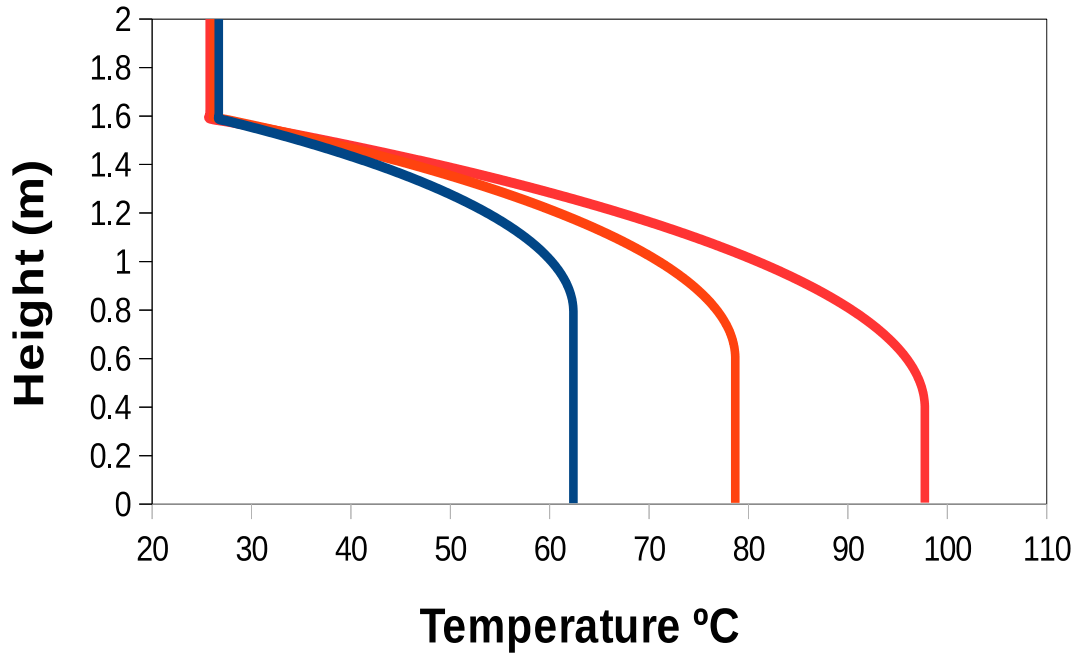

FIGURE 4.8. Libya SGSP steady-state temperature profile after running the SGSP for 90 days at different zone thicknesses ratios, ■ NCZ = 0.8 m, ■ NCZ = 1 m, ■ NCZ = 1.2 m.

However, any further increase in the NCZ thickness beyond 1.2 m, more likely will be unprofitable for a 2 m SGSP. Because less thermal energy W/m^2 will be available in the lower zone to be withdrawn; however, this should be justified according to the application; in addition to that, the question arises wither the SGSP will be hydrodynamically stable at an extremely tiny LCZ thickness. Therefore, the optimum thickness of the NCZ depends significantly on how much energy is needed for a particular application and how the SGSP stability will be affected. A two-dimensional study is needed to be conducted where velocity factors are activated, and the movement of the fluid could be simulated.

In the lower convective zone. The highest temperature is achieved when the lower convective zone thickness is decreased, and NCZ thickness increased. However, a minimum depth limit of the LCZ might be required in order to hinder any erosion of the non-convective zone when extracting heat from the lower zone and also for the beforementioned stability reasons. On the other hand, when the LCZ thickness is increased, the heating process needs more time in order to heat the lower convective zone. As a consequence, the diurnal increase in temperature of the lower convective zone is degraded. The succeeding option is not practical for three main reasons; (I) the lower convective zone does not reach high temperature as that could be obtained when LCZ thickness is smaller, (II) the longer heat-up period for a large LCZ, and (III) the high salt requirements for a thicker lower convective zone which could not be justified economically. Therefore, and for all reasons mention earlier, a lower convective zone thickness of 0.4 m is seen as optimal for the proposed SGSP. However, a 2-D hydrodynamic stability study is still needed to be conducted to examine the stability of the SGSP.

To conclude, the NCZ acts as a thermal insulator and plays a crucial role in SGSP thermal behaviour. It is observed that the temperature increases with respect to the depth of the gradient zone NCZ, the deeper the gradient non-convective layer, the higher is the average temperature obtained and the minimum is the upward heat losses. However, the financial (thermo-economical) implications of increasing or decreasing the thickness of the NCZ must be evaluated in order to justify what is optimum. As mentioned, any increase or decrease should always justify the capital and operating expenditure. Additionally, a two-dimensional numerical study is needed in order to investigate the effect of zone thickness on the hydrodynamic stability of the pond. The 2-D study is conducted in chapter 6.

4.4.3 SGSP thermal behaviour

This section explains how the temperature profile evolves with time. The depth of the non-convective layer considered is 1.2 m, depth of UCZ and LCZ are 0.4 m and 0.4 m respectively as the best results were obtained at these thicknesses. The underpinning logic for choosing this thickness is explained in the previous section. 4.4.2.

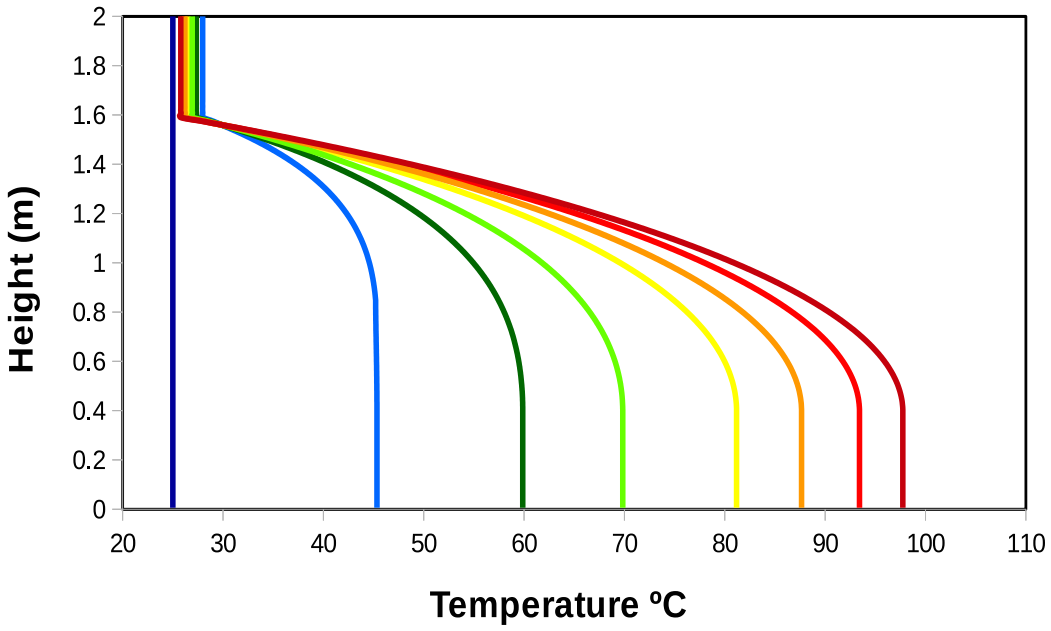

FIGURE 4.9. Libya SGSP temperature profile development at NCZ (1.2 m), ■ Initial, ■ 20 Days, ■ 40 Days, ■ 50 Days, ■ 60 Days, ■ 70 Days, ■ 80 Days, ■ 90 Days (Steady State). The thermal energy output at 98 °C LCZ temperature = 68 W/m^{-2}.

The simulation starts at the beginning of June and ends at the end of August. Meanwhile, once solar radiation hits the top surface of the SGSP, a portion of the incident, solar radiation is absorbed. The maximum temperature occurs just below the UCZ. Afterwards, a portion of the NCZ starts to heat up. Later the peak temperature moved towards the LCZ as more absorption is taking place in the bottom, as shown in Fig. 4.9. The non-convective layer works as a transparent insulator permits heat to be trapped in the bottom layer. Providing that the water has a low thermal conductivity, the heat is trapped and stored in the lower convective zone. The only significant heat loss from the SGSP is through the UCZ.

Simulation results show that the temperature in the LCZ exceeded 90 °C at zero heat extraction rate according to Libya meteorological data as shown in Fig. 4.9. Which corresponds to the thermal energy output = 68 W/m^{-2} at 98 °C LCZ temperature with a Carnot efficiency of 25%. The heating in the lower convective zone slightly slowed in August due to lower solar intensity in this month in comparison to July. Moreover, the SGSP was close to reaching its steady-state; thus, the heat absorption and conduction processes become extremely slow. Figure. 4.9 Indicates that the thermal performance for such a stable and

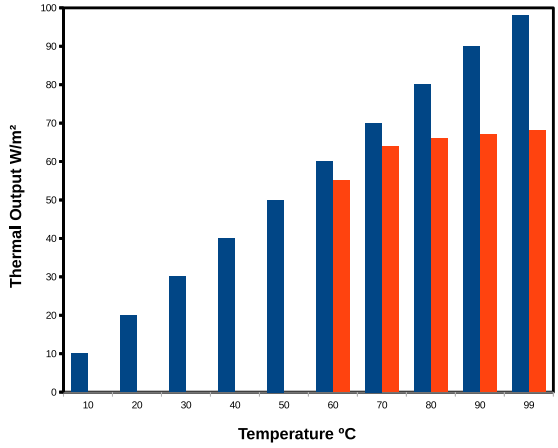

(A) Thermal energy output at temperatures higher than TBT of MED-TV units 60-65 °C .

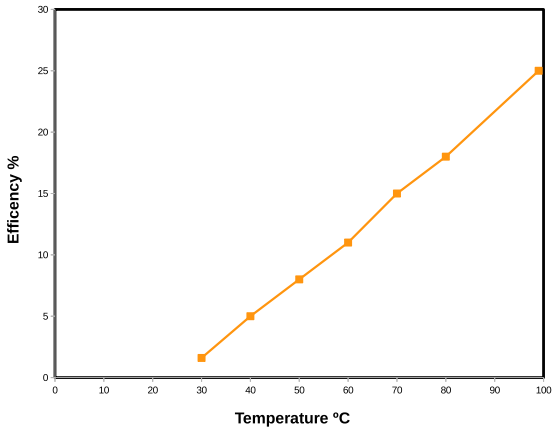

(B) Carnot efficency of the system for different SGSP LCZ temperatures.

FIGURE 4.10. Thermal energy output and carnot efficency figures ■ Temperature, ■ Thermal energy output in W/m^{-2}, and ■ Carnot efficency of the system.

steady SGSP is promising. However, to elaborate further on the SGSP thermal performance, a year around thermal behaviour is to be conducted later in this thesis.

4.4.4 SGSP solutal behaviour

This section describes the simulation results for the mass transfer process inside the SGSP. Before the start of the operation. The UCZ starts with a low initial salt concentration of 0 $kg\,m^{-3}$, the LCZ has a significantly higher salt concentration of 300 $kg\,m^{-3}$. The non-convective zone is considered to have a linear-gradient salt concentration profile. Fig. 4.11 illustrates the salt concentration profile inside SGSP at initial stage. The SGSP was then run for 180 days. As shown in Fig. 4.11, the salt concentration in the UCZ has increased after 180 days of simulation whereas, the salt concentration for the LCZ has slightly decreased. The increase in the salt concentration level in the UCZ is due to the diffusion of the salt inside the SGSP or in other words the occurrence of mass transfer from the higher concentration areas, which are the NCZ and the LCZ to lower concentration region which is the UCZ.

The SGSP cannot work without a stable concentration profile in the NCZ, as the main concept of creating a SGSP is maintaining that gradient profile throughout

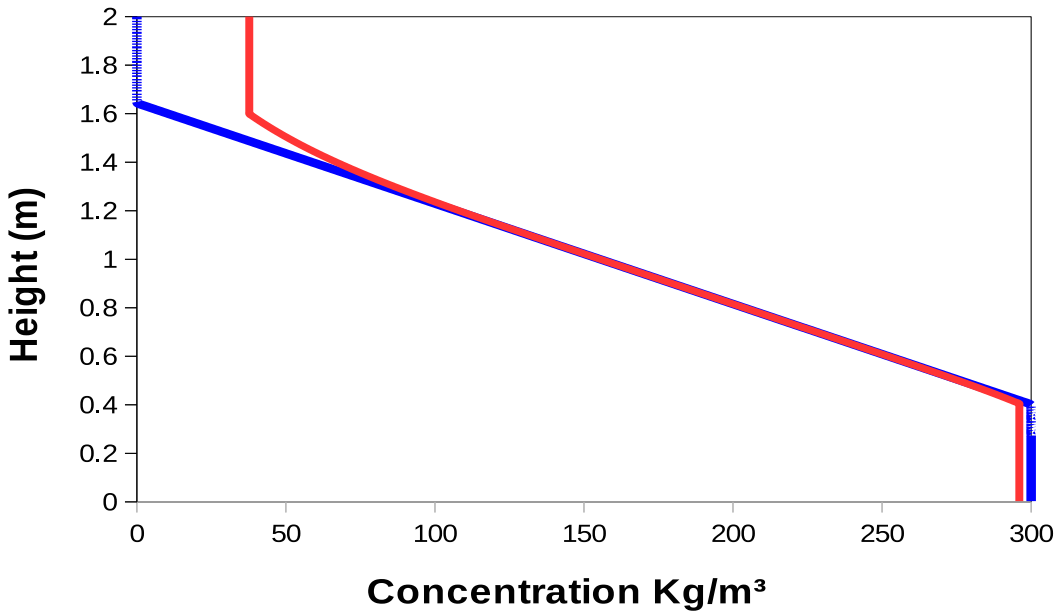

FIGURE 4.11. Libya SGSP density profile at NCZ (1.2 m), ■ Initial profile, ■ After 180 days.

the operation. This means the concentration should be increased downwards to hinder any gravitational overturn. A weak salt gradient can cause instability in the gradient layer, and subsequently, this will negatively affect the SGSP thermal performance.

This emphasises that the dynamics of salt diffusion is a crucial aspect to study and to keep under control. If diffusion occurs inside the SGSP, the non-convective zone stratification will be disturbed. Subsequently, the stratification of the SGSP needs modifying, which can be achieved by flushing the UCZ and adding fresh-water, while adding high salt concentration solution in the lower convective zone. A coupled two-dimensional study will be conducted in the next chapter in order to elaborate more on the effect of salt diffusion on the operational stability of the pond.

4.4.5 Heat recovery

Heat recovery is the purpose of creating a SGSP, but it is also a form of heat loss as it lessens the lower convective zone temperature. A pattern of constant heat extraction Q_{ext} is simulated. This investigation aims only to examine the

practicality, suitability and potential of SGSP generating heat for desalination units. To this end, the simulation is run with a constant imposed extraction rates of 45 W/m^2 55 W/m^2.

The pond started heating up in January, whereas, the heat extraction started by the end of April, as shown in Fig. 4.12. Heat extraction was chosen to start at this time due to desalination systems specifications (Top Brine Temperature Requirments). The heat was extracted assuming that the pond is operating and the temperature has been accumulated from previous months (startup time). Fig. 4.12 illustrates that the lower convective zone temperature at the end of each month and compares it with the ambient for the same month. To compare with solar intensity, see Fig. 4.7. It can be noticed that the lower convective zone temperature increased to a peak in July, August and beginning of September 98 °C, then decreased to almost 70 °C in December. The lower convective zone temperature significantly depends on the solar radiation absorbed by the lower convective zone, the ambient temperature and the amount of heat extracted from the SGSP.

To elaborate more on heat recovery. The periodical variation of the temperature in the lower convective zone with continuous heat recovery over a period of two years has been investigated; the results are shown in Fig. 4.12. The SGSP was able to store heat during the second year and maintain thermal performance. The temperature profile shows an increase during summer, as anticipated, immediately interrupted during the winter season as the solar radiation is not as intense (it is advisable to do do the maintenance during this time if needed). In the following second year, the LCZ displays more resistance to seasonal variation. The minimum LCZ temperature is 70 °C at the end of January, and the maximum LCZ temperature is 98 °C by the end of August and beginning of September.

The thermal behaviour of the salinity gradient solar pond is tested with two loadings of 45 and 55 W/m^2 and compared with the no-load scenario. Repeatedly, the SGSP is located in the city of Tripoli and with zone thicknesses of 0.4 m for the UCZ, 1.2 m for the NCZ and 0.4 m for the LCZ. Thicknesses of the upper convective zone, non-convective zone and lower convective zone are justified (see, section. 4.4.2). It is evident that the lower convective zone temperature changes according to the heat extraction rate specified. With a 45

W/m^2 heat extraction load, the lower convective zone temperature gradually builds to reach a peak of 91 °C (about 6 °C below the temperature achieved in no-load scenario), and that is by the end of August and later decreases to almost 70 °C by the end of the year which is about (5 °C below the temperature achieved no load scenario). The same behaviour is witnessed with a load of 55 W/m^2, however lower values of maximum and minimum temperatures were observed. With both loads, it has been illustrated that there was a slight sudden temperature decrease at the (start of operation) in the second year. Nevertheless, the temperature increases again and begins to decline after August; The causative factor of this behaviour is that when the heat is removed from the SGSP it decreased the lower convective zone temperature, yet after short period of time the incident solar radiation on the SGSP substitutes the heat loss and the temperature starts to rise until it reaches steady-state in the mid of the summer season.

As shown in Fig. 4.12, the heat recovery process cannot be performed at the start of the operation, and that is to let the SGSP heat up. The LCZ temperature reaches approximately 70 °C by the end of April, (perfect time to extract heat for the case of ME-TVC units because the temperature in the LCZ is higher than 70 °C in this month which is enough to generate heat for ME-TVC unit that works at top brine temperature of 60-65 °C. However, this temperature should be maintained throughout the Year. Large surface area SGSP might be required to generate enough energy for desalination units at 55 W/m^2.

4.4.6 Thermal potential: Integration with desalination

This section discusses the thermal potential of SGSP in driving thermal desalination units. MSF units require a top brine temperature of 90 °C [132]. It is not recommended option as SGSP can not supply enough hot water at this temperature to operate an MSF unit throughout the year.

Multi-Effect Desalination MED units require a top brine temperature of 64-70 °C [7, 132]. The time of the establishment of thermal extraction mechanism suitable to power a MED unit is then 6 months during the first year of operation. Also, 8 months during the second year, as shown in Fig. 4.12.

MED-TVC desalination units require a top brine temperature of 60-65 °C [48, 49, 50]. The period of thermal extraction regime suitable for heat extraction in order to power a MED-TVC unit is nine months during the first year of operation and 12 months during the second year, as shown in Fig. 4.12. That indicates if this particular load 55 W/m^2 is implemented for particular desalination unit (ME-TVC) that require 60 °C, there is no need to hold heat extraction process as shown in Fig. 4.12. Additionally, the heat extraction process could start earlier than other configurations. However, if the required temperature is more than 60 °C as in other desalination application MED and MSF, heat recovery should be held in November and begun again in March.

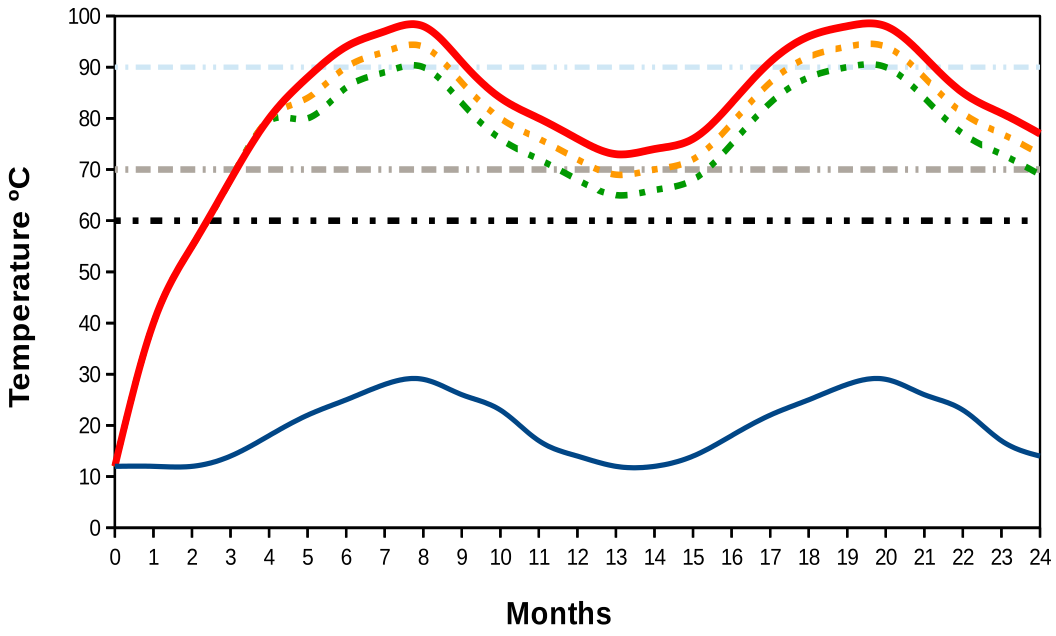

FIGURE 4.12. SGSP-thermal desalination potential, ■ Ambient temperature, ■ SGSP LCZ Temperature Profile, ■ 55 W/m^2 , ■ 45 W/m^2, ■ No load. ■ MED-TVC Top brine temperature requirements 60 °C, ■ MED Top brine temperature requirements 70 °C , ■ MSF Top brine temperature requirements 90 °C.

For ME-TVC plant that requires a top brine temperature of 60-65 °C [48, 49, 50], an LCZ thickness of 0.4 m is suitable and cost-effective as no high amounts of salt required to achieve this target. Increasing the LCZ thickness will decrease the zone temperature, slow the heating process, which both mean a need to stop the SGSP for several months, and increase in the capital and operational cost. The thickness used for the LCZ depends mainly on the type of the application coupled with the SGSP and how much thermal energy is required in order to justify economics.

To further elaborate on the temperature profile results, at average annual insolation of about 2000 kW hr m^{-2} per year. Considering a solar pond efficiency of about 25% [133]. This means each m^2 collects around 500 kW hr m^{-2} per year. The Carnot efficiency of a SGSP operating between 98 °C and 25 °C becomes about 25%. However, a practical Rankine cycle has a smaller temperature difference, because of the temperature drop in the evaporator and condenser. Thus, the resulting cycle efficiency is approximately 10%. This indicates that in the case of power production, each m^2 produces 50 kWh per year. Each kW installed for baseload operation therefore requires a SGSP surface area of 1 x 24 x 365/50 = 175.2 m^2. Provided that the operational stability of the SGSP is not disturbed due to the DDC effect or any other mechanical source of instability. Assuming the desalination plant has an average economy ratio of 10:1. Assuming the same average rate of annual radiation. According to the beforementioned figures and assumptions, the freshwater production will then be 10 x 500 x 860 (kcal/mm^2 per year)/550,000 (kcal/m^3) = 7.80 m^3/m^2. This indicates that the SGSP area required to supply heat for desalination for a 1 m^3 per day is about 1 x 365/7.80 = 46.8 m^2.

4.5 Summary

The result obtained from the one-dimensional transient model indicates that SGSP technology is suited to Libya, owing to the abundance of solar radiation. The maximum temperature obtained is 98 °C. A temperature above 70 °C is sustained during winter. SGSP can provide hot water at a temperature exceeding 70 °C most of the Year to drive ME-TVC unit.

The salt concentration profile gave an indication to an import aspect of SGSP operation, which is the operational stability. The gradient profile of the NCZ could be damaged due to the diffusion of salt. However, that happens slowly over time, as shown in the results; it can have a destabilising effect. The temperature distribution created by the absorption of solar radiation can also have a destabilising influence on the SGSP because hot salt-water is lighter than cold salt-water at the same salt concentration level. Subsequently, the potential thermal energy stored can be diffused by small perturbations and this diffusion yield in mixing. Thus, SGSP can be subject to hydrodynamic instability due to

both effects. The 1-D model can not describe the hydrodynamic, the velocity fields and the convection. It requires two dimensions to occur. A 2-D study to address the operational stability of the SGSP is to be conducted.

Furthermore, the results show that thickness change has a significant influence on the lower convective zone temperature. The 1-D study shows that the larger the NCZ, the better insulation it provides, and subsequently, the better the SGSP thermal performance. However, the answer to what is the optimum NCZ: LCZ zone thickness ratio needs a more complicated model to be determined. The 1-D model can not predict the hydrodynamic stability of the system. A 2-D study that investigates the zone design thicknesses in more detail is also to be conducted.

Chapter 5

2-D hydrodynamic, heat and mass transfer

5.1 Overview

In the previous chapter, a one-dimensional numerical study was conducted in order to study the thermal potential of SGSPs as a source of thermal energy for desalination units according to the geographical and climate conditions of Libya. The results indicated that SGSP is perfectly suited to arid and semi-arid regions like Libya, and it has the potential to provide the heat required for desalination units such as ME-TVC in the most part of the year. The 1-D study assumes that SGSP is a stable system where the temperature and concentration are uniform in the entire upper convective and lower convective zones with a stable instantaneous mixing in these zones which is a simplifying hypothesis. The 1-D model can provide a prediction to SGSP thermal performance and an insight into the individual components of SGSP behaviour for short and long periods of operation; however, it cannot describe the hydrodynamic behaviour and the operational stability of the SGSP as it requires at least two dimensions to occur.

In reality, an SGSP is subject to instability due to the double-diffusive convection effect DDC, where convective movement is induced by buoyancy force in which two components (salt concentration and temperature) that have different diffusivity and behaviour get activated concurrently and subsequently drive an opposing destabilising effect to the vertical density gradient. Whereas previous studies have provided an insight into some aspects of the SGSP thermal and hydrodynamic behaviour, to the best of the author's knowledge, studies that

explain in detail how the NCZ becomes unstable have not been conducted. In particular, questions of how, when, and where convection current starts to form inside the NCZ have not been explained in sufficient detail.

This chapter aims to study the hydrodynamic stability of SGSP by (I) Firstly, investigating the hydrodynamic behaviour of the transient fluid flow developed in the UCZ, NCZ and LCZ during the absorption of solar energy in and the presence of the DDC effect, (II) Secondly, investigating the changes that occur to the zones during operation due to the DDC effect and answering the questions of how and where convection currents start to form in the non-convective zone, and (III) Finally, comparing the thermal performance of the hydrodynamically stable 1-D SGSP where the SGSP is assumed to be stable and the 2-D model where the SGSP is subject to the DDC effect and interfaces motion.

In this chapter, the following second section discusses the physical model and the governing equations. The third section deals with the numerical method, where the finite element discretisation of the governing equations adopting the Crank–Nicolson scheme is performed. Moreover, the numerical code precision is compared and validated. The fourth section deals with the numerical solution of the equations where the thermo-hydrodynamic behaviour and hydrodynamic instability of the SGSP are investigated under a semi-arid climate of Libya. The fifth section discusses the movements of the internal interface. This chapter further provides a comparative study between the 1-D SGSP thermal performance where the SGSP is assumed to be hydrodynamically stable and the 2-D study where the double-diffusive convective effect is considered. Finally, a summary of the chapter is presented.

5.2 Physical model and governing equations

The model configuration is depicted in Fig. 3.1. The model is for the proposed Libya SGSP. The assumptions that are made for this model do not modify the principles of the study. The sidewalls and the bottom are considered to be well insulated. The incident solar radiation on the SGSP is assumed to be constant and fixed with an average solar intensity value in transient regime. The solar radiation that arrives at the bottom of the SGSP is entirely absorbed. The

salt and water mixture is supposed to be incompressible and Newtonian. Initially, the water-salt mixture is deemed to be stagnant and in a stable condition, and at ambient temperature. Thus, the pressure, temperature, salt concentration and fluid velocities have initial values that are similar to their reference values. The SGSP has a uniform initial temperature (0 dimensionless temperature, which is equivalent to 25°C) in the entire SGSP. The non-convective zone is established with gradient salt concentration profile, ranges between 0 and 1 in dimensionless units, which is equivalent to 0 kg m^{-3} and 300 kg m^{-3} respectively. The temperature, concentration and velocity variation in the Y-axis direction are regarded to be small and negligible. Consequently, the temperature, concentration, and velocity distributions in the SGSPs are 2-D (Z,X). In the next sections, the governing dimensionless equations Eqs. 3.53 - 3.62 of continuity, momentum, heat and mass which were described in chapter 3 t are to be solved numerically.

5.3 Numerical method

In this section, the mesh, the discretisation method, the numerical solution approach, and the computing platform FEniCs are all explained.

5.3.1 Mesh generation

The computational domain consists of 30 grid points (Triangular mesh of the 2D rectangle (H) x (L)). The class rectangle mesh creates a mesh on a rectangle with one corner in (X0, Z0) and the opposite corner in (X1, Z1). nX and nZ specify the number of cells in the X- and Z-directions. In the mesh, the default direction ("right") of the diagonal is used. A uniform grid spacing and a Crank Nicolson ϑ equal to 0.5 is adequate for yielding results in a moderate computed time.

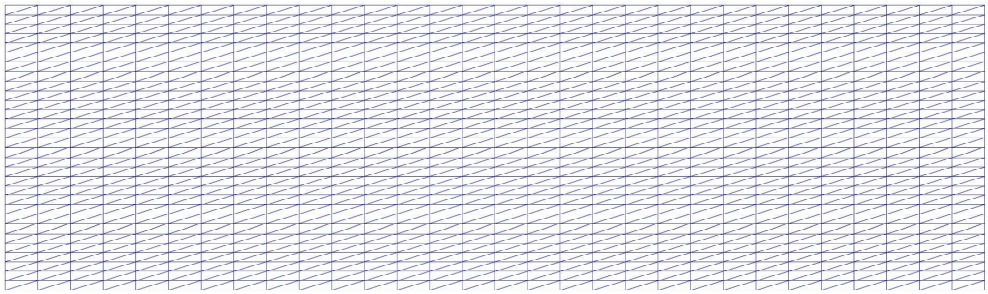

FIGURE 5.1. Demonstration of the rectangular mesh.

5.3.2 Discretization of governing equations

The discretization in time and space of the governing equations of of continuity, momentum, heat and mass in section. 3.6.5 is based on the respective weak formulations. The weak form of the governing equations is obtained by multiplying components by test functions ϕ, then integrating in (X) and finally applying integration by parts to reduce the derivatives current order. In the solutions for all the equations in the model:

$$\theta(X,Z,t) \simeq \sum_j \theta_j(t)\phi_\theta{}^j(X,Z) \tag{5.1}$$

$$\varphi(X,Z,t) \simeq \sum_j \varphi_j(t)\phi_\varphi{}^j(X,Z) \tag{5.2}$$

$$V_X(X,Z,t) \simeq \sum_j V_j(t)\phi_V{}^j(X,Z) \tag{5.3}$$

$$V_Z(X,Z,t) \simeq \sum_j V_j(t)\phi_V{}^j(X,Z) \tag{5.4}$$

$$P(X,Z,t) \simeq \sum_j P_j(t)\phi_P{}^j(X,Z) \tag{5.5}$$

Discretisation or integration is accomplished by adopting Crank Nicolson scheme

[134]. Crank Nicolson is a finite element scheme applied to solve partial differential equations numerically. The scheme is named after the developer John Crank and Phyllis Nicolson who introduce it in the mid 20th century [134]. It is a second-order method; it is implicit in time, and also numerically stable method. The method has two advantages over the explicit method; which are stability and improved convergence. The discretisation in time has been specified in order to have fewer restrictions on time stepping in terms of stability. Using the Crank-Nicolson scheme, the variable naturally finds its place at the midpoint between i and i+1. In Crank Nicolson $\vartheta = \frac{1}{2}$, it is unlike the BDF scheme, though, no modifications are strictly necessary on the first time step since the convection term simply will be reduced to the first-order accurate.

The general form of a non-linear algebraic equation discretization can be written as:

$$\frac{\partial y}{\partial t} - F(y,t) = 0 \tag{5.6}$$

$$\frac{y^{i+1} - y^i}{\Delta t} = \vartheta F(y^{i+1}, t \quad i) + (1-\vartheta)F(y^i, t \quad i+1) \tag{5.7}$$

The superscript i and i+1 are the solution current and the next time steps. Thus, the Crank Nicolson is a combination of the forward Euler at i and the backward Euler at i+1; however, the method is not the average of those two, as the later has an implicit dependence on the solution. The Navier Stokes discretization in time and space is explained in Appendix A.

5.3.3 Computing platform FEniCs

Having explained how the governing equations are discretised in the previous section. This section deals with the computing platform that is used to perform the simulation. FEniCs [135] is open-source software that is transparent, and the researcher has much more control over the model that would have in most software if not all. It is the latest powerful tool in FEM, implementing all the latest tools like PETSc, etc. Unlike many other platforms, it allows the

researcher to understand the problem from an elementary level, i.e., the weak and robust form (PDEs), and solving the problem from there. It allows the researcher to fully control and understand the physical model when dealing with PDE, stability, time and space discretisation, parallel decomposition, computational algorithms, etc.. [136, 135, 137].

In the present study, FEniCs has been used as a programming package to solve partial differential equations PDEs that governs the system based on the FEM. FEM is the adopted discretisation method, as it can readily support complex geometries, it divides infinite geometry elements which are quite infinitesimal small sections across the model. It also supports complex boundary conditions and can readily handle mixed linear and non-linear behaviours in a single model; then it executes the boundary conditions as many times as the number of meshes. Additionally, FEM provides comprehensive result sets much near to the practicality results, forming the physical answer of the system at any location, and that includes ones that could have been ignored in an analytical approach [135].

To sum up, FEniCs is an open-source (LGPLv3) computing platform that enables the user to swiftly interpret scientific models into an effective FEM code utilising the significantly high-level Python and C++ interfaces to FEniCS. This includes also features for automated error control and adaptivity, and a comprehensive finite elements library[136, 135, 137]. The DOLFIN solve() function is used to solve the variational problem where Newton Raphson scheme is utilised to resolve the non-linear algebraic equations where FEniCs attacks the non-linear variational problem directly. The next section deals with the numerical study, assumptions, parameters and the simulation results.

5.4 Validation of the model

To check the developed numerical code precision in simulating the operation of the SGSP. A validation study is conducted by performing computational simulation for double-diffusive convection and compared to [72]. The study is performed with the following parameters Internal Rayleigh Number (Ra_I)= 1.4$\times$ 10^8, Thermal Rayleigh Number (Ra_T) = 1.0$\times$ 10^7, Pr = 6 and A = 3. Figure 5.2

shows the salt concentration profile in the SGSP for two different studies.

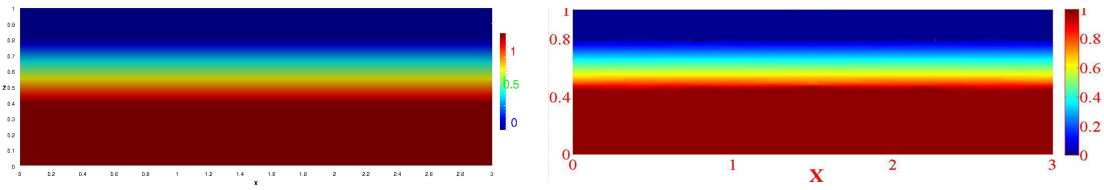

(A) Present Study.

(B) Previous Study [72].

FIGURE 5.2. Salt concentration profile inside the SGSP, internal Rayleigh number (Ra_I)= 1.4$\times$ 10^8, thermal Rayleigh number (Ra$_T$) = 1.0$\times$ 10^7, Pr = 6, A = 3 and a dimensionless time t= 0.05.

The codes successfully simulate the concentration profile for two different studies with the same parameters and aspect ratio. The present model shows a good agreement with the simulated data from [72].

Time step sensitivity analysis

A time step sensitivity study of different time schemes is conducted, as shown in Fig. 5.3. The study shows that the same output can be achieved by applying lower-order or higher-order time schemes. Thus, it is possible to reduce or increase the time steps required to predict the evolution of concentration, temperature or velocity profiles till steady state is reached; however, smaller size of time step results in increased total number of iterations. The analysis for the 2-D numerical study shows that the numerical method provides a good balance between size of time step and number of iterations.

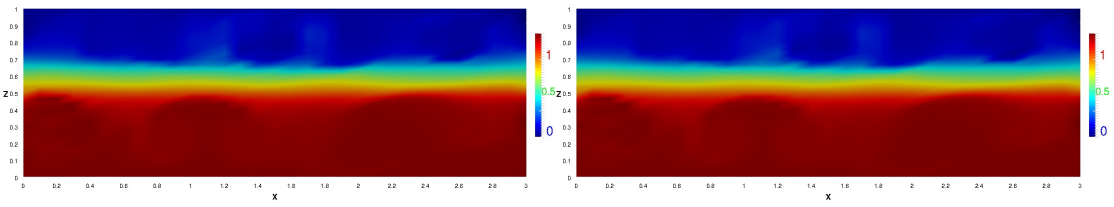

(A) Time step = 1 s.

(B) Time step = 10 s.

FIGURE 5.3. The evolution of salt concentration profile inside the SGSP till SGSP steady state, internal Rayleigh number (Ra_I)= 1.4$\times$ 10^8, thermal Rayleigh number (Ra$_T$) = 1.0$\times$ 10^7, Pr = 6, A = 3 and at different time steps.

Consequently, a time step of 10 seconds found to be appropriate and gives the shortest runs tim. The previous studies reviewed in chapter 2 neither explain the operational stability, nor the essence (when, how and where) of the hydrodynamic instability in sufficient detail. In this study, salt concentration and velocity profiles along with the temperature profile, will be generated in order to explain the hydrodynamic instability in sufficient detail.

5.5 2-D Study of SGSP thermo-hydrodynamic

The aims of this investigation are (I) to numerically predict the hydrodynamic, thermal and solutal behaviour in the upper convective zone, non-convective zone and lower convective zone during absorbing and collecting solar energy in order to understand the thermo-hydrodynamic behaviour of the system, (II) to investigate the the transient hydrodynamic behaviour of the zones, and (III) to compare results of the 2-D DDC SGSP with the results from the 1-D SGSP, which assumes a stable system.

In the present numerical study, the SGSP is made up of a rectangular cavity with an aspect ratio A = W/H. The SGSP is considered to be full of a salt-water mixture. The zones of the SGSP have different salt concentration levels forming (upper convective, non-convective and lower convective). In transient scenarios, the analysis of the flow structure temperature, concentration and velocity distributions in the SGSP is extremely complicated because of the number of physical phenomena that happen inside the SGSP and also at the SGSP boundaries. Accordingly, and before proceeding it is beneficial to point out all the crucial hypotheses that do not alter the basic concept and the principles of the SGSP but created to help to investigate the transient heat and mass transfer in the salinity gradient solar pond alongside the hydrodynamics.

The assumptions are, (I) the properties of the system in the Y dimension of the rectangular cavity is deemed to be uniform and constant. Accordingly, the distributions of temperature, concentration and velocity in the SGSP are 2-D, (II) the SGSP has three different zones, upper convective zone, non-convective zone and lower convection zone, (III) The bottom and sidewalls are well insulated while the UCZ of the SGSP is subject to heat losses via convection (iv) the solar radiation reaching the SGSP bottom is considered to be consistent and entirely absorbed.

The mathematical model developed in section 5.2 includes equations that govern the concentration, temperature and velocity, besides the constitutive association between temperature and density. The resolution of Eqs. 3.53 - 3.62 with the boundary conditions represented in Eqs. 3.56- 3.61 is conducted numerically using finite element method. Also, as it has been mentioned earlier, FEniCs is

the programming package used to attack the non-linear variational problem directly. The parameters used in this particular study are introduced in the next section.

5.5.1 Parameters

The transient heat and mass transfer and hydrodynamic in the SGSP are studied under the parameters illustrated in Table. 5.1.

TABLE 5.1. Illustrates, parameters and values of all parameters in the dimensionless equations which correspond to an average characteristics of salt–water mixtures.[125, 72, 131]

Term (symbol)	Value
Internal Rayleigh number (Ra_I)	1.4×10^8
Thermal Rayleigh number (Ra_T)	1.0×10^7
Biot number (Bi)	500
Aspect ratio (A)	$\frac{3}{1}$
Schmidt number (Sc)	1000
Prandtl number (Pr)	6
Lewis number (Le)	166.6

The simulation starts with the fluid at a uniform initial temperature (0 dimensionless temperature, which is equivalent to 25°C) in the entire SGSP. The non-convective zone is established with gradient salt concentration profile, as shown in Fig. 5.4 ranges between 0 and 1 in dimensionless units, which is equivalent to 0 kg m^{-3} and 300 kg m^{-3} respectively. Note that all values correspond to the proposed Libya SGSP discussed in chapter 4.

The parameters used in the present study correspond to the properties of water-NaCl solutions. Also, they have been designed to actively opposing buoyant

conditions. Thermal Rayleigh number of 1.0×10^7, internal Rayleigh number of 1.4×10^8, these values represent the limit of salt stratification stability, and they correspond to experimental SGSPs. The buoyancy ratio N = 4, which represent a high salt concentration at the bottom of the SGSP in comparison to the top surface.

The dimensionless thicknesses of the upper convective zone, non-convective zone and lower convective zone are equal to 0.2, 0.6 and 0.2, which are equivalent to 0.4, 1.2 and 0.4 meters respectively, in dimensional form, and in compatibility with the 1-D study in chapter 4. In order to understand the evolution of temperature with time, the SGSP has been run for an extended period of time (Until SGSP became unstable).

5.5.2 Thermo-hydrodynamic behaviour

The present section provides a thorough exploration of the evolution of the velocity, concentration and temperature components during the absorption and storing of solar energy. It also provides a detailed explanation of the hydrodynamic instability of the SGSP. The initial set-up for the SGSP is shown in Fig. 5.4.

At the start of the simulation, a portion of the incident solar radiation transmits and arrives at the bottom of the SGSP where it heats the salt-water mixture there, as shown in Fig. 5.5. The NCZ acts as an insulating zone not permitting any upward heat loss from the bottom to the top of the SGSP, from areas of high temperature (hot) to areas of lower temperature (cold). This insulation or in other words the suppression happens due to the presence of the salt gradient profile shown in Fig. 5.4. At this gradient zone, the fluid is heated, and its density is insignificantly reduced but still higher than that of the layer just above it due to nature and the way it has been created. So, in the beginning, there is no upward movement of the hot fluid induced by the buoyancy force. And the heat loss from the lower convective zone is halted. There is also no other form of heat losses by conduction through bottom and sidewalls of the SGSP as they have been well insulated; thus, the lower convective zone heats up and sustains the thermal energy.

The portion of incident radiation absorbed in the upper convective zone also contributes to the heating of the UCZ, as shown in Fig. 5.5, leading to the growth of several thin thermal cells (convection currents which are represented by velocity fields) in the UCZ, as shown in Fig. 5.6. The temperature never exceeds 60 C° even though almost 20% of solar radiation is absorbed just beneath the surface of the SGSP, which can be observed more clearly in Fig. 5.5. The increase of temperature in the surface seems to be less notable and significant due to the high convective heat transfer coefficient, which makes the surface of this zone always close to the ambient.

On the other hand, in the LCZ, the rise of temperature seems to be more significant due to the vast amount of solar radiation absorbed and stored in the bottom of the SGSP. In the first period of operation, the solar energy absorbed in the bottom of the SGSP is transferred mainly by conduction to the nearby

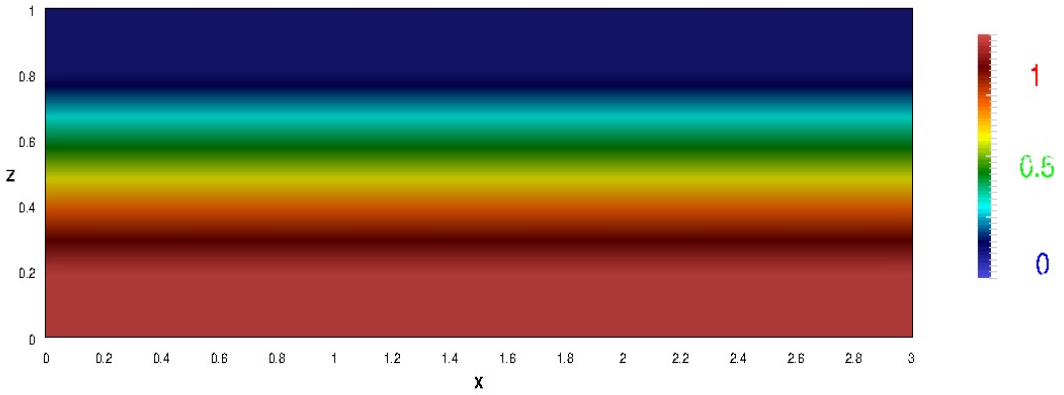

(A) Salt Concentration Profile At Initial State t=0. ■ φ=0, $C \equiv 0$ kg m^{-3}, ■ Salinity Gradient, ■ φ=1 $\equiv C = 300$ kg m^{-3}.

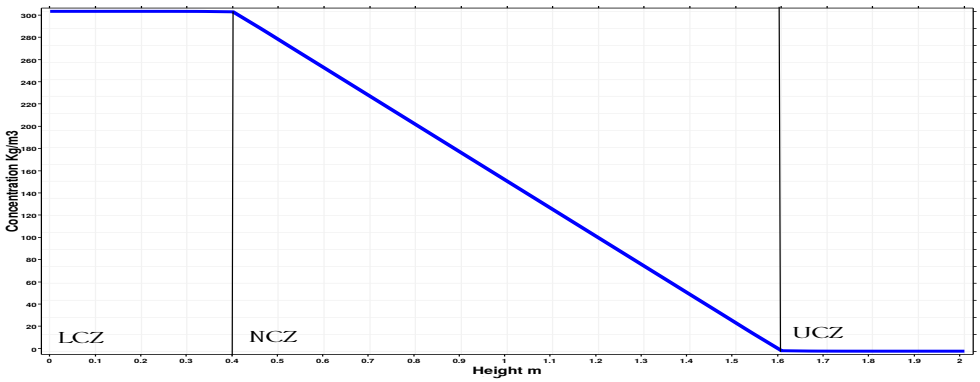

(B) Salt concentration profile shape at initial state t=0.

FIGURE 5.4. Initial set-up, concentration profile

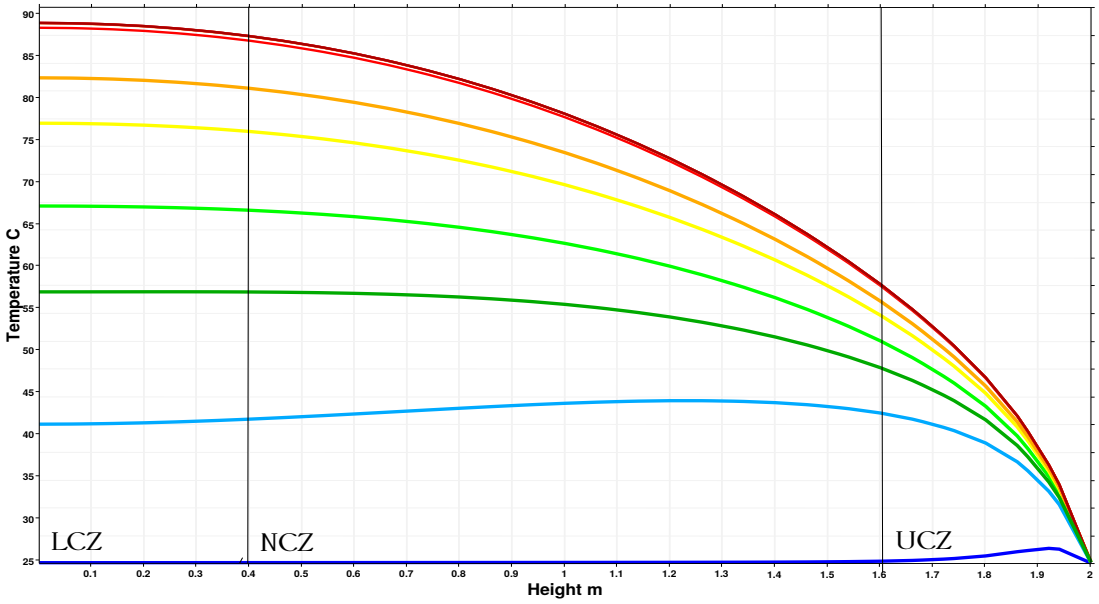

FIGURE 5.5. Evolution of temperature with time, ■ 1 Day, ■ 20 Days, ■ 40 Days, ■ 50 Days, ■ 60 Days, ■ 70 Days, ■ 80 Days. ■ 180 Days.

fluid layers. This explains that the uniform temperature in the LCZ, as shown in Fig. 5.5. The region under the interface of the NCZ-LCZ is also mainly dominated by conductive heat transfer; however, small dehomogenizing convective cells are also developed. Interestingly, the profile in Fig. 5.6 shows that the convective currents are a bit aggressive and dominant in the upper part of the LCZ, which could be related to the vulnerability of NCZ-LCZ interface area (density difference at the interfaces). While a conductive heat transfer still occurs in the lower part near the bottom of the SGSP.

Additionally, a vertical temperature gradient begins to develop just above the LCZ, as shown in Fig. 5.5, with time, this thermal gradient expands across the non-convective zone and becomes stronger forming a gradient shape profile in the non-convection zone. This could be related to the conductive heat transfer consistent progression from the LCZ to the UCZ, eventually driving to the creation of a temperature profile that is decreasing in the upward direction of the LCZ. Similar behaviour was noticed in the transient 1-D numerical, which was conducted earlier in chapter 4.

The lower convective zone temperature increases with time, as shown in Fig. 5.5. After 60 days of exposition to solar radiation, the temperature has undergone a noticeable increase, as shown in Fig. 5.5. After 80 Days, the LCZ temperature

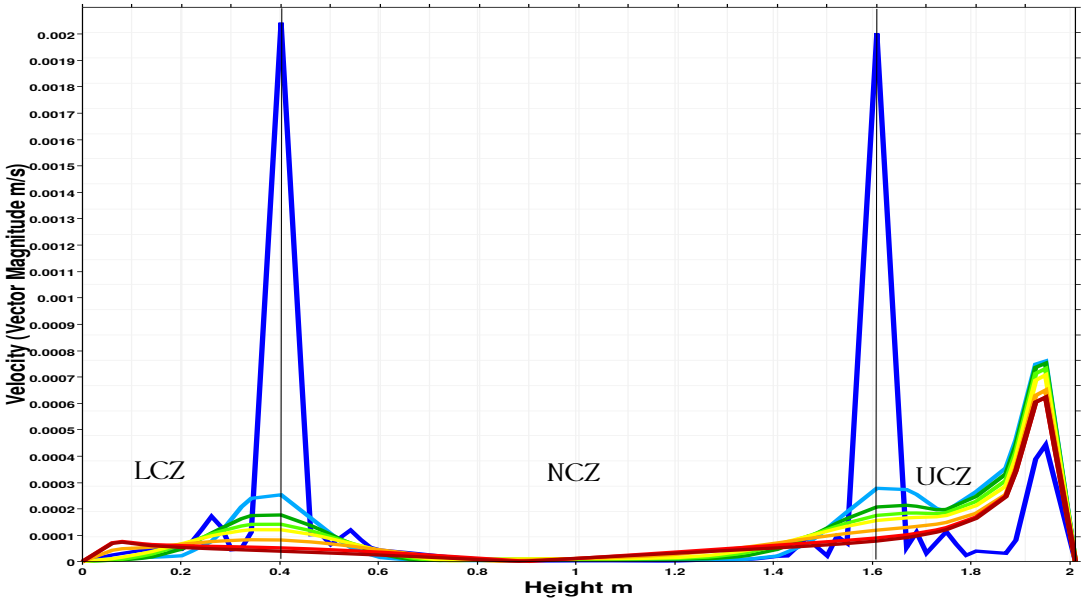

FIGURE 5.6. Evolution of Velocity (Vector magnitude) ■ 1 day, ■ 20 days, ■ 40 days, ■ 50 days, ■ 60 days, ■ 70 days, ■ 80 days, ■ 180 days (Become Unstable).

has significantly increased from the solar pond commissioning where the highest temperature occurred in the area located close to the bottom of the SGSP. The pond reached a steady-state temperature after almost ±80 days of operation. The SGSP heating rate was not constant during the operation period; in order to understand this variation in thermal behaviour, it is essential to understand the thermal behaviour and hydrodynamic behaviour collectively.

The evolution of velocity with time is shown in Fig. 5.6. The figure shows that the highest velocities appear at the initial stages of the SGSP operation. The highest velocity is noticed at the (UCZ-NCZ), (NCZ-LCZ) interfaces; however, these high velocities which represent the presence of convection currents did not deteriorate the NCZ performance in the short term. It is noteworthy to observe that when the NCZ thickness insignificantly decreased, the NCZ still able to suppress convection currents and does not permit overturn of the SGSP; however, after running the SGSP for a longer time, it has been noticed that these velocities which represent convection currents decreases in magnitude, but have expanded in size to cause shrinking of the NCZ thickness to an extreme limit which means the complete erosion of the zone. After almost 180 days of operation, the NCZ has become completely eroded and unstable, as shown in Fig. 5.7. The formation of convection currents in the non-convective zone deteriorated the SGSP thermal performance by reducing the NCZ thickness and subsequently insulation and resistance abilities to heat loss.

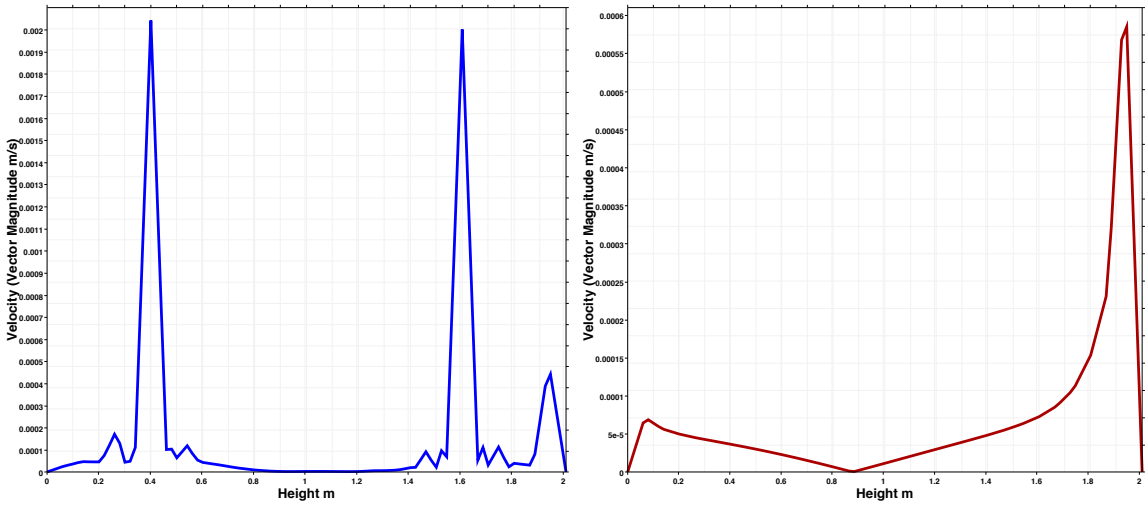

(A) Start up. (B) The moment SGSP became unstable

FIGURE 5.7. Zoom of velocity vectors, ■ t=0.1 day, ■ t=180 days.

The simulated velocities in the present study are in a good agreement with other velocities measurement of SGSP reported in the literature, which has never exceeded 0.02 m/s [9]; however, slightly higher velocities have been recorded at the start of operation in this study than that in the literature, and that can be justified to the high solar intensities considered in this study. The maximum velocity in the SGSP was witnessed at the UCZ and interfaces. Interestingly, the convective cells represent by velocity are found to be irregular-shaped, hinting that the continuous heat of the SGSP does not give time to develop a regular shape, so as was noticed in some steady-state experiments [59].

To further elaborate on how the SGSP became hydrodynamically unstable. The hydrodynamic instability could also be attributed to the distribution of temperature generated by the absorption of solar radiation which has a destabilising impact on the SGSP; the hot fluid becomes less dense than cold fluid at the same level of concentration. Following these conditions, the potential thermal energy collected in the temperature gradient is released by small perturbations, and this release yield is mixing and consequently the hydrodynamic instability of the SGSP. The stability of the gradient layer requires maintaining a net positive salt concentration and temperature distributions as a function of depth. The destabilising convective regimes observed in the UCZ and LCZ (Convection motions dominant in large part of the UCZ and LCZ due to the heating effect), could not be predicted by the 1-D numerical study since the 1-D model

assumes uniform temperatures in the upper convective zone and the lower convective zone. Consequently, the results obtained based on the later assumptions utilised in the 1-D model are of less precision. This highlights the significance of using at least 2-D models to describe the hydrodynamics within SGSP alongside other variables.

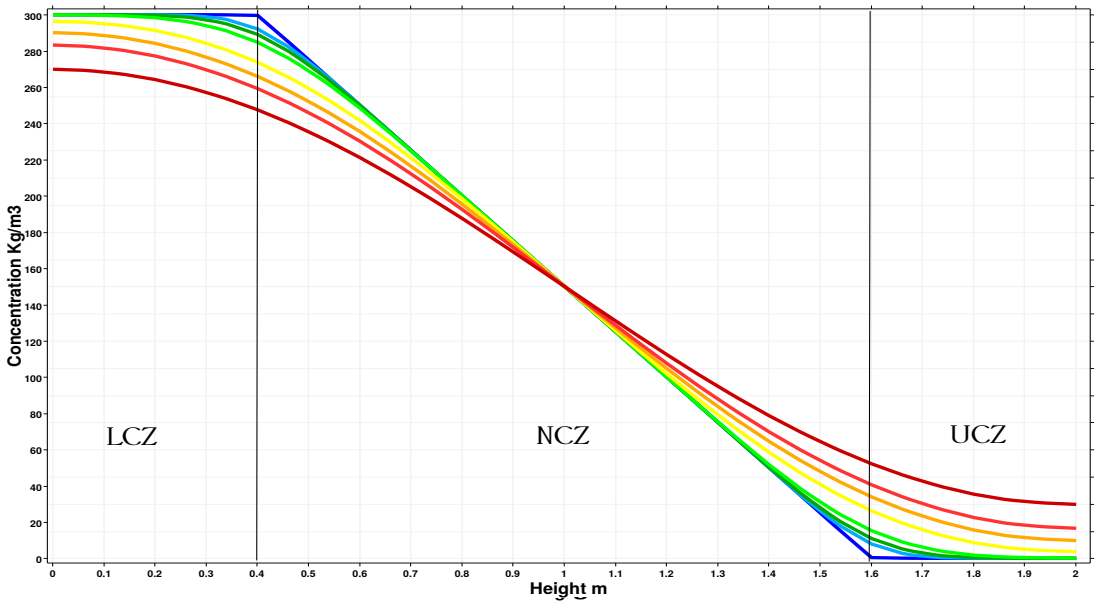

FIGURE 5.8. Evolution of Concentration with Time ■ 1 day, ■ 20 days, ■ 40 days, ■ 50 days, ■ 60 days, ■ 70 days, ■ 80 days, ■ 180 days.

It is important to relate the solutal behaviour in order to fully explain the hydrodynamic behaviour of the SGSP. The evolution of salt concentration profile inside the SGSP is shown in Fig. 5.8. It is apparent that there is no change in the concentration profile inside the SGSP from the start of operation; this indicates that the SGSP is stable, and the salt gradient does not require any maintenance; however, when the SGSP was run for a longer time, it has then been noticed that the salt concentration in the UCZ has slightly increased. This increase is due to the salt diffusion in the SGSP, and the occurrence of the mass transfer from the higher concentration zones, which is NCZ and LCZ to lower concentration zone, which is the UCZ. Similar behaviour was noticed in the transient 1-D numerical study in chapter 4; however, another primary reason for the mass transfer of salt was the convection currents developed at the interface of UCZ-NCZ, which could not be described by the 1-D model due to neglecting the hydrodynamic of the fluid.

Throughout the beginning stages of initiating the SGSP, the movement of salt might be beneficial to form and strengthen the structure of the salt gradient.

The pace in which the gradient is created and the movement of salt are proportional. But, after the gradient profile is established, the diffusion of salt will have a counterproductive effect. And it will affect the SGSP stability if no action is taken. Fig. 5.8 shows that the erosion of the non-convective zone as a result of mass diffusion from high concentration region to lower concentration regions and subsequently, the occurrence of convection due to the difference in densities. This occurrence, even if so slow, it degrades the salt gradient profile with time. In order to minimise the effect of this natural phenomenon and sustain the SGSP in operation for long periods of time, it is vital to add concentrated brine at and underneath the boundary between the lower convective zone and the non-convective zone and to flush the upper convection zone with low salinity water or freshwater.

The work of Newell et al. [98] has shown that a surface salt concentration of 5% is tolerable. Gupta [97] has stated that the UCZ concentration could be between 2% and 5% and above that, a surface flushing has to be done. Niel [138] in his experiment, no freshwater was added to the upper convective zone until the non-convective zone became extremely thin due to the mixed effect of heat loss from the top surface of the SGSP and the salt diffusion inside the SGSP. Thus, the insulating effect of the non-convective zone was declined, and the lower convective zone heat absorption decreased significantly. The UCZ was flushed with fresh water to solve the issue. According to this study observations, a 5% UCZ salinity is tolerable, and an increase of salt concentration above 15% leads to a complete turnover of the SGSP.

However, the salt concentration gradient in the NCZ can not be maintained by only if the UCZ water is quiescent. This is because of the effects of diffusion from the bottom to the top. The diffusion process is, in fact, too slow but because it is integrative and the regions involved are significant, a significant amount of salt diffuses upwards and towards the UCZ. Thus a number of measures have to be considered, (I) for best operational stability, the UCZ should be regularly flushed, and freshwater added, (II) substituting the diffused salt upwards by injecting more salt or by hindering the diffusion even though the latter option does not seem to be possible; however, with the current rapid technological advancement, this option could be possible in the future.

5.5.3 Motion of interfaces

One of the most significant advantages of the 2-D double-diffusive convection model over 1-D models is that it has the capability to describe the SGSP interfaces behaviour in a way that allows tracking and observing the evolution of the zones created by the diffusion of salt and the formation of convective current.

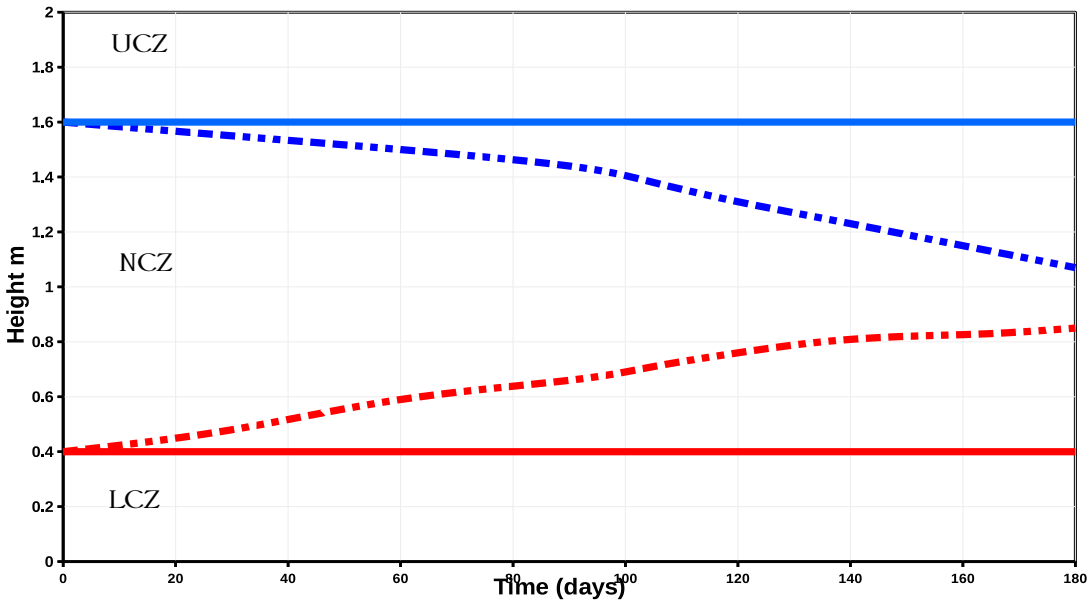

FIGURE 5.9. Illustration of the erosion of NCZ Thickness due to mass diffusion and expansion of convection currents. ■ UCZ/NCZ interface, ■ NCZ/LCZ interface. Dotted lines show the evolution of both interfaces with time defined by highest velocity area (Interfaces) where velocity is higher then ≈ 0.0001 m/s. The SGSP became unstable after 180 days.

Figure 5.9 shows the evolution and changes that occur to the zones during operation. Moreover, it demonstrates the upper convective zone/non-convective zone, and lower convective zone/non-convective zone interfaces shift from their particular original locations (see, initial salt concentration profile). This also shows that the intermediate zone is progressively eroded from both sides due to the expansion of convection currents. The interface location at the beginning was defined by the salt concentration profile, which is set at the stage of initiating the pond operation; however, during the SGSP operation period, it is not possible to identify the interfaces of the zones due to the convection currents formed at those regions. Thus, in order to identify the interface location, the evolution of velocity was computed. The interface was defined according to the velocities (Dotted lines show highest velocity area (Interfaces) where velocity higher then ≈ 0.0001 m/s.), as it has been noticed after one day of operation

that the highest velocities were at interfaces as shown in Fig. 5.6. The convection currents start to expand from the interfaces and move inward the NCZ, any area with a velocity higher than 0.001 m/s is considered a convective area and no more a part of the non-convective zone. Thus, points with lower velocities indicate the location of the non-convective zone (no convective motion). As shown in Fig. 5.9, quantitatively, the non-convective zone thickness changes from 1.2 m (initial thickness) to less than 0.12 m (thickness just before the end of simulations), which indicates that it experiences a reduction of around 80%, as shown in Fig. 5.9. The UCZ and the LCZ both have expanded to the detriment the non-convective zone (the dotted lines in the latter figure shows the evolution of both interfaces with time which was the distinct boundaries can be determined by highest velocity area (Interfaces) when velocity is higher then $\approx$ 0.0001 m/s) as shown in Figs. 5.7 and 5.9.

The stability of the interface can be attributed to the thermal gradient and its relation to the salt gradient. Any thermal gradient change causes a change of the salt gradient, which means that the outcome of this change is systematically followed by a change ins the location of the interface. In other words, instability occurs when the temperature gradient is large enough to make the buoyancy force goes down a particular critical value. The competition or the ratio between thermal and solute Rayleigh/buoyancy forces determines the state of the fluid and controls the expansion of convection currents. The effect of buoyancy ratio N on the hydrodynamic behaviour and long term stability of SGSP is a vital factor to investigate. In order to further understand the hydrodynamic stability of the SGSP, this matter will be investigated in more detail in the next chapter.

It can be concluded from the present study that, the operational stability of the SGSP is strongly governed by maintaining its zones at their specified thickness (mainly, maintaining the NCZ structure). It can be no more stressed than that the non-convective zone is unstable from both a thermodynamic and dynamic perspective. The factor that causes shrinking of this layer is mainly; the rising thermal gradients which accelerate the disposition of the interfaces and not allow the recovery of the solutal equilibrium gradient, which drives to the erosion of the non-convective zone (thickness decrease) and gradual deterioration of the salinity gradient solar pond stability. To the best of the author's knowledge, this findings and precise illustration of where and how the convection

currents start to develop and expand on the interfaces have never been shown nor explained in this detail in the literature. It can not be more emphasised that it is crucial to keep zone thicknesses at their specified height, Fig. 5.6 shows that there is a critical limit to NCZ thickness, where SGSP will become hydrodynamically unstable. This conclusion raises the question of what is the optimal NCZ/LCZ zone thickness ratio that will provide best thermal performance and longest term of stability, to the best to the researcher knowledge this question has not been answered anywhere in the literature considering the SGSP hydrodynamic (DDC effect). The next chapter will examine different NCZ to LCZ zone thickness ratios in order to find out the optimum zone thicknesses ratio.

5.5.4 Comparing findings with other 2-D simulation studies

In the present study, a 2-D numerical model was developed to study the hydrodynamic stability of the zones and consequently the SGSP operational stability. To the best of the author's knowledge, only [59, 72] have addressed the SGSP hydrodynamic stability numerically in a scale of 1 m height SGSP; however, as it has been mentioned earlier, neither the operational stability has been fully explained, nor the essence (when, how and where) of the hydrodynamic instability has been simulated in sufficient detail. Interestingly, Boudhiaf [72] has detected in his simulation results the presence of two fluid circulation zones, one located in the top of the SGSP while the other one was witnessed in the lower zone of the SGSP. He concluded that the expansion of these cells could lead to the SGSP instability. Boudhiaf conclusions are reasonable, and it matches the results were obtained in this study; however, Boudhiaf study does not show how, when and where the NCZ has eroded.

In the present study, velocity and concentration fields evolution with time are explained, the questions of why, where and how SGSP has gone hydrodynamically unstable are also answered by the clear illustration of the build and growth of convective motion inside the non-convective zone represented by velocity fields and interfaces motion as shown in Figs. 5.6, 5.7 and 5.9, respectively.

5.5.5 Comparative performance evaluation of the 2-D study and the 1-D study

Most previous theoretical studies have been conducted with simplified models adopting the one-dimensional approach [139, 87, 87], (only the energy equation was solved) neglecting the double-diffusive convection. That was the case in the 1-d study in chapter 4. The 1-D models can provide a good indication of stable SGSP thermal performance but not the SGSP stability. The main difference between the 1-D model and 2-D model is the assumptions have been made in the case of the 1-D model, i.e., unconditional stability of the SGSP neglecting of the double-diffusion effect. The aim of this study is to compare the thermal behaviour of the 1-D SGSP and the 2-D SGSP. For the purpose of this comparative study, the study is conducted using an average solar intensity of 300 W/m^2 to heat both SGSPs for almost 90 days. The initial temperature is 25 °C. The same parameters adopted in the previous 1-D and 2-D studies are used accordingly.

The result obtained from the one-dimensional transient model indicates that SGSP is perfectly suited to Libya geographical and climate conditions. SGSP can provide hot water with a temperature surpassing 60 °C most of the year which is hot enough water temperature to feed thermal destination units such as the MED-TVC (TBT = 60 °C). The same temperature was also obtained in the case of the 2-D, as shown in Fig. 5.10, which means the SGSP still has the same potential in deriving thermal energy to ME-TVC units. The only difference is that the 2-D SGSP shows that more time needed for the SGSP to reach 60 °C (almost 60 Days) than that predicted by the 1-D.

In the case of the 1-D SGSP, a temperature as high as 93°C (steady-state) is obtained after almost 75 days of operation with an average solar intensity while in the case of 2-D SGSP almost 85 days needed to reach 89°C (steady-state) as shown in Fig. 5.5, that is due to the double-diffusive effect (the upward heat loss via heat diffusion at the beginning of operation in addition to the formation of thermal convective cells). In the 1-D study the main heat loss from the pond is the heat loss from the top surface, while in the 2-d study, heat is also lost from the LCZ to upper layers due to the DDC effect. In the 1-d study, all heat has been absorbed in the lower layer remains at that layer, and that explains why the SGSP has a slightly higher temperature than the 2-D pond.

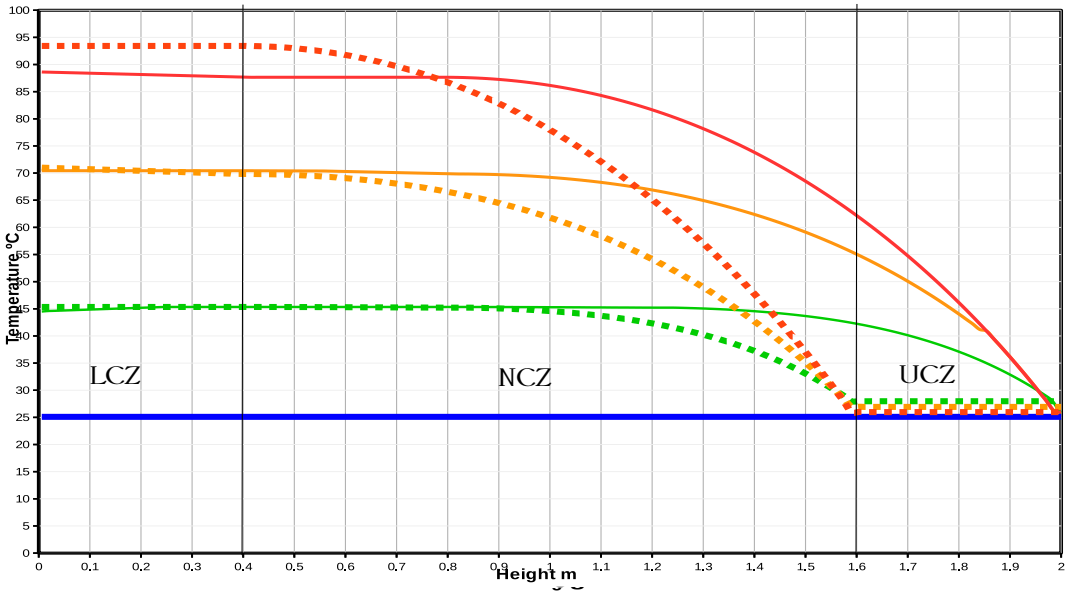

FIGURE 5.10. SGSP thermal behaviour (- - - -) 1-D SGSP, no DDC effect, and (——) 2-D SGSP, with DDC effect, ■ Initial profile, ■ 22/25 days, ■ 52/56 days, ■ 82/88 days, respectevily. Both 1-D and 2-D SGSPs are run for the same period (90 days) and using the same average solar intensity.

A sharp edge has been noticed in the UCZ/NCZ interface in the 1-D SGSP while they disappeared in the 2-D SGSP. The reason for that is explained earlier in Fig. 5.6, the reason is that in the 1-D SGSP, the velocity fields have been neglected. High velocity is always obtained at the (UCZ-NCZ), (NCZ-LCZ) interfaces and top surface, this convective movement at the interfaces will not allow any sharp edges to form. These convection currents after running the SGSP for long times expands (shrinking the NCZ thickness) to reach almost the middle of the NCZ, which leads to the erosion of the zone and affect it is performance. In the 1-D study, the salinity gradient solar pond was assumed to be always stable.

To conclude, Fig. 5.10 shows that the SGSP needs slightly more time to reach high temperatures in the case of 2-D SGSP in comparison to the 1-D SGSP. The inclusion of DDC inside the SGSP led to the erosion of the NCZ. If DDC effect does not exist, the erosion of the non-convective zone would not exist either, and both 1-D and 2-D SGSPs will reach the same steady-state temperature and at the same time.

5.6 Summary

The present chapter deals with the hydrodynamic stability problem of the SGSP. The study is conducted implementing and considering the effect of double-diffusive convection which was neglected in the 1-D study. The model applies Hull improved model for the absorption of the solar radiation with proper attention to the boundary conditions used in order to investigate the complex flow structure velocity, temperature and concentration in transient form.

Fenics code based on the finite element method was developed and used. The solution of the non-dimensional Navier–Stokes governing equations plus the equations of heat and mass provides sufficient detail data for the operational stability of SGSP.

Indeed, the first presence of convection current was noticed at the upper convective zone and the lower convective zone interfaces with the non-convective zone, which led to the erosion of the boundaries of the non-convective zone. The expansion of these convective current led to the shrinking of the non-convective zone thickness, as shown in Figs. 5.6 and 5.8. Thus, the formation and growth of any convective currents in this non-convective zone, cause mixing, deteriorate SGSP thermal performance, cause hydrodynamic instability and eventually destabilise the SGSP. For these reasons, interventions need to be planned in order to rectify the salt gradient. The way and the nature of interventions depend certainly on the characteristics of the non-convective zone (and mainly the thickness). The non-convective zone should be nearly a motionless layer to act as a transparent insulating zone, permitting energy capture and storage in the LCZ.

The DDC effect slows down the SGSP heating process after comparing the 1-D and the 2-D ponds; however, the temperature required to provide heat to thermal desalination units is still achievable in both ponds.

The next chapter aims to study the long term operational stability of SGSP, by studying the effect of zone thicknesses, buoyancy force and heat recovery on salinity gradient solar pond performance and operational stability, subsequently, providing some characteristic quantities for optimum zones thickness ratio and procedure that will enhance the SGSP long term operational stability.

Chapter 6

Zone thicknesses and Operational Stability

6.1 Overview

In chapter 5, the hydrodynamic stability of SGSP was investigated using a 2-D model. At the start of the SGSP operation, the fluid temperature and salinity both increase with depth, with thermal and salt concentration gradients being such that their respective contributions to the density gradient are balanced, and the fluid density is uniform; thus, the SGSP was stable, as there was no buoyancy force to drive large scale motion; however, with continuous solar radiation absorption and heating, convection currents build over time due to the double-diffusive convection (DDC) phenomena. The first appearance of the convection cells was at the boundaries of the NCZ, and they expanded with time. The DDC directly or indirectly led to the erosion of the boundaries of the insulating layer and reduces its thickness due to the continuous expansion of convection currents until a limit where continuous mixing in the NCZ took place, and the SGSP became completely eroded; as a result, the SGSP became hydrodynamically unstable. It is crucial to maintain the zones of the SGSP, especially the NCZ, at a thickness where the SGSP can always operate efficiently.

In hindsight to chapter 4, the 1-D study conducted illustrated that increasing the thickness of the NCZ helps to increase the LCZ temperature. A thicker NCZ provides better insulation for the LCZ, retaining heat absorbed in the LCZ and minimising heat loss via conduction from the LCZ where high temperatures exist to the UCZ where the temperature is low and close to ambient; however, it can be argued that increasing the NCZ thickness to an extremely large value

could lead to a reduced amount of solar radiation of which reaches the LCZ, which in return will slow down the LCZ heating process; thus, the LCZ could experience salt diffusion before it reaches high temperatures.

Other questions are, how the SGSP would hydrodynamically react if the NCZ is too large in comparison to the LCZ, or if they are equal in height, or if the NCZ is too small in comparison to the LCZ. The 1-D models can not answer and describe the hydrodynamic stability of the zones when altering their thickness; subsequently, a 2-D numerical study is considered.

The present chapter aims to study the effect of zone thicknesses on SGSP thermal behaviour and long term operational stability. The present study will also examine the effect of characteristics quantities such as buoyancy ratio and heat recovery on the operational stability of the SGSP. This chapter consists of three main sections that deal with, (I) The effect of zone thicknesses, (II) The effect of buoyancy ratio, and (III) The effect of heat recovery. Where in the first section, different zone thickness ratios are to be investigated for a SGSP that has a total height of 2 m. The aim of this section is to find the optimum (longest operational period with best thermal performance) NCZ: LCZ zone thickness ratio. The second section aims to investigate the effect of buoyancy ratio (altering the concentration levels in the SGSP zones) on the operational stability of the SGSP where different buoyancy ratios are assessed, and the final section deals with the effect of heat recovery, where a systematic heat recovery procedure is introduced, the SGSP is tested under two scenarios, (with no heat recovery) and (with heat recovery) in order to examine the impact of heat recovery on the SGSP long term operational stability. Finally, a summary of the chapter is presented.

6.2 Effect of zone thicknesses

This section investigates the effect of zone thicknesses on the SGSP thermal performance and operational stability. The proposed SGSP is located in Tripoli within the latitude and longitude of 32.54° N, 13.11° E and subject to the local climate. Different zone thickness ratios are to be examined for a SGSP that has a total height of 2 m. The bottom and the walls of the SGSP are considered to

be fully insulated; the UCZ thickness is kept at 0.4 m. The underpinning logic of choosing this particular height for the UCZ was explained in chapter 2. The same parameters used in chapter 5 is utilised to perform this study; however, this time, the UCZ is assumed to be flushed with freshwater to minimise heat losses to the environment. The SGSP has a uniform initial temperature which is equivalent to the ambient 25 °C throughout the SGSP zones and for all zone thickness settings.

6.2.1 Parameters

The transient heat and mass transfer and hydrodynamic in the SGSP are studied under the parameters illustrated in Table. 6.1. The parameters used in the present study correspond to the properties of water-NaCl solutions. Also, they have been designed to actively opposing buoyant conditions. Thermal Rayleigh number of 1.0×10^7, internal Rayleigh number of 1.4×10^8, these values represent the limit of salt stratification stability, and they correspond to experimental SGSPs. The buoyancy ratio N = 4, which represent a high salt concentration at the bottom of the SGSP in comparison to the top surface. The simulation starts with the fluid at a uniform initial temperature (0 dimensionless temperature, which is equivalent to 25°C) in the entire SGSP. The non-convective zone is established with gradient salt concentration profile, as shown in Fig. 5.4 ranges between 0 and 1 in dimensionless units, which is equivalent to 0 kg m^{-3} and 300 kg m^{-3} respectively. Note that all values correspond to the proposed Libya SGSP discussed in chapter 4.

The transient hydrodynamic, heat and mass behaviour in the SGSP with internal heating of the fluid due to solar radiation absorption is governed by non-dimensionalized continuity, momentum, thermal energy and mass transfer equations coupled with the equation of fluid density Eqs. 3.53 - 3.62, explained in Chapter 5. The parameters considered in this study are also listed in Table. 5.1. While Fig. 6.1 shows the schematic view of the SGSP set-ups (Initial concentration profiles and zone thicknesses) to be investigated in this particular study. Considering the NCZ thickness as a reference value.

TABLE 6.1. Illustrates, parameters and values of all parameters in the dimensionless equations which correspond to an average characteristics of salt–water mixtures.[125, 72, 131]

Term (symbol)	Value
Internal Rayleigh number (Ra_I)	1.4×10^8
Thermal Rayleigh number (Ra_T)	1.0×10^7
Biot number (Bi)	500
Aspect ratio (A)	$\frac{3}{1}$
Schmidt number (Sc)	1000
Prandtl number (Pr)	6
Lewis number (Le)	166.6

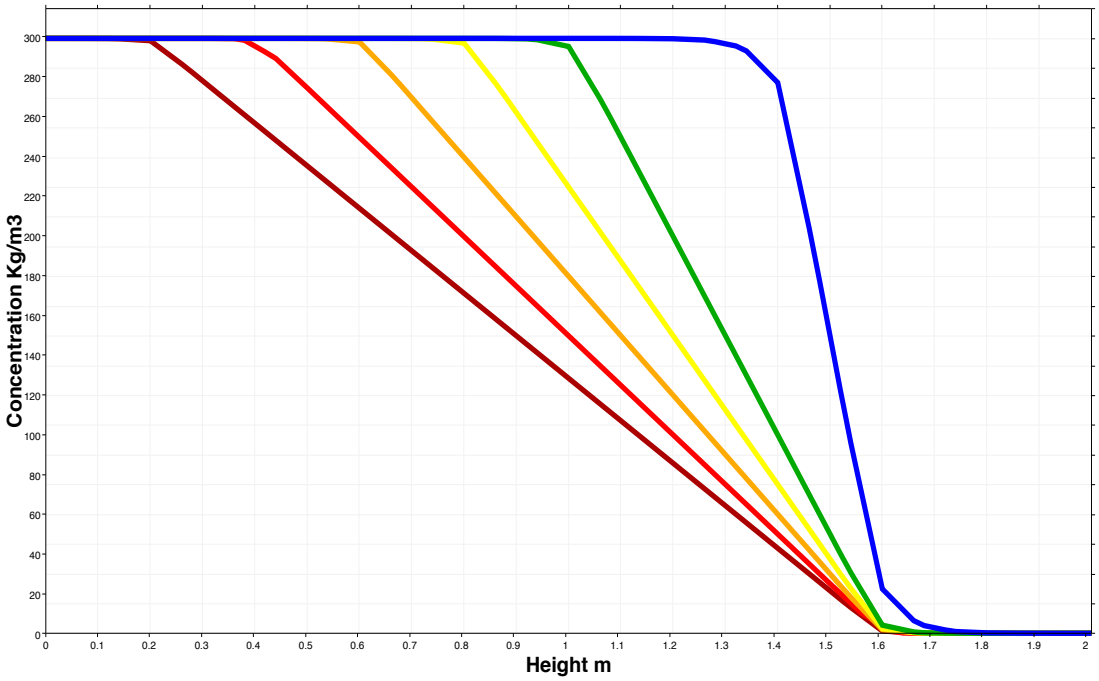

FIGURE 6.1. Different zone thicknesses set-ups, ■ NCZ= 0.2 m, ■ NCZ= 0.6 m, ■ NCZ= 0.8 m, ■ NCZ= 1 m, ■ NCZ= 1.2 m, ■ NCZ= 0.7.

6.2.2 A typical pond with no established zones

Before proceeding with studying the effect of the zone thicknesses on a salinity gradient solar pond, it is beneficial to explain why SGSPs have zones at first place. Consequently, the behaviour of a typical pond with no zones established is studied. This particular study considers the behaviour of a pond filled with salty water without an established salinity gradient in the middle. The pond bottom and sidewalls are well insulated, and it is subjected to high solar radiation. As part of the incident, solar radiation is absorbed in the upper part of the pond. It warms the water in that region. While another portion of incident solar radiation gets absorbed in the lower regions and also warms the water at that region. The hotter water in the pond rises to the top via conduction and convection. The cold water becomes heavy and sinks to the bottom. Convection currents are formed everywhere inside the pond (white convection cells), as shown in Fig. 2.1. Because of this continuous mixing, it is impossible to concentrate and store solar energy as thermal energy in a particular region of the pond. More specifically, in the lower region of this particular pond, the flow of the fluid is driven only by the thermal buoyancy force, and there is no mechanism to suppress and concentrate the thermal convection currents at the lower region and subsequently store useful heat at the bottom of the pond.

Figure 2.1 shows the importance of dividing the pond into zones that have different salt concentration levels; an upper convective zone (almost freshwater) to minimise heat loss to the environment, a non-convective zone (gradient increasing downward) to suppress heat in the bottom, and lower convective zone (high salt content) to store this heat. It is fundamental to create this insulating non-convection zone in the middle to suppress thermal convection currents at the bottom of the pond in order to store thermal energy, as without this particular zone continuous mixing in the entire pond will always occur, and no heat will be stored at the bottom of the pond as shown in Fig. 2.1. Therefore, the gradient zone is the main zone in SGSP design and operation.

6.2.3 SGSP at different zone thicknesses

This section investigates the optimum (longest operational period with best thermal Performance) NCZ: LCZ zone thickness ratio. The NCZ: LCZ zone thicknesses to be examined are illustrated in Table. 6.2. The initial concentration profiles for each SGSP set-up is shown in Fig. 6.1. The effect of zone thicknesses ratios is numerically investigated.

TABLE 6.2. Different NCZ: LCZ zone thicknesses set-ups.

Case	UCZ	NCZ	LCZ	NCZ: LCZ
1	0.4 m	0.2 m	1.4 m	1:7
2	0.4 m	0.6 m	1.0 m	1:2
3	0.4 m	0.8 m	0.8 m	1:1
4	0.4 m	1.0 m	0.6 m	2:1
5	0.4 m	1.2 m	0.4 m	3:1
6	0.4 m	1.4 m	0.2 m	7:1

The simulation starts with the fluid at a uniform initial temperature which is equivalent to the ambient 25 °C throughout the salinity gradient solar pond zones and for all zone thickness settings. On the first day of operation, the salinity gradient solar pond heats to about 1 °C, as shown in Fig. 6.2a, and it continues to heat gradually and steadily during the first 30 days, as shown in Fig. 6.2b, which means that solar radiation is trapped and stored in the LCZ as thermal energy. It should be noted that the salinity gradient solar pond zone thickness variations have similar thermal behaviour during the first 30 days of operation; all lines almost identical, as shown in Figs. 6.2a and 6.2b. Although insignificant, and slightly different thermal performances (temperature profiles) differences are noticed. This indicates that the competition between concentration and thermal forces has not changed largely in magnitude where solutal Rayleigh is still higher in comparison to thermal Rayleigh; thus, the SGSP heats up slowly and steadily, and heat diffusion dominates heat transfer process in the SGSP.

Therefore, at the start of the operation, the SGSP is stable, and there is no change in buoyancy force to drive significantly large scale motion. Interestingly, the initial thermal behaviour of the 2-D model is similar to that of the 1-D transient

model in chapter 4, where heat diffusion also dominates heat transfer in SGSP, but in the 1-D model, the double-diffusive convection effect was neglected; thus, the pond is assumed to be stable throughout its operational time.

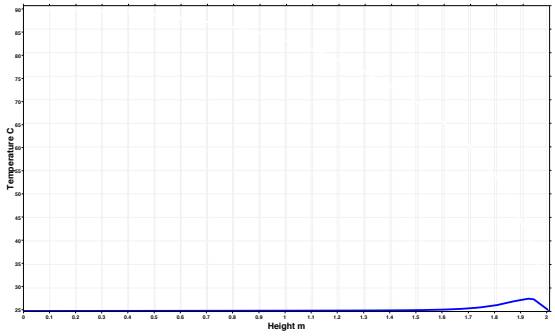

(A) One day of operation.

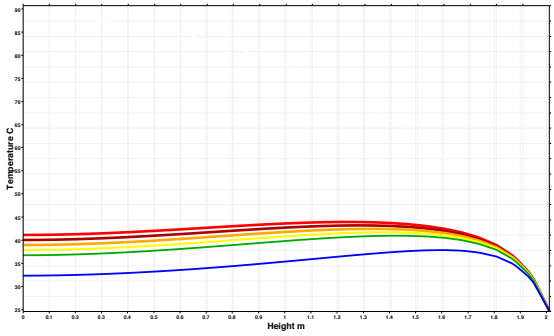

(B) 30 days of operation.

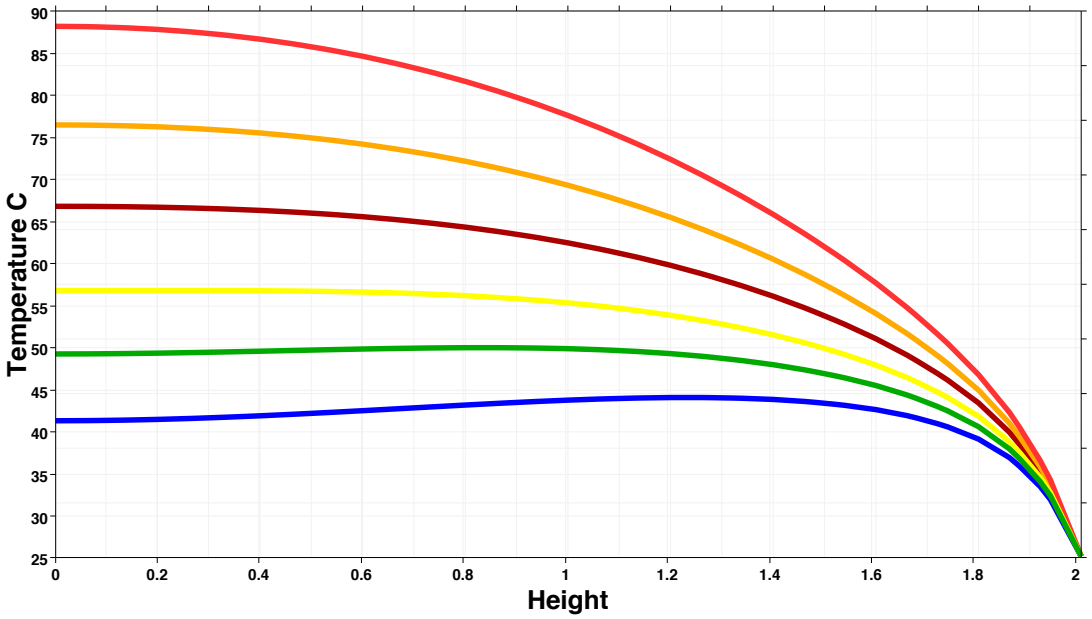

(C) Temperature profile before SGSP become unstable.

FIGURE 6.2. Temperature Profile, ■ NCZ= 0.2 m, ■ NCZ= 0.6 m, ■ NCZ= 0.8 m, ■ NCZ= 1 m, ■ NCZ= 1.2 m, ■ NCZ= 1.4 m.

The simulation is then run until the temperature profile reached steady-state, and that is for all zone thicknesses ratios. Fig. 6.2c shows the steady-state temperature, which is at the same time resembles the highest temperature achieved for all the thickness variations. From the figure, it is clear that the thermal behaviour and performance have varied after running the pond for a long period. After heating the SGSP for a longer period (ca. one month), convection currents start to grow at and beyond the boundaries. They expand gradually to erode the insulating layer at various rates for the different set-ups, as shown

TABLE 6.3. SGSP thermal performance and operation period at different NCZ: LCZ zone thicknesses ratios.

Case	NCZ (m)	NCZ:LCZ	Time to reach steady-state (days)	Maximum T °C	operation period (days)
1	0.2	1:7	36	42	36
2	0.6	1:2	60	49	91
3	0.8	1:1	65	58	110
4	1.0	2:1	75	76	150
5	1.2	3:1	88	89	220
6	1.4	7:1	70	68	120

in Fig. 6.6b. This explains why the thermal behaviour and performance varies, see Fig. 6.2b (during a short period of operation) and Fig. 6.2c (during the more extended period of operation). Table. 6.3 illustrates the time the pond needed to reach steady-state, the operational lifetime of the SGSP and the maximum steady-state temperature achieved for the different zone thicknesses ratios.

When the NCZ thickness is set at an extremely small limit of 0.2 m (blue line) which is equivalent to NCZ: LCZ thickness ratio of 1:7, the lowest thermal performance was achieved (lowest LCZ temperature), as shown in Fig. 6.2c. On the other hand, when the NCZ thickness is increased to an extremely large limit of 1.4 m (brown line), the thermal performance achieved is not as high as other NCZ thickness variations 1.0 m and 1.2 m. The best thermal performances (highest LCZ temperature) is achieved when NCZ: LCZ thickness ratios is 3:1, which represent NCZ/H = 1.2 m (red line). This could indicate that the system has the best hydrodynamic stability at this particular ratio. Fig. 6.2c shows clearly that an extreme reduction or increase of the NCZ thickness has a counterproductive effect on the SGSP thermal performance. The reason is attributed to the weak insulation capabilities when NCZ thickness is small, and subsequently, more heat loss from the bottom to the top. The second reason is the reduction of the amount of solar radiation reaching the LCZ when NCZ is extremely large.

Thus, for the best thermal performance, two points should be considered by the operator while adjusting the thickness of NCZ. The increase of NCZ thickness causes an increase in the LCZ temperature. This increase is the result of

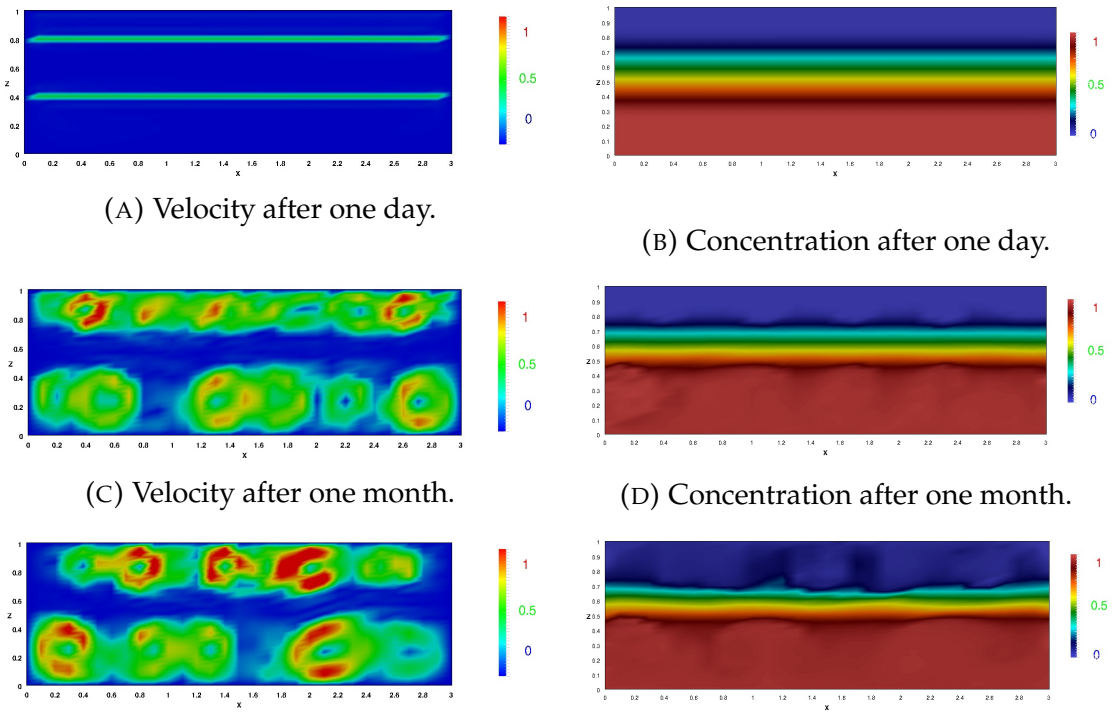

(A) Velocity after one day.

(B) Concentration after one day.

(C) Velocity after one month.

(D) Concentration after one month.

(E) Velocity at instability.

(F) Concentration at instability.

FIGURE 6.3. Illustration of the hydrodynamic behaviour and the salt concentration profiles inside the SGSP at NCZ: LCZ = 1:1.

the high insulation provided by a thicker NCZ which minimises the upward heat loss from the lower convective zone. The second point is, in the case of increasing the NCZ to an extremely large thickness, the radiation reaching the LCZ decreases (radiation has to pass through a more significant path with consequent higher absorption before it reaches the lower convective zone), which brings down the temperature of the LCZ. This is manifested in Fig. 6.2c when the NCZ thickness is set to 1.4 m (brown line). Consequently, this adverse effect offset the beneficial effect of reduced heat loss. At an NCZ thickness of 1.2 m, the effect of reduction in radiation input is still equal in magnitude to that due to heat loss, and at this stage, the SGSP has maximum collection efficiency. Table. 6.3 illustrates the time the pond needed to reach steady-state, the operational lifetime of the SGSP and the maximum steady-state temperature achieved for the different zone thicknesses ratios.

In order to understand the hydrodynamic behaviour, and answer the operational stability question of why the non-convective zone has become unstable more quickly when it has an extremely small or extremely large thickness, it is crucial to link the heat, the mass and the hydrodynamic behaviour collectively.

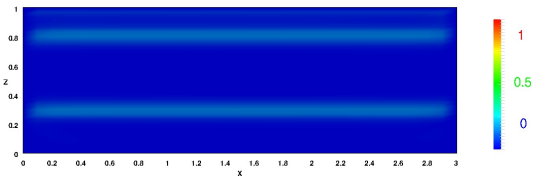

(A) Velocity after one day.

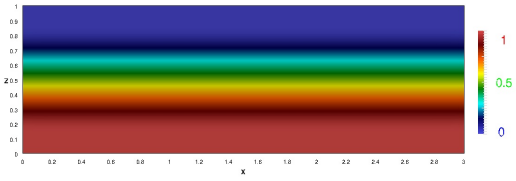

(B) Concentration after one day.

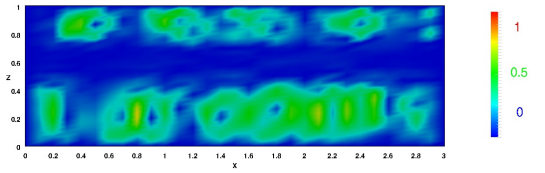

(C) Velocity after one month.

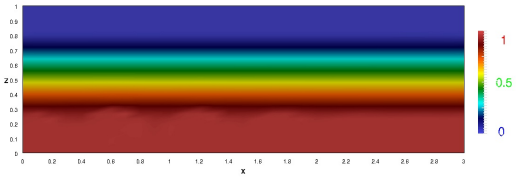

(D) Concentration after one month.

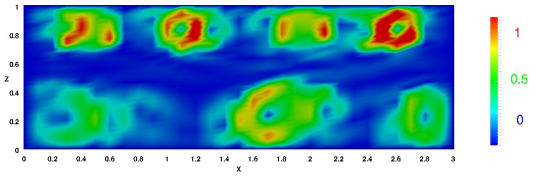

(E) Velocity at instability.

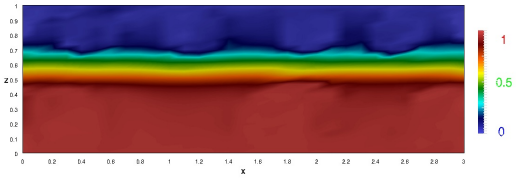

(F) Concentration at instability.

FIGURE 6.4. Illustration of the hydrodynamic behaviour and the salt concentration profiles inside the SGSP at NCZ: LCZ = 2:1.

Consequently, the evolution of the velocity fields is generated for all zone thicknesses ratios. When the salty water is heated, convection cells build and grow over time (convection currents) as shown in Figs. 6.4 and 6.3. It is interesting to observe that it first develops thermal gradients at the most vulnerable parts, which are the interfaces of the salinity gradient solar pond, as shown in Figs. 6.4, 6.3 and 6.6a. The velocity figures reflect both the speed and at the same spirit the location of convective motion as shown in Figs. 6.6a and 6.6b (during a short period of operation) and Fig. 6.6c (during the more extended period of operation). Clearly, there are significant differences in velocity magnitude at the interfaces depending on the NCZ: LCZ thickness ratio specified.

Another observation is, with decreasing NCZ thickness, the convection currents at the interfaces become higher in magnitude, and their expansion and damage to the NCZ is faster, as shown in Figs. 6.6a, 6.6b and 6.6c. Thus, the thinner the NCZ, the faster it will reach a critical limit (Tiny insulating layer, as

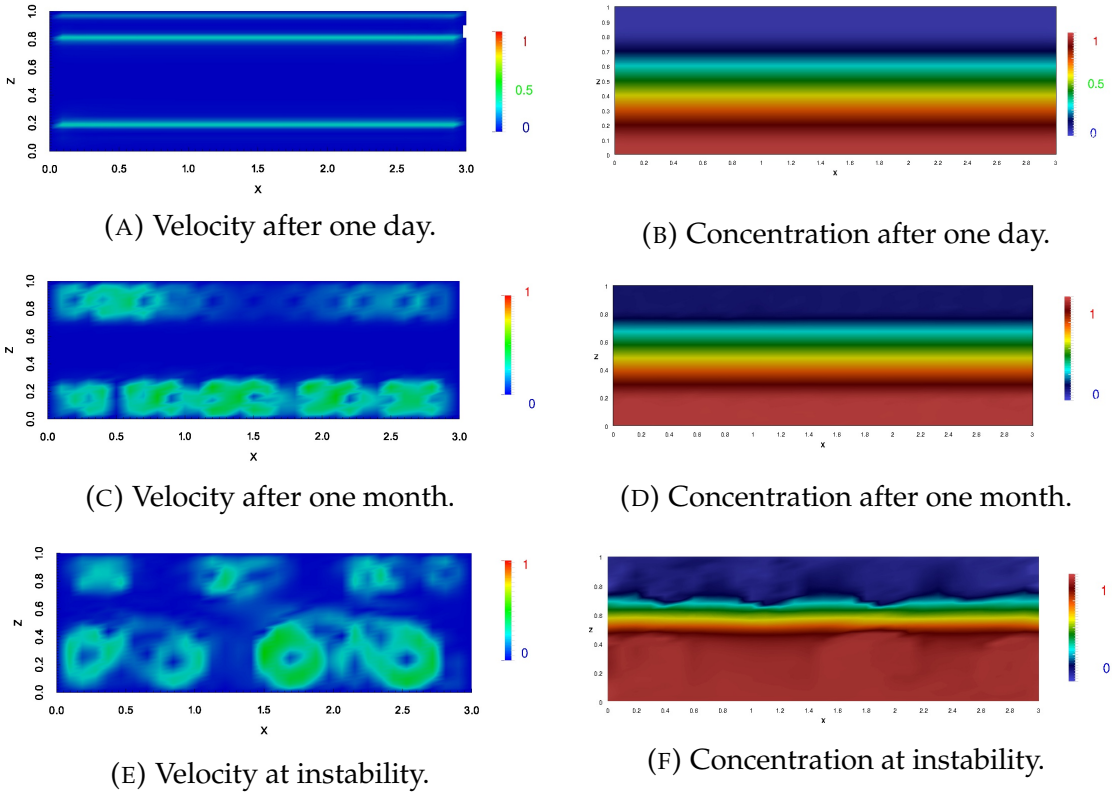

(A) Velocity after one day.

(B) Concentration after one day.

(C) Velocity after one month.

(D) Concentration after one month.

(E) Velocity at instability.

(F) Concentration at instability.

FIGURE 6.5. Illustration of the hydrodynamic behaviour and the salt concentration profiles inside the SGSP, NCZ: LCZ = 3:1.

a result of the fast expansion of the convective current) where it becomes unstable and unable to store any heat as shown in Fig. 6.2c. In the case of a thick NCZ, the SGSP hydrodynamic response to the effect of daily solar radiation is slow in terms of fluid motion, as shown in Figs. 6.6a, 6.6b and 6.6c; thus, the erosion from buoyancy-driven flows is also small. Both the thermal performance and hydrodynamic stability of the SGSP deteriorates according to the amount of the damage (shrinking) that occur to the insulating layer, and the thicker the NCZ, the more its resistance to the DDC effect; however, an extreme NCZ design thickness (i.e. 1.4 m) has a counterproductive consequence as it could not tolerate as small LCZ that diffuses salt and heat faster as shown in Figs. 6.7c, 6.6c and illustrated in Table. 6.3. This indicates that there is an optimum NCZ to LCZ thickness ratios where SGSP is more resistance to the DDC effect, which should be considered.

For an NCZ: LCZ zone thicknesses ratio of 3:1, the effect of reduction in radiation input becomes equal in magnitude to that due to the reduction in heat loss, and at this stage, the pond has a maximum solar collection efficiency. The best

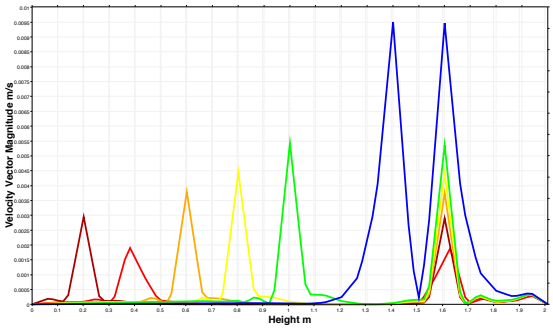

(A) One day of operation.

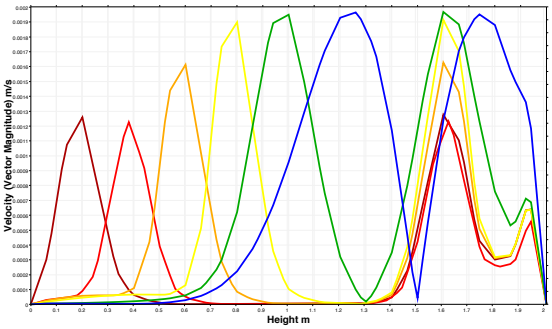

(B) 30 days of operation.

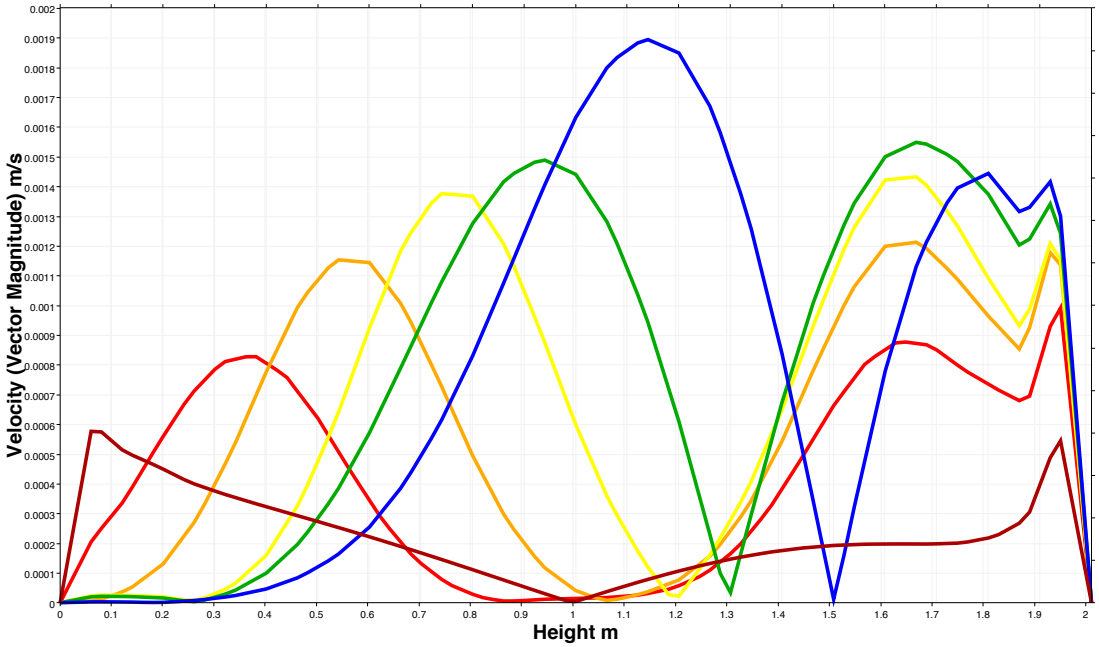

(C) Velocity profile at the time before SGSP become unstable.

FIGURE 6.6. Velocity profile, ■ NCZ= 0.2 m, ■ NCZ= 0.6 m, ■ NCZ= 0.8 m, ■ NCZ= 1 m, ■ NCZ= 1.2 m, ■ NCZ= 1.4 m.

operational stability is also obtained at this ratio as the SGSP hydrodynamic response to the effect of daily solar radiation is slow in terms of fluid motion as shown in Figs. 6.7c, 6.6c and 6.2c.

To further understand the effect of zone thicknesses on the hydrodynamic stability of the SGSP, it is fundamental to relate it to the solute behaviour inside the SGSP. The NCZ is established with a gradient salt concentration profile, as shown in Fig. 6.7a. This concentration profile ranges from low salt content in the UCZ to high salt content in the LCZ which are equivalent to 0 kg m^{-3} and 300 kg m^{-3}, respectively. The evolution of the salt concentration profile has been simulated for one day, 30 days, and until the time SGSP becomes unstable,

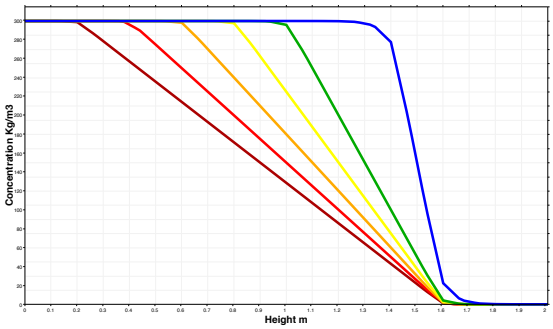

(A) One day of operation.

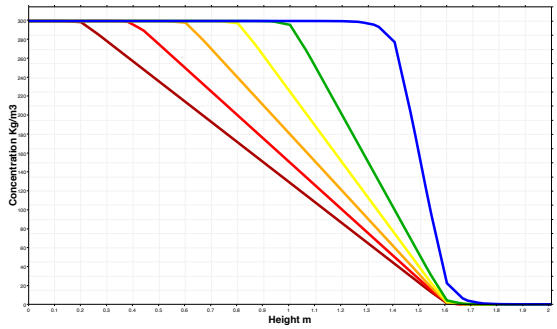

(B) 30 days of operation.

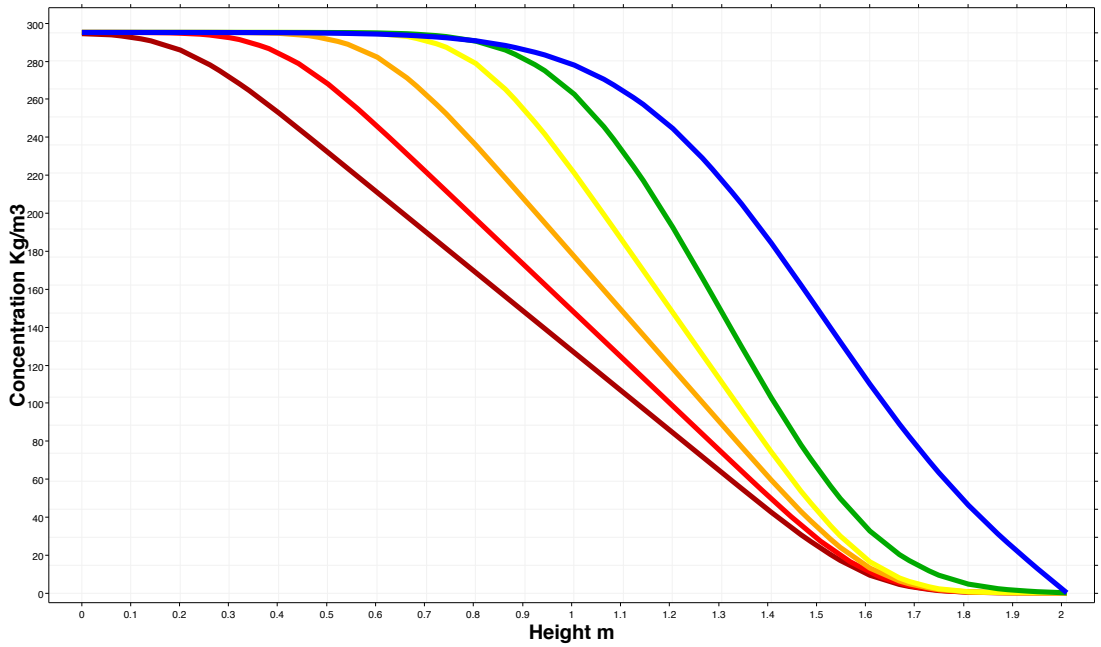

(C) Concentration profile the time before SGSP become unstable.

FIGURE 6.7. Concentration profile, ■ NCZ= 0.2 m, ■ NCZ= 0.6 m, ■ NCZ= 0.8 m, ■ NCZ= 1 m, ■ NCZ= 1.2 m, ■ NCZ= 1.4 m.

as shown in Figs. 6.7a, 6.7b and 6.7c, respectively. It is noticed that salt diffusion is a slow process in comparison to heat diffusion.

In the NCZ, the solutal behaviour appears to be similar and reveal almost an identical average salt concentration at all thickness ratios examined as shown in Figs. 6.7a, 6.7b and 6.7c; however, it can be noticed that there is a decrease or degradation of the level of salt in the most vulnerable parts, which are the boundaries of the NCZ. This degradation is due to the diffusion of salt from areas where the salt concentration is high to areas where the salt concentration is less. For NCZ/H = 1.4 m, which resembles an NCZ: LCZ thickness ratio of (Extremely large NCZ), the salt diffusion from the relatively small LCZ to

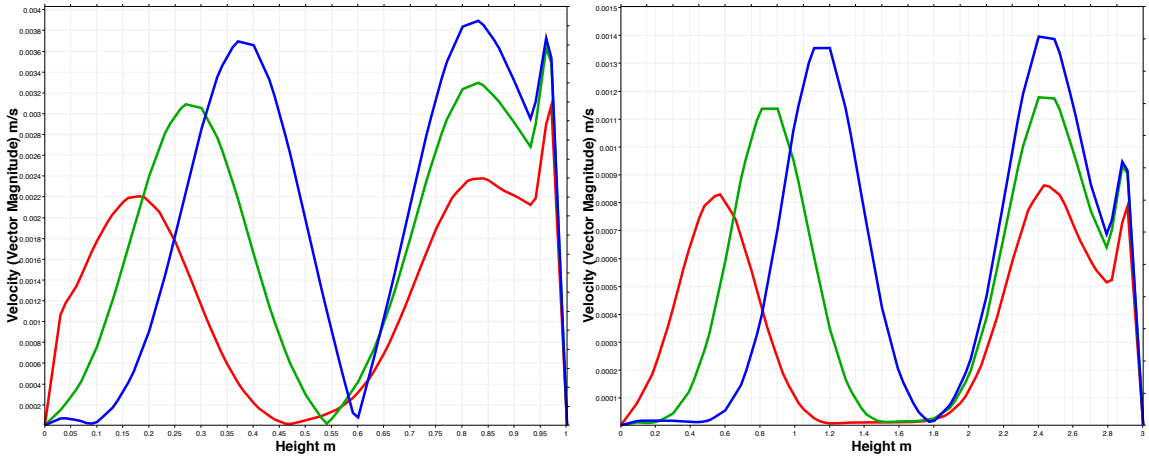

(A) One meter SGSP. (B) Three meter SGSP.

FIGURE 6.8. Effect of zones thickness ratio on SGSP long term stability for different SGSP heights (t = 90 days), ■ NCZ:LCZ= 1:1 , ■ NCZ:LCZ= 2:1, ■ NCZ:LCZ= 3:1. Velocity profiles indicates that the SGSP has the longest term of stability at NCZ:LCZ zone thickness ratio 3:1 (Lowest NCZ errosion percentage is obtained at this ratio).

NCZ was significant and eventually contributed to mixing and destabilising the SGSP in a short period. This breaks the rule that the larger the NCZ, the better, thus, this is another illustration that a large NCZ cannot tolerate the negative impact of small LCZ due to the rapid diffusion of salt. Therefore, an optimised and balanced NCZ: LCZ thickness ratio where SGSP performs with the best thermal performance and for the longest period is a key for an effective, efficient and stable system.

At a thickness ratio of 3:1 (red line), the concentration profile drops significantly, as shown in Fig. 6.7c, that can be attributed to the long period of operation which, exceeded 180 days in comparison to other thickness ratios where the operational lifetime of the pond has not exceeded 135 days. Although the change in all concentration profiles is not significant, this change has a significant impact, as it contributed indirectly to eroding the NCZ. The reduction of the level of salt concentration at the boundaries contributes to change in densities and consequently, the formation of the convection currents in the non-convective zone. Therefore, the dynamic of salt diffusion is critical to keep under control.

To summarise, the present 2-D study explains the effect of SGSP zone thicknesses on the SGSP thermal performance and operational stability in sufficient detail. Although salinity gradient solar ponds at all NCZ: LCZ zone thickness ratios eventually become unstable (at different times) due to the DDC effect.

The DDC effect leads to the growth of convection cells, which expand with time due to the continuous heating, causing inward damaging convective motion at the interfaces that lead to the shrinking of the non-convective zone to a critical limit where SGSP becomes unstable; however, as illustrated earlier, the SGSP thermal performance and operational lifetime (stability time) differ from one NCZ: LCZ zone thickness ratio to another.

According to the simulation results, a ratio of 3:1 (NCZ/H = 1.2 m) is found to be the optimum zone thickness ratio for an average height 1, 2 and 3-meter SGSPs, the longest stability (Operational Time) is obtained at this particular ratio as shown in Fig. 6.8; however in the case of 1 m SGSP an 0.2 m LCZ could not be an ideal thickness for this particular zone as heat extraction process need larger zone area to avoid mechanical instability. In the case of the average height SGSP with 2 m height; an NCZ: LCZ thickness ratio of 3:1 which corresponds to 0.4 m for UCZ, 1.2 m for the NCZ and 0.4 m for the LCZ can also be the most cost-effective option for a 2 m SGSP. One should not neglect that the increase in salt requirements that will follow the increase in the thickness of LCZ if other NCZ: LCZ thickness ratios such as 2:1 or 1:1 are to be considered, which will add to the capital cost.

For desalination applications, a regular temperature just above 60-65°C is needed to operate a MED-TVC desalination unit. This temperature should be maintained throughout the year. If any NCZ: LCZ thickness ratio is considered, it is crucial to assure a temperature above 60-65 °C is always maintained (long term stability). The financial (thermo-economical) implications of increasing or decreasing the thickness of the NCZ must also be assessed in order to justify what is optimum. As mentioned, any increase or decrease should always justify the capital and operating expenditure.

The thermal behaviour observed at the start of operation is interesting, as SGSP tends to heat up gradually and steadily in all the three zones regardless of the NCZ: LCZ zone thicknesses ratio set. This indicates that the competition between concentration and thermal forces is balanced at the start of operation where solutal Rayleigh is higher in comparison to thermal Rayleigh, thus, the SGSP is stable, and it heats up slowly and steadily where conduction dominates heat transfer process in the SGSP. In other words, there is no significant

change in buoyancy force to drive large scale motion. Subsequently, it is important to keep the relative balance of temperature and concentration contributions to the density field intact in order to minimise the double-diffusive effect and maintain the stability of the pond. Buoyancy force represents this competition between thermal and solute Rayleigh, which determines the state of the fluid.

6.3 Effect of buoyancy ratio

This section aims to study the effect of buoyancy ratio on the hydrodynamic behaviour and operational stability of the SGSP. The SGSP with the optimum zone thicknesses (UCZ = 0.4 m, NCZ = 1.2 m, LCZ = 0.4 m) is examined under different buoyancy ratio; (I) N = 0.1, (II) N = 1, (III) N = 2, (IV) N = 4 and, (V) N = 6. The buoyancy ratio approximation is given by [45]:

$$N = \frac{\beta_C \Delta C_s}{\beta_T \Delta T} \tag{6.1}$$

where N is the buoyancy ratio, β_C and β_T are the thermal and solutal expansion coefficient, respectively, given by [45]. ΔC_s is the salinity difference and ΔT is the temperature difference. From an operator point of view, this investigation explains if a procedure like increasing the buoyancy force (increasing the level of salt concentration at LCZ in order to make the fluid at the bottom dense enough) helps to minimise the DDC effect and consequently enhance the long term operational stability of the SGSP. Table. 6.4 provides an indication of the salt requirements according to salinity and Buoyancy.

TABLE 6.4. Buoyancy, salinity, density, concentration estimates for NaCl solution [140].

Salinity C_s wt %	Density kg m^{-3}	LCZ concentration kg m^{-3}	Buoyancy ratio
1	1018	10.18	0.1
5	1048	52.4	1
10	1078	107.8	2
25	1168	299	4
35	1230	430.5	6

For the purpose of this study, some assumptions are made. The SGSP is run from steady-state where the temperature at the LCZ is 100 °C, the NCZ is well established, and the temperature at the UCZ equals to the ambient 25 °C. Thus, at the start of the operation, ΔT between the LCZ and UCZ equals 75 °C. The UCZ salt concentration equals 0 while the LCZ concentration varies according to the buoyancy ratio specified, (see Table. 6.4). The fluid is assumed to be stagnant at the start of the operation; thus, velocity equals 0 everywhere inside the pond. The study is conducted, incorporating the assumptions, governing equations and parameters used in the zone thicknesses study.

SGSP at different buoyancy ratios

The first simulation starts with a buoyancy ratio N = 0.1, which is a ratio that violates the stability criteria in Section 2.8.3 that is suggested by [20]. For this particular ratio N= 0.1, after running the SGSP for two weeks, no heat was stored in the LCZ due to the continuous mixing inside the non-convective zone that led to complete turnover as shown in Fig. 6.9a. The presence of convection currents in the non-convective zone violates the main design concept of salinity gradient solar pond which is maintaining the gradient and insulating layer as a non-convective zone above the lower convective zone in order to function as an insulation barrier suppressing thermal convective currents generated in LCZ. Therefore, the stability condition suggested by [45] is valid and should always be met.

For N = 1 the stability condition is met, the competition between thermal and solute buoyancy forces becomes the same order of magnitude. The convective motion induced by the absorption of solar radiation is suppressed at the upper and lower convective layers, as shown in Fig. 6.9b; however, the NCZ has still been eroded to some extent at this ratio. For N = 1, there is not enough gravitational resistance to the mixing caused by the DDC effect, and the temperature rise also weakened the density distribution. Thus, meeting the stability criteria could not be enough when considering long term operation stability. Higher buoyancy ratios (Salt concentration should be heavy enough to prevent convection current from eroding the NCZ) are required for better protection to NCZ from erosion and subsequently longer operational stability.

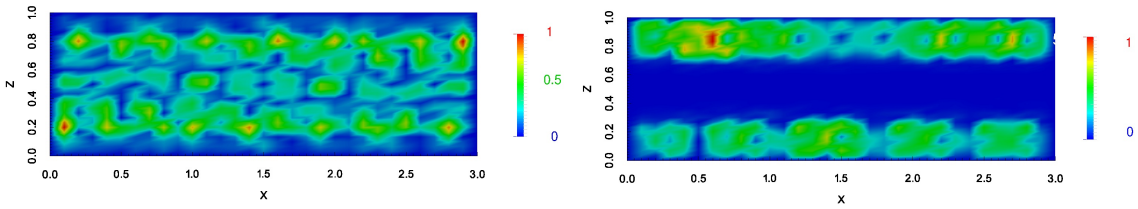

(A) Velocity profile illustrates the continues mixing when stability condition is violated. N = 0.1, SGSP instantly after 3 days of operation becomes Unstable (0 lowest velocity and 1 highest).

(B) Velocity profile when the stability condition is met. N = 1, at Two weeks of operation from steady-state (0 lowest velocity and 1 highest).

FIGURE 6.9. Effect of buoyancy ratios on the SGSP hydrodynamic behaviour.

For buoyancy ratios of 2, 4 and 6, no significant fluid motion is observed in the NCZ after one day of operation as shown in Figs. 6.10a; Hence, the competition between thermal and solute buoyancy forces is high. The convection currents induced by the absorption of solar radiation are significantly suppressed by the NCZ, while just smaller circulation eddies are generated in the UCZ (with relatively high velocities). Other convective cells are observed in the NCZ-LCZ interface. These velocities are larger than those observed when N = 1. This could be attributed to the high competition between thermal and solutal forces. At the start of the operation, diffusion dominates thermal and mass transfer process, considering that the solution is dense enough in the bottom at these ratios (N = 2, 4 and 6). Diffusion is the dominant heat and mass transfer process at this stage, and it is an extremely slow process.

However, after running the SGSP for a longer period (two weeks), convection currents start to evolve, grow and expand with time to erode larger parts of the NCZ at different rates. When N = 1 and 2, the erosion was significant, as shown in Fig. 6.10b. At a buoyancy ratio of 4 and 6, the solution in the LCZ is dense enough to prevent convection from eroding the NCZ; consequently, the SGSP is more resistance to the DDC effect. At N = 6, the SGSP has better stability (hydrodynamic stability) than when the buoyancy ratio is 4, as shown in Fig. 6.10c; however, from an economic point of view, at N = 6, the salt requirement is going to be the highest. Table. 6.5 illustrates the operational time of the SGSP at different buoyancy ratios. The operational lifetime is less than those observed in the previous study, as in this study, the SGSP is assumed to be operated from steady-state (maximum LCZ temperature); however, the N and operational lifetime figures in the table give an indication of a procedure

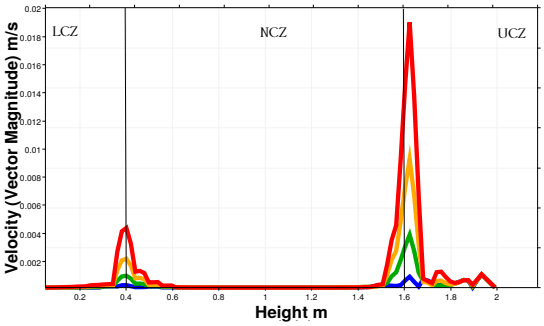

(A) One day of operation.

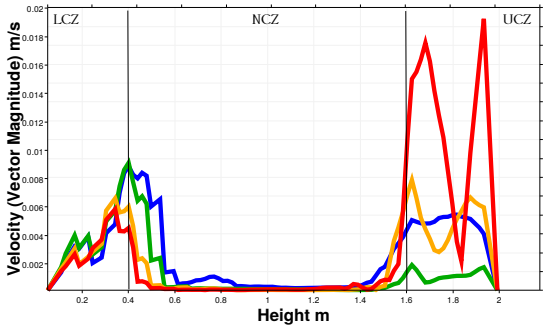

(B) Two weeks of operation.

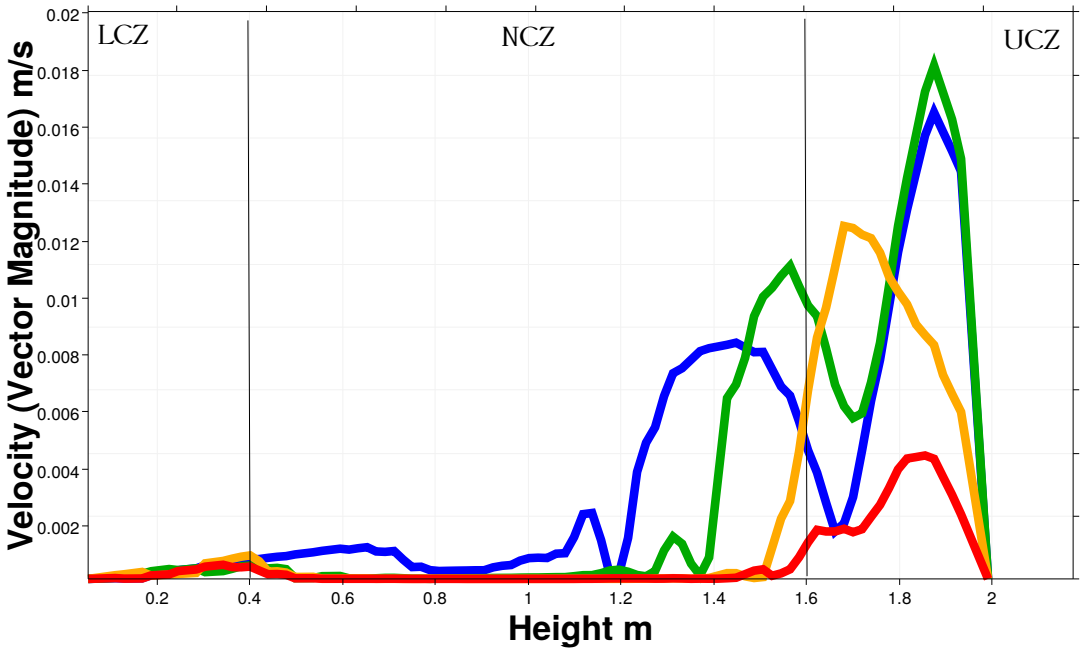

(C) Velocity profile the time before SGSP becomes unstable.

FIGURE 6.10. Velocity profiles, ■ N= 1, ■ N = 2, ■ N= 4, ■ N= 6.

such as increasing the buoyancy ratio (increasing salt content) helps to extend the operational lifetime of an on operation SGSP. It is clear that with adjusting the buoyancy ratio (N=6, LCZ salt concentration = 430.5 kg/m^3), the SGSP can be operative for another 150 days from steady-state.

In order to further understand the effect of buoyancy ratio on thermal behaviour, the distribution of temperature, concentration and velocity in the salinity gradient solar pond are studied collectively. For a buoyancy ratio N = 1, the convective motion induced by the absorption of solar radiation easily disturbs the system. Thermal convective currents transfer heat to the upper zone where the transferred heat causes a rise in temperature to that zone (potential heat losses)

TABLE 6.5. SGSP operation stability at different N ratios.

i	Buoyancy ratio N	LCZ T °C	Operational time (days)
1	0.1	31	Instantious mixing
2	1	91	50
3	2	92	75
4	4	95	130
5	6	97	150

as shown in Figs. 6.11a and 6.11b.

When the buoyancy ratio is increased to value equals to 6, the fluid in the bottom becomes dense enough. This hinders both salt diffusion and convection currents from growing fast and from expansion; thus conduction dominates heat transfer process in SGSP. Fig. 6.11c clearly shows that the increase of buoyancy ratio from 1 to 6 helps to maintain the stored energy in the LCZ, and minimises the heat loss from the LCZ to the UCZ.

To elaborate further on the operational stability of the system. Concentration profiles are also generated. The concentration profiles illustrate the difference in the solutal behaviour for the four buoyancy ratios examined, as shown in Figs. 6.12a, 6.12b and 6.12c. At N = 6 and 4, the concentration profile is the most stable and the least affected by DDC effect, whereas at a smaller buoyancy ratios N = 1 and N = 2 the concentration profile shows a significant increase in the concentration level in the UCZ and parts of the gradient layer, that is due to the mass transfer of salt via diffusion and convection.

The concentration profile in Fig. 6.12c clearly shows that the increase of buoyancy ratio helps to maintain the average salt concentration to almost zero in the UCZ, and also helps to maintain the shape of salt concentration profile in the gradient non-convective layer. At N = 4 and 6, it is possible for the SGSP to be operative for months; however, in order to compensate for salt diffused to upper layers, regular addition of saturated brine in the LCZ is still needed. The concentration profile, as shown in Fig. 6.12c, also indicates that it is only the

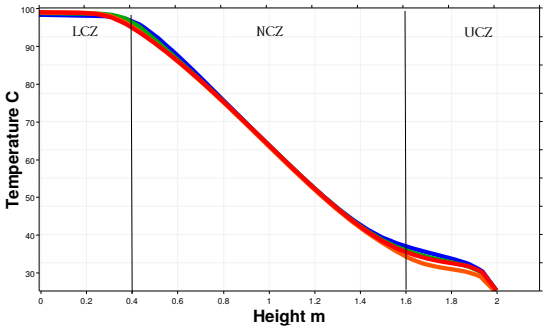

(A) One day of operation.

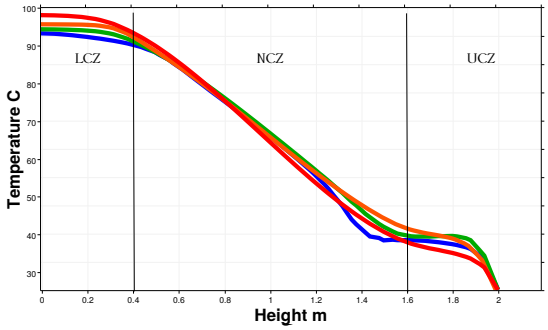

(B) Two weeks of operation.

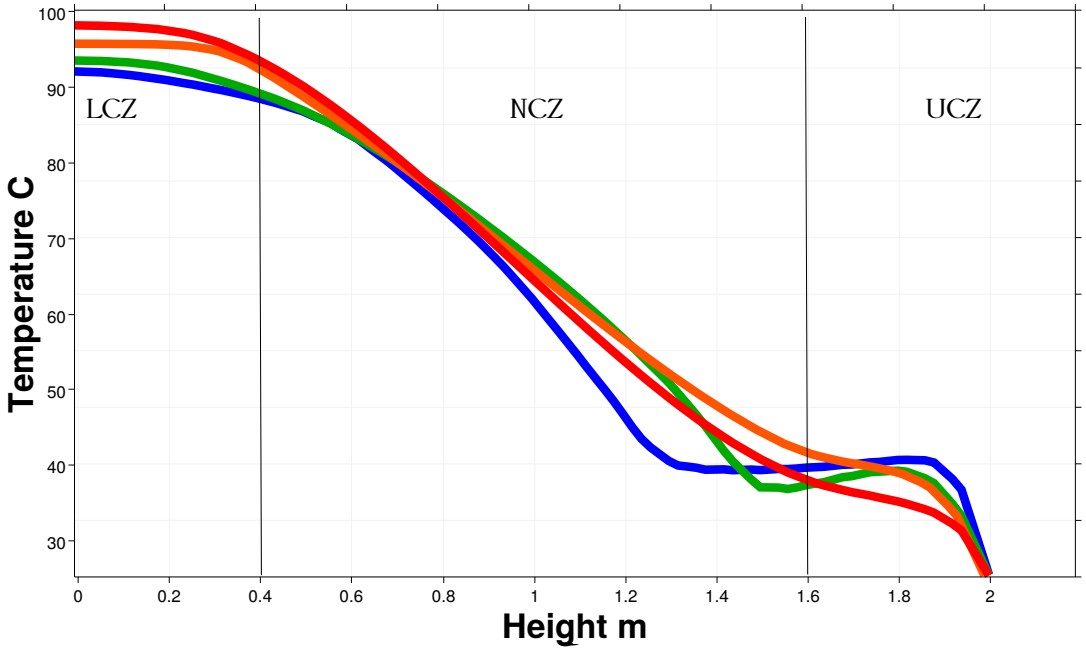

(C) Temperature profile the time before SGSP becomes unstable.

FIGURE 6.11. Temperature profile, ■ N= 1, ■ N = 2, ■ N= 4, ■ N= 6.

contribution of the salinity distribution that provides enough gravitational resistance to the mixing because the temperature rises only weakens the density distribution. In order to compensate for this intrinsic source of instability, the salt contribution $\beta_C \Delta C$ to the local net density must be sustained more significant than the temperature contribution $\beta_T \Delta T$.

For the operator in the field, this means injecting salt regularly to the LCZ in order to strengthen the salt concentration profile is crucial, see Table. 6.4 for more reflection on buoyancy and salt requirements. According to the results, the concentration difference between the UCZ and LCZ should be at least 300 kg/m^3 of NaCl concentration to maintain the SGSP temperature. It can be concluded that

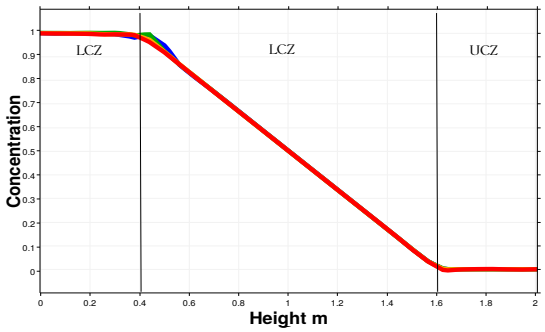

(A) One day of operation.

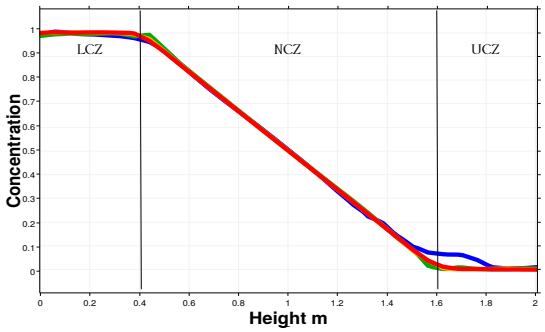

(B) Two weeks of operation.

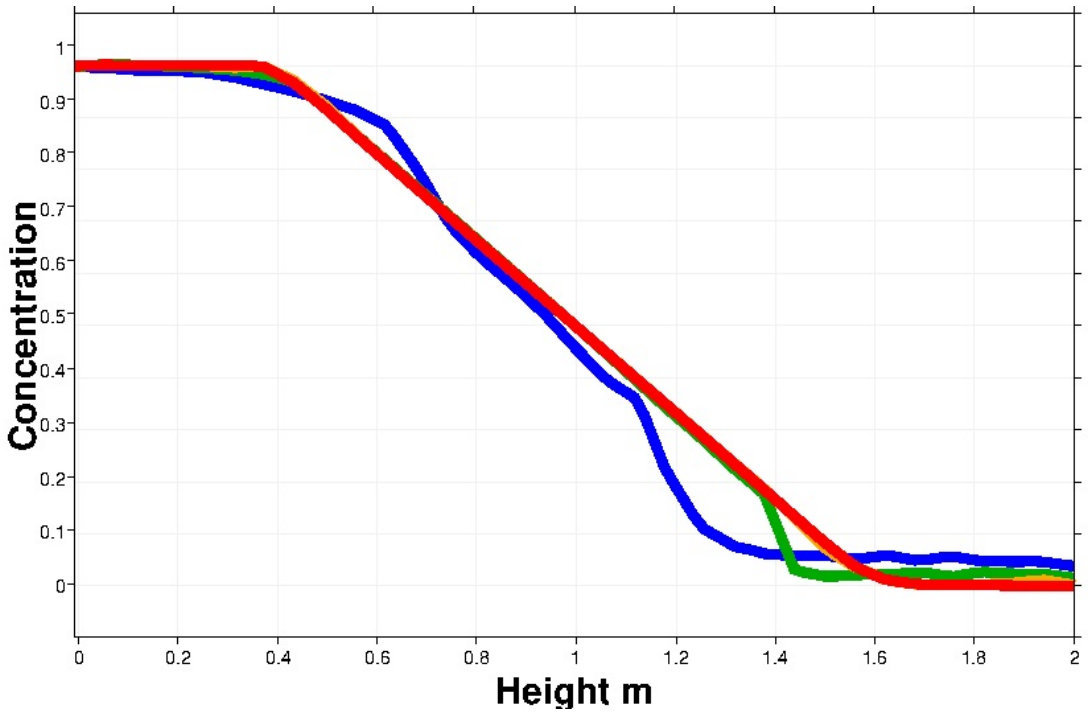

(C) concentration profile the ime before SGSP become unstable.

FIGURE 6.12. Concentration profile, ■ N= 1, ■ N = 2, ■ N= 4, ■ N= 6.

if a SGSP salt injection process is correctly planned, surface regularly flushed, then storing the attained thermal energy for a long period of time is possible.

Table. 6.6 summaries the buoyancy ratio effect on SGSP operational stability. To conclude, the buoyancy ratio plays a great role in stabilising the layers of salty water in the solar pond and subsequently hindering convective motions in the UCZ and LCZ from expanding and causing fluid mixing in the NCZ which will eventually destabilise the pond. The NCZ is progressively eroded by convective mixing above and below when the buoyancy ratio is small in comparison to a large buoyancy ratio. This thickness reduction reduces the efficiency of the

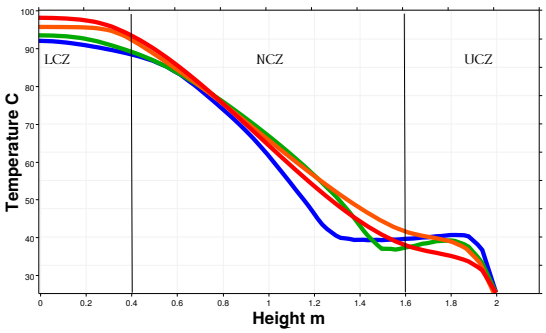

(A) Temperature profile.

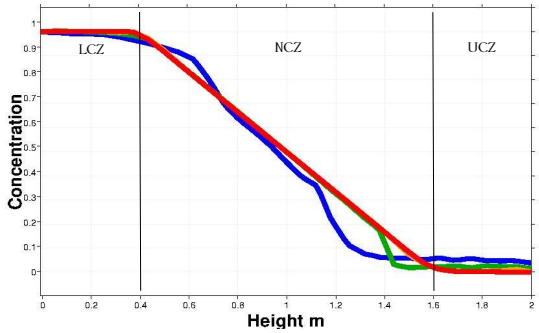

(B) Concentration profile.

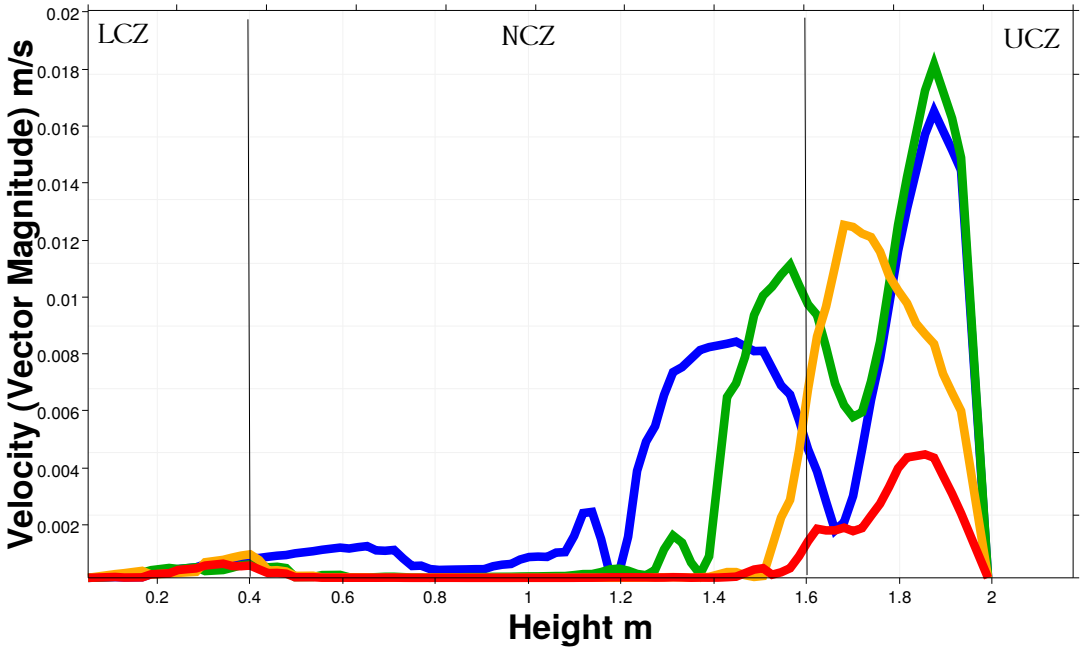

(C) Velocity profile.

FIGURE 6.13. Temperature, concentration and velocity profiles at the time SGSP becomes unstable, ■ Buoyancy ratio= 1, ■ Buoyancy ratio = 2, ■ Buoyancy ratio= 4, ■ Buoyancy ratio= 6. Operational stability period from steady-state ≈, 50, 75, 130 and 150 days respectively.

SGSP. It is important to note that even though the NCZ thickness slightly decreased, it still suppresses convection and does not allow complete overturn of the pond.

However, the progressive and continuous expansion of convection currents will eventually make SGSP go unstable if no measures are taking. A high buoyancy ratio adds to the salt requirement, but in return, it sustains the system for a longer time. A heat recovery procedure is required in order to avoid SGSP overheating. Overheating is a causative factor to enhance DDC phenomena

TABLE 6.6. Effect of buoyancy ratio on SGSP operational stability.

i	Buoyancy ratio	Operatinal stability period from steady-state	instability causative factor
1	<1	Becomes unstable instantly after 3 days	Instant continous mixing inside the non-convective zone that led to complete turnover.
2	1	50 days	Weak gravitational resistance to the mixing caused by the DDC effect
3	2	75 days	No enough gravitational resistance to the mixing caused by the DDC effect
4	4	130 days	Relatively high gravitational resistance to the mixing caused by the DDC effect; however, salt diffusion and overheating weakened the density gradient in the NCZ.
5	6	150 days	High Resistence to DDC effect; however, salt diffusion and overheating weakened the density gradient in the NCZ.

and the expansion of convective cells. Thus, the effect of heat recovery on SGSP operational stability study is to be conducted in the next section.

6.4 Effect of heat recovery

A crucial aspect of SGSP technology is heat recovery. Typically, heat recovery is carried out in two ways: by using a submerged heat exchanger located on the bottom of the pond, or by pumping brine from the lower convective

zone to an external heat exchanger and then returning it to the pond. The first method implies high costs for the maintenance of the heat exchanger, as it is fully submerged in the hot brine, which is a highly corrosive medium. The second method generates local temperature differences, whose final effect is to destabilise the non-convective zone because this brine extraction/injection process is performed at a specific point of the solar pond, generally close to the centre of the pond [9].

Heat extraction/recovery is always treated as a mechanical source of instability. This study focuses only on hydrodynamic instability sources. Subsequently, mechanical instability factors such as the mechanical heat extraction process (injection and extraction of the fluid) are assumed to be well designed, and all sources of mechanical instability and shearing flows are curtailed. Therefore, the primary purpose of this study is to determine whether overheating can play a role in destabilising SGSP when the DDC effect is minimised by increasing the salt content at the bottom of the pond to a level of saturation where the solution is heavy enough to prevent convection currents from expansion.

The same SGSP investigated in the buoyancy ratio study will be further examined, where, N = 4 and NCZ: LCZ thickness ratio 3:1. For the purpose of this study, some assumptions are made. The SGSP is run from steady-state. The fluid in the SGSP is assumed to be stagnant at the start of the operation, $V = 0$ throughout the pond. Temperature and salt concentration at LCZ is maximum 100°C . The NCZ is well established. Also, temperature and concentration at UCZ are equal to ambient. The system is operating in a transient state. The amount of the absorbed energy is assumed to be significantly high, an internal Rayleigh (Ra_I) equals 10^9. The SGSP is at a state where heat extraction occurs at a constant rate from the start of the simulation. Two scenarios are studied; (I) No heat extraction, and (II) With heat extraction. The study is conducted, incorporating the same governing equations and parameters used in Chapter 5.

At no heat extraction scenario (red lines). The SGSP initial temperature profile (blue line), is shown in Fig. 6.14b. The salinity gradient solar pond was run until it became unstable (complete erosion of NCZ) as shown in Fig. 6.14c. It has been noticed that at the end of the simulation, the LCZ temperature dropped almost 5°C due to the rapid heat diffusion from LCZ to the upper zone at the

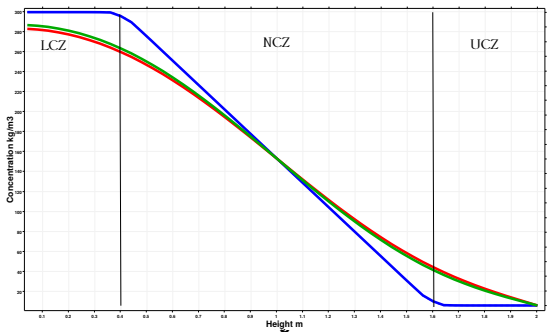

(A) Concentration profiles.

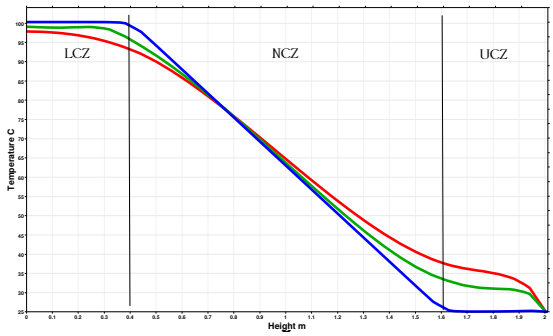

(B) Temperature profiles.

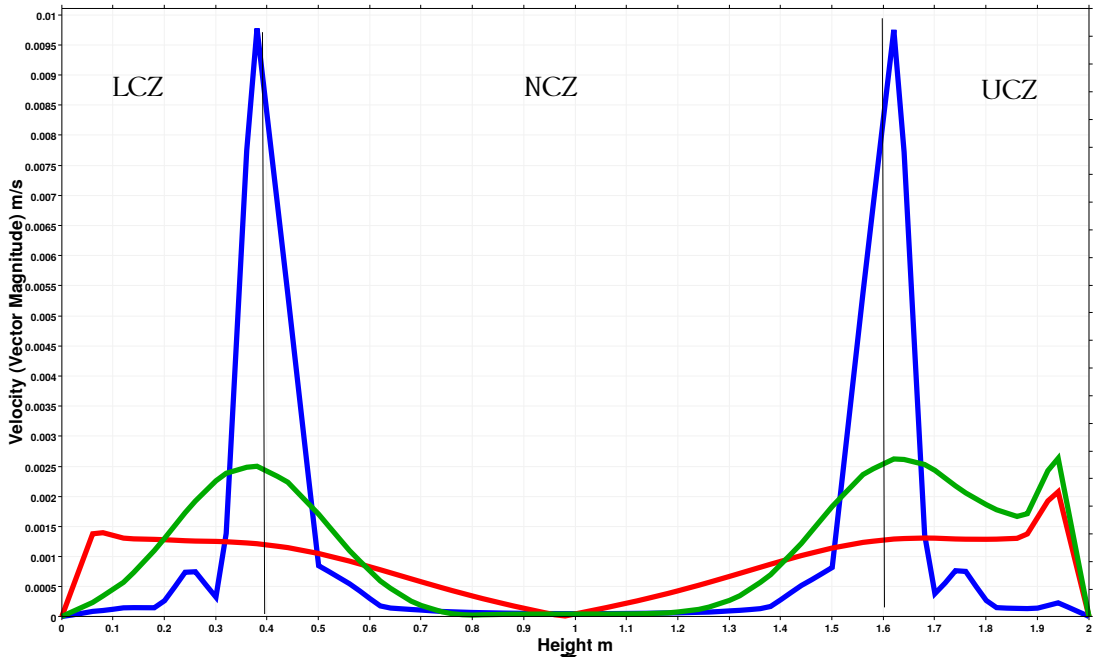

(C) Velocity profiles.

FIGURE 6.14. SGSP Thermal behaviour and operational stability studied under two scenarios, ■ = With heat recovery (Unstable after 158 days), ■ = No heat recovery (Unstable after 90 days). ■ = Initial profile for both scenarios. SGSP Run from steady-state (Maximum LCZ temperature) and with $Ra_I = 10^9$ (extremely high solar intensity)

no-heat extraction scenario. The overheating of the pond, without any procedure to extract heat led to the rapid formation of thermal convective currents. The expansion of the thermal convection currents destabilises the temperature gradient in the NCZ and subsequently destabilising the salinity gradient solar pond after almost 90 days of operation, and that is mainly due to the overheating which enhanced the rapid diffusion of salt and the DDC effect., as shown in Fig. 6.14c. The excessive increase in the LCZ temperature weakens the temperature gradient. Therefore, overheating of the LCZ affect the stability of the

NCZ in two ways. Firstly, the excessive heat in the lower convective zone temperature enhanced the destabilising temperature gradient. Secondly, thermal convective currents rising from the bottom of the pond entrained fluid from the gradient into the lower convective zone, decreases the thickness of the gradient. It is, therefore, essential to extract enough heat to avoid overheating counterproductive consequences.

At heat recovery scenario (green lines) during the heat extraction period at high solar intensity, the rate of decrease in the temperature of the LCZ was insignificant. The decrease in this scenario is in terms of useful heat. In this short loading period, the salinity gradient solar pond thermal behaviour slightly changed, as shown in Fig. 6.14b. The LCZ temperature drop is insignificant; this decrease was mainly due to the extraction of heat. The salinity gradient solar pond became unstable after almost $\approx$ 160 days of operation, and that is mainly due to the Mainly Salt Diffusion. Injecting salt to the LCZ and keeping flushing the UCZ with fresh water is crucial to protect the gradient layer. It is recommended that the SGSP excess energy is extracted when necessary to avoid overheating.

A salinity gradient solar pond can serve as a source of thermal energy, and it can be used continuously as an energy reserve, but with an appropriate salt control measurement and heat control procedure. Based on the result the heat extraction is crucial in order to avoid pond overheating in geographical latitude like in Libya, especially during the summer season. Instrumentations, such as thermocouples, transmitter, control valves and controllers can help to control the LCZ and avoiding any overheating that might occur. To conclude, for long term operation, flushing the UCZ and adding fresh water to minimise heat losses and wind erosion, injecting salt to the LCZ to sustain the competition between thermal and solutal Rayleigh balanced (buoyancy control) and an appropriate heat recovery procedures are mandatory.

6.5 Summary

The present chapter deals with the effect of zone thickness on SGSP thermal performance and operational stability. The 2-D study was conducted implementing the double-diffusive convection phenomenon. The optimum NCZ/LCZ

thickness ratio for an average salinity gradient solar pond of 2 m height is 3:1. The longest stability period and best SGSP thermal performance were obtained at these ratios.

The interfaces are the most vulnerable parts as week density (salt concentration) gradients exist in this region. Interestingly, for all zone thicknesses, the expansion of the convective cells at UCZ/NCZ and NCZ/LCZ interfaces eventually contributes to eroding the NCZ boundaries, and subsequently the dehomogenization of the non-convective layer, which eventually leads to shrinking of the zone until reaching a tiny limit where SGSP can not function. This happens at different rates and periods of time. At a thickness ratio of 3:1 (NCZ = 1.2 m), the NCZ was the most resistance to the DDC effect and had the best thermal performance and operational stability. Moreover, The SGSP was examined under different buoyancy ratios.

At a buoyancy ratio 4-6, the longest term of stability was obtained. Buoyancy ratio has an important rule in keeping the NCZ at its desired thickness and minimise the DDC effect. At these ratios, the solution inside the pond is heavy enough to prevent convection currents from forming rapidly and subsequently eroding the NCZ. The effect of overheating on SGSP stability has also been investigated. It has been found that overheating the lower convective zone can reduce the stability of the gradient and in turn, the pond unstable. To conclude, controlled heat recovery, regular injection of brine to LCZ and flushing the UCZ with fresh water are three fundamentals to sustain SGSP operational stability.

Chapter 7

Conclusion

7.1 Introduction

In Libya, the demand for freshwater is soaring, but the freshwater supply is limited. The water deficit in 1998 is estimated at 1154 Mm^3/year. In the absence of a sound water supply strategy, the deficit tends to increase to 4339 Mm^3/year in 2025 [1]. The current supply-driven approaches have been incapable of delivering freshwater security and sustainability on the national level. Seawater desalination has evolved into the only viable alternative water supply option. Unfortunately, seawater desalination is an energy-intensive process. Thus, the conclusions for energy and freshwater sustainability for future generations are twofold. On the input side: choosing how desalination is powered before Libyan oil depletes in probably 20 years. On the output side: viewing radical and efficient water conservation strategies in agriculture use, by far the country's highest consumer of freshwater. The sooner desalination plants can be powered by inexpensive and sustainable energy sources such as solar energy; the sooner Libya will become sustainable.

This thesis investigates the thermal potential and operation of salinity gradient solar ponds to be one of a mix of technologies helping to lead Libya to a future more based on renewable energy. To achieve this goal, the following specific objectives were therefore set out; (I) to model the thermal performance for a proposed SGSP located in Libya within the latitude and longitude of 32.54° N, 13.11° E, (II) to investigate the operational stability of the SGSP, by studying the formation and changes occur to the zones of the SGSP during operation, finally (III) to find the optimum zone design thicknesses, and also to develop

a procedure that helps to sustain the operational stability of the SGSP for an extended periods of time.

This chapter summarises; (I) the SGSP potential as a source of thermal energy to drive desalination units in Libya, (II) SGSP thermal behaviour and operational stability, and (III) SGSP optimum zone design thicknesses and the procedure for best thermal performance and long term stability. Finally, practical recommendations for future research are also presented in this concluding chapter.

7.2 SGSP thermal potential

Referring to the first objective (see, Section 1), this research has utilized a one-dimensional model to study and predict the potential of a salinity gradient solar pond as a source of thermal energy for thermal desalination application according to the geographical and climate conditions of Libya (Detailed results were reported in chapter 4).

The accuracy of the 1-D model used to conduct the SGSP thermal potential study was validated against results from published experimental data. The simulated temperature distribution output from the developed Python FiPy code was validated with data from El Paso and Granada solar ponds. It is concluded that the simulated and experimental temperature profiles are in good agreement.

The results obtained from the one-dimensional transient model for the proposed SGSP indicates that salinity gradient solar pond technology is ideally suited to Libya geographical and climate conditions. The starting up period for the SGSP takes 60 - 120 days depends on what time of the year to start the pond operation. Preferably, starting the SGSP during the winter season, although the SGSP will take longer time (ca. 120 days) before useful heat can be extracted, on the other hand, the SGSP will work at its full thermal potential during spring and summer where solar intensity is higher.

The maximum LCZ temperature obtained is 98 °C in August and beginning of September. During the winter, a temperature above 70 °C was sustained

throughout the second year of operation. Thus, constructing a SGSP for providing thermal energy for desalination units such as multi-effect distillation thermal vapour compression MED-TVC unit is applicable, as the SGSP is able to provide hot saline water with a temperature exceeding 65 °C most of the year except for a start-up period in the beginning. It has been reported that multi-effect distillation thermal vapour compression MED-TVC units have been successfully working at a top brine temperature TBT of almost 60 - 65 °C [141, 48, 49, 50].

The multi-effect distillation MED systems, are more convenient than Multi-stage flashing, as the MSF TBT is 90 °C and the typical multi-effect distillation TBT is 70 °C as shown in chapter 4. MED-TCV operates at the lowest TBT amongst these mature desalination units and costs less in terms of operation and construction; however, its production capacity is lower.

Salinity gradient solar pond, similar to all solar energy systems, can experience variations in thermal performance due to weather fluctuations; however, its unique characteristic is that it can store, preserve and provide thermal energy for the majority of months of the year, as shown in Fig. 4.12. The free storage feature in the SGSP assures consistency in providing sufficient heat throughout the year in the case for the MED-TVC desalination units.

Another advantage of SGSPs over other solar technologies is the utilization of reject brine. The environmental impacts of the rejected hypersaline brine should always be integrated. Brines is disposed of prudently as it often considered a waste product. In the case of SGSP, this brine can be used as a foundation to create the SGSP. This is a significant feature when considering SGSPs for inland freshwater production.

SGSPs are less costly than other solar collectors. Moreover, they provide the handiest and least costly choice for heat storage. That is very important, both for operational and economic viewpoints if regular and inexpensive water production is required. Efficiency alone may determine the practical feasibility. For example, even if fuel farms (a wood-burning power plant) could produce low-cost energy as illustrated in Table 7.1, it implies a large area requirement; thus, it should be excluded when land area is limited [9]. Flat plate solar collectors are a shallow box typically mounted on a roof that heats water using the solar

TABLE 7.1. Relative collector costs for several solar technologies [9]

Low temperature heat	Flat plate collector	SGSP (Average Site)	Fuel farm
Collector cost($\$/m^2$)	300	50	0.30
Collection efficiency	0.30	0.25	0.0030
Thermal output (W/m^2)	60	50	0.6
Area per k W thermal (m^2/kW)	17	20	1667
Collector cost ($\$/kW$)	5000	1000	500

energy has a very high collector per area cost ($\$/m^2$), and Collector per energy produced cost ($\$/kW$) which does not make it economically efficient compared to SGSPs [9].

To conclude, SGSP, as an integral device for receiving, collecting and storing solar energy is a potential heat supplier and attractive answer for powering thermal desalination in a country like Libya. The simplicity in design and operation and low cost of SGSP pose the question as to why they are not already in widespread use in arid and semi-arid regions where solar radiation intensity is high. There are several difficulties and limitations which are now under intensive study and for which viable solutions seem in sight. One of the limitations is the hydrodynamic stability of the system. Salinity gradient solar pond is a double-diffusive convective system, and it is subject to hydrodynamic instability.

7.3 Thermal behaviour and operational stability

Referring to the second objective (see, Section 1), the operational stability of the salinity gradient solar pond have been studied numerically using a 2-D model (see, chapter 5). After the solar radiation reaches the SGSP, the portion that crosses the surface gets absorbed at the bottom of the pond. This attenuation causes internal heating of the pond. Consequently, convection is activated. Thus, a slow continuous mixing in the LCZ takes place; the continuous mixing

leads to a uniform temperature everywhere inside the LCZ. Thus, the assumption of homogeneous temperatures in the LCZ, considered in the 1D models found to be a reasonable assumption as a relatively uniform temperature has been noticed throughout this layer; however, interfaces motion has also been noticed after heating the SGSP, that could not be detected using the 1-D model.

The interfaces motion is due to the DDC effect, and it has been noticed during the simulation at the UCZ-NCZ interface and NCL-LCZ interface. Convective currents appeared first at the interfaces and started to expand gradually to erode and damage the NCZ completely. This middle insulating layer should be nearly a motionless layer to act as a transparent insulating layer, allowing energy entrapment in the LCZ, and to maintain the stability of the pond.

For the operators sustaining the concentration profile of the non-convective zone is crucial to the successful operation and stability. The aim of operational stability can not be accomplished except when the slat concentration gradient is faultlessly sustained, and the diffusion of salt inside the SGSP is successfully controlled.

7.4 Zone thicknesses and long term stability

Referring to the third objective (see, Section 1). The thicknesses of the zones are a critical parameter in SGSP operation. The optimum NCZ: LCZ zone thicknesses ratio for an average salinity gradient solar pond of 2 m height is found to be 3:1. The longest term stability and the best SGSP thermal performance were obtained at this ratio. An NCZ: LCZ zone thicknesses ratio of 3:1 corresponds to 0.4 m for the UCZ, 1.2 m for the NCZ and 0.4 m for the LCZ. This ratio can also be the most cost-effective option for a 2 m SGSP. One should not neglect that the increase in salt requirements that will follow the increase in the thickness of LCZ if other NCZ: LCZ thickness ratios such as 2:1 or 1:1 are considered, which will add to the capital cost.

For MED-TVC plant that requires a top brine temperature around 60 - 65 °C, an LCZ thickness of 0.4 m for 2 m ponds, is found to be suitable and cost-effective, increasing the LCZ thickness will decrease the zone temperature which means

a need to stop the pond for several months when LCZ temperature of 60 - 65 °C can not be obtained. Increasing the LCZ thickness also increases the capital cost due to the high salt requirements. The financial (thermo-economical) implications of increasing or decreasing the thickness of the NCZ must be evaluated in order to justify what is optimum. As mentioned, any increase or decrease should always justify the capital and operating expenditure.

The buoyancy ratio has a critical impact on preventing convection motions induced by solar radiation absorption from destabilizing SGSP. The increase of buoyancy ratio (increasing the salt concentration to a level where the solution becomes heavy enough to prevent convection) reduces the UCZ temperature by minimizing upward heat losses and will also preserve the thermal energy in the LCZ. For a buoyancy ratio of 4 and 6, the salt concentration gradient is strong, and the salt concentration in the LCZ is heavy enough to prevent convection from eroding the LCZ in rapid time. For the operator, a salt (Na Cl) concentration difference between the UCZ and LCZ should be approximately between 300 kg m^{-3} to achieve a buoyancy ratio of 4 This makes the competition between concentration and thermal forces high and the solutal Rayleigh is higher in comparison to thermal Rayleigh; thus, the SGSP is stable, and conduction dominates heat transfer process in the SGSP. In other words, there is no significant change in buoyancy force to drive large scale motion. Subsequently, it is vital to keep the relative balance of temperature and concentration contributions to the density field intact in order to minimize the double-diffusive effect and maintain the stability of the pond.

Referring to chapter 6, the procedure for maintaining zone thicknesses can be summarized for the operator in three points. (I) Regularly flushing UCZ with freshwater (I) Controlling buoyancy ratio (measuring the concentration level and injecting brine solution to LCZ to a level that is heavy enough to prevent convection accordingly), and (III) A systematic heat recovery procedure from the pond to avoid pond overheating.

7.5 Overall conclusion

Salinity gradient solar pond technology is ideally suited to Libya geographical and climate conditions. The starting up period for the SGSP takes 60 - 120 days depends on what time of the year to start the pond operation. The maximum LCZ temperature obtained is 98 °C in the summer. During the winter, a temperature above 70 °C was sustained throughout the second year of operation. Thus, constructing a SGSP for providing thermal energy for desalination units such as MED-TVC unit is applicable, as it can provide hot saline water with a temperature exceeding 64 °C most of the year except for a start-up period in the beginning. MED-TVC plants have been successfully in operation at TBT of almost 60 - 65 °C.

At a heat extraction of 55 W m^{-2} per hour and for 14 hours per day (Average sunlight hours), yields 55 x 14 = 770 W m^{-2} per day and about 2400 kW hr m^{-2} per year. Considering a solar pond efficiency of about 22% [133]. This means each m^2 collects around 500 kW hr m^{-2} per year. The Carnot efficiency of the SGSP operating between 98 °C and 25 °C becomes about 25%; however, a practical Rankine cycle has a smaller temperature difference, because of the temperature drop in the evaporator and condenser. Thus, the resulting cycle efficiency is approximately 10%. This indicates that in the case of power production, each m^2 produces 50 kWh per year. Each kW installed for baseload operation therefore requires a SGSP surface area of 1 x 24 x 365/50 = 175.2 m^2. Provided that the operational stability of the SGSP is not disturbed due to the DDC effect or any other mechanical source of instability. Assuming the desalination plant has an average economy ratio of 10:1. Assuming the same average rate of annual radiation. According to the beforementioned figures and assumptions, the freshwater production will then be 10 x 500 x 860 (kcal/mm^2 per year)/550,000 (kcal/m^3) = 7.80 m^3/m^2. This indicates that the SGSP area required to supply heat for desalination for a 1 m^3 per day is about 1 x 365/7.80 = 46.8 m^2.

The design thickness of the zones has a significant impact on SGSP thermal performance and stability. A thickness ratio of 3:1 (corresponds to 0.4 m for the UCZ, 1.2 m for the NCZ and 0.4 m for the LCZ) found to be an optimum ratio for long term operational stability and thermal performance. Flushing UCZ with freshwater, controlling the buoyancy ratio (injecting brine solution

to LCZ to a level that is heavy enough to prevent convection, salt concentration difference between the UCZ and LCZ interfaces of 300 kg m^{-3} achieves a buoyancy ratio of 4 which makes the competition between concentration and thermal forces high where the solutal Rayleigh is high enough in comparison to thermal Rayleigh during operation; thus, the SGSP is stable, and conduction dominates heat transfer process in the SGSP), and a systematic heat recovery procedure are all crucial for best thermal performance and long term stability.

7.6 Recommendations for further research

Today, Libya has two strategies for freshwater sustainability: first, stringent water conservation and second, powering desalination with sustainable energy sources. It is recommended to promote the use of SGSPs to drive medium-scale desalination units; this research shows the potential of using SGSPs as a thermal-energy supply.

A number of issues remain and are the subject of intense R. & D. activity. Further research could be carried out to study, the brine injection process to the LCZ, by investigating a system where the brine injection is accomplished automatically during the SGSP operation. Additionally, simulating the upper convective zone flushing and addition of freshwater processes using more complicated models where the system can detect when the salt concentration in this particular layer is above the salinity limit that was indicated in the present study. Accordingly, the model should allow flushing and adding freshwater to the UCZ. Automating the flushing and salt injecting processes could improve the operational stability of the pond. Thus, modelling and simulating a fully automated SGSP could lead to understanding how to design a system that solves the stability issue altogether.

Manufacturing a transparent absorbent that could be floated within the upper convective zone to absorb any salt in this layer, or developing a procedure that hinders the salt diffusion from the LCZ, even though the latter options does not seem to be possible currently; however, with the rapid current technological advancement, this option could be possible in the future. It could be useful if this option is investigated.

In the SGSP operation, the SGSP reaches a point where there is no enough gravitational resistance to the mixing caused by the DDC effect, as the temperature rise will always weaken the density distribution. Coupling a salinity gradient solar pond with a covered pond may improve the operational stability and support the gained heat by adopting this procedure; preheating by the gradient pond and storing the heat in a cover pond. This coupling could result in more temperature control and heat gain. It could be useful if this kind of system is studied in the future.

Appendix A

Appendix

The Navier Stokes discretization in time fore Eqs. 3.53 - 3.62 can be written as follows:

Continuity and Momentum

$$\nabla \cdot \mathbf{V}^{i+1} = 0 \tag{A.1}$$

$$\frac{\mathbf{V}^{i+1} - \mathbf{V}^{i}}{\Delta t} + \vartheta(\mathbf{V}^{i+1} \cdot \nabla)\mathbf{V}^{i+1} + \vartheta(\mathbf{V}^{i} \cdot \nabla)\mathbf{V}^{i} - Pr\vartheta\Big(\nabla^2\mathbf{V}^{i+1} + \nabla^2\mathbf{V}^{i}\Big) = \nabla P^{i} \tag{A.2}$$

$$\vartheta(\mathbf{V^{i+1}} \cdot \nabla\mathbf{V^{i+1}} - Pr\nabla^2\mathbf{V^{i+1}}) - \frac{1}{\rho}\nabla P^{i+1}) = (1-\vartheta)(\mathbf{V^{i}} \cdot \nabla\mathbf{V^{i}} - Pr\nabla^2\mathbf{V^{i}} + \nabla P^{i}) \tag{A.3}$$

Energy Equation

$$\frac{\theta^{i+1} - \theta^{i}}{\Delta t} + \vartheta\cdot(\mathbf{V}^{i+1}\cdot\nabla)\theta^{i+1} + (1-\vartheta)\mathbf{V}^{i}\cdot\nabla\theta^{i+1} - Pr(\vartheta\cdot\nabla^2\theta^{i+1} + (1-\vartheta)\nabla^2\theta^{i}) = \frac{Ra_I}{Ra_T}\sigma(Z) \tag{A.4}$$

Mass Equation

$$\frac{\varphi^{i+1}-\varphi^{i}}{\Delta t}+\vartheta\cdot(\mathbf{V}^{i+1}\cdot\nabla)\varphi^{i+1}+(1-\vartheta)(\mathbf{V}^{i}\cdot\nabla)\varphi^{i}-\frac{1}{Le}\Big(\vartheta\cdot\nabla^{2}\varphi^{i+1}+(1-\vartheta)\nabla^{2}\varphi^{i}\Big)=0 \tag{A.5}$$

Weak form of the Governing Equations

$$\begin{aligned}\int dx\varphi^{i+1}(x)\phi_i(x)-\int dx\Delta t\frac{1}{Le}(\vartheta\cdot\nabla^{2}\varphi^{i+1}(x)\phi_i(x)\\ +(1-\vartheta)\nabla^{2}\varphi^{i}(x)\phi_i(x))=\int dx\varphi^{i}(x)\phi_i(x)\\ +\int dx\Delta t\vartheta(v^{i+1}\cdot\nabla)\varphi^{i+1}(x)\phi_i(x)\end{aligned} \tag{A.6}$$

Apply Integration by parts:

$$\begin{aligned}-\int dx\Delta t\frac{1}{Le}(\vartheta\cdot\nabla^{2}\varphi^{i+1}(x)\phi_i(x)\\ =-\int_s dx\vartheta n\cdot\frac{1}{Le}\Delta t\nabla\varphi^{i+1}(x)\phi_i(x)+\int dx\frac{1}{Le}\nabla\varphi^{i+1}\nabla\phi_i(x)\end{aligned} \tag{A.7}$$

$$\begin{aligned}-\int dx\Delta t\frac{1}{Le}(1-\vartheta)\nabla^{2}\varphi^{i}(x)\phi_i(x))\\ =-\int_s dx(1-\vartheta)n\cdot\frac{1}{Le}\Delta t\nabla\varphi^{i}(x)\phi_i(x)+\int dx\frac{1}{Le}\nabla\varphi^{i}\nabla\phi_i(x)\end{aligned} \tag{A.8}$$

$$-n\cdot(\frac{1}{Le}\nabla\varphi)=0 \tag{A.9}$$

$$\begin{aligned}\sum_j \left[\int dx\phi_i(x)\phi_j(x)\right]\varphi_j^{i+1} + \sum_j \left[\int dx\Delta t(1-\vartheta)\frac{1}{Le}\nabla\phi_i(x)\nabla\phi_j(x)\right]\varphi_j^i \\ + \sum_j \left[\int dx\Delta t\vartheta\frac{1}{Le}\nabla\phi_i(x)\nabla\phi_j(x)\right]\varphi_j^{i+1}\Bigg] \\ = \sum_j \left[\int dx\phi_i(x)\phi_j(x)\right]\varphi_j^i \\ + \sum_j \left[\int dx\Delta t\vartheta(V^{i+1}\cdot\nabla)\varphi^{i+1}(x)\phi_i(x)\phi_j(x)\right].\end{aligned} \tag{A.10}$$

$$M_{ij} = \int dx\phi_i(x)\phi_j(x) \tag{A.11}$$

$$K_{ij} = \Delta t\frac{1}{Le}(1-\vartheta)\int dx\nabla\phi_i(x)\nabla\phi_j(x) \tag{A.12}$$

$$\sum_j M_{ij}\varphi_j^{i+1} - \sum_j K_{ij}\varphi_j^{i+1} - \sum_j E_{ij}V^{i+1}\varphi_j^{i+1} = \sum_j K_{ij}\varphi_j^i + \sum_j M_{ij}\varphi_j^i \tag{A.13}$$

$$\begin{aligned}\int dx\theta^{i+1}(x)\phi_i(x) - \int dx\Delta t(\vartheta\cdot\nabla^2\theta^{i+1}(x)\phi_i(x) \\ +(1-\vartheta)\nabla^2\theta^i(x)\phi_i(x)) = \int dx\theta^i(x)\phi_i(x) \\ + \int dx\Delta t\vartheta(v^{i+1}\cdot\nabla)\theta^{i+1}(x)\phi_i(x) + \int dx\Delta tS_t(x)\phi_i(x)\end{aligned} \tag{A.14}$$

Apply integration by parts:

$$\begin{aligned}-\int dx\Delta t(\vartheta\cdot\nabla^2\theta^{i+1}(x)\phi_i(x) \\ = -\int_s dx\vartheta \quad n\cdot\Delta t\nabla\theta^{i+1}(x)\phi_i(x) + \int dx\nabla\theta^{i+1}\nabla\phi_i(x)\end{aligned} \tag{A.15}$$

$$\begin{aligned} &- \int dx \Delta t (1-\vartheta) \nabla^2 \theta^i(x) \phi_i(x)) \\ = &- \int_s dx (1-\vartheta) n \cdot \Delta t \nabla \theta^i(x) \phi_i(x) + \int dx \nabla \theta^i \nabla \phi_i(x) \end{aligned} \tag{A.16}$$

$$-n \cdot \nabla \theta = Bi\theta \tag{A.17}$$

$$\begin{aligned} \sum_j \left[\int dx \phi_i(x) \phi_j(x) \right] \theta_j^{i+1} + \sum_j \left[\int dx \Delta t (1-\vartheta) \nabla \phi_i(x) \nabla \phi_j(x) \right] \theta_j^i \\ + \sum_j \left[\int dx \Delta t \vartheta \nabla \phi_i(x) \nabla \phi_j(x) \right] \theta_j^{i+1} \Bigg] \\ = \sum_j \left[\int dx \phi_i(x) \phi_j(x) \right] Bi \theta_j^i \\ + \sum_j \left[\int dx \Delta t \vartheta (V^{i+1} \cdot \nabla) \theta^{i+1}(x) \phi_i(x) \phi_j(x) \right] + \sum_j dx \Delta t S_t(x) \phi_i(x) \phi_j(x) \end{aligned} \tag{A.18}$$

$$R_{ij} = \Delta t (1-\vartheta) \int dx \nabla \phi_i(x) \nabla \phi_j(x) \tag{A.19}$$

$$E_{ij} = \Delta t \int dx \phi_i(x) \nabla \phi_j(x) \tag{A.20}$$

$$H_{ij} = \Delta t (1-\vartheta) \int dx \nabla \phi_i(x) \nabla \phi_j(x) \tag{A.21}$$

$$\sum_j M_{ij} \varphi_j^{i+1} - \sum_j K_{ij} \theta_j^{i+1} - \sum_j E_{ij} V^{i+1} \theta_j^{i+1} V^{i+1} + \sum_j R_{ij} V^{i+1} \theta_j^{i+1} = \sum_j M_{ij} Bi \theta_j^i + \sum_j H_{ij} \varphi_j^i \tag{A.22}$$

Discretization in space or spatial discretization converts the PDE to a set of non-linear algebraic equations for the coefficient for the expressions in times of finite element. The scheme and variational forms without time derivative in previous or current times read:

Continuity and Momentum

$$\int \mathbf{dr}(\nabla \cdot \mathbf{V})\boldsymbol{\phi}_P = 0 \tag{A.23}$$

$$\int \mathbf{dr}\mathbf{V} \cdot \nabla V\boldsymbol{\phi}_V + \int \mathbf{dr}\nabla V \cdot \nabla\boldsymbol{\phi}_V + \int \mathbf{dr}\nabla \cdot \mathbf{V}\boldsymbol{\phi}_P = -\int \mathbf{dr}Ra_T(\theta - N\varphi)e_z\boldsymbol{\phi}_V \tag{A.24}$$

The scheme and variational forms for thermal and mass diffusion equations without time derivative in previous or current time read:

Energy Equation

$$\int \mathbf{dr}\nabla\theta \cdot \nabla\boldsymbol{\phi}_\theta + \int \mathbf{dr}\mathbf{V} \cdot \nabla\theta\boldsymbol{\phi}_V + \int \mathbf{dr}Bi \cdot \nabla\theta\boldsymbol{\phi}_\theta(ds) = \int \mathbf{dr}\frac{Ra_I}{Ra_T}\sigma(Z)\boldsymbol{\phi}_\theta \tag{A.25}$$

Mass Equation

$$\frac{1}{Le}\int \mathbf{dr}\nabla\varphi \cdot \nabla\boldsymbol{\phi}_\varphi + \int \mathbf{dr}\mathbf{V} \cdot \nabla\varphi\boldsymbol{\phi}_P = 0 \tag{A.26}$$

where $\boldsymbol{\phi_V}, \boldsymbol{\phi}_\theta, \boldsymbol{\phi}_\varphi$ are test functions.

References

[1] E Wheida and R Verhoeven. "Review And Assessment Of Water Resources In Libya". In: *Water International* 31.3 (2006), pp. 295–309.

[2] Robert Goodland. "How Libya Could Become Environmentally Sustainable". In: *Libyan Studies* 39 (2008), pp. 145–160.

[3] Muhammad Mohsin et al. "Assessment Of Drinking Water Quality And Its Impact On Residents Health In Bahawalpur City". In: *International Journal of Humanities and Social Science* 3.15 (2013), pp. 114–128.

[4] World Health Organization. *Guidelines For Drinking-water Quality*. Vol. 1. World Health Organization, 2004.

[5] A-KM Hussain and RMY Edaayf. "Seawater Desalination By Using Salinity–gradient Solar Pond Technologies". In: *WIT Transactions on Ecology and the Environment* 78 (2004).

[6] *Libya Water Map*. https://www.economist.com/node/21016792. Accessed: 2015-09-30.

[7] Akili D Khawaji, Ibrahim K Kutubkhanah, and Jong-Mihn Wie. "Advances In Seawater Desalination Technologies". In: *Desalination* 221.1-3 (2008), pp. 47–69.

[8] *Libya Solar Energy Map*. https://www.solarpaces.org/libya. Accessed: 2018-09-30.

[9] John R Hull, J Nielsen, and Peter Golding. "Salinity Gradient Solar Ponds". In: (CRC Press (31 Dec. 1988)).

[10] Lourdes Garcia-Rodriguez, Ana I Palmero-Marrero, and Carlos Gómez-Camacho. "Comparison Of Solar Thermal Technologies For Applications In Seawater Desalination". In: *Desalination* 142.2 (2002), pp. 135–142.

[11] A Saleh, JA Qudeiri, and MA Al-Nimr. "Performance Investigation Of A Salt Gradient Solar Pond Coupled With Desalination Facility Near The Dead Sea". In: *Energy* 36.2 (2011), pp. 922–931.

[12] Mehmet Karakilcik, Ibrahim Dincer, and Marc A Rosen. "Performance Investigation Of A Solar Pond". In: *Applied Thermal Engineering* 26.7 (2006), pp. 727–735.

[13] Hershel Weinberger. "The Physics Of The Solar Pond". In: *solar Energy* 8.2 (1964), pp. 45–56.

[14] John Ralph Hull. "Physics Of The Solar Pond". In: (Digital Repository@ Iowa State University, http://lib. dr. iastate. edu/, 1979).

[15] AA El-Sebaii et al. "History Of The Solar Ponds: A Review Study". In: *Renewable and Sustainable Energy Reviews* 15.6 (2011), pp. 3319–3325.

[16] Harry Tabor and R Matz. "A Status Report On A Solar Pond Project". In: *Solar Energy* 9.4 (1965), pp. 177–182.

[17] H Tabor. "Solar ponds". In: *Solar Energy* 27.3 (1981), pp. 181–194.

[18] Nicolas Chepurniy and Stuart B Savage. "An analytical and experimental investigation of a laboratory solar pond model". In: (1974).

[19] N Chepurniy and SB Savage. "Effect Of Diffusion On Concentration Profiles In A Solar Pond". In: *Solar Energy* 17.3 (1975), pp. 203–205.

[20] F Zangrando. "On The Hydrodynamics Of Salt-gradient Solar Ponds". In: *Solar Energy* 46.6 (1991), pp. 323–341.

[21] H Tabor. "Non-convecting solar ponds". In: *Philosophical Transactions of the Royal Society of London A: Mathematical, Physical and Engineering Sciences* 295.1414 (1980), pp. 423–433.

[22] Ari Rabl and Carl E Nielsen. "Solar Ponds For Space Heating". In: *Solar Energy* 17.1 (1975), pp. 1–12.

[23] Duffie Beckman. "Solar Engineering Of Thermal Process". In: (John Wiley & Sons (2014)).

[24] Amit Kumar and VVN Kishore. "Construction And Operational Experience Of A 6000 M2 Solar Pond At Kutch, India". In: *Solar Energy* 65.4 (1999), pp. 237–249.

[25] Huanmin Lu and Andrew HP Swift. "El Paso Solar Pond". In: *Journal of Solar Energy Engineering* 123.3 (2001), pp. 178–178.

[26] Jimmy Leblanc et al. "Heat Extraction Methods From Salinity-gradient Solar Ponds And Introduction Of A Novel System Of Heat Extraction For Improved Efficiency". In: *Solar Energy* 85.12 (2011), pp. 3103–3142.

[27] A Alcaraz et al. "Design, Construction, And Operation Of The First Industrial Salinity-gradient Solar Pond In Europe: An Efficiency Analysis Perspective". In: *Solar Energy* 164 (2018), pp. 316–326.

[28] Huanmin Lu et al. "Advancements In Salinity Gradient Solar Pond Technology Based On Sixteen Years Of Operational Experience". In: *Journal Of Solar Energy Engineering* 126.2 (2004), pp. 759–767.

[29] H Xu, AHP Swift, and P Golding. "'Two Gradient Failure and Repair Events as Experienced at the El Paso Solar Pond". In: *Solar Engineering-Proceedings of ASME International Solar Energy Conference*. Maui, HI. 1992, pp. 665–671.

[30] Huanmin Lu, John C Walton, and Andrew HP Swift. "Desalination coupled with salinity-gradient solar ponds". In: *Desalination* 136.1-3 (2001), pp. 13–23.

[31] Tamás Szacsvay, Patrick Hofer-Noser, and Mario Posnansky. "Technical And Economic Aspects Of Small-scale Solar-pond-powered Seawater Desalination Systems". In: *Desalination* 122.2-3 (1999), pp. 185–193.

[32] G Caruso and A Naviglio. "A Desalination Plant Using Solar Heat As A Heat Supply, Not Affecting The Environment With Chemicals". In: *Desalination* 122.2-3 (1999), pp. 225–234.

[33] J Srinivasan. "Solar pond technology". In: *Sadhana (Academy Proceedings in Engineering Sciences)*. Vol. 18. Indian Academy of Sciences. 1993, pp. 39–55.

[34] Keith Lovegrove and Mike Dennis. "Solar Thermal Energy Systems In Australia". In: *International Journal Of Environmental Studies* 63.6 (2006), pp. 791–802.

[35] Bradford S Sherman and Jörg Imberger. "Control Of A Solar Pond". In: *Solar Energy* 46.2 (1991), pp. 71–81.

[36] *Libya-Map*. https://www.britannica.com/place/Libya. Accessed: 2019-10-1.

[37] *Meteorological Data Libya*. https://power.larc.nasa.gov/. Accessed: 2016-09-30.

[38] Ahmad Aizaz and Rizwan Yousaf. "Construction and analysis of a salt gradient solar pond for hot water supply". In: *European Scientific Journal* 9.36 (2013).

[39] Hüseyin Kurt, Mehmet Ozkaymak, and A Korhan Binark. "Experimental And Numerical Analysis Of Sodium-carbonate Salt Gradient Solar-pond Performance Under Simulated Solar-radiation". In: *Applied Energy* 83.4 (2006), pp. 324–342.

[40] V Vitagliano. "Determinazione Delle Mobilita Ioniche Per Le Soluzioni Aquose Di Nacl A Diverse Temperature". In: *Gazzetta Chimica ltaliana* 90 (1960), pp. 1847–1858.

[41] F Zangrando. "A Simple Method To Establish Salt Gradient Solar Ponds". In: *Solar Energy* 25.5 (1980), pp. 467–470.

[42] F Zangrando and HW Johnstone. "'Effect of Injection Parameters on Gradient Formation". In: *Solar Engineering-1988* (1988), pp. 95–99.

[43] Guzman C Venegas. "Development Of A Simple And Practical Method To Modify The Structure Of The Salinity Gradient Of A Solar Pond." In: (2001).

[44] Carl E Nielsen. "Experience with a prototype solar pond for space heating". In: *Sharing the Sun: Solar Technology in the Seventies, Volume 5*. Vol. 5. 1976, pp. 169–182.

[45] F Zangrando and HC Bryant. "Demonstration salt gradient solar pond[Ph. D. Thesis]". In: (University of New Mexico, 1979).

[46] A Akbarzadeh and RWG MacDonald. "Introduction Of A Passive Method For Salt Replenishment In The Operation Of Solar Ponds". In: *Solar Energy* 29.1 (1982), pp. 71–76.

[47] R Collins and D Frederiksen. *Alice Springs Solar Pond Project*. Department of Primary Industries and Energy, 1987.

[48] T Michels. "Recent Achievements Of Low Temperature Multiple Effect Desalination In The Western Areas Of Abu Dhabi. Uae". In: *Desalination* 93.1-3 (1993), pp. 111–118.

[49] FN Alasfour, MA Darwish, and AO Bin Amer. "Thermal analysis of ME—TVC+ MEE desalination systems". In: *Desalination* 174.1 (2005), pp. 39–61.

[50] AO Bin Amer. "Development and optimization of ME-TVC desalination system". In: *Desalination* 249.3 (2009), pp. 1315–1331.

[51] Hisham M Ettouney et al. "Evaluating The Economics Of Desalination". In: *Chemical Engineering Progress* 98.12 (2002), pp. 32–40.

[52] Hisham T El-Dessouky and Hisham Mohamed Ettouney. *Fundamentals Of Salt Water Desalination*. Elsevier, 2002.

[53] Jimmy Leblanc, Aliakbar Akbarzadeh, and John Andrews. "Modelling solar-thermal desalination systems". In: *Australian and New Zealand Solar Energy Society (ANZSES)–2005 Solar Conference*. 2005, pp. 28–30.

[54] Andrea Cipollina, Giorgio Micale, and Lucio Rizzuti. "Seawater desalination". In: *Con-ventional and Renewable Energy Processes. Berlin & Heidelberg: Springer-Verlag* (2009).

[55] MA Sharaf, AS Nafey, and Lourdes García-Rodríguez. "Thermo-economic Analysis Of Solar Thermal Power Cycles Assisted Med-vc (multi Effect Distillation-vapor Compression) Desalination Processes". In: *Energy* 36.5 (2011), pp. 2753–2764.

[56] Jagadeesh Mallikarjunaiah Kyathsandra. "Performance Of A Solar Pond Coupled Multistage Flash Desalination System." In: (2001).

[57] Jose Manuel Barron. "Installation and operation of multi-effect multistage separator coupled with a solar pond." In: (2001).

[58] FB Alagao, A Akbarzadeh, and PW Johnson. "The Design, Construction, And Initial Operation Of A Closed-cycle, Salt-gradient Solar Pond". In: *Solar Energy* 53.4 (1994), pp. 343–351.

[59] Hwataik Han and Thomas H Kuehn. "Double Diffusive Natural Convection In A Vertical Rectangular Enclosure—i. Experimental Study". In: *International Journal Of Heat And Mass Transfer* 34.2 (1991), pp. 449–459.

[60] Hüseyin Kurt, Fethi Halici, and A Korhan Binark. "Solar Pond Conception—experimental And Theoretical Studies". In: *Energy conversion and management* 41.9 (2000), pp. 939–951.

[61] Hüseyin Kurt, Mehmet Ozkaymak, and A Korhan Binark. "Experimental And Numerical Analysis Of Sodium-carbonate Salt Gradient Solarpond Performance Under Simulated Solar-radiation". In: *Applied Energy* 83.4 (2006), pp. 324–342.

[62] Ali A Dehghan, Alireza Movahedi, and Mohsen Mazidi. "Experimental Investigation Of Energy And Exergy Performance Of Square And Circular Solar Ponds". In: *Solar energy* 97 (2013), pp. 273–284.

[63] Hershel Weinberger. "The Physics Of The Solar Pond". In: *Solar Energy* 8.2 (1964), pp. 45–56.

[64] HC Bryant and Ian Colbeck. "A Solar Pond For London?" In: *Solar Energy* 19.3 (1977), pp. 321–322.

[65] VVN Kishore and Veena Joshi. "A Practical Collector Efficiency Equation For Nonconvecting Solar Ponds". In: *Solar Energy* 33.5 (1984), pp. 391–395.

[66] D Subhakar and S Srinivasa Murthy. "Saturated Solar Ponds: 1. Simulation Procedure". In: *Solar Energy* 50.3 (1993), pp. 275–282.

[67] John R Hull. "Computer Simulation Of Solar Pond Thermal Behavior". In: *Solar Energy* 25.1 (1980), pp. 33–40.

[68] Hillel Rubin, Barry A Benedict, and Stefan Bachu. "Modeling The Performance Of A Solar Pond As A Source Of Thermal Energy". In: *Solar Energy* 32.6 (1984), pp. 771–778.

[69] Safwan Kanan, Jonathan Dewsbury, and Gregory Lane-Serff. "A Simple Heat and Mass Transfer Model for Salt Gradient Solar Ponds". In: *International Journal of Mechanical, Industrial Science and Engineering* (2014), pp. 27–33.

[70] TS Jayadev and Jon Henderson. *Salt Concentration Gradient Solar Ponds: Modeling And Optimization*. Tech. rep. Solar Energy Research Inst., Golden, CO (USA), 1979.

[71] Zahra Panahi, J Clair Batty, and JP Riley. "Numerical Simulation Of The Performance Of A Salt-gradient Solar Pond". In: *Journal of Solar Energy Engineering* 105.4 (1983), pp. 369–374.

[72] Ridha Boudhiaf, Ali Ben Moussa, and Mounir Baccar. "A Two-dimensional Numerical Study Of Hydrodynamic, Heat And Mass Transfer And Stability In A Salt Gradient Solar Pond". In: *Energies* 5.10 (2012), pp. 3986–4007.

[73] PD Lund and RS Keinonen. "Radiation Transmission Measurements For Solar Ponds". In: *Solar Energy* 33.3 (1984), pp. 237–240.

[74] Ridha Ben Mansour, Cong Tam Nguyen, and Nicolas Galanis. "Numerical Study Of Transient Heat And Mass Transfer And Stability In A Salt-gradient Solar Pond". In: *International Journal of Thermal Sciences* 43.8 (2004), pp. 779–790.

[75] Feliciano B Alagao. "Simulation Of The Transient Behavior Of A Closed-cycle Salt-gradient Solar Pond". In: *Solar Energy* 56.3 (1996), pp. 245–260.

[76] Margarida Canedo Giestas, Jorge P Milhazes, and HL Pina. "Numerical Modeling Of Solar Ponds". In: *Energy Procedia* 57 (2014), pp. 2416–2425.

[77] A Ramalingam and S Arumugam. "Performance prediction results of a 500 square metres Pondicherry salt gradient solar pond". In: *International Journal of Energy Technology and Policy* 11.1 (2015), pp. 1–12.

[78] KR Ranjan and SC Kaushik. "Thermodynamic And Economic Feasibility Of Solar Ponds For Various Thermal Applications: A Comprehensive Review". In: *Renewable and Sustainable Energy Reviews* 32 (2014), pp. 123–139.

[79] MR Jaefarzadeh and A Akbarzadeh. "Towards The Design Of Low Maintenance Salinity Gradient Solar Ponds". In: *Solar Energy* 73.5 (2002), pp. 375–384.

[80] H Lu and AHP Swift. "Reconstruction and Operation of the El Paso Solar Pond with a Geosynthetic Clay Liner System/University of Texas at El Paso. 1996". In: *American Society of Mechanical Engineers* ().

[81] MA Lichtwardt and H Remmers. "'Advanced Solar Pond Liner Technologies". In: 13 (1995).

[82] David Edwin Daniel. *Geotechnical Practice For Waste Disposal*. Springer Science & Business Media, 2012.

[83] MA Lichtwardt and AI Comer. "Geosynthetics In Salinity-gradient Solar Ponds". In: *Geotechnical Fabrics Report* 15 (1997), pp. 24–28.

[84] GR Ramakrishna Murthy and KP Pandey. "Scope Of Fertiliser Solar Ponds In Indian Agriculture". In: *Energy* 27.2 (2002), pp. 117–126.

[85] Ismail Bozkurt et al. "Performance Assessment Of A Magnesium Chloride Saturated Solar Pond". In: *Renewable Energy* 78 (2015), pp. 35–41.

[86] M Hassairi, MJ Safi, and S Chibani. "Natural brine solar pond: an experimental study". In: *Solar Energy* 70.1 (2001), pp. 45–50.

[87] CF Kooi. "The Steady State Salt Gradient Solar Pond". In: *Solar Energy* 23.1 (1979), pp. 37–45.

[88] MA Garmana and MA Muntasserb. "Sizing And Thermal Study Of Salinity Gradient Solar Ponds Connecting With The Med Desalination Unit". In: *Desalination* 222.1-3 (2008), pp. 689–695.

[89] H Tabor and B Doron. "Solar Ponds-Lessons learned from the 150 kW (e) power plant at Ein Boqek". In: *Proc. of the ASME Solar Energy Div., Anaheim, California* (1986).

[90] MM El-Refaee and AM Al-Marafie. "Numerical Simulation Of The Performance Of The Kuwait Experimental Salt-gradient Solar Pond (kesgsp)". In: *Energy Sources* 15.1 (1993), pp. 145–158.

[91] SM Patel and CL Gupta. "Experimental Solar Pond In A Hot Humid Climate". In: *Sunworld* 5.4 (1981), pp. 115–118.

[92] ND Kaushik and PK Bansal. "Transient Behaviour Of Salt Gradient Stabilised Shallow Solar Ponds". In: *Applied Energy* 10.1 (1982), pp. 47–63.

[93] Y Jaluria and CK Cha. "Heat Rejection To The Surface Layer Of A Solar Pond". In: *Journal of heat transfer* 107.1 (1985), pp. 99–106.

[94] YS Cha, WT Sha, and WW Schertz. "Modeling Of The Surface Convective Layer Of Salt-gradient Solar Ponds". In: *Journal of Solar Energy Engineering* 104.4 (1982), pp. 293–298.

[95] YF Wang and A Akbarzadeh. "A Parametric Study On Solar Ponds". In: *Solar Energy* 30.6 (1983), pp. 555–562.

[96] F Sabetta, M Pacetti, and P Principi. "An Internal Heat Extraction System For Solar Ponds". In: *Solar energy* 34.4-5 (1985), pp. 297–302.

[97] ND Kaushika. "Solar Ponds: A Review". In: *Energy Conversion And Management* 24.4 (1984), pp. 353–376.

[98] TA Newell et al. "Construction And Operation Activities At The University Of Illinois Salt Gradient Solar Pond". In: *Solar Energy* 45.4 (1990), pp. 231–239.

[99] MNA Hawlader and BJ Brinkworth. "An Analysis Of The Non-convecting Solar Pond". In: *Solar Energy* 27.3 (1981), pp. 195–204.

[100] KR Agha. "The Thermal Characteristics And Economic Analysis Of A Solar Pond Coupled Low Temperature Multi Stage Desalination Plant". In: *Solar Energy* 83.4 (2009), pp. 501–510.

[101] Celestino Angeli, Erminia Leonardi, and Luca Maciocco. "A Computational Study Of Salt Diffusion And Heat Extraction In Solar Pond Plants". In: *Solar Energy* 80.11 (2006), pp. 1498–1508.

[102] CE Nielsen. "Experience with heat extraction and zone boundary motion". In: *Proc. Annu. Meet.-Am. Sect. Int. Sol. Energy Soc.;(United States)* 6.CONF-830622- (1983).

[103] Joseph F Atkinson and DRF Harleman. "A Wind-mixed Layer Model For Solar Ponds". In: *Solar Energy* 31.3 (1983), pp. 243–259.

[104] SG Schladow. "The Upper Mixed Zone Of A Salt Gradient Solar Pond: Its Dynamics, Prediction And Control". In: *Solar Energy* 33.5 (1984), pp. 417–426.

[105] John Chipman. "The Soret Effect". In: *Journal of the American Chemical Society* 48.10 (1926), pp. 2577–2589.

[106] CE Nielsen. "Surface Zone Behavior In Solar Ponds". In: *Am. Soc. Mech. Eng.,(Pap.);(United States)* 82.CONF-821101- (1982).

[107] Herbert E Huppert and J Stewart Turner. "Double-diffusive convection". In: *Journal of Fluid Mechanics* 106 (1981), pp. 299–329.

[108] JP Leshuk et al. "Solar Pond Stability Experiments". In: *Solar Energy* 21.3 (1978), pp. 237–244.

[109] Hua Wang, Maozhao Xie, and Wen-ce Sun. "Nonlinear Dynamic Behavior Of Non-convective Zone In Salt Gradient Solar Pond". In: *Solar Energy* 85.9 (2011), pp. 1745–1757.

[110] Ridha Boudhiaf. "Numerical temperature and concentration distributions in an insulated salinity gradient solar pond". In: *Renewables: Wind, Water, and Solar* 2.1 (2015), p. 10.

[111] Francisco Suárez, Scott W Tyler, and Amy E Childress. "A Fully Coupled, Transient Double-diffusive Convective Model For Salt-gradient Solar Ponds". In: *International Journal of Heat and Mass Transfer* 53.9-10 (2010), pp. 1718–1730.

[112] Muhammad Iqbal. *An Introduction To Solar Radiation*. Elsevier, 2012.

[113] Jui Sheng Hsieh. "Solar energy engineering". In: (Prentice-Hall, Inc., Old Tappan, NJ, 1986).

[114] R Almanza and HC Bryant. "Observations Of The Transmittance In Two Solar Ponds". In: *Journal of Solar Energy Engineering* 105.4 (1983), pp. 378–379.

[115] YA Cengel and MN Özişik. "Solar Radiation Absorption In Solar Ponds". In: *Solar Energy* 33.6 (1984), pp. 581–591.

[116] JA Palyvos. "A survey of wind convection coefficient correlations for building envelope energy systems' modeling". In: *Applied Thermal Engineering* 28.8 (2008), pp. 801–808.

[117] Noam Lior. "Thermal Theory And Modelling Of Solar Collectors". In: *Solar Collectors, Energy* (1991).

[118] William H MacAdams and William H McAdams. *Heat transmission*. McGraw-Hill New York, 1954.

[119] W CQJR Swinbank. "Long-wave Radiation From Clear Skies". In: *Quarterly Journal of the Royal Meteorological Society* 89.381 (1963), pp. 339–348.

[120] MS Sodha, ND Kaushik, and SK Rao. "Thermal Analysis Of Three Zone Solar Pond". In: *International Journal of Energy Research* 5.4 (1981), pp. 321–340.

[121] BW Davis. "Solar Ponds: Performance Of Bottom-insulation And Performance Of Aboveground And Underground Thermal Storage". In: *Arab International Solar Energy Conference. 1*. 1983, pp. 347–354.

[122] John R Hull. "Solar Pond Ground Heat Loss To A Moving Water Table". In: *Solar Energy* 35.3 (1985), pp. 211–217.

[123] Celestino Angeli and Erminia Leonardi. "A One-dimensional Numerical Study Of The Salt Diffusion In A Salinity-gradient Solar Pond". In: *International Journal Of Heat And Mass Transfer* 47.1 (2004), pp. 1–10.

[124] Subrahmanyan Chandrasekhar. *Hydrodynamic And Hydromagnetic Stability*. Courier Corporation, 2013.

[125] Mostafa H Sharqawy, John H Lienhard, and Syed M Zubair. "Thermophysical Properties Of Seawater: A Review Of Existing Correlations And Data". In: *Desalination And Water Treatment* 16.1-3 (2010), pp. 354–380.

[126] Henk Kaarle Versteeg and Weeratunge Malalasekera. *An introduction to Computational Fluid Dynamics: The Finite Volume Method*. Pearson education, 2007.

[127] Jonathan E Guyer, Daniel Wheeler, and James A Warren. "Fipy: Partial Differential Equations With Python". In: *Computing in Science & Engineering* 11.3 (2009), pp. 6–15.

[128] J. E. Guyer, D. Wheeler, and J. A. Warren. "FiPy: Partial Differential Equations with Python". In: *Computing in Science and Engineering* May/June (2009), pp. 6–15. URL: http://www.ctcms.nist.gov/fipy.

[129] *Meteorological data Granada*. https://power.larc.nasa.gov/. Accessed: 2016-10-01.

[130] *Meteorological data El Paso*. https://power.larc.nasa.gov/. Accessed: 2016-09-30.

[131] Kishor G Nayar, Mostafa H Sharqawy, Leonardo D Banchik, et al. "Thermophysical Properties Of Seawater: A Review And New Correlations That Include Pressure Dependence". In: *Desalination* 390 (2016), pp. 1–24.

[132] Henry Shih. "Evaluating The Technologies Of Thermal Desalination Using Low-grade Heat". In: *Desalination* 182.1-3 (2005), pp. 461–469.

[133] Mohammad Reza Jaefarzadeh. "Heat Extraction from a Salinity-Gradient Solar Pond Using in Pond Heat Exchanger". In: *Applied Thermal Engineering* 26.16 (2006), pp. 1858–1865.

[134] J Crank and P Nicolson. "A Practical Method For Numerical Evaluation Of Solutions Of Partial Differential Equations Of The Heat-conduction Type". In: *Adv. Comput. Math* 6 (1947), pp. 207–226.

[135] J. Hake A. Johansson B. Kehlet A. Logg C. Richardson J. Ring M. E. Rognes M. S. Alnaes J. Blechta and G. N. Wells. "The FEniCS Project Version 1.5". In: vol. Archive of Numerical Software, vol. 3, 2015, [DOI].

[136] Anders Logg et al. "The fenics project". In: *Workshop on Multiscale Problems and Methods, Simula Research Laboratory*. 2011.

[137] Todd Dupont et al. *The FEniCS project*. Chalmers Finite Element Centre, Chalmers University of Technology, 2003.

[138] Zhen Nie et al. "Experimental Study Of Natural Brine Solar Ponds In Tibet". In: *Solar Energy* 85.7 (2011), pp. 1537–1542.

[139] K Al-Jamal and S Khashan. "Parametric Study Of A Solar Pond For Northern Jordan". In: *Energy* 21.10 (1996), pp. 939–946.

[140] M Haynes William, DR Lide, and TJ Bruno. *Crc Handbook Of Chemistry And Physics*. 2011.

[141] Ali Al-Karaghouli and Lawrence L Kazmerski. "Energy Consumption And Water Production Cost Of Conventional And Renewable-energy-powered Desalination Processes". In: *Renewable and Sustainable Energy Reviews* 24 (2013), pp. 343–356.